THE DESIGN AND TESTING OF

TURBINE BLADES

THE AERODYNAMIC DESIGN AND TESTING OF HIGH TURNING ANGLE TURBINE BLADES

BY

J.H. STANNARD B.Sc. (Eng), M.Sc.(Eng)

A Thesis

Submitted to the Faculty of Graduate Studies

in Partial Fulfilment of the Requirements for

the Degree of Doctor of Philosophy

McMaster University

April 1975

DOCTOR OF PHILOSOPHY (1975) McMASTER UNIVERSITY
(Mechanical Engineering) Hamilton, Ontario.

TITLE: The Aerodynamic design and testing of High Turning Angle Turbine Blades.

AUTHOR: J.H. STANNARD B.Sc.(Eng), M.Sc.(Eng), Southampton University, (U.K.)

SUPERVISOR: Dr. J.H.T. Wade

NUMBER OF PAGES: 230, xii

SCOPE AND CONTENTS:

Continuous development of Gas Turbines to realise higher work output has necessitated the design of turbine blades having large turning angles.

Improvements to existing calculation methods have been carried out to better describe the potential flow near the leading and trailing edges of a blade originally designed by R.K. Malhotra at McMaster University. An incompressible turbulent boundary layer program has been extended to calculate compressible flows, taking into account the adverse and favourable pressure gradients, and it has been used to describe the flow in the region near to the blade surface.

A test facility of the intermittent blow-down type was constructed and instrumented to test two-dimensional blade cascades. Some of the blades were instrumented to measure the surface pressure distribution. The performance of the blades has been analysed both theoretically and experimentally over a range of angles of attack and pressure ratios. The effect of stagger angle was also investigated to

show its effect on performance. The experimental results were compared to those obtained theoretically, and the agreement substantiates the main thrust of the thesis, which was to develop a rational design technique.

ACKNOWLEDGEMENTS

The author is grateful to Dr. J.H.T. Wade for his continuous support and guidance as supervisor of this work. The assistance of Dr. S.K. Gupta in the preparation of the boundary layer program is also acknowledged with thanks.

The financial support provided through the National Research Council Operating Grant A1585 is gratefully acknowledged.

CONTENTS

SYMBOLS

A_τ	Turbulent Mixing Coefficient (Eqn 24)
b	Blade Axial Chord
b'	Wake Width
c	Speed of Sound
C'	Constant c_o/C_pT_w
C_{LZ}	Zweifel Life Coefficient
C_p	Specific Heat at Constant Pressure
C'_p	Pressure surface Curvature (inverse of Radius)
C'_s	Suction surface Curvature (inverse of Radius)
E	Non-dimensional Eddy Viscosity (Eqn 26)
H_{12}	Shape Factor
k	Thermal Conductivity
l	Distance measured along mean centre line in Wake
l_m	Mixing length
$\dot{m}$	Mass Flow
M	Mach number
$\underline{M}$	Line Parallel to x-direction in Finite Difference Grid
n	Distance along a Quasi-Orthogonal measured from the suction surface
n_o	Length of Quasi-Orthogonal

p	Pressure
P	Non-dimensional pressure
P_r	Prandtl Number
P_{RT}	Turbulent Prandtl Number
R_c	Radius of Curvature
R_{crit}	Critical Reynolds Number
$R_{\delta 2}$	Reynolds Number based on Momentum Thickness
S	Pitch
T	Temperature
$\overline{T}_u$	Free Stream Turbulence % R.M.S.
u	Velocity, x-direction
U	Non-dimensional Velocity in x-direction (Eqn 26)
v	Velocity, y-direction
V	Non-diemnsional y-direction velocity (Eqn 26)
x	Coordinate measured along Wall
X	Non-Dimensional coordinate measured along Wall (Eqn 26)
$\overline{x}$	Coordinate measured normal to Blade Cascade
$\mathfrak{K}$	Pressure Gradient Parameter = $\frac{\delta_2^2}{\gamma}\frac{du}{dx}$
y	Coordinate measured normal to Wall
Y	Non-dimensional Coordinate measured normal to Wall (Eqn 26)
y^+	Van Driest damping factor (Eqn 39)

$\underline{y}$	Coordinate measured parallel to Blade Cascade
$\underline{z}$	Coordinate measured parallel to Blade Trailing Edge

Greek Symbols

α_1	Angle of Attack
δ	Boundary Layer Thickness
δ_1	Boundary Layer Displacement Thickness
δ_2	Boundary Layer Momentum Thickness
ε	Eddy Viscosity
ε_H	Eddy Conductivity
θ	Angular Deviation
$\overline{\theta}$	Dimensionless Temperature
μ	Dynamic Viscosity
ν	Kinematic Viscosity
ζ	Density
τ	Shear stress
λ	Stagger Angle
ψ	Angular Deviation (Tunnel Test Section)
γ	Ratio of the Specific Heats

Subscripts

m	Grid line in x-direction
mid	Mid Channel
n	Grid Line in y-direction
p'	Pressure Surface

s	Static
s'	Suction surface
a	Atmosphere
t	Turbulent
w	Wall
∞	Free Stream
o	Stagnation

Superscript

—	Time Averaged Quantity
'	Fluctuating Quantity
A_n, B_n, C_n, D_n	Coefficients in the Finite Difference Momentum Equations
F_n, G_n, H_n, I_n	Coefficients in the Finite Difference Energy Equations

CHAPTER 1.0 INTRODUCTION

Turbine design has traditionally been a semi-empirical process using large amounts of experimentally derived information such as profile loss coefficients to develop families or series of related blade shapes with similar performance. Typically a lift coefficient such as that defined by Zweifel is used to determine optimum blade spacing (1,2). With the widespread use of high speed computers it has become possible to better analyse the flow in detail over a cascade of airfoils, and finite element computation schemes are available which solve the two-dimensional equations of motion, momentum and energy in the transonic regime. Naturally attention has turned to analysis of the flow near the surface of the blades which gave rise to simple design methods in which the blade shape was corrected to allow for boundary layer displacement thickness.

More recently certain authors, particularly Le Foll (3), have suggested that the correct way to derive the most efficient general airfoil shape is to design an optimum boundary layer and thus derive a potential flow solution to satisfy the upstream and downstream constraints, together with the prescribed surface velocity distribution. This idea has generally met some resistance from industry because such blades have extremely long thin trailing edges and are thus difficult to manufacture and prone to excessive vibration in service, despite attempts to keep the 1st natural frequency well away from forcing

frequencies at design operating conditions.

The aim of the present work is to establish a rational design method based on computation schemes developed by the author, and to test the predicted aerodynamic performance of the blades in a cascade wind tunnel. A design method similar to that described in Reference 4 is used (Fig. 1). The modular approach enables the updating of the various computational blocks as improvements are made. The work to date has been two-dimensional in nature and it is thought that the methods developed are applicable to actual turbine design since the highly loaded high pressure turbines in modern designs have very short blades in relation to hub diameter with only small amounts of blade twist. However the three-dimensional effects due to secondary flows induced by the rotational force field, and the effect of hub and tip end-wall boundary layers deserve further study.

The potential flow solutions are generated by a simple streamline curvature method which calculates velocities and pressures at various design points in the flow passage. This is a development of methods dating back to the late 1950's (5), but a number of important improvements have been made which are detailed in Chapter 2.0. This method has the advantage of being extremely cheap and quick in operation, at the expense of a slight loss of accuracy under transonic conditions. The blade design method using this calculation is also described in Chapter 2.0. One of the chief features of interest with this type of blade is the fact that the blade system is choked, that is we have a sonic condition at the narrowest part of the blade passage. The exact

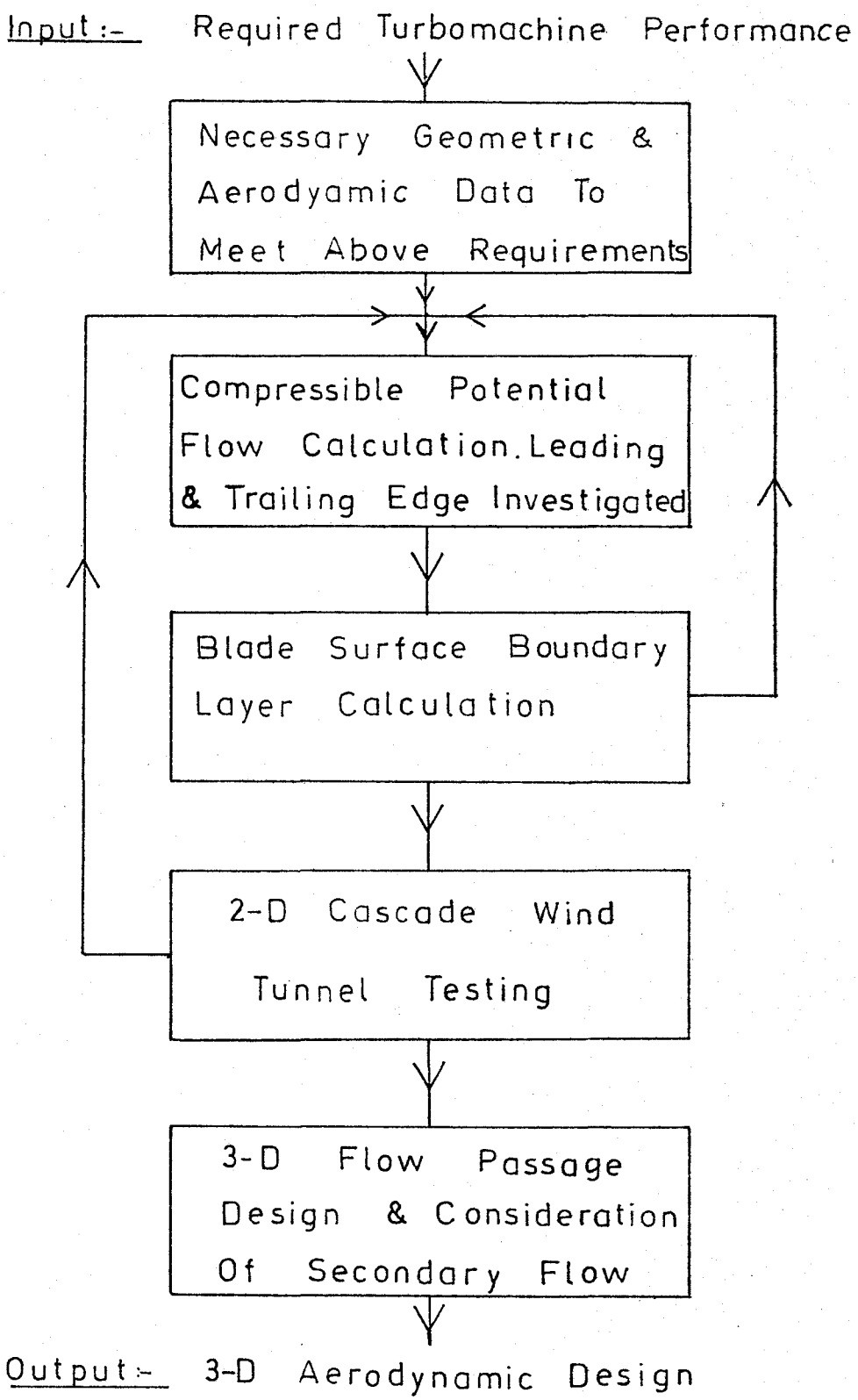

Figure 1 Illustration of the Design Process

shape and position of the sonic line affect performance to a considerable degree.

In Chapter 3.0 the boundary layer flow is analysed from a theoretical viewpoint. A compressible flow, turbulent boundary layer computation scheme has been developed to describe the flow over a curved surface, with or without heat transfer. A transition point is calculated within the program taking into account free stream turbulence, momentum thickness and pressure gradient. To this point no allowance has been made for the effects of surface curvature (other than pressure gradient) or surface roughness. The aim is to calculate displacement thickness to allow improvement of the potential flow solution, particularly in the throat region.

To test the blades so designed an intermittent blow-down cascade wind tunnel was developed using the basic design of the A.V. Roe Gas Turbine Group at Orenda Engines Ltd. This wind tunnel had been used previously to test compressor blades. The original tunnel was modified extensively to a blow-down design enabling the surface pressure distribution and upstream and downstream flow to be measured over a range of pressure ratios up to 3:1 at varying angles of attack. To reduce capital and running costs an intermittent facility was built enabling some fifteen seconds of running time at a pressure ratio of 2:1. The upstream pressure is controlled by a feedback control loop. This cascade wind tunnel is described in Chapter 4.0.

The instrumentation and testing performed are described in later chapters, with the emphasis being place on obtaining sufficient

experimental results so that our theoretical model of the flow through the cascade could be verified.

CHAPTER 2.0 TWO-DIMENSIONAL DESIGN AND POTENTIAL FLOW SOLUTION

The type of blade designs of interest to this work have very high surface curvatures with total turning angles of the order of 130° and Zweifel lift coefficients of the order of 0.8 to 1.2. A typical blade shape is shown with the surface pressure distribution that results in Fig. 2. Notable features of the pressure distribution curve are the rapid expansion and recompression near the leading edge followed by a further expansion and compression on the suction surface. The pressure surface is typified by a large portion of the surface at nearly constant pressure followed by an expansion towards the trailing edge.

There exists a number of computation schemes used for design in this area but many of them break down when applied to very high surface curvatures. Traditionally methods such as that of Martensen (6) or Stanitz (7) have been applied to blade profile design. That of Martensen is difficult to apply to modern designs since it is essentially an incompressible method. Stanitz's method is mathematically laborious since it involves the relaxation solution of a potential function along the blade surface. With the widespread use of large scale computers, a number of finite difference and finite element solutions to the equations of motion, momentum and energy have been developed. Good examples are those used by McDonald (8) and Davis and Millar (9).

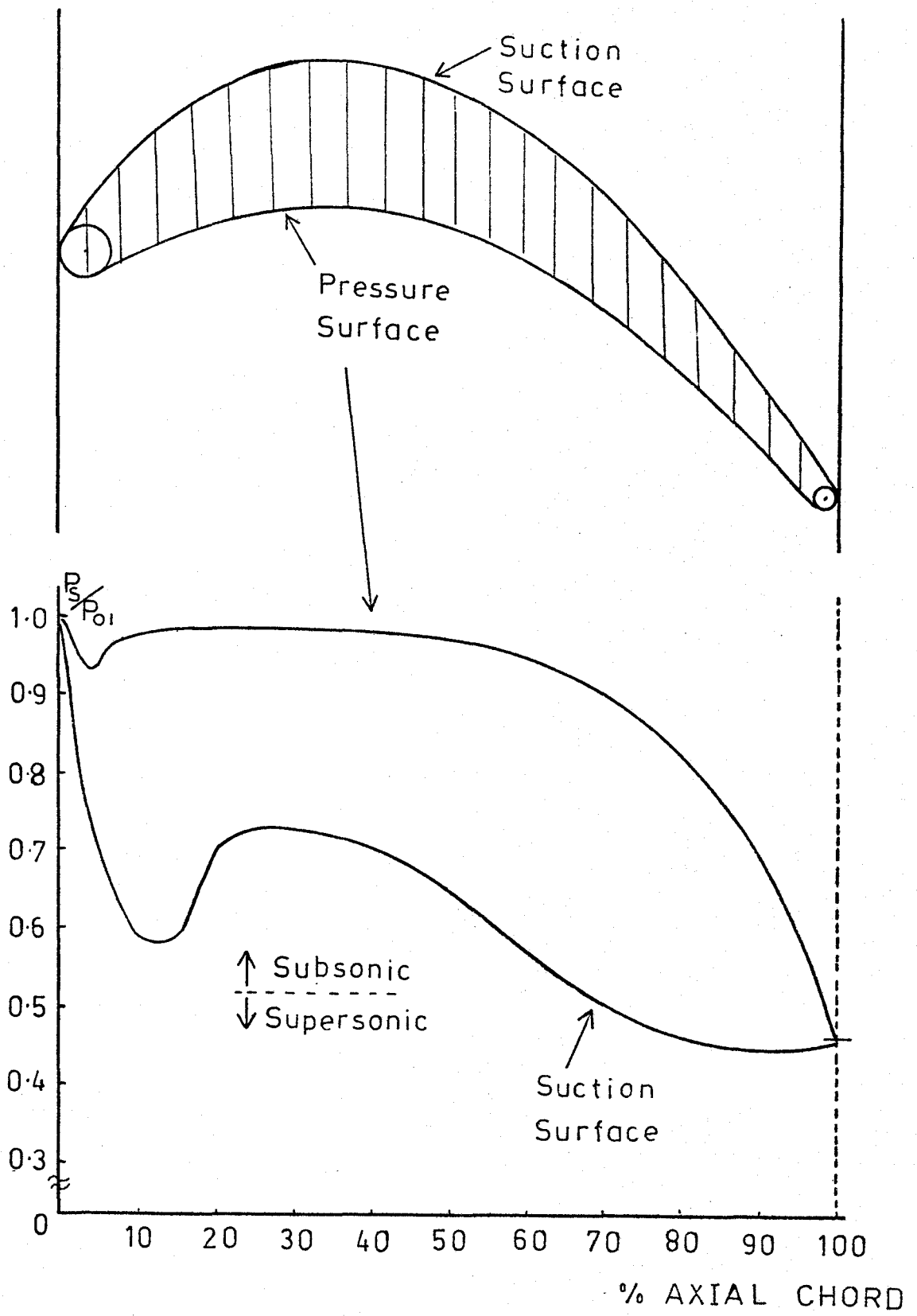

Figure 2 Typical Pressure Distribution Over a Turbine Blade

These methods in general have the advantage that the flow is described extremely accurately throughout the blade passage. However, to obtain this accuracy a large number of nodal points, or elements, of the order of 1000, is needed, thus increasing the difficulty and length of time needed for data preparation. A further disadvantage is the need for relatively large computer core size for storage of the arrays of elements in the calculation. In addition McDonald's solution requires a rough solution to the flow field as a starting point. The advantages of these methods include the ability to handle additional mass flows, such as cooling air, and heat transfer to and from the blade.

However there still exists a need for a direct and easy-to-use method of obtaining surface pressure and velocity distributions for such blade designs. In this chapter an extension of the streamline curvature method as described by Kumar (10), Malhotra (11) and Johnsen (5) is developed. The existing methods were subject to the following major criticisms:

(a) As turning angle increased the portion of the blade covered by the method decreased. (Region B Fig.3)

(b) As the blade nears choke the basic assumptions inherent in the method break down.

These problems are dealt with in section 2.3 and 2.4 of this chapter.

The present work takes as its starting point the blade design method described by Malhotra (11) as detailed in section 2.1.0.

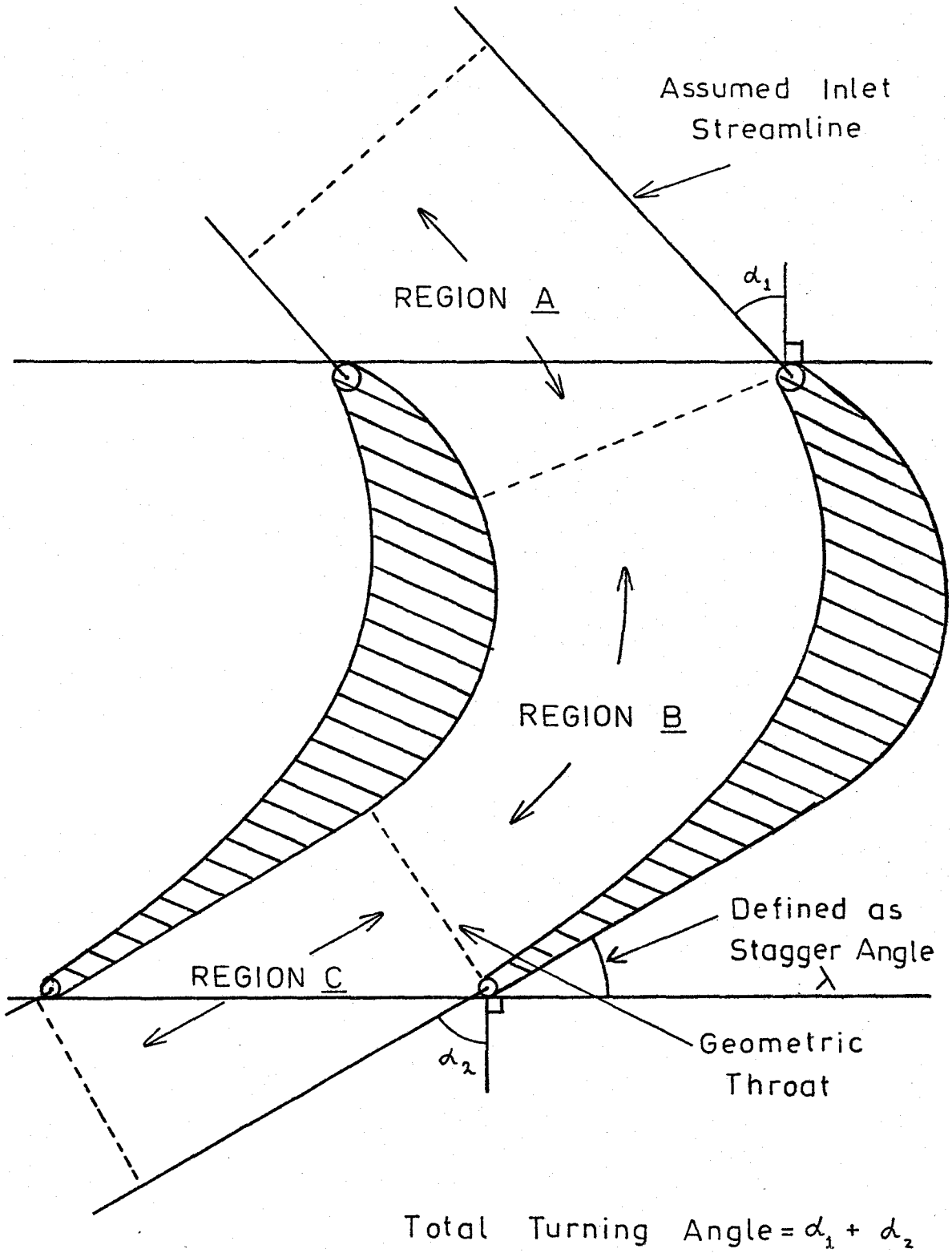

Figure 3 Region of Interest in the Blade Passage

The reasoning behind the derivation of the blade shape is explained and the calculation of the flow over the characteristic flat back of the blade by conventional methods is described in section 2.5.

2.1.0 Derivation of the Blade Shape

The chief requirement of the design process was to achieve a given total turning angle at different pressure ratios without unfavourable development of, or separation of the boundary layer. We have deliberately fixed the lift coefficient desired to say a value of 1.0 and thus for a given inlet and outlet angle, usually specified by considerations for the turbomachine as a whole, we have a fixed blade pitch or spacing as determined by the Zweifel criterion:

$$C_{Lz} = 2\frac{s}{b}[\cos^2 \alpha_2](\tan \alpha_1 - \tan\alpha_2) \qquad (1)$$

The problem thus reduces to specifying the variation of surface curvature, particularly on the suction surface, to eliminate wherever possible adverse pressure gradients. We are not absolutely tied to the Zweifel criterion for blade spacing but it is one design rule which has been tried and tested with success (1, 10, 11, 12). It is obvious from the pressure distribution diagram (Fig. 2) that velocities in the trailing edge region are high, reaching sonic speeds for reasonable blade pressure ratios of say greater than the choking pressure ratio of approximately 1.9:1. Thus very small changes in

surface curvature can give rise to rapid and large changes in surface pressure and velocity near the surface. These changes are not necessarily smooth and continuous as in wholly subsonic flow (8).

A good starting point for such a blade design is thus the "flat-back" type of blade in which the region of the blade suction surface downstream of the throat is flat, thus effectively eliminating adverse pressure gradients in a region where the boundary layer is thickest and most prone to separation. Thus the blade design can be carried out using the following steps:

(a) Given the outlet angle and a flat-back blade design the throat dimension is effectively fixed by the blade spacing. It is assumed that typical trailing edge radii are known from considerations of manufacturing and service life. (See Fig. 4)

(b) It is known from empirical data (10) that the nose radius* will effectively supply up to about 15^{o} of the total turning angle. Thus the remaining amount of turning is supplied by the region of the suction surface between the tangent to the nose radius and the throat. From simple geometrical considerations (Fig. 5) it can be seen that:

$$|\sin \beta_{s1}| + |\sin \beta_{s2}| = \left(\frac{x}{b}\right) / \left(\frac{R_s}{b}\right) = \left(\frac{x}{b}\right) \cdot \left(\frac{b}{R_s}\right) \qquad (2)$$

*When this radius is large enough for considerations of Life and Cooling

This equation can be represented in the form of a rectangle of area $|\sin \beta_{s1}| + |\sin \beta_{s2}|$ on a graph with coordinates $\frac{x}{b}$ and $\frac{b}{R_s}$ (Fig. 6). The area now represents the blade suction surface curvature.

(c) The essence of the blade design is in redistributing the area of the rectangle in the form of a histogram to obtain the desired suction pressure distribution. It should be noted that although the histogram is discontinuous the actual blade curvature when drawn is necessarily continuous.

(d) The pressure surface is drawn to provide a monatonically decreasing channel width in a manner similar to nozzle design.

(e) Using the method described in later portions of this chapter the histogram is manipulated if necessary to give a better pressure distribution.

Further details on this procedure are given in Refs. (10) and (11). Using the above method and the original version of the pressure distribution program a series of such blades was designed by Malhotra at McMaster University with lift coefficients varying from 0.8 to 1.2 and total turning angles from 115° to 140°.

One particular blade with a lift coefficient of 1.0 and a design total turning angle of 128° 30' was chosen for further analysis and development.

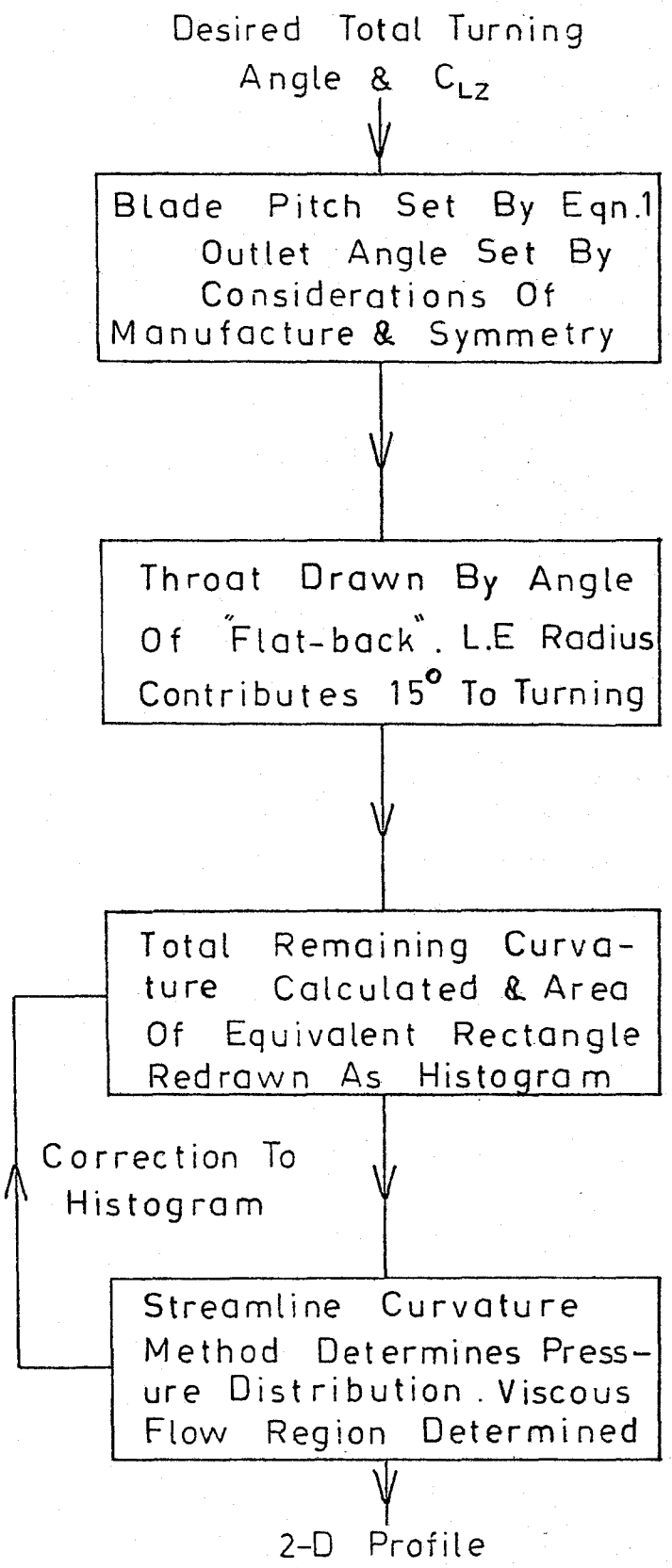

Figure 4 Illustration of Two-Dimensional Profile Design

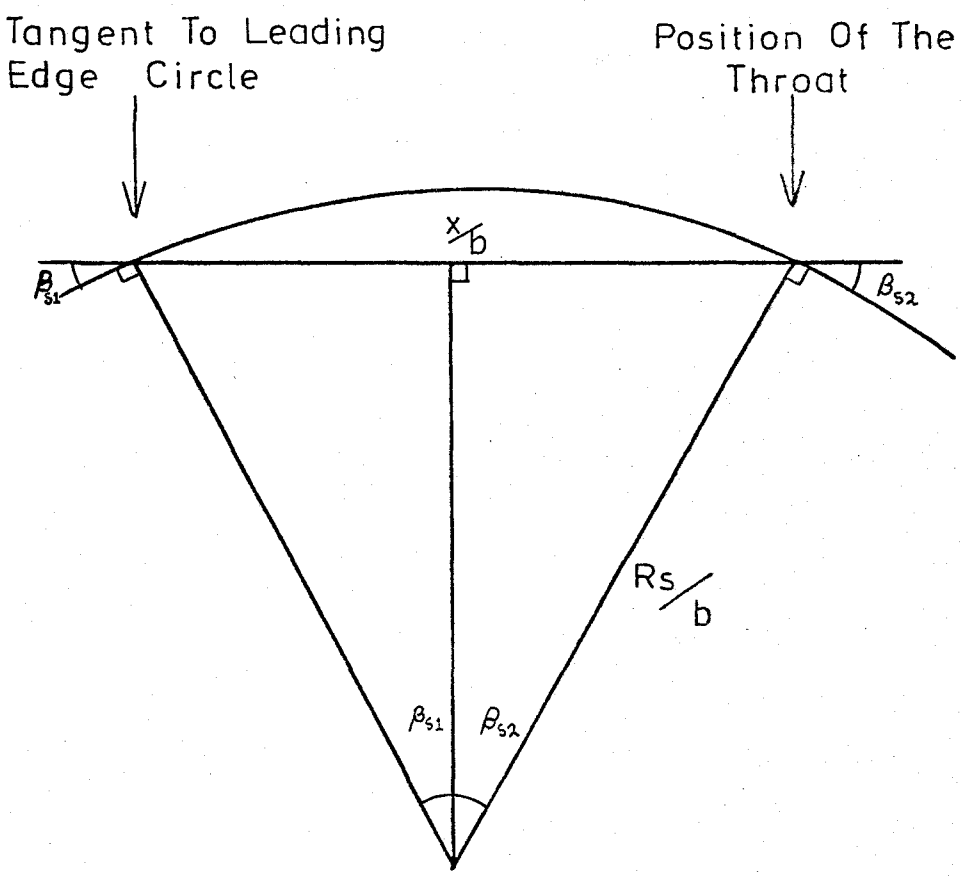

$$\left|\text{Sin } \beta_{s1}\right| + \left|\text{Sin } \beta_{s2}\right| = \frac{x/b}{Rs/b}$$

$$= \left(\frac{x}{b}\right) \cdot \left(\frac{b}{Rs}\right)$$

= Area Of Histogram

Figure 5 Geometry of Suction Surface Curvature

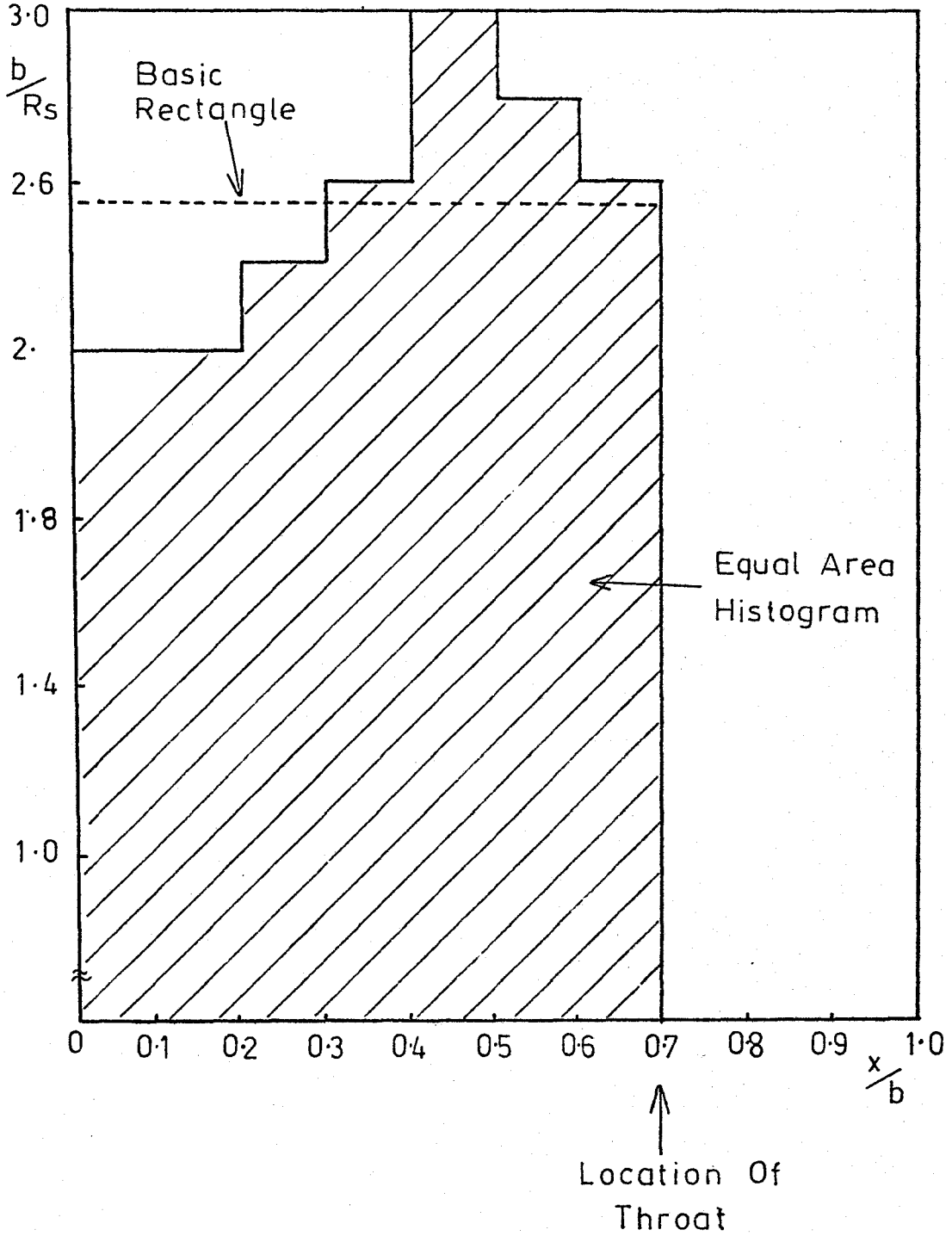

Figure 6 Redistribution of Total Suction Surface Curvature

2.2.0 Derivation of the Streamline Curvature Method

This follows exactly the derivation of Kumar (10) and Malhotra (11) and further detail can be obtained from these works.

2.2.1 The Streamline and Quasi-Orthogonal System

A system of quasi-orthogonal lines is drawn across the passage which, as accurately as can be determined by drafting methods, resemble equi-potential lines. These are then divided up at each station down the passage into an arbitrary number of equal width portions, thus the smoothly drawn curves between corresponding points down the passage define an elementary stream-tube system (see Fig. 7). No effort is made to generate exact locations of the stream-lines since this cannot be determined at this stage. Usually the pressure and velocities are needed at the blade surfaces, which are indeed true streamlines. The number of quasi-orthogonals used is left to the designer and one might choose to use more in some critical areas than others. The number of streamtubes is set to nine in this work as it has been found to give the maximum possible accuracy without unduly complicating computation.

2.2.2 Derivation of the Equations

The following are assumed in the derivation:

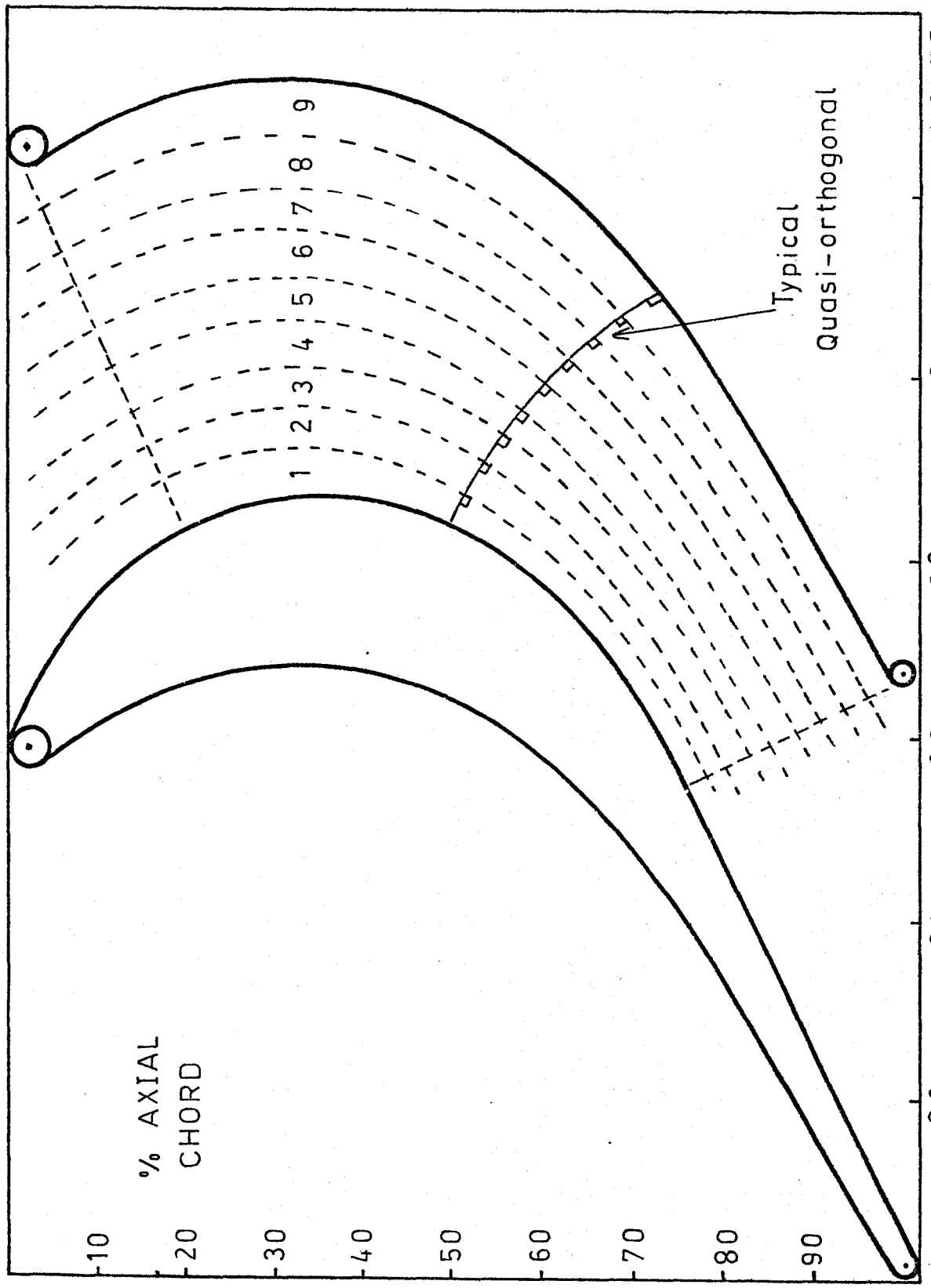

Figure 7 The Elementary Stream Tube System

(a) The fluid is considered inviscid but compressible.

(b) The flow is steady.

(c) The flow is two-dimensional.

(d) The flow is isentropic

(e) The mid-passage line is defined as a streamline.

The continuity equation for flow through any orthogonal can be written as:

$$\dot{m} = \int_{o}^{n_o} \zeta \, V \, d \, n \tag{3}$$

While the momentum equation assumes the form:

$$\zeta \, . \, V \, . \, V\frac{\partial \theta}{\partial s} = \frac{\partial p}{\partial n} = \frac{\zeta V^2}{R} \tag{4}$$

Since $\frac{\partial \theta}{\partial s}$ is by definition the curvature at a point on a streamline and curvature is the inverse of radius of curvature R_c.

The momentum equations along an orthogonal and a streamline become respectively:

$$-\frac{1}{\zeta}\frac{dp}{dn} = -\frac{V^2}{R} \tag{5}$$

and

$$-\frac{1}{\zeta}\frac{dp}{ds} = V\frac{dV}{ds} \tag{6}$$

Equation (6) can be rearranged to give:

$$\frac{dp}{\zeta} = -V \, d \, V \tag{7}$$

Substituting for $\frac{dp}{\rho}$ in (5) we obtain:

$$V \frac{dV}{dn} = - \frac{V^2}{R} \tag{8}$$

Which is rearranged to give:

$$\frac{dV}{V} = - \frac{dn}{R} \tag{9}$$

Using our definition of curvature

$$\frac{dV}{V} = - C \, d \, n \tag{10}$$

At this point in the derivation it is normal to assume some relationship for the variation of streamline curvature across the passage. The process will be illustrated by assuming that the curvature varies linearly across the passage, so that if "n" is the distance along an orthogonal measured from the suction surface

$$C = C_{s'} + (C_{p'} - C_{s'}) \frac{n}{n_o} \tag{11}$$

which can be differentiated to give:

$$d \, C = 0 \; + (C_{p'} - C_{s'}) \frac{dn}{n_o} \tag{12}$$

Substituting for "dn" in Equation (10) and integrating we obtain:

$$V = e^{-\frac{n_o}{2(C_{p'} - C_{s'})} \cdot C^2} \tag{13}$$

which defines the velocity at a point on a quasi-orthogonal as a function of curvature. This can be rearranged to give the velocity as a function of mid-channel velocity:

$$\frac{V}{V_{mid}} = e^{-\frac{n_o}{2(C_{p'} - C_{s'})} \{C^2 - \frac{(C_{p'} + C_{s'})^2}{4}\}} \tag{14}$$

Using the alternative simple assumption that radius of curvature varies linearly across the passage:

$$\frac{V}{V_{mid}} = \left(2 \left\{ \frac{C_{p'} + (C_{s'} - C_{p'}) \frac{n}{n_o}}{C_{p'} + C_{s'}} \right\} \right)^{\frac{n_o \cdot C_{p'} \cdot C_{s'}}{C_{p'} - C_{s'}}} \tag{15}$$

By simple algebraic manipulation it is possible to obtain similar expressions for velocity as a function of velocity on the pressure curve. (Assuming linear variation of curvature)

$$\frac{V}{V_{press}} = e^{\frac{n_o}{2} \left(C_{p'} + C_{s'} - 2C_{s'} \frac{n}{n_o} - (C_{p'} - C_{s'}) \frac{n^2}{n_o^2} \right)} \tag{16}$$

We now have the basis for a computation scheme since we can numerically integrate the mass flow across an orthogonal using an expression similar to Simpson's rule.

The mass flow per unit area in each stream-tube is derived from the velocities calculated from Eqns. 14 or 16 and known inlet conditions using the isentropic flow relations and the ideal gas law. Thus we can iterate using the mid-channel velocity as the variable until we converge to a total mass flow equal to that allowed by choking or to some other design inlet mass flow. In this work the assumption of linear variation of curvature was found to give the most consistently accurate results. A computer program based on this derivation is included as Appendix 2 to this thesis. A flow chart and Fortran IV listing are given together with sample results.

2.3.0. Extension of the Method to the Leading Edge

Previously this method has been used to calculate surface pressure distribution in Region B (Fig. 3) these calculations being described in Refs. (10) and (11). However, the leading edge portion of the blade on the suction side is vital to the following flow processes:

(a) High turning angle blades (greater than 100^{o} total turning) often exhibit supersonic flow patches near the leading edge which can terminate in shocks and cause considerable flow blockage and disturbance. This is especially true at positive angles of attack although the design point may be"safe".

(b) There is generally a region of rapidly accelerating flow followed by a region of marked deceleration.

This region has a great influence on boundary layer development. (Fig. 2) Incorrect design can cause separation or early transition of the boundary layer.

(c) The nature and extent of the secondary flow systems depend to a large extent on pressure gradients on the blade suction and pressure surfaces near the leading edge. (Region A)

Thus, having established a necessity for flow in this region to be described by the method it was necessary to develop an improvement compatible with the main body of the calculation. Similar to the suggestion by Kumar in Ref. (10) it was decided to adopt an arbitrary inlet streamline shape, to which the existing calculation along quasi-orthogonals could be applied. A good approximation to the flow, especially at high inlet Mach numbers (say 0.5 to 0.7) is to consider the inlet stagnation streamlines to be straight lines focussed on the centre of the leading edge circle. The angle with the cascade is the appropriate inlet air angle desired. (see Fig. 3)

If these inlet streamlines are drawn on the large scale drawing of the blades used to generate data for the existing program, then it is easy to draw the necessary remaining quasi-orthogonals near the leading edge.

This method can be successfully applied to the variation of pressure distribution with angle of attack. Inaccuracies due to uncertain placement of the quasi-orthogonals is minimized in plotting pressure distributions since it occupies a small proportion of axial chord.

2.4.0 Alternative Choke Calculations

Hitherto the program has generally caused problems at a choked throat because it depends upon iterating the mid-channel velocity to calculate mass flow. Unfortunately, a feature of a choked throat is that the sign of $d\varsigma/dA$ changes at this point, that is the mass flow per unit area is a maximum. The result is that the program diverges from a solution as it hunts for the correct mass flow using a simple algorithm. This can be avoided by assuming only small curvature at the throat which yields a small supersonic patch of flow near the suction surface. This is generally unsatisfactory since it leaves us with an unchoked region near the pressure surface, also most practical blades have considerable curvature in this region and the choke line is not necessarily the geometric throat, though close to it.

If we adhere to our simple flow tube description of the system we can show that flow will choke in the streamtube closest to the suction surface first, then progressively towards the pressure surface (see Fig. 8). In an effort to describe the flow in this region an additional calculation was used in the program so that if conditions at a geometric throat reached a critical Mach number, then the velocity distribution was calculated from the pressure surface towards the suction surface using Eqn. 16. To start the calculation it is assumed that the flow on the pressure surface is just choked. This assumption is justified for a convergent passage, however highly curved, since the pressure surface streamline reaches the critical pressure ratio at this point.

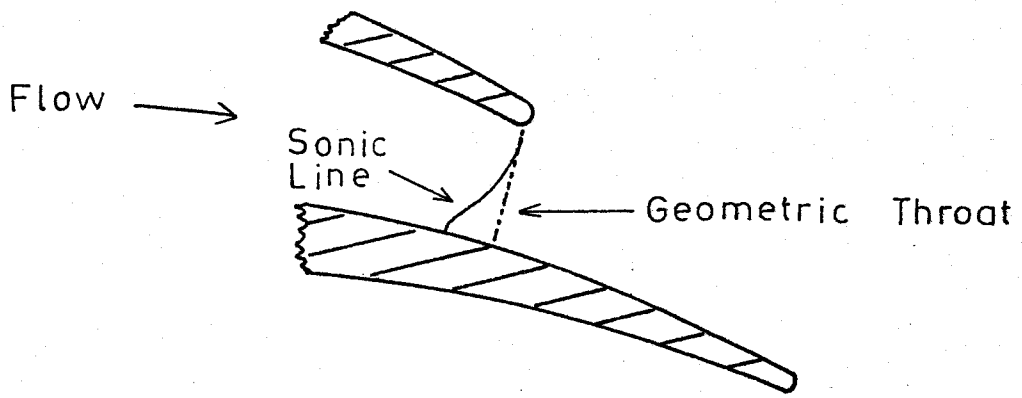

Figure 8a Illustration of the Sonic Line in Highly Curved Pasaage

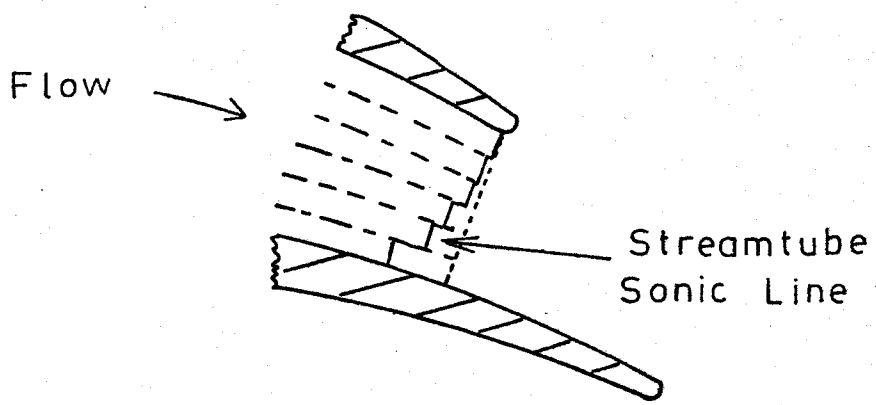

Figure 8b Illustration of the Streamtube Approximation to the Sonic Line

Downstream of the trailing edge the pressure is everywhere either at or below this critical pressure.

For a real viscous flow with finite trailing thickness to be taken into account, consequent boundary layer and wake effects will perhaps move the point of choking on the pressure surface, but only by a fraction of a percent of axial chord. This first order approximation to the flow is, however, accurate enough for generating potential flow solutions which can be used as free-stream data for boundary layer calculations.

The principal shortcomings of this calculation are that we retain the assumption of linear rate of change of curvature across the throat, and mass flow calculated is generally a little less than the design geometric throat value (see Examples in Section 2.6). The former assumption, however, still gives reasonable pressures at the suction surface, which correspond well with experimental data.

2.5.0 The Trailing Edge Region

This region (C) can represent a large proportion of the suction surface of some highly loaded blades. It is also a larger proportion of axial chord than the uncovered leading edge region (A). Knowledge of the pressure, velocity and temperature distribution is vital to the following:

(a) Blade loading

(b) Aerodynamic moments about the neutral axis

(c) Blade vibration and flutter (usually the thinnest section of the blade is involved)

(d) Boundary layer behaviour and wake thickness

(e) Cooling air exit pressure necessary for preliminary design.

For fully choked flat-back blades we can determine the position of the choke line and the fluid properties. For any back pressures lower than the critical we can assume an expansion system of waves similar to that described by Horlock (1). The thickness of the trailing edge is neglected and a Prandtl-Meyer expansion fan radiates from the centre of the trailing edge circle. A complementary shock wave exists as shown in Fig. 9. At a small distance downstream from the cascade the wave system cancels out leaving a net flow deviation and a reduced static pressure. (Fig. 10). The system can be drawn for 1^{o} or 2^{o} waves depending on the accuracy required. For pressure ratios greater than 4:1 the introduction of non-linearities and entropy changes would cause a more complicated wave pattern with perhaps gradients of temperature and pressure.

For this last case, and for blades in which there exists significant trailing edge curvature the method of characteristics is more suitable. (see Fig. 11) This method is also compatible with the existence of a considerable Mach number distribution across the throat.

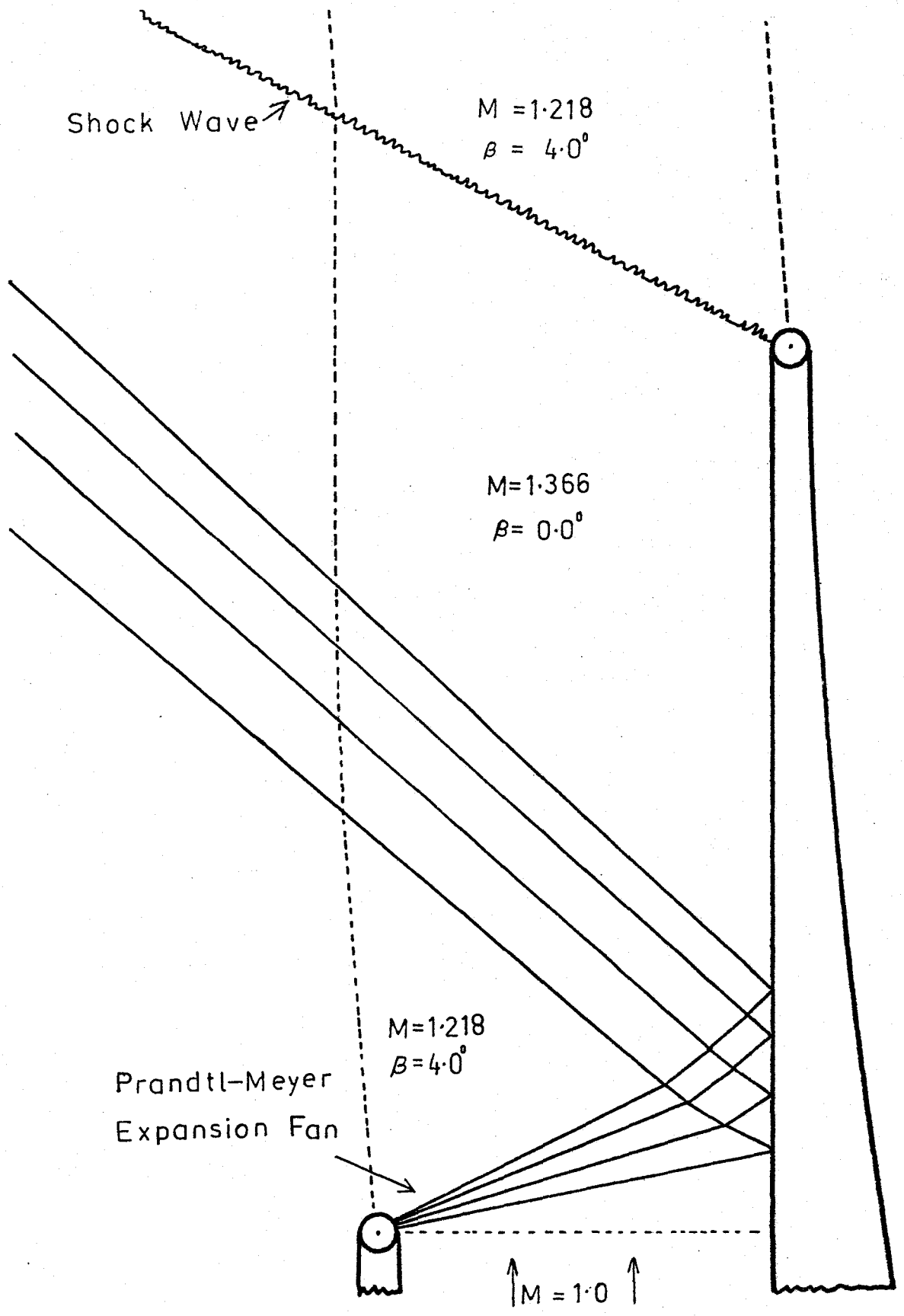

Figure 9 Expansion Wave System for Underexpanded Flow with a "Flat-back" Blade. P_{01}/P_a = 2·47

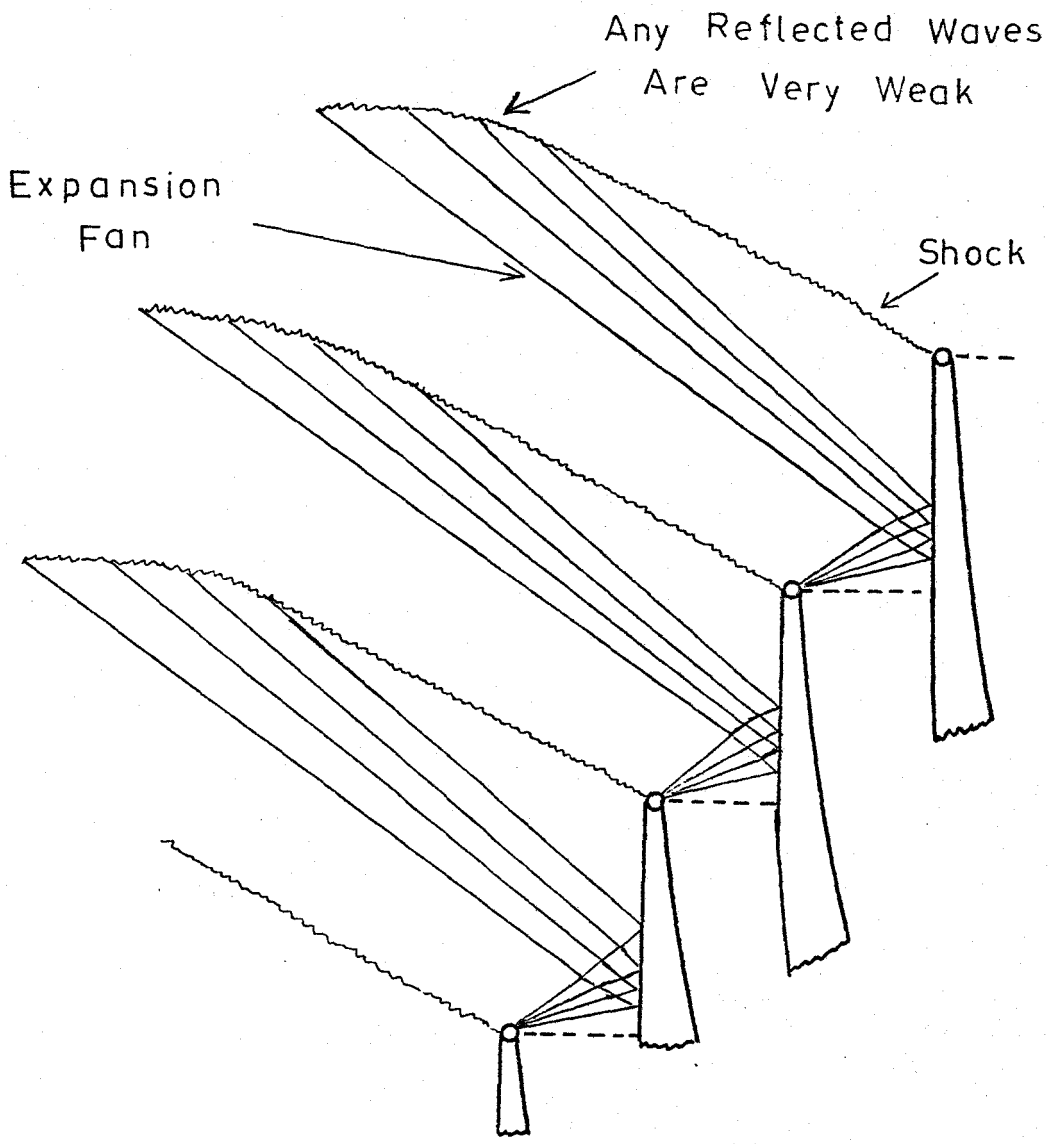

Figure 10 Cancellation of the Simple Wave System for the case shown in Fig. 9.

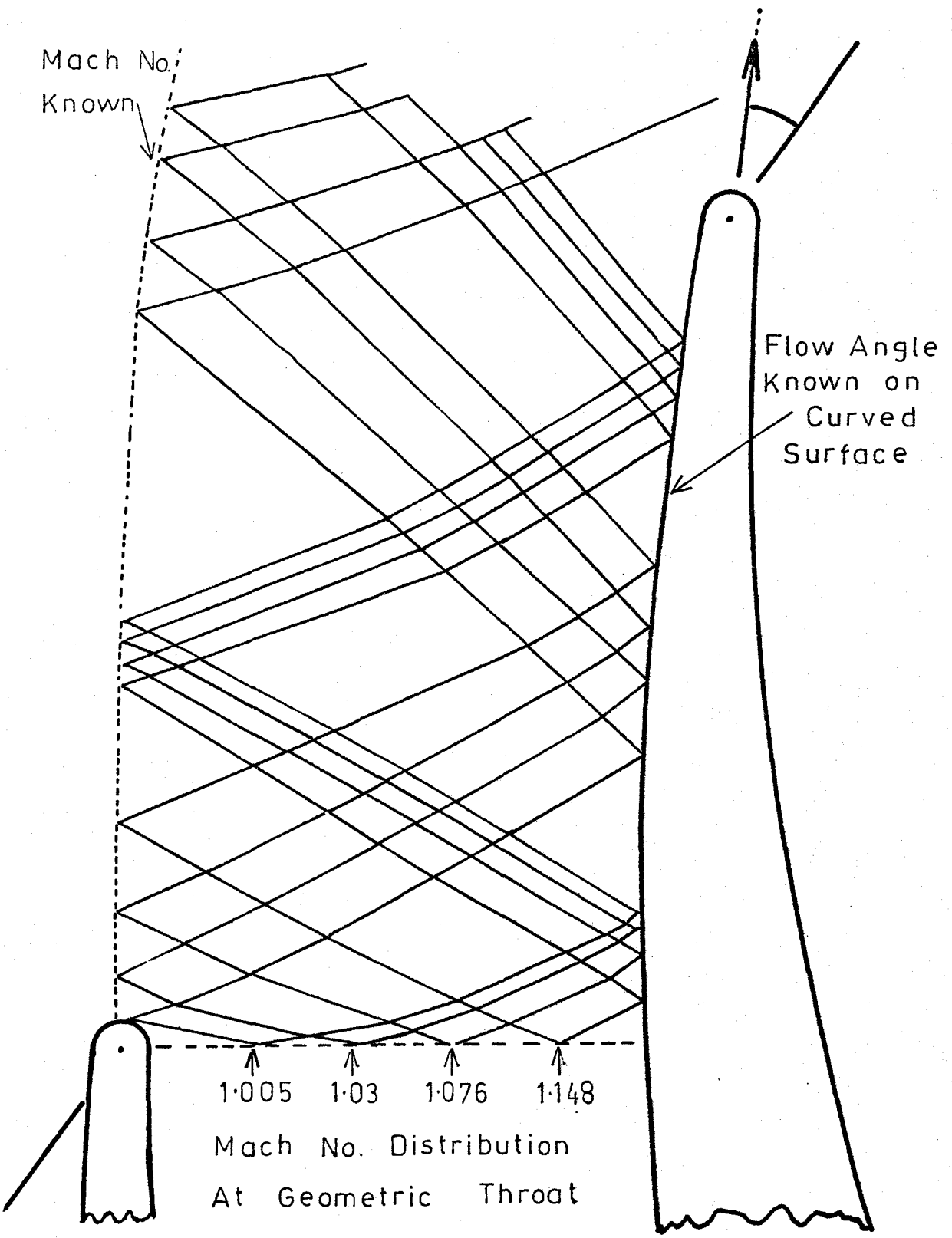

Figure 11 Method of Characteristics Applied to a Blade with considerable Curvature near the Trailing Edge.

2.6.0 Application of the Method

2.6.1. Design of a High-turning Angle Blade

Using the design procedure laid out by Kumar (10) and Malhotra (11), a high turning angle blade (one of a series) was designed at McMaster University. The original program was used by Malhotra to develop pressure distributions of the sort shown in Fig. 12. Leading particulars of the blade are summarized in Table 1. As can be seen from the graph a smooth variation of pressure from the forward limit of the calculation to the stagnation point was assumed consistent with overall blade loading determined by momentum calculations. Pressure in the flat-back region was assumed constant, which is adequate at the critical pressure ratio.

Using the improvements to the calculation specified above the pressure distribution was re-calculated and is shown in Figs 13 and 14. The curves now show all the features of this class of turbine blades. Especially near the leading edge the description of the flow is considerably different. The expected effects of angle of attack and leading edge blockage are shown. The pressure distribution for a pressure ratio greater than that for choking is shown in Fig. 15. This was calculated using the system of waves shown in Fig. 9.

2.6.2 Calculation of Flow for an Existing Blade

To test the applicability of the method the program was used

TABLE 1

LEADING PARTICULARS OF McMASTER BLADE

Total Turning Angle	$128^{\circ}30'$
Inlet Air Angle	64°
Outlet Air Angle (at Choke)	$64^{\circ}30'$
Lift Coefficient (Zweifel)	1.0
Pitch	0.650 inches
Axial Chord	1.00 inches
Uncovered Turning	0°
Geometric Throat	0.257 inches
Inlet Choking Mach No.	0.68

TABLE 2

LEADING PARTICULARS OF McDONALD BLADE

NOTE: Values marked thus * estimated

Total Turning Angle (Air)	116°
Total Turning Angle (Geometric)*	109°
Uncovered Turning*	8°
Inlet Air Angle	55°
Outlet Air Angle	61°
Geometric Throat*	0.308 inches
Axial Chord	1.00 inches
Outlet Mach No.	1·08
Pitch	0.675 inches
Zweifel Lift Coefficient	1.025
Inlet Choking Mach No.	0.61

to calculate the pressure distribution for one of the blades chosen by McDonald (8). This blade was chosen since the inlet Mach number and air angle and outlet Mach No. and air angle were all typical of highly loaded blades. Also drawings of the blade were included in the report (8), (although small in scale). In the paper, McDonald compares his calculations with experimental results. Leading particulars of the blade are included in Table 2.

The three sets of results are compared in Fig. 16. Application of the method of characteristics as shown in Fig. 11 was partially unsuccessful in that it was found to give incompatible results near the trailing edge. However, this method is extremely sensitive and very dependent on surface curvature distribution and errors can be cumulative. However, the surface pressure distribution is shown in this region as a dotted line for the sake of completing the diagram.

2.7.0 Discussion of the Theoretical Results

Comparing our results with those given by McDonald for the same blade:

(a) The general features of the flow are reproduced using our program except for the rapid rise of pressure just upstream of the trailing edge. This is a strong function of surface curvature and possible shock-wave/boundary layer interaction and better input data would improve our solution.

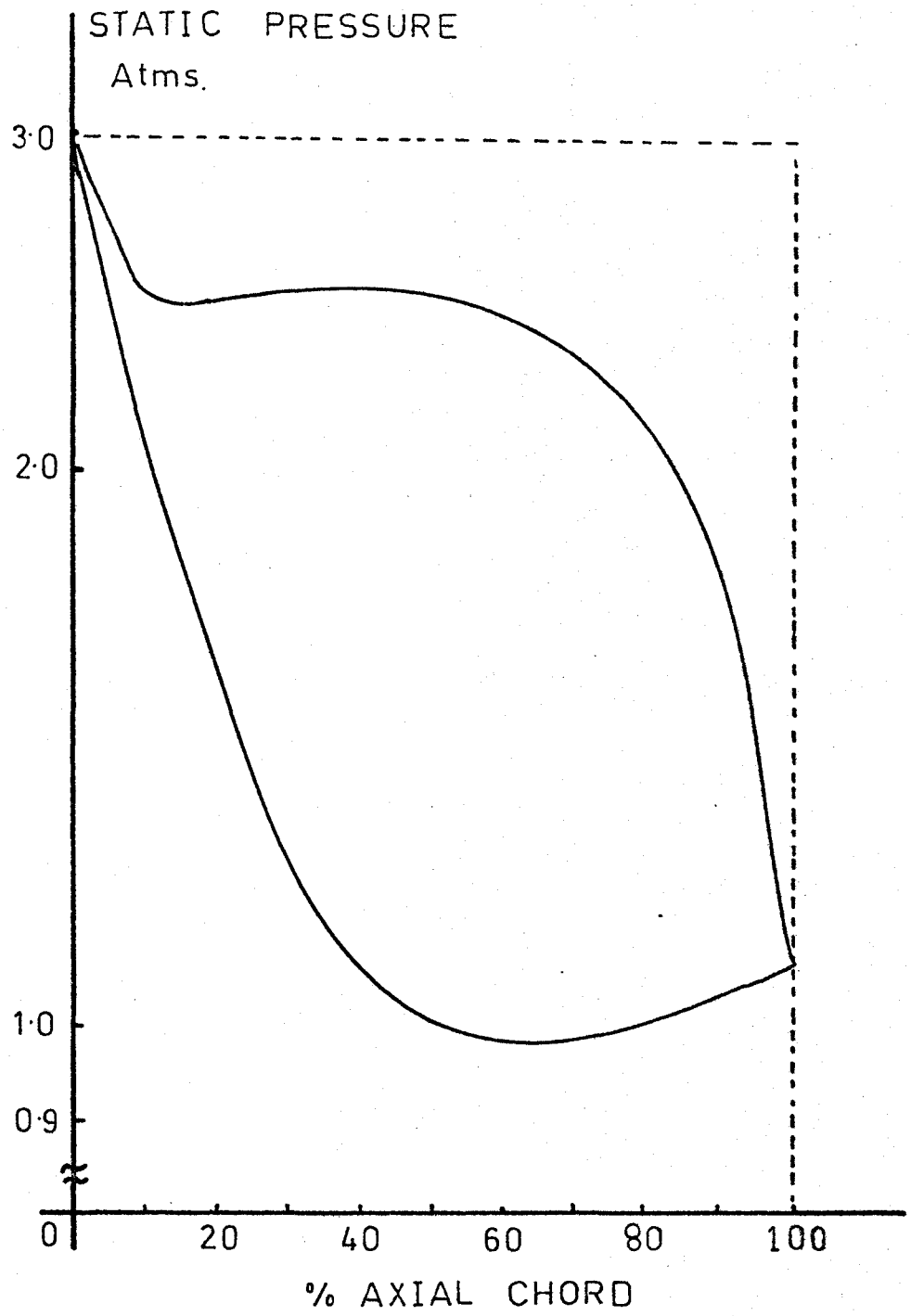

Figure 12 Pressure Distribution for the McMaster Blade.
Calculation by Malhotra

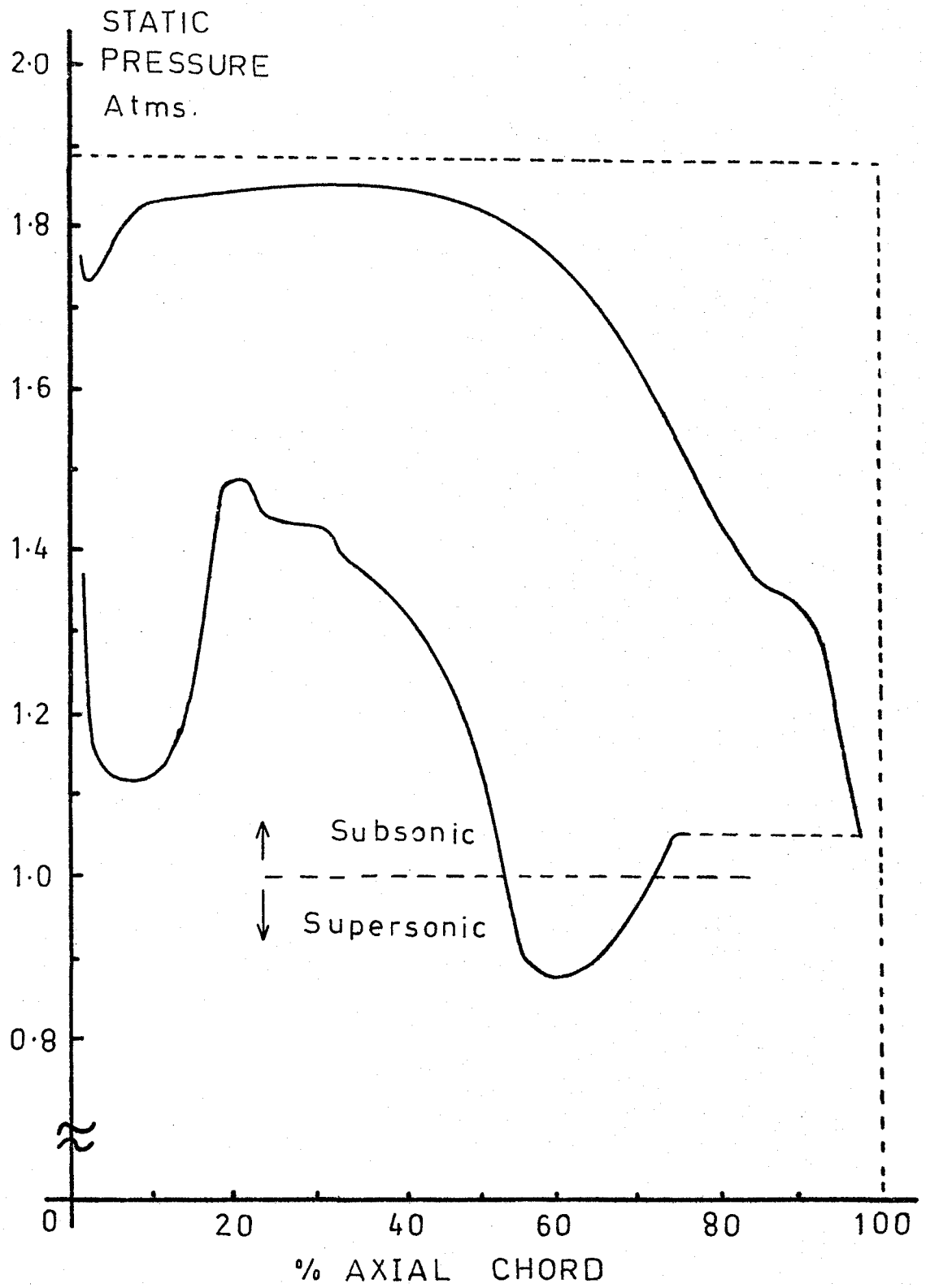

Figure 13 Calculation showing the Leading Edge Suction Peak using Improved Program (McMaster Blade)

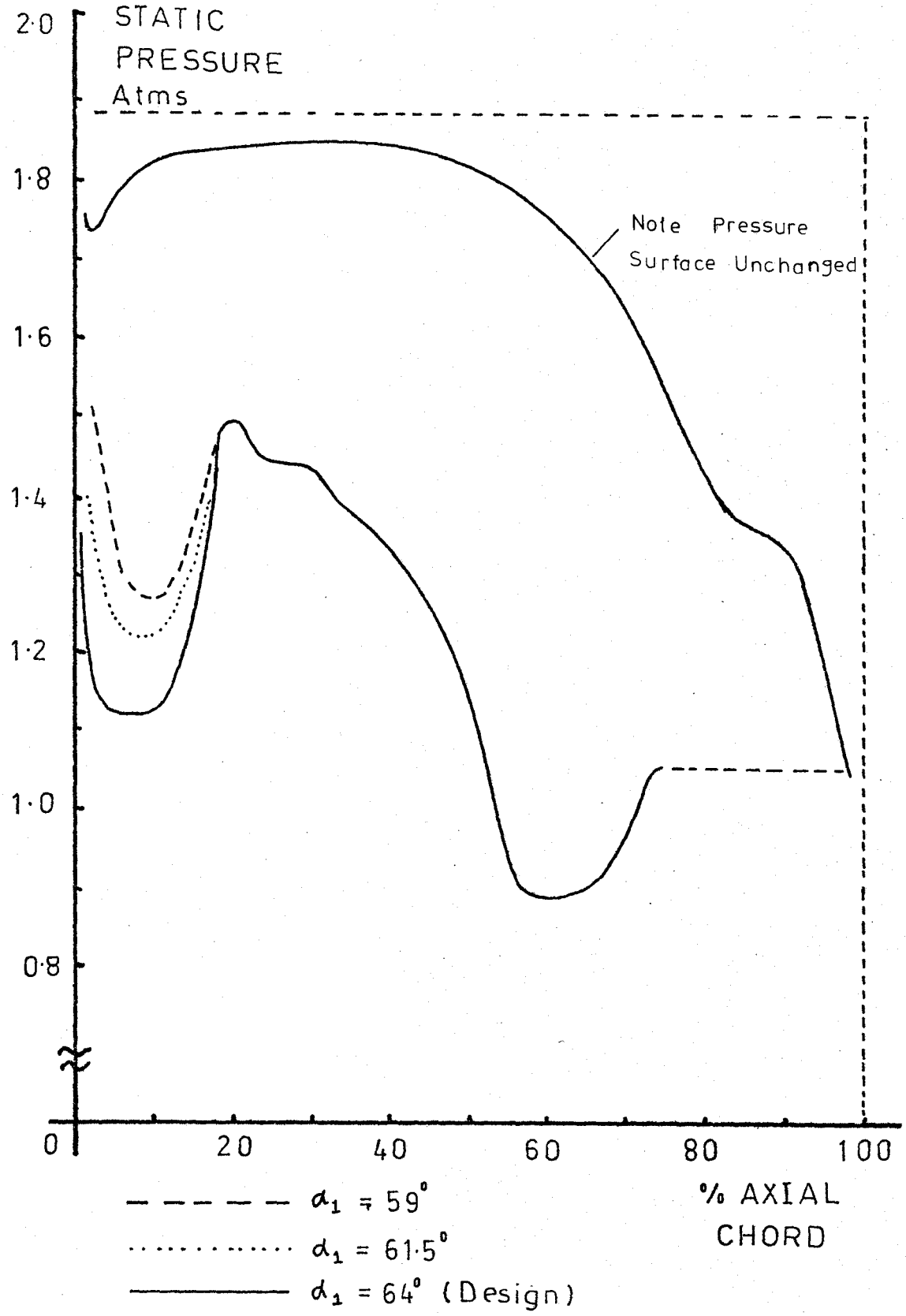

Figure 14 Theoretical Analysis of the Change in Pressure Distribution with Angle of Attack α_1 (McMaster Blade)

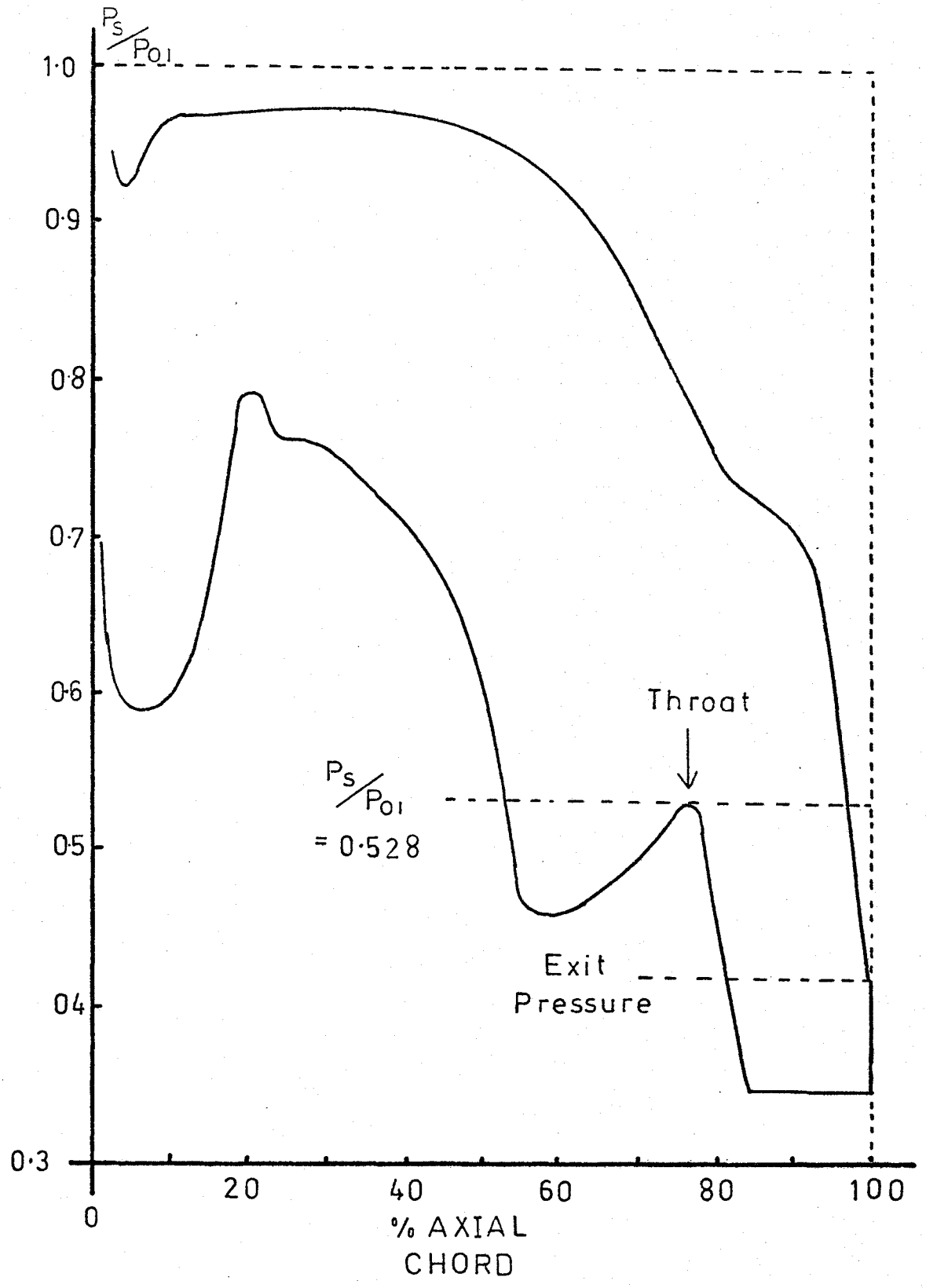

Figure 15 Theoretical Analysis of Trailing Edge Pressure Distribution using Wave System in Figure 9 (McMaster Blade).

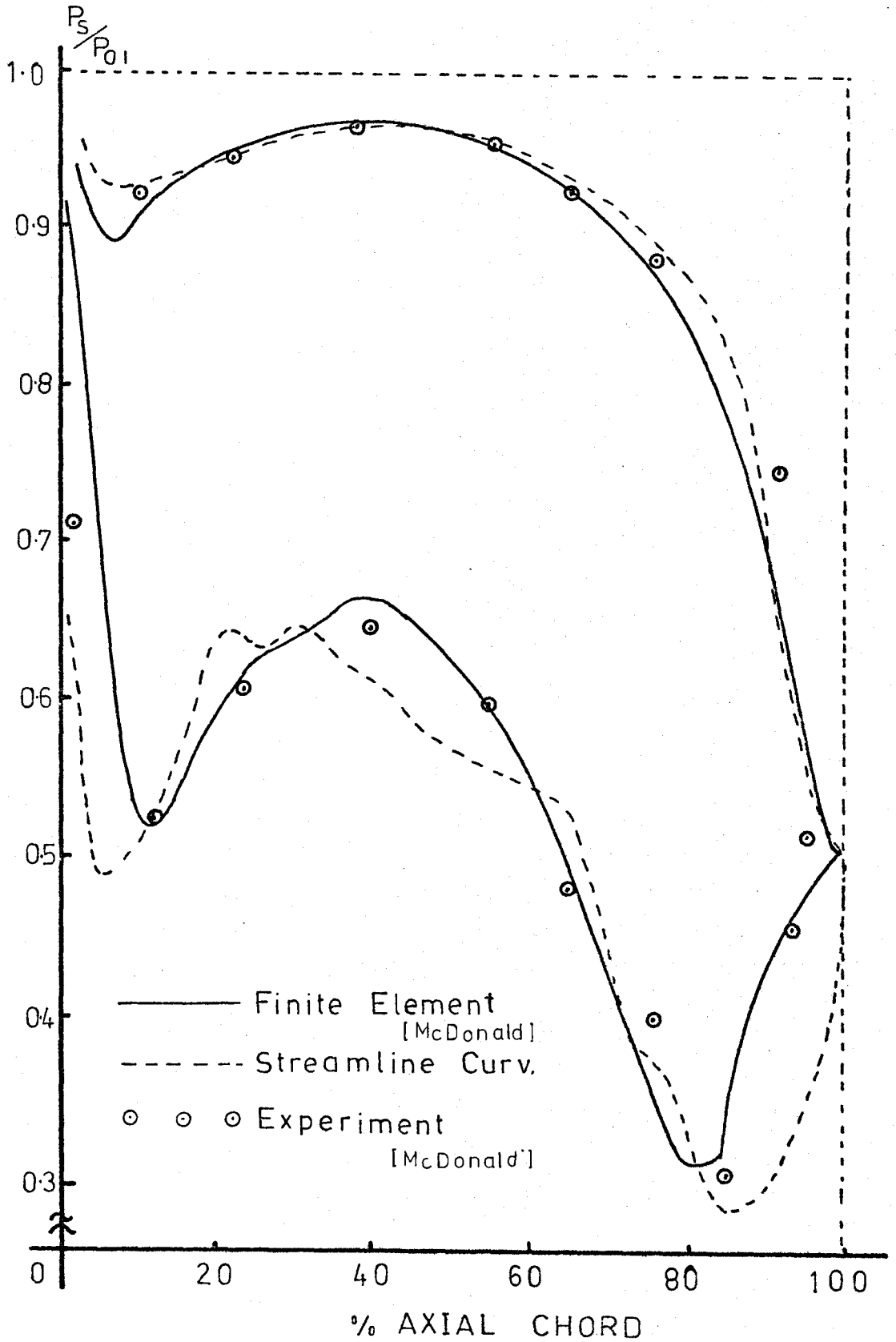

Figure 16 Comparison of Results for the Blade Described by McDonald including the Experimental Results

(b) The accuracy of the pressure distribution is satisfactory for design purposes, being closer to the experimental results than McDonald's results in some regions.

(c) The overall tangential force calculated by integrating the pressure differential between the suction and pressure surfaces agrees with the value calculated from momentum considerations within 6.0%(Table 3).

For the McMaster blade we can conclude the following from the theoretical study to this point.

(d) The general features of the distributions and changes with angle of attack are as expected awaiting experimental verification.

(e) For underexpanded flows, a favourable pressure gradient exists upstream of the trailing edge on the suction surface.

(f) The overall tangential force calculated from pressure distributions agrees well with momentum calculations (within 4%) (Table 3).

The above conclusions indicate that the extended computation method is good enough for design purposes. It is further felt that any increased sophistication of the method would not only be unnecessary but counter-productive since the essential simplicity of the method would be lost. The short running times of the computation (A few seconds on a C.D.C. 6400) and small demands on core size make the program ideal for an iterative design procedure whereby potential flow

solutions are used to generate viscous and secondary flow information until a suitable blade shape is arrived at.

TABLE 3 NET TANGENTIAL FORCE

METHOD A CALCULATION FROM FLUID MOMENTUM

METHOD B INTEGRATION OF STATIC PRESSURE

BLADE	METHOD	FORCE/UNIT HEIGHT lbs	% ERROR Relative To A
McMaster	A	8.14	------
	B	7.81	-4
McDonald	A	9.99	------
	B McDonald Results	8.55	-12
	B Expl. Results	8.92	-10.7
	B McMaster Results	9.40	-5.92

CHAPTER 3.0 ANALYSIS OF THE BOUNDARY LAYER FLOW OVER THE TURBINE BLADE SURFACE

The analysis of the viscous flow region near a turbine blade surface is complicated by a number of factors:

(a) A high degree of surface curvature

(b) A high degree of free stream turbulence, up to 5% being typical.

(c) Considerable forced convection heat transfer, usually from the air-stream to cooled blade.

(d) Significant variations in both surface pressure and velocity.

(e) The possibility of supersonic flow patches and change in flow direction may result in shock waves, causing discontinuous change of pressure.

(f) The possibility that the surface roughness, although small in absolute terms is significant when related to boundary layer thickness.

(g) The flow is compressible over a great portion of the blade passage.

In this work a computer program was developed with the aim of describing the flow in this region with engineering accuracy. The starting point in our analysis was an incompressible turbulent boundary layer program developed at Queens University by P.H.Oosthuizen (13).

In this program a simple empirical turbulence model due to Van Driest was used to describe the distribution of eddy diffusivity within the boundary layer. The method of formulation was the same as that used by R.H. Pletcher at an earlier date (14). The approach used by Oosthuizen was to non-dimensionalise the turbulent incompressible boundary layer equations, and to use an implicit finite difference computation to reduce these partial differential equations to a system of linear algebraic equations. The system of equations was then solved using the Thomas algorithm approach.

In the present program the compressible equations which take into account variable fluid properties were treated in the same manner. Using Morkovin's hypothesis as reported by H. McDonald and R.W. Fish (15) it was permissible to view the turbulence structure as independent of Mach number provided that the variable fluid properties were properly taken into account (15, 16). Thus the same turbulence model was used in the new compressible flow program. The modular nature of the program enabled the turbulence model, or any other part of the program, to be updated without interfering with the overall strategy leading to a solution.

No attempt has been made to include the effects of surface roughness, or the pressure gradients normal to the surface caused by surface curvature. Free stream turbulence was only included indirectly in that its influence on transition was calculated. Surface curvatures on a turbine blade are usually of an order such that the commonly used criterion of boundary layer thickness δ being less than $R_c/300$ is not met.

Bradshaw (17) has used an analogy with buoyancy to explain the de-stabilising effect of convex surface curvature on the boundary layer. On concave surfaces it is possible for Gortler vortices to form with their axes parallel to the flow direction (18). It is felt by the present author that with the primary objective of improving the passage analysis these effects are small when applied to displacement thickness, but that this is not necessarily true of more sensitive parameters such as heat transfer.

In the following sections of this chapter the compressible turbulent boundary layer equations are reduced to a non-dimensional form, and with the aid of an implicit finite difference scheme are further reduced to a system of linear algebraic equations.

3.1 The Compressible Turbulent Boundary Layer Equations

The compressible steady state boundary layer equations can be written in the following conventional form: (For example see references, 15, 19,20).

Continuity:-
$$\frac{\partial}{\partial x}(\bar{\zeta}\bar{u}) + \frac{\partial}{\partial y}(\bar{\zeta}\bar{v}) = 0 \qquad (17)$$

x-momentum:
$$\bar{\zeta}\bar{u}\frac{\partial \bar{u}}{\partial x} + \bar{\zeta}\bar{v}\frac{\partial \bar{u}}{\partial y} = -\frac{\partial \bar{p}}{\partial x} + \frac{\partial}{\partial y}(\bar{\mu}\frac{\partial \bar{u}}{\partial y}) + \frac{\partial T_T}{\partial y} \qquad (18)$$

y-momentum:
$$\frac{\partial \bar{p}}{\partial y} = 0 \qquad (19)$$

Energy:
$$\bar{\zeta}_u \frac{\partial(\bar{c}_p\bar{T})}{\partial x} + \bar{\zeta}_v \frac{\partial(\bar{c}_p\bar{T})}{\partial y} = \bar{u}\frac{\partial \bar{p}}{\partial x} + \frac{\partial}{\partial y}\left(\bar{k}\frac{\partial \bar{T}}{\partial y}\right) + \frac{\partial qt}{\partial y} + (\mu + A\tau)\left(\frac{\partial \bar{u}}{\partial y}\right)^2 \quad (20)$$

State:
$$\frac{\bar{\zeta}\,\bar{T}}{\bar{p}} = \text{constant} \quad (21)$$

The conventional boundary layer assumption is implicit in equation (19) and thus we can reduce $\frac{\partial \bar{p}}{\partial x}$ to $\frac{d\bar{p}}{dx}$. In the above equations the time averaged quantities are signified by a bar(-). The turbulent transport terms are also defined as:

$$q_t = \bar{\zeta}\,\bar{C}_p\,\varepsilon_H\,\frac{\partial \bar{T}}{\partial y} \quad (22)$$

also
$$T_t = \bar{\zeta}\,\varepsilon\,\frac{\partial \bar{u}}{\partial y} \quad (23)$$

and
$$A_\tau = \bar{\zeta}\,\varepsilon\,. \quad (24)$$

To further reduce the number of variables it is known that over the wide range of Mach numbers and Reynolds numbers of interest to turbine designers it is possible to write.

$$\frac{\varepsilon_H}{\varepsilon} = P_{RT} \simeq \text{CONSTANT} \quad (25)$$

The turbulent Prandtl number (P_{RT}) has thus an analogous role to that

of the molecular Prandtl number ($\frac{\mu C_p}{k}$). The constant value normally taken for air at the pressures and temperatures of interest is 0.9.

The equations shown above were non-dimensionalised using a system based on two primary reference values:

T_o: a reference temperature usually chosen to be close to the stagnation temperature

c_o: The speed of sound at the reference temperature

All reference fluid properties were derived at the reference temperature T_o thus the reference values are:-

$$\begin{aligned} U &= \bar{u}/c_o & V &= \bar{v}/c_o \\ P &= \bar{p}/\tfrac{1}{2}\zeta_o c_o^2 & \zeta^* &= \bar{\zeta}/\zeta_o \\ \mu^* &= \bar{\mu}/\mu_o & k^* &= \bar{k}/k_o \\ E &= \varepsilon/\nu_o & P_{RT} &= \varepsilon/\varepsilon_H \\ X &= x\, c_o/\nu_o & Y &= y\, c_o/\nu_o \end{aligned} \qquad (26)$$

We also define two non-dimensional temperatures θ_x and θ which vary parallel to, and normal to, the wall respectively:-

$$\theta_x = \frac{T_1}{T_w} \qquad \text{and} \qquad \theta = \frac{T_w - \bar{T}}{T_w - T_1} \qquad (27)$$

We note that in the computer program to follow, $T_w = T_o$ the reference temperature so that the numerical value of T_o was chosen to avoid computational difficulties when $(T_w - T_1)$ reached a value of zero in the computer.

Using these non-dimensionalising variables the boundary layer equations are reduced to the following non-dimensional form. (These are described in detail in Ref. 21).

$$\text{Continuity:} \quad \frac{\partial}{\partial X}(\zeta^* U) + \frac{\partial}{\partial Y}(\zeta^* V) = 0 \tag{28}$$

$$\text{Momentum (X):} \quad U\frac{\partial U}{\partial X} + V\frac{\partial U}{\partial Y} = -\frac{1}{2\zeta^*}\frac{\partial P}{\partial X} + \frac{1}{\zeta^*}\frac{\partial}{\partial Y}\left(\mu^*\frac{\partial U}{\partial Y}\right) + \frac{1}{\zeta^*}\frac{\partial}{\partial Y}\left(\zeta^* E\frac{\partial U}{\partial Y}\right) \tag{29}$$

$$\text{Momentum (Y):} \quad \frac{\partial P}{\partial Y} = 0$$

$$\text{Energy:} \quad U\frac{\partial \theta}{\partial X} + V\frac{\partial \theta}{\partial Y} = \frac{1}{\zeta^* P_{ro}}\frac{\partial}{\partial Y}\left(k^*\frac{\partial \theta}{\partial Y}\right) + \frac{1}{\zeta^*}\frac{\partial}{\partial Y}\left(\zeta^* P_{RT}\frac{E}{}\frac{\partial \theta}{\partial Y}\right) + \frac{1}{(\theta_x - 1)}\left\{\frac{C'U}{2\zeta^*}\frac{dP}{dX} + \frac{C'(\zeta^* E + \mu^*)}{\zeta^*}\left(\frac{\partial U}{\partial Y}\right)^2\right.$$

$$\left. - \frac{U.\theta}{(\theta_x - 1)}\frac{d\,\theta x}{dX}\right. \tag{30}$$

where C' is a convenient constant defined by:

$$C' = \frac{c_o^2}{C_p\, T_w} \tag{31}$$

The equation of state is effectively handled in the program by externally supplying data in which fluid properties, including density,

are tabulated as a function of temperature. This does not take compressibility into account because the data is tabulated at a reference pressure of one atmosphere. It is reasonable in the range of Mach numbers of interest to assume that μ, C_p and k only vary with temperature. (16, 19, 20) The problem of variable density is handled by extracting data by interpolation from the table supplied at the correct temperature, and then correcting for free stream static pressure since it is known that $\frac{\partial \bar{p}}{\partial y} = 0$

$$\text{Thus:} \qquad \zeta^* = \{\zeta^* (T)\} \times \frac{P_\infty}{P_{ref}}$$

$$\text{where} \qquad P_{ref} = 1 \text{ atmosphere} \tag{32}$$

It is quite possible to use polynomial expressions to calculate the variable fluid properties internally, a good example being that of Sutherland's Law for calculating viscosity as a function of absolute temperature. The existing method has the advantage of being easily changed to accommodate different gases or gas mixtures.

3.2 The Finite Difference Calculation Scheme

The set of four non-dimensional boundary layer equations (28 to 31) can be solved by employing a finite difference grid in the boundary layer, with a series of M-lines normal to the wall and a series of N-lines parallel to the wall as shown in Fig. 17. This grid

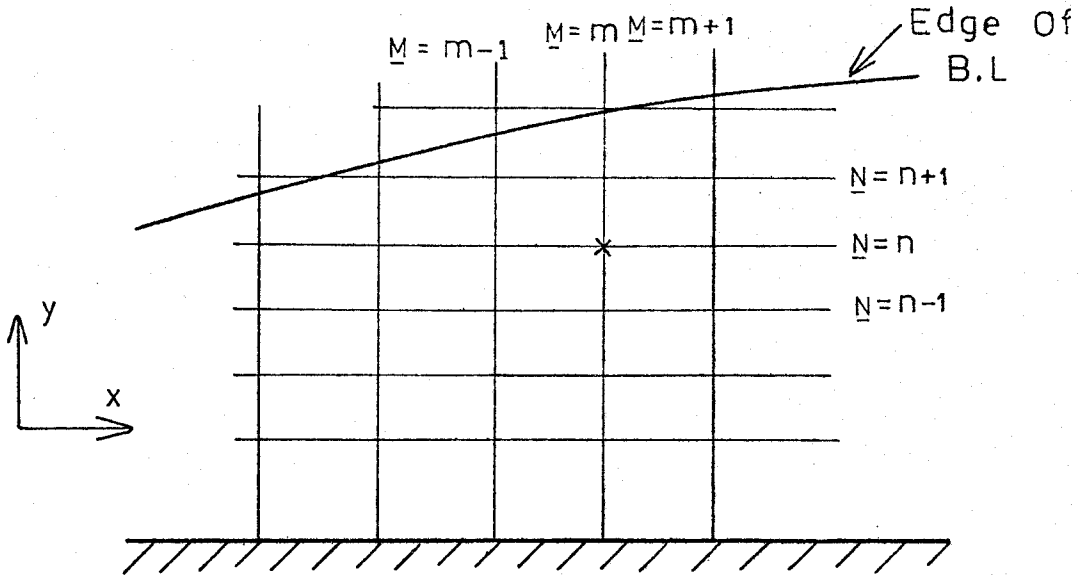

Figure 17 The Finite Difference Grid

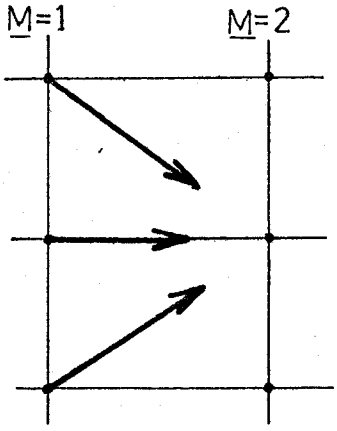

Figure 18 Illustration of an Explicit Calculation

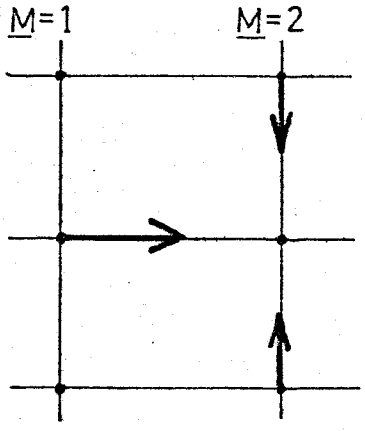

Figure 19 Illustration of an Implicit Calculation

is consistent with the normal boundary layer coordinate system that we have used in which x is measured parallel to the wall and y normal to it. We denote the values of the variables at a given nodal point using a simple subscripting system. e.g. $U_{2,4}$ refers to the X-direction dimensionless mean velocity at the intersection of the $\underline{M} = 2$ and $\underline{N} = 4$ lines.

In the boundary layer problem conditions at the nodal points along one $\underline{M}$-line will be known, and finite difference approximations to the governing equations can be used to determine conditions on the next $\underline{M}$-line downstream. For example if conditions are known on the $\underline{M} = 1$ line then the X-wise derivatives can be approximated by equations of the form (using the dimensionless variables).

$$\frac{\partial U}{\partial X} = \frac{U_{2,n} - U_{1,n}}{X_2 - X_1} \tag{33}$$

We note the different use of 'n', here it is a subscripting variable unlike the usage in Chapter 2.0.

The y-direction (or Y-direction) derivatives can be derived in two ways:-

(a) In the explicit solution process the y-derivatives are calculated using only data from the $\underline{M} = 1$ line as represented by Fig. 18. This has the disadvantage that the wall and free stream conditions on the $\underline{M} = 2$ line do not enter directly into the calculation, allowing the possibility of numerical instability. For example errors arising from the round-off errors in the finite difference approximation

can be amplified.

(b) Using the present implicit solution process y-derivatives are approximated from values on the $\underline{M}$ = 2 line, thus values of the variables at the grid points on the $\underline{M}$ = 2 line use information from both the $\underline{M}$ = 1 and the $\underline{M}$ = 2 lines. (see Fig. 19). This generally increases stability at the expense of slightly increased computer storage requirements.

As an example of the implicit derivative process we can write the formulation for $\frac{\partial^2 U}{\partial Y^2}$ in the following way:

$$\left.\frac{\partial^2 U}{\partial Y^2}\right|_n = \frac{\left[\frac{U_{2,n+1} - U_{2,n}}{Y_{n+1} - Y_n}\right] - \left[\frac{U_{2,n} - U_{2,n-1}}{Y_n - Y_{n-1}}\right]}{\left[\frac{Y_{n+1} - Y_n}{2}\right] - \left[\frac{Y_n - Y_{n-1}}{2}\right]} \tag{34}$$

If we carry out this process in detail for every term we obtain a set of linear algebraic equations of the form:

$$\text{X-momentum:} \qquad A_n U_{2,n} + B_n U_{2,n+1} + C_n U_{2,n-1} = D_n \tag{35}$$

where: A_n, B_n, C_n and D_n are functions of U, V and E on the $\underline{M}$ = 1 line. Similarly we can derive from the energy equation:

$$\text{Energy:} \qquad F_n \theta_{2,n} + G_n \theta_{2,n+1} + H_n \theta_{2,n-1} = I_n \tag{36}$$

again the coefficients F_n , G_n , H_n , and I_n are found from the solution for the $\underline{M} = 1$ line.

At this point the advantage of the implicit calculation scheme becomes more obvious. Equations (35) and (36) represent a set of linear algebraic equations and both $U_{2,1}$ (the velocity at the wall) and $U_{2,N'}$ (the velocity in free stream) are known. Similarly we know $\theta_{2,1}$ and $\theta_{2,N'}$. Thus we have two sets of equations with $N' - 2$ equations and $N' - 2$ unknowns. This system is solved in our case by the Thomas Algorithm method. We still need at this point to be able to describe the variation of eddy diffusivity (E) across the $\underline{M} = 1$ line.

3.3. The Calculation of the Eddy Diffusivity Term

In common with many other theoretical solutions to the turbulent boundary layer equations we have used Prandtl's mixing length concept whereby one can define an eddy diffusivity in terms of a mixing length in the form:

$$\varepsilon = l_m^2 \left| \frac{\partial u}{\partial y} \right| \tag{37}$$

From physical arguments (see Refs 14, 22) it is considered that the mixing length is independent of the velocity gradient, but dependent on local wall shear stress and distance from the wall in the form:

$$l_m/\delta = \text{Function } \{y/\mu \sqrt{\tau_w/\zeta}\ )\ \ (y/\delta\ )\} \tag{38}$$

We will also find it useful to define a dimensionless variable y^+ such that:

$$y^+ = y/\mu \sqrt{\tau_w/\zeta} \tag{39}$$

Thus our equation (38) can be recast in the form:

$$l_m/\delta = \text{Function } F(y^+)\ (y/\delta) \tag{40}$$

The function (F) in equation (40) is an empirical curve first described by Van Driest, and used by Pletcher (14) in the following numerical form:

$$\text{For } y/\delta < 0.1 \qquad L_m/\delta = 0.41\ (1 - e^{-y^+/26})(y/\delta)$$

$$0.1 < \frac{y}{\delta} < 0.6 \quad l_m/\delta = 0.41\ (1 - e^{-y^+/26})\ (y/\delta)$$

$$- 1.535\ (y/\delta - 0.1)^2 + 2.756\ (y/\delta - 0.1)^3$$

$$+ 1.884\ (y/\delta - 0.1)^4$$

$$\text{and } 0.6 < \frac{y}{\delta} < 1.0 \quad l_m/\delta = 0.089 \tag{41}$$

It can be seen that each component of Equation 41 describes the mixing length in a certain region of the boundary layer and that when they are plotted on a single graph as a function of y/δ the result is a continuous curve as shown in Figure 20.

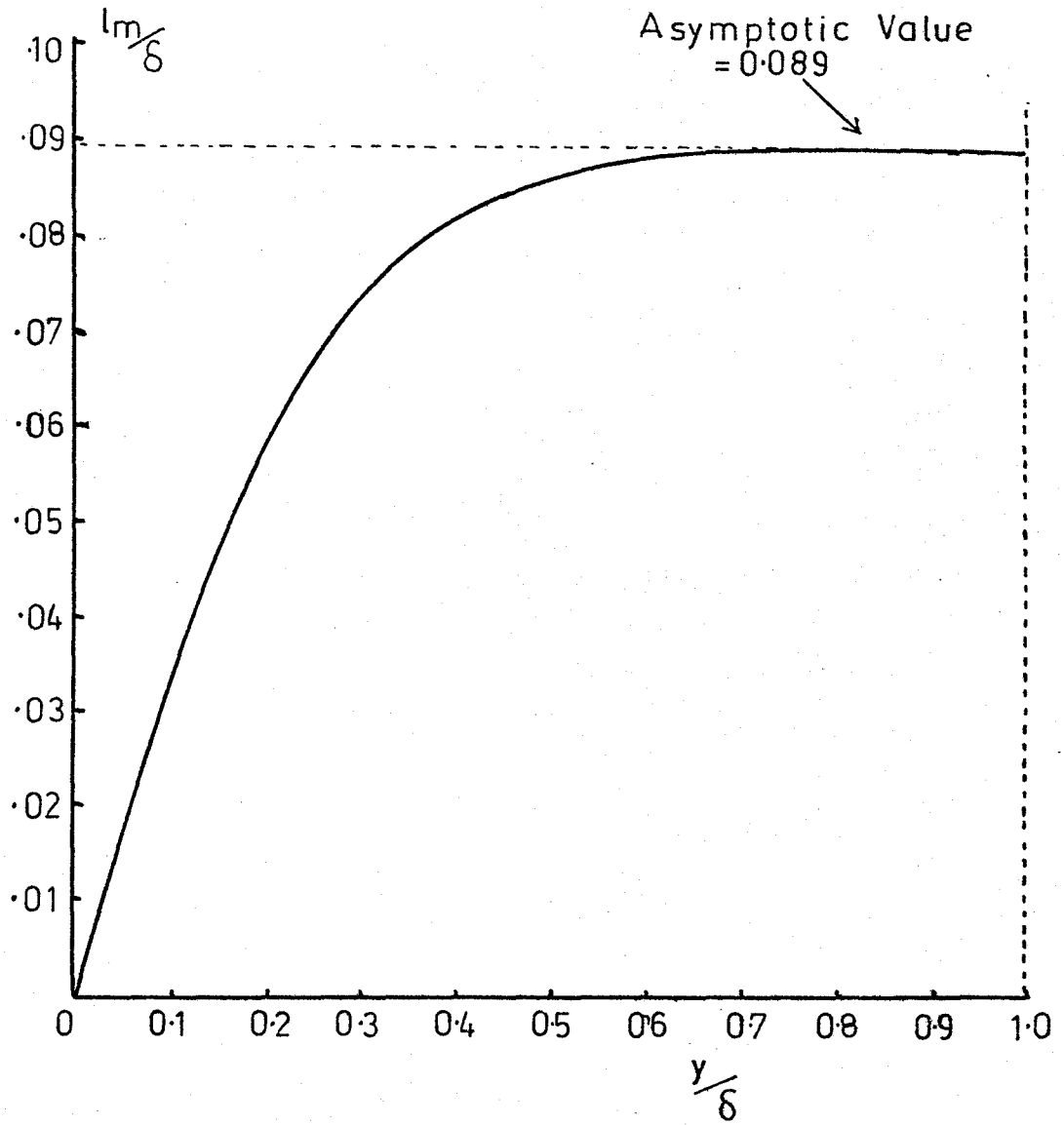

Figure 20 Variation of the Non-Dimensional Mixing Length l_m/δ with distance normal to the wall y/δ

In the region close to the wall we can neglect the turbulent and inertial terms in the x-momentum equation (Eqn. 18) and thus we can write:

$$\mu \frac{\partial^2 \bar{u}}{\partial y^2} = \frac{d\bar{P}}{dx} \tag{42}$$

Therefore integrating with respect to 'y' it can be shown that

$$\mu \frac{\partial \bar{u}}{\partial y} = \frac{d\bar{P}}{dx} .y + C' \tag{43}$$

but at the wall where y = 0 we have $T_w = \mu \frac{\partial \bar{u}}{\partial y} \Big|_{wall}$ by definition thus:

$$\mu \frac{\partial \bar{u}}{\partial y} = \frac{d\bar{p}}{dx} .y + T_w \tag{44}$$

Integrating further we obtain:

$$\mu.\bar{u} = \frac{d\bar{p}}{dx} \frac{y^2}{z} + T_w.y + C'' \tag{45}$$

Once again defining our boundary conditions at y = 0 we know that $\bar{u} = 0 \quad \therefore \quad C'' = 0.$

Hence $$T_w = \{\frac{\mu\bar{u}}{y} - \frac{dP}{dx} \frac{y}{2}\} \tag{46}$$

It should be noted that equation (4 6) can be calculated at each M-line and then substituted in equation (39) enabling the value of l_m/δ to be

computed at each point on the M-line.

3.4 Initial Conditions for the Computer Program

It is necessary to start the computation by specifying the velocity and temperature distribution on the first M-line in the calculation. This can be done in a number of ways:

(a) One can feed into the program either a known or assumed set of boundary layer parameters for that station, taking the form of either a simple theoretical model such as the power law velocity profile, or possibly experimental results.

(b) One may start the calculation using a suitable shape factor (H_{12}) and momentum thickness, which can be taken from the literature as long as they are physically realistic for the case to be computed.

(c) One may also start the calculation from a front stagnation point, with $\bar{U}$ and $\bar{T}$ away from the wall specified as U_∞ and T_∞, the free stream values.

Of these methods it has been found that method 'c' is unattractive in seeking a solution since very small x-steps and y-steps have to be chosen to achieve numerical stability. This necessarily increases the cost and computer running time needed for a given problem.

Method 'a' is to be preferred, based on our experience, because the calculation reaches stable values very quickly. Method 'b' which starts by approximating the flow by a simple shape factor and one

thickness parameter,and thereafter calculating the other boundary layer parameters within the program using approximations such as the power law boundary layer equation etc., works well if one is familiar with the particular sort of flow to be calculated. Experience gained in operation can eliminate the choice of unsuitable shape factors for example.

3.5 The Computer Program

As we have previously noted in the introduction to this chapter the program based on the foregoing calculation method is modular in nature. Virtually all the calculation steps, such as calculating the eddy diffusivity term are carried out in sub-routines. Also the function of preparing the data in a suitable form for the program, of non-dimensionalising the data, and printing out results are carried out in further sub-routines. The function of the main program is to provide control of the process and continuity between calculation steps. The sub-routines are described in detail together with a flow-chart and program listing in Appendix 3.

The program starts by reading in all input data and preparing it in a suitable form. Depending on the value assigned to certain control cards (see Appendix 3) the program can be set at this point to run in either the laminar ($l_m = 0$) or turbulent mode, with or without the energy equation. If necessary the energy equation can be replaced by the Crocco-Busemann relationship:

$$\bar{T} = T_w + (T_{aw} - T_1) \frac{\bar{u}}{u_1} - \frac{r\bar{u}^2}{2 C_p} \qquad (47)$$

This effectively specifies the temperature field, once the velocity field is known assuming a value for the recovery factor (r). The value of 'r' is chosen as 0.89 for turbulent flows in the Mach number range 0.5 to 1.0 which is entirely suitable for turbine blade flow analysis (16,19).

Using the input conditions, the flow variables on the $\underline{M}$ = 1 line are calculated, and thus ζ^*, μ^*, C_p^*, k^* and E can be calculated. Normally it is assumed that the y-direction velocity V is zero on this $\underline{M}$ = 1 line. This assumption has proved satisfactory in service. Using the finite difference approximations velocity and temperature on the $\underline{M}$ = 2 line are calculated. The calculated values of temperature and velocity are used to improve our solution for the $\underline{M}$ = 2 line by updating the physical value of such variables as ζ^* and ε. It has been found that very few iterations, of the order of two or three, are necessary to achieve satisfactory accuracy. The flow variables so obtained can be used to determine such important boundary layer characteristics as momentum thickness, displacement thickness and shape factor.

If the flow has been started in the laminar mode a simple empirical criterion is used to determine the possibility of transition. This is in a form suggested by Dunham (23) for use in turbine blade calculations and it is written in the following way:

Transition occurs for $R_{\delta 2} < R_{crit}$

$$\text{where } R_{crit} = \{ 0.27 + 0.73e^{-0.8\bar{T}u} \} \{ 550 + 680(1+\bar{T}u-21\chi)^{-1} \} \qquad (48)$$

No attempt has been made to calculate an exact transition length since existing calculations are somewhat unreliable (23, 15). Thus it has been assumed that transition occurs over an arbitrary small number of x-steps. This has the dual advantage of providing both a realistic physical situation, since eddy diffusivity is allowed to increase linearly from zero in this number of x-steps, and it also allows the numerical calculation to proceed in a smooth continuous manner with no instabilities due to a sudden change at the values of various parameters in the finite difference equations. Whether transition is detected or not the results for the $\underline{M} = 2$ line are transferred to the $\underline{M} = 1$ line and a number of important parameters of interest to the designer are printed out, forexample the skin friction coefficient.

This computation process continues as described until it ends in one of two ways:-

(a) If the flow is well behaved it continues to the last x-step.

(b) If the pressure gradient is sufficiently adverse to cause separation, this is usually shown in the program by a tendency for velocity values in the x-direction in the lower part of the boundary layer to become negative and the skin friction drops sharply. These negative x-velocities cause some of the finite difference terms to become negative, which in some cases is computationally unacceptable. At this point the calculation is rejected by the machine.

3.6 Application of the Program to Two-Dimensional Turbine Blade Flow

The program has been tested on a number of flows of interest in the Mach number range 0.1 to 4.95 (see Ref. 21) with encouraging results. Of particular interest to the problem at hand were the experimental results for heat transfer and velocity distribution over a typical turbine blade reported by Dunham and Edwards (24). The particular case chosen for computation of a number described in Reference 24 had an outlet Mach number from the blade passage of 0.9 which suggests that compressibility effects are present in the results. In our numerical analysis a simple transition test was used (Eqn 48) and the temperature chosen to be approximately $10^{o}F$ above the free stream stagnation temperature. This value was chosen to approximate as closely as possible the described conditions of the test (24). As can be seen from Figure 21 the heat transfer coefficients calculated vary in a manner which echoes the experimental results closely, although the absolute values are in error. This discrepancy is probably due to the estimates made for input data to the program, since actual wall temperatures were not specified in the report.

The program has also been applied to the McMaster blade and the results are shown in Figure 22. Values for displacement thickness, momentum thickness, shape factor and skin friction coefficient are shown in Figures 23, 24, 25, 26. With the values of displacement thickness obtained it is possible to modify the existing blade shape by hypothetically adjusting the wall position, and thus computing a new potential flow solution. In the design of a new blade shape it

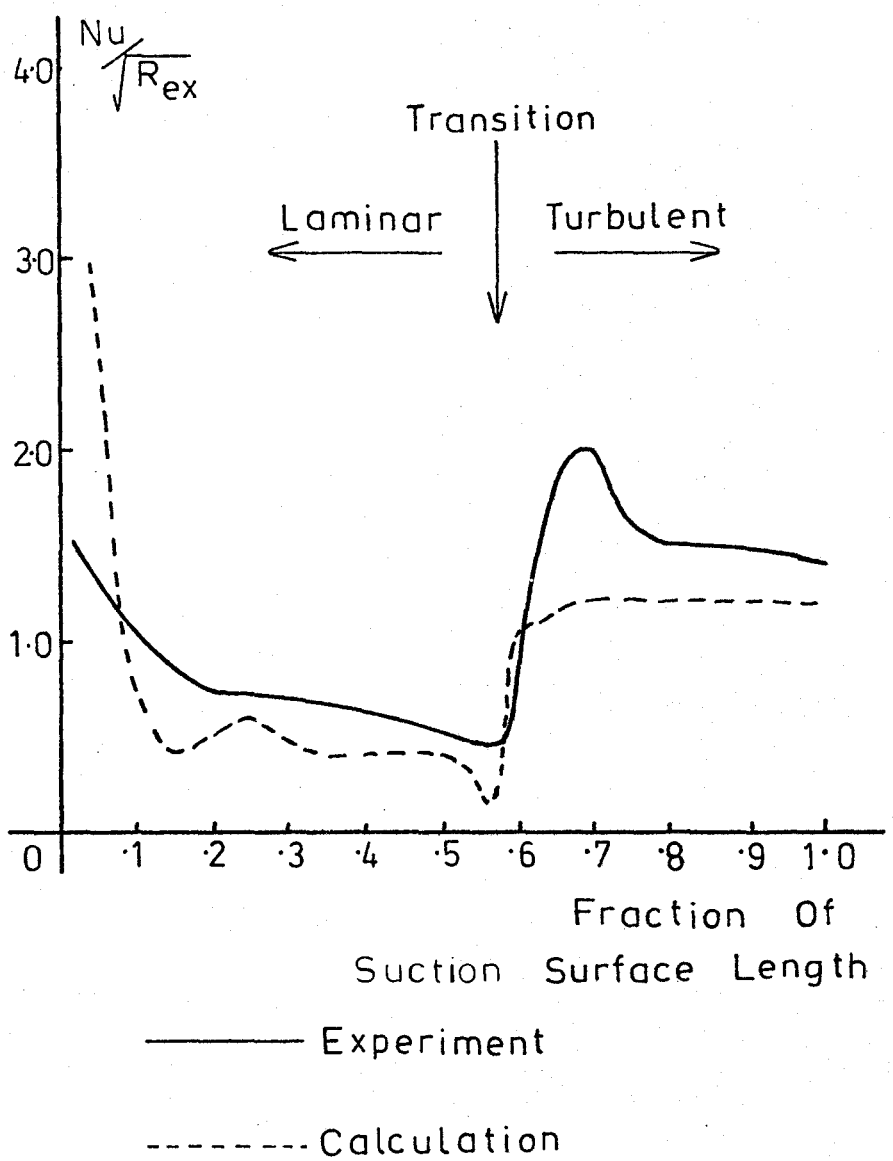

Figure 21 Comparison of Theoretical Results using McMaster Program with Heat Transfer Measurements for a Turbine Blade.

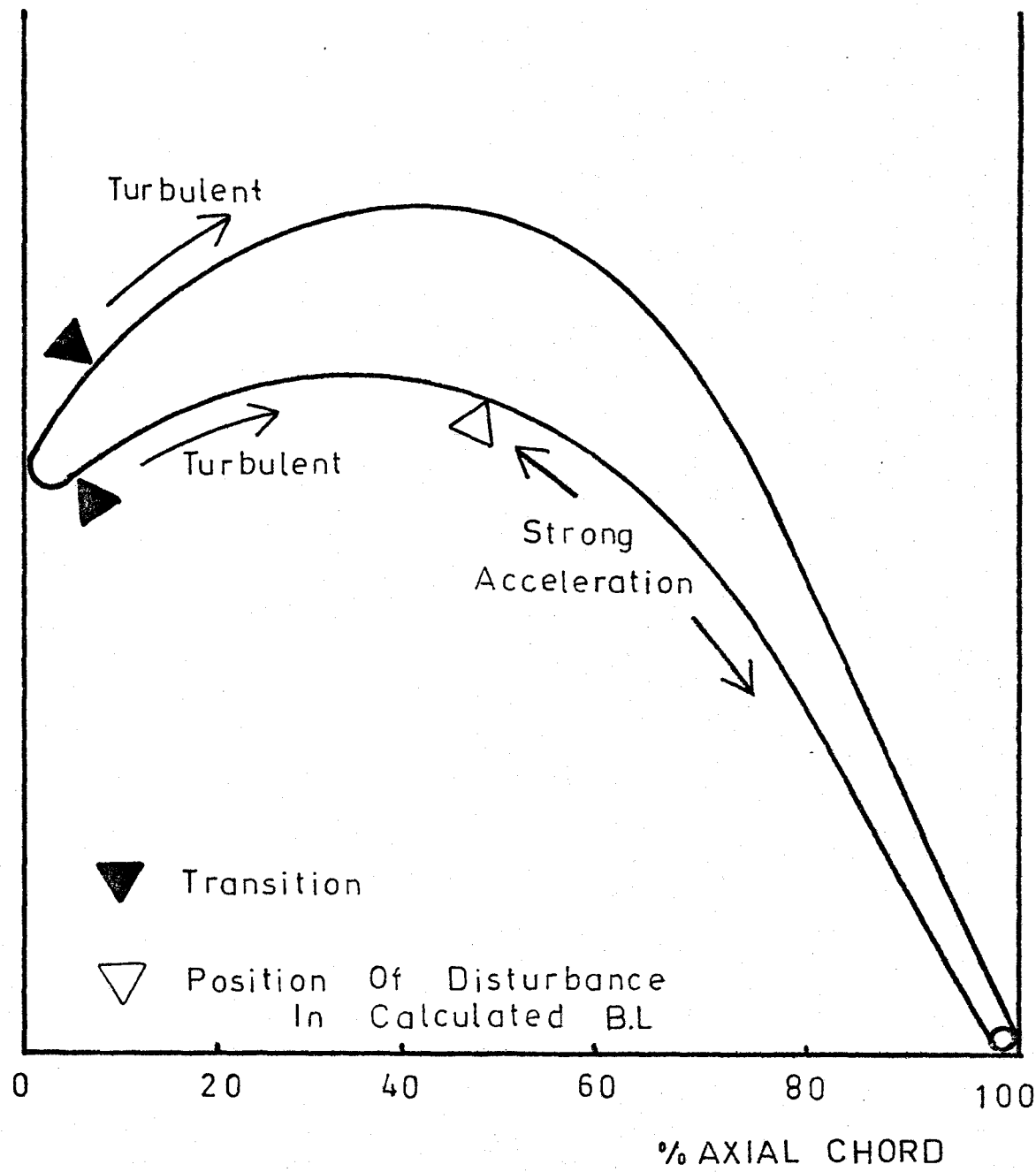

Figure 22 Calculated Points of Transition on the McMaster Blade

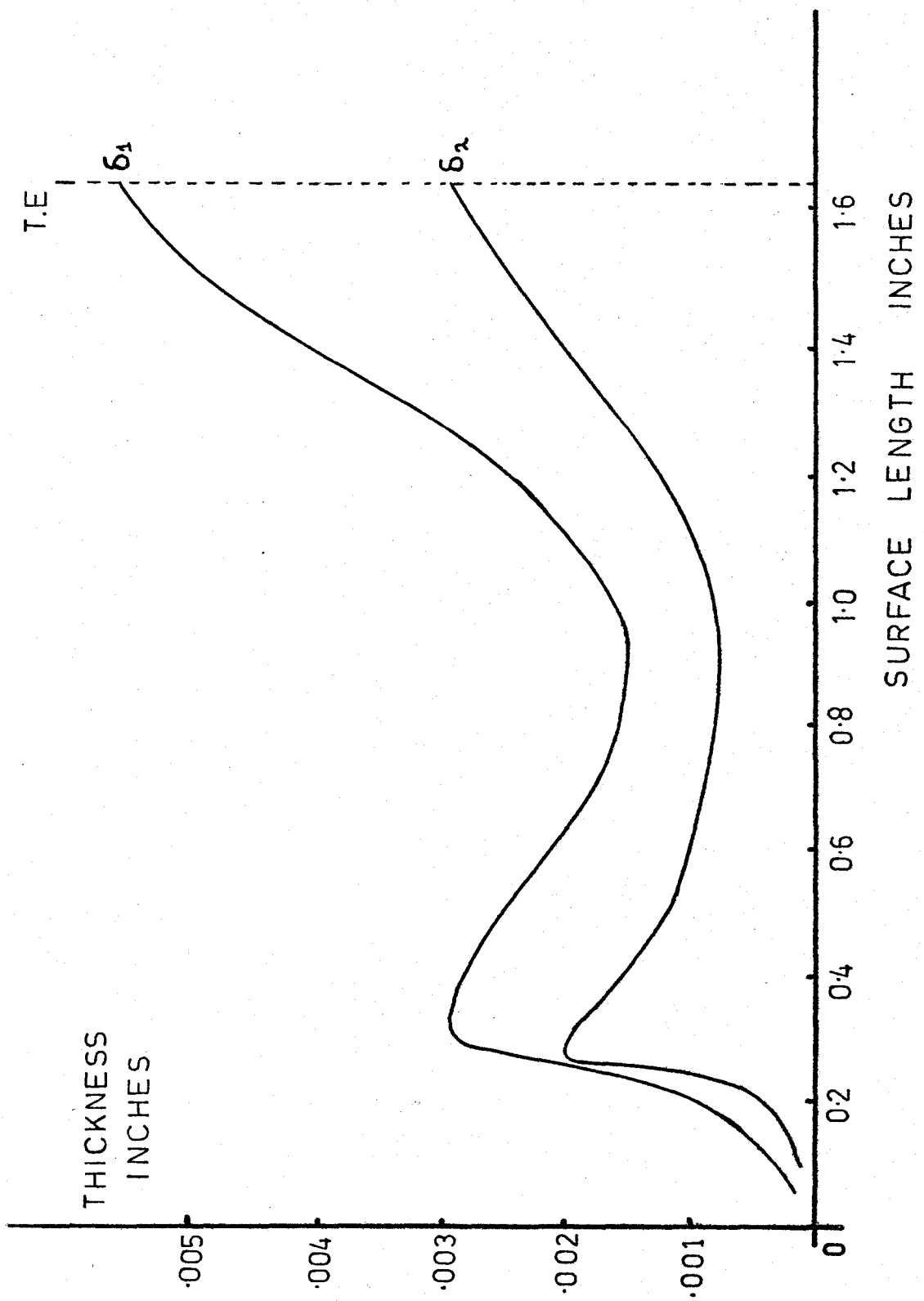

Figure 23 Calculated distribution of Displacement Thickness (δ_1) and Momentum Thickness (δ_2) for McMaster Blade (Suction Surface)

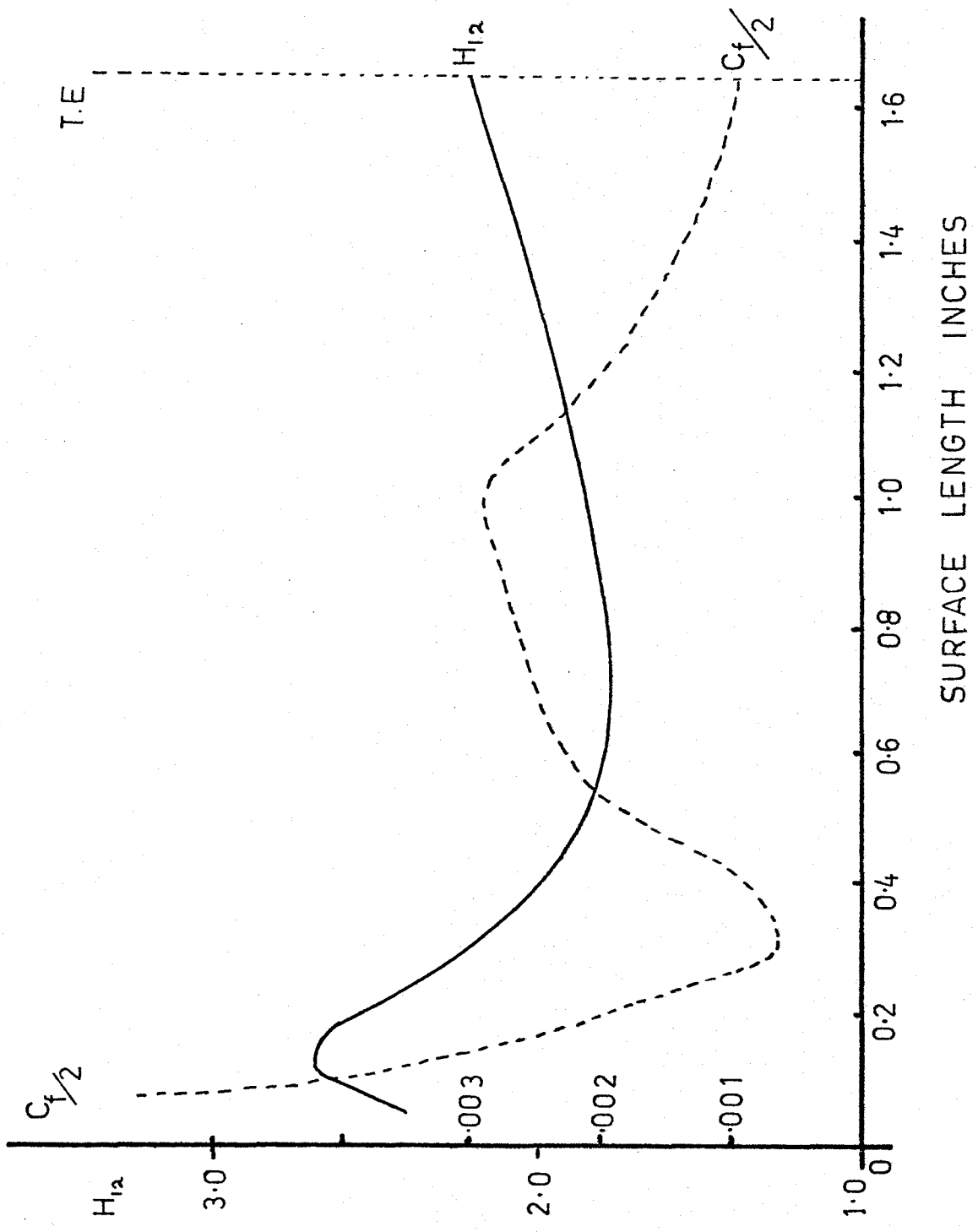

Figure 24 Calculated Distribution of Local Skin Friction Coefficient C_f and Shape Factor H_{12} for McMaster Blade (Suction Surface) $\frac{C_f}{2}$

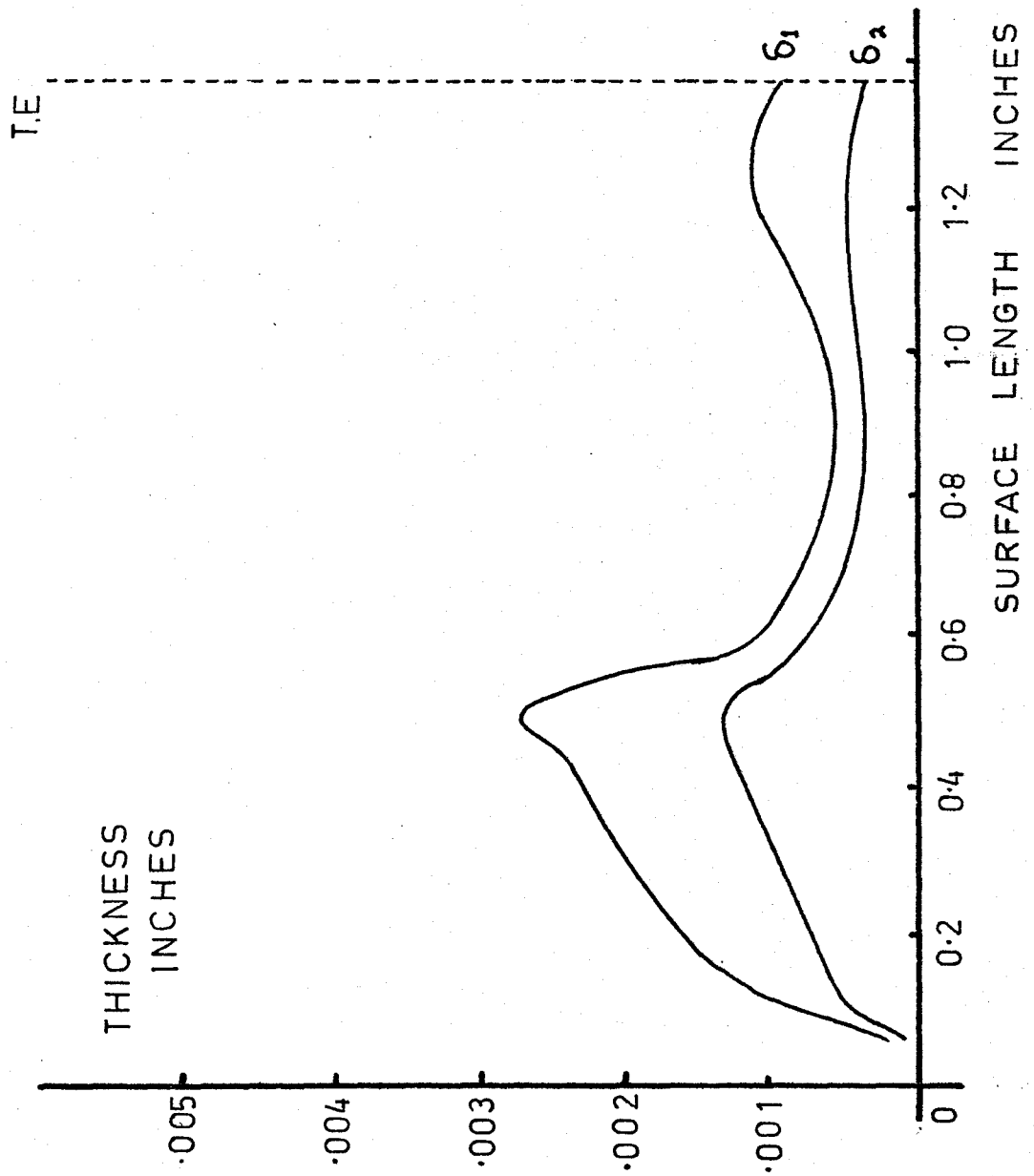

Figure 25 Calculated Distribution of Displacement thickness (δ_1) and Momentum Thickness (δ_2) for McMaster Blade(Pressure Surface)

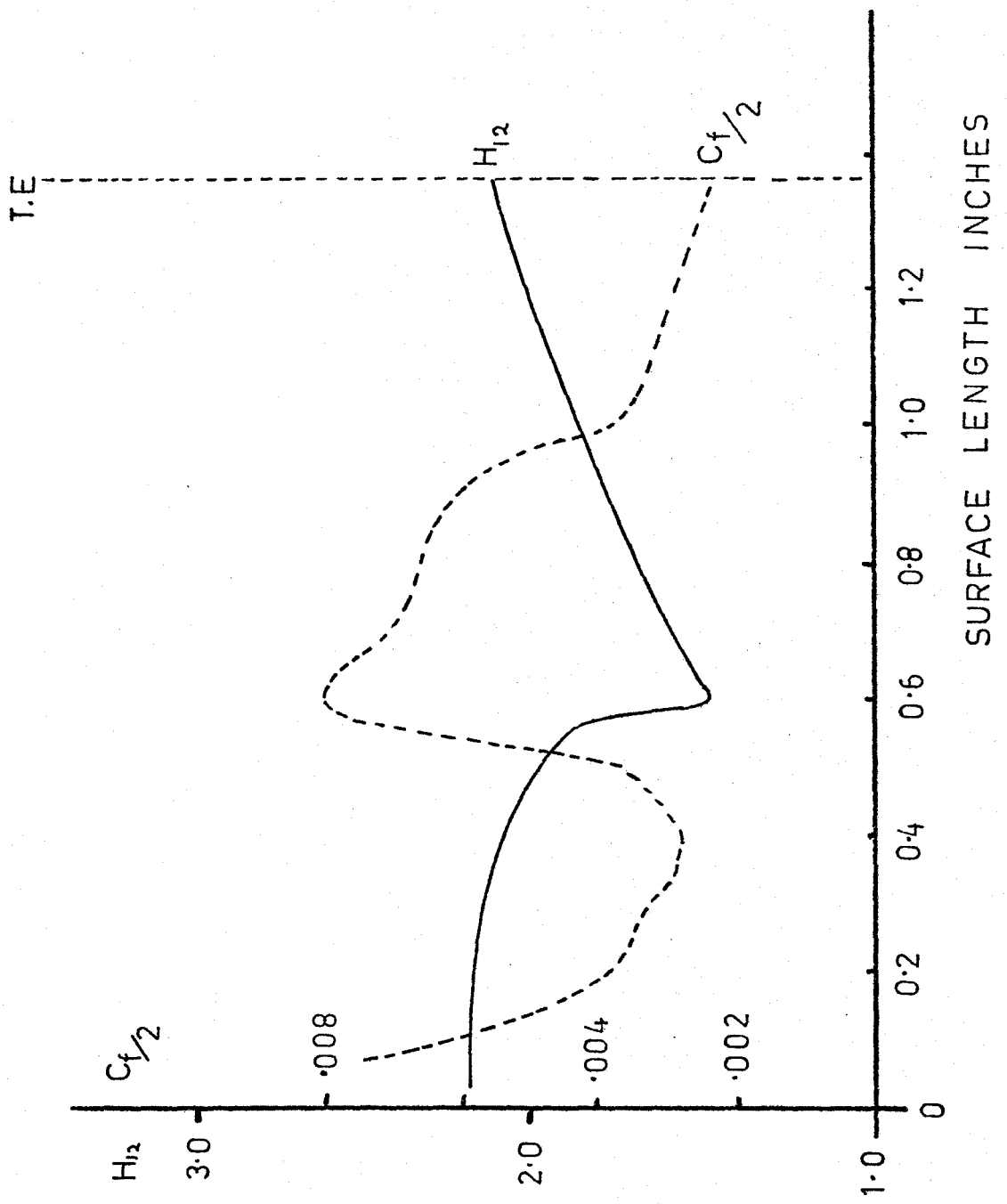

Figure 26 Calculated Distribution of Local Skin Friction Coefficient C_f and Shape Factor H_{12} for McMaster Blade (Pressure Surface) $\frac{}{2}$

would be possible at this point to correct for boundary layer effects. If it was found that separation or undesirable thickening of the boundary layer occurred according to our theoretical analysis, then the blade pressure distribution could be altered via the curvature histogram. In our case we are concerned with testing a particular blade, thus the streamline curvature method was used to recompute the pressure distribution described in Chaper 2.0. The new pressure distribution is compared to the original calculation results in Figure 27. The chief effect of the boundary layer is the reduction in mass flow and a reduction in the amount of leading edge suction, where the boundary layer is thin.

An interesting feature is visible on Figure 26. It can be seen that although the computed transition was near the leading edge there are sharp changes in the skin friction coefficient and shape factor at a position which corresponds to the beginning of the sharp acceleration of the boundary layer. It has been suggested in the literature (15) that the boundary layer on the pressure surface is in fact neither truly turbulent, nor truly laminar, and that strong accelerations could cause relaminarisation on a generally transitional type of flow. In these types of flow our present program is not entirely satisfactory, although the integral parameters such as displacement thickness are not disturbed to such an extent.

3.7 The Effect of the Boundary Layer at the Trailing Edge

In section 2.5 we described the method of calculating the pressure

distribution over the exposed trailing edge of the blade for cases of underexpanded flow. We assumed at that point that no boundary layers existed and that the trailing edge expansion fan and complementary shock wave were focussed on the centre of the trailing edge circle. In a real flow with finite boundary layers and trailing edge thickness we would have the situation shown in Figures 28 and 29 for correctly expanded and underexpanded flows respectively. It can be seen from the diagram that the net effect is a displacement a very short distance downstream of the expansion and shock-wave system. At high pressure ratios considerable thickening of the wake would be expected. (Refs. 25, 26).

For the blade described by McDonald (8) it is possible that the rapid rise in pressure near the trailing edge is in fact a shock-wave which follows an overexpansion of the flow. (Fig. 16). Rapid thickening or even separation of the boundary layer with greatly increased profile loss coefficients would be expected in this situation. For the flat-back blade the pressure distribution in this region is much more favourable to boundary layer development. (Figure 15).

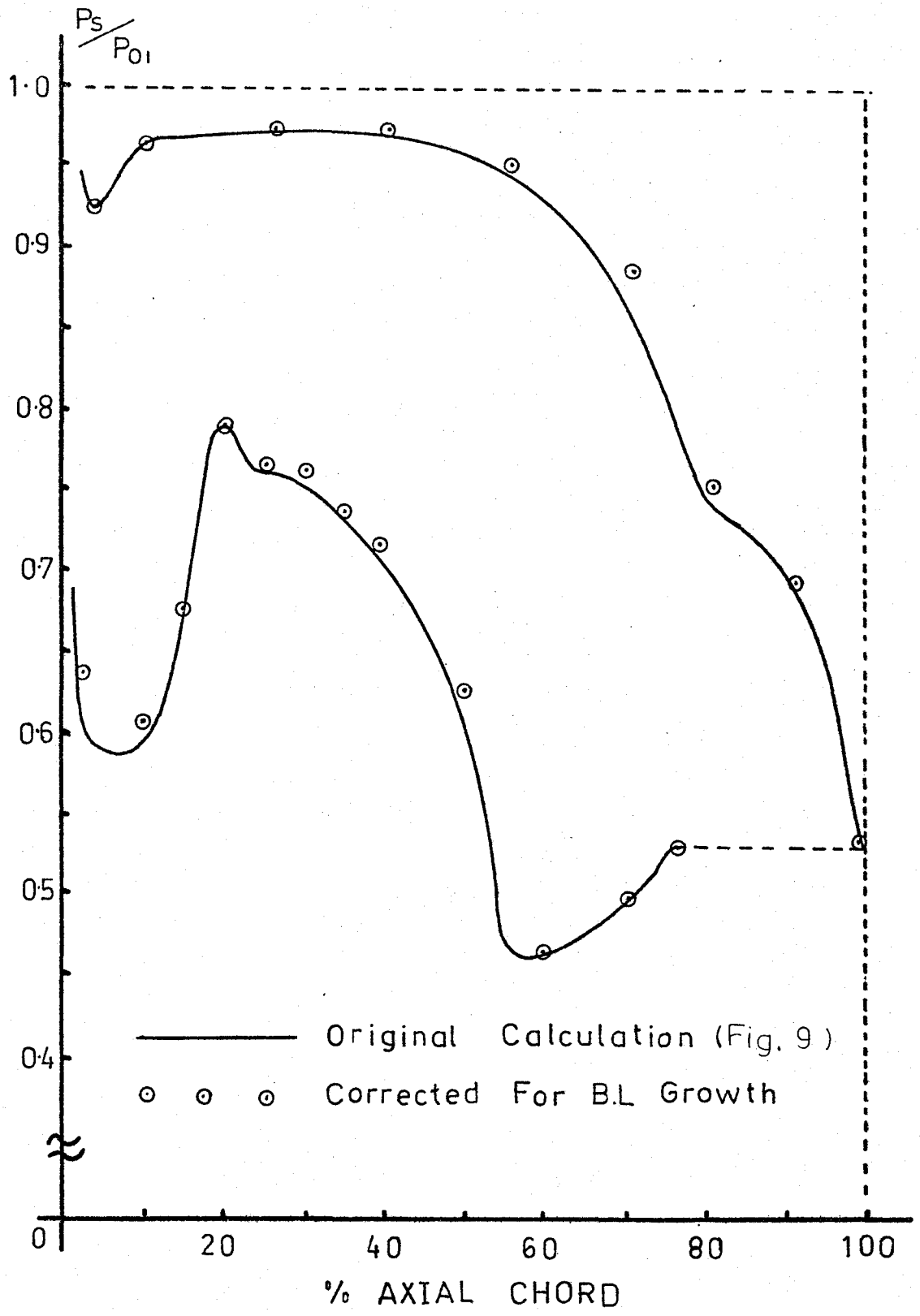

Figure 27 Correction to Calculated Pressure Distribution using Displacement Thickness Data (McMaster Blade)

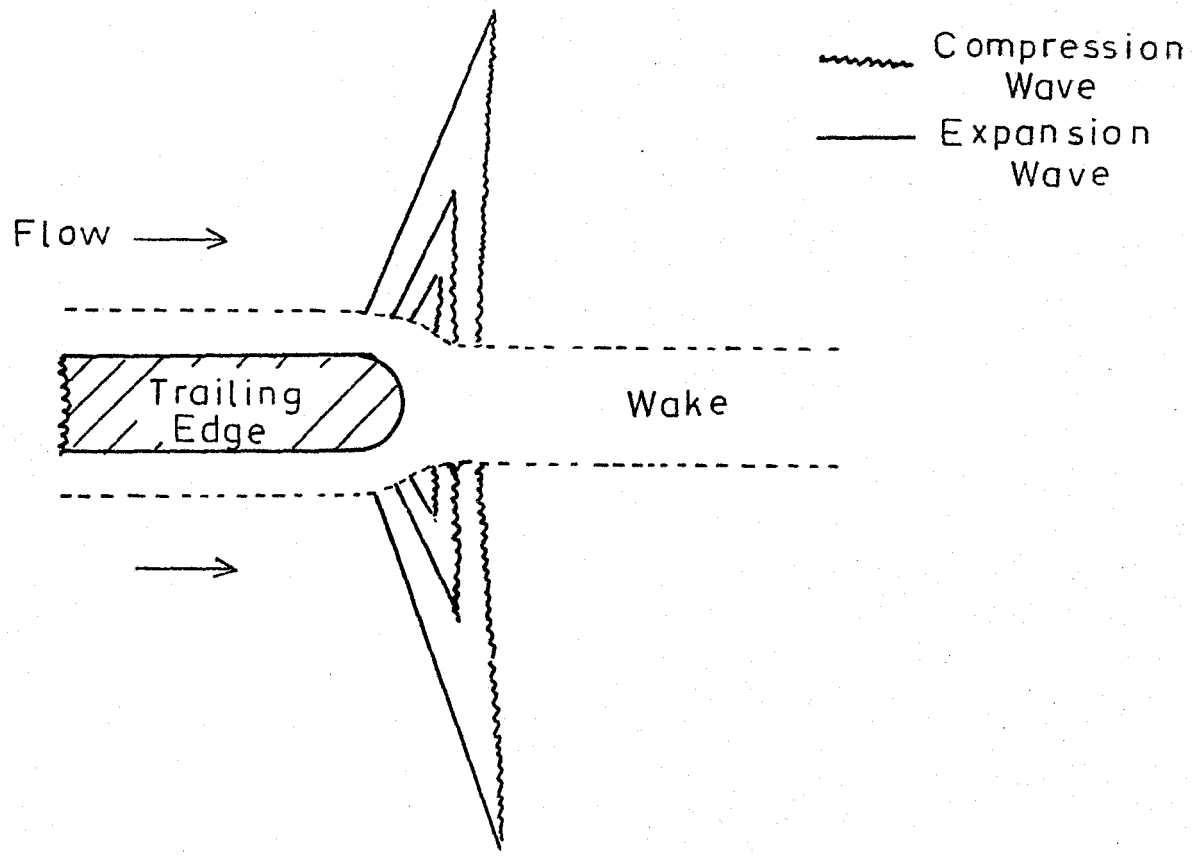

Figure 28 Illustration of Expansion System at the Trailing Edge with a Finite Boundary Layer Thickness

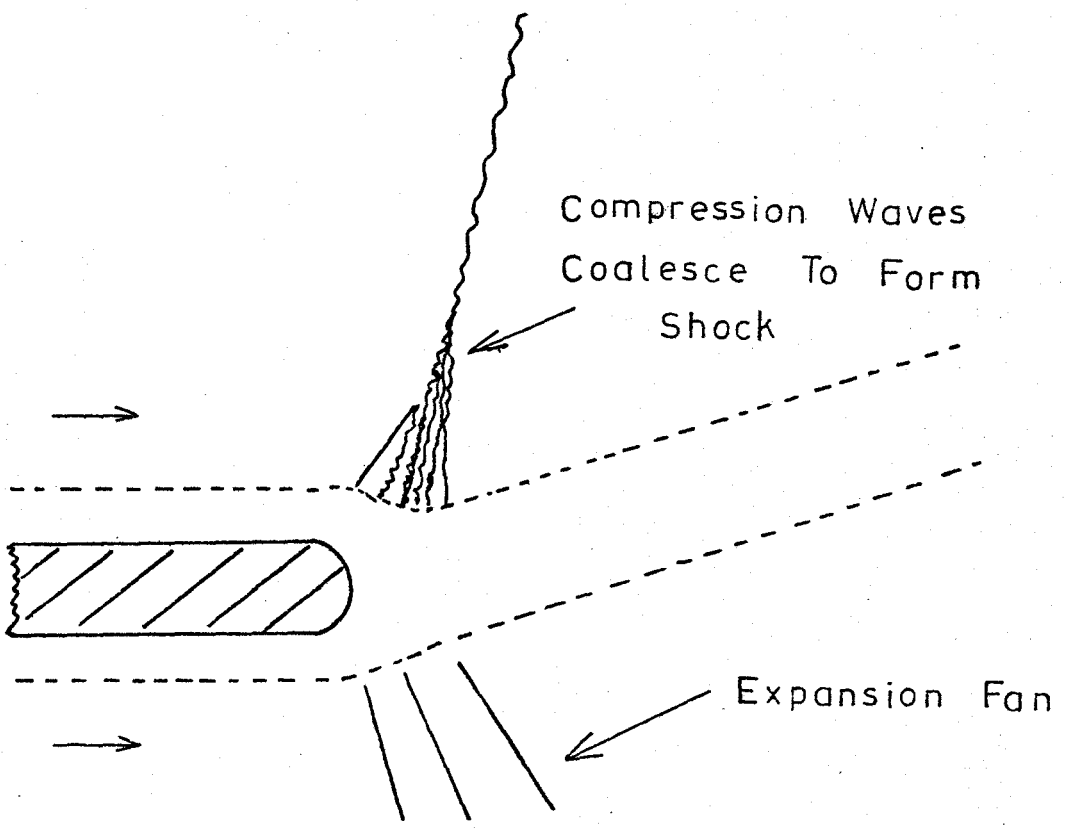

Figure 29 Illustration of the Expansion System for the Underexpanded Flow Case with a Boundary Layer

CHAPTER 4.0 THE DEVELOPMENT AND TESTING OF THE CASCADE WIND TUNNEL

The principal requirements for testing rectilinear cascades of turbine blades in a realistic manner are summarised in point form below:

(a) Modern turbine designs are usually operated with choked blades. Test pressure ratios of up to 3:1 are thus required for the underexpanded flow case.

(b) In common with most wind tunnel design the inlet flow to the test section should be straight and distortion free.

(c) The total pressure should be constant across the inlet passage.

(d) For use at a university the capital and running costs should be low.

The higher capital and running costs needed for continuous operation at representative mass flows dictated the design of an intermittent blow-down system with exhaust from the blades at atmospheric pressure. In the present system air is stored at pressure (100 psig.) in cylindrical storage vessels. The flow through the working section is initiated by opening a butterfly valve. An automatic control system monitors pressure in the working section and controls the position of a ball valve to maintain the working pressure within close limits.

The air is initially supplied by a large V-twin oil-free compressor through an after-cooler and chemical dessicator. (Figure 30). The running time varies as a function of the flow area, storage pressure, and desired pressure ratio. The effect of these variables and the various feedback control parameters available is described in later sections of this chapter. An optimum method of setting up the control system to achieve maximum running time at any desired pressure ratio is described

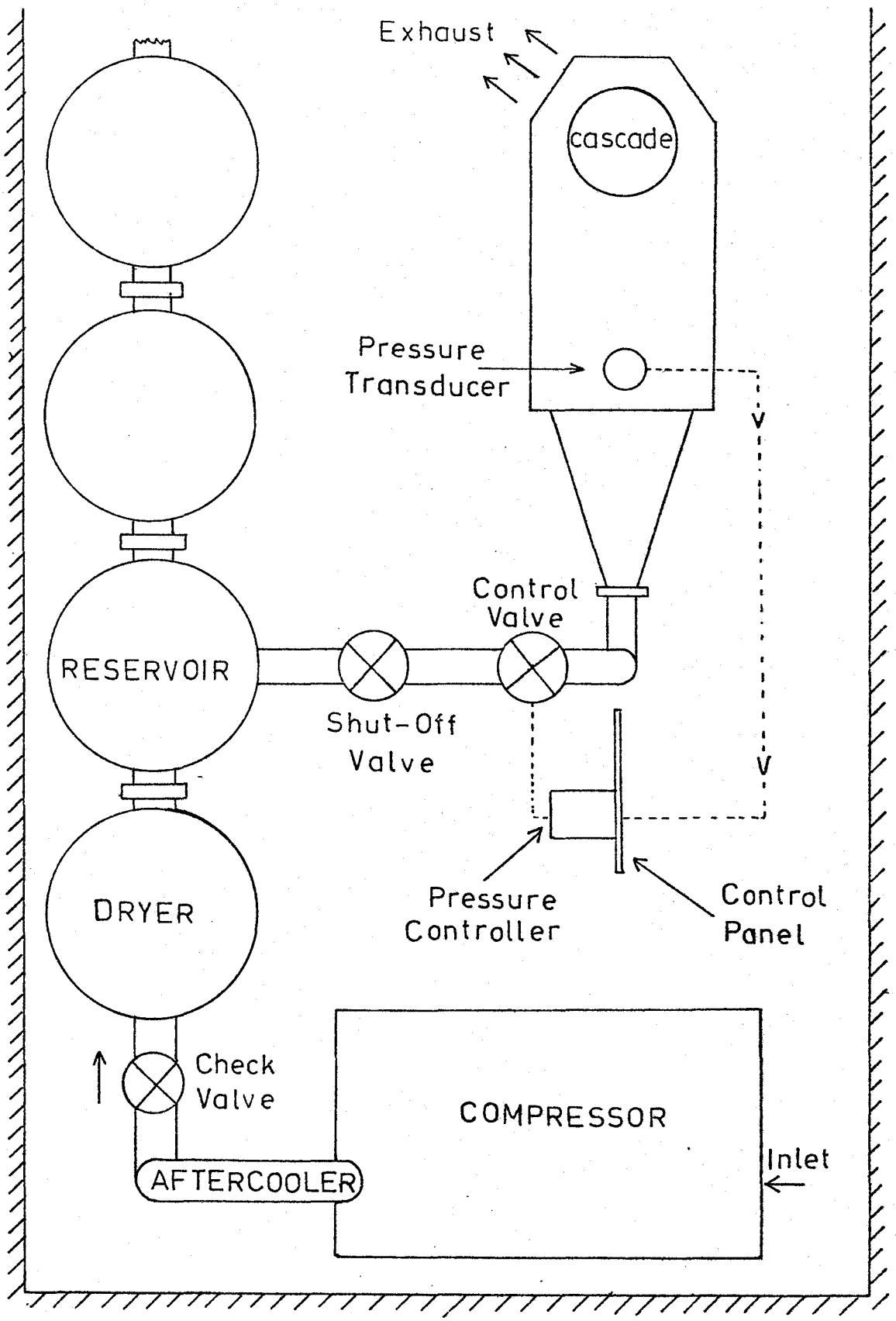

Figure 30 Plan View of the Test Rig

4.1 The Cascade Wind-Tunnel and Associated Equipment

The blowdown installation is for clarity of description broken down into the following major components: The air supply, The cascade tunnel, and the control system. Each is described in a following subsection. A general view of the system is shown in Figure 31.

4.1.1 The Air Supply

Air is taken from the atmosphere and compressed using a Broom-Wade VC500 compressor. This machine is of the dry cylinder, double acting, type and is designed to supply air at 100 psig at a rate of 500 S.C.F.M. The piston rings and seals are manufactured of carbon which enables the delivery air to be uncontaminated by oil. Power is supplied by a 3-phase 100 H.P. electric motor.

Air passes from the high pressure stage of the compressor through a water-cooled after cooler and a one-way valve to an air dryer. This dryer is manufactured by Van-Air Ltd. and in operation the air is filtered through a bed of chemical dessiccant. The dryer is capable of reducing the dew-point by 22°F at its rated pressure of 100 psig but performance is reduced during the typical discharge and recharge cycle of the blow-down wind-tunnel.

The storage volume is made up of four cylindrical vessels 3'6" in diameter and 28' high. This provides a total storage capacity of 1080 cu. ft. excluding the dryer and pipework. The line connecting the reservoirs to the tunnel is 4" in diameter. The two main control

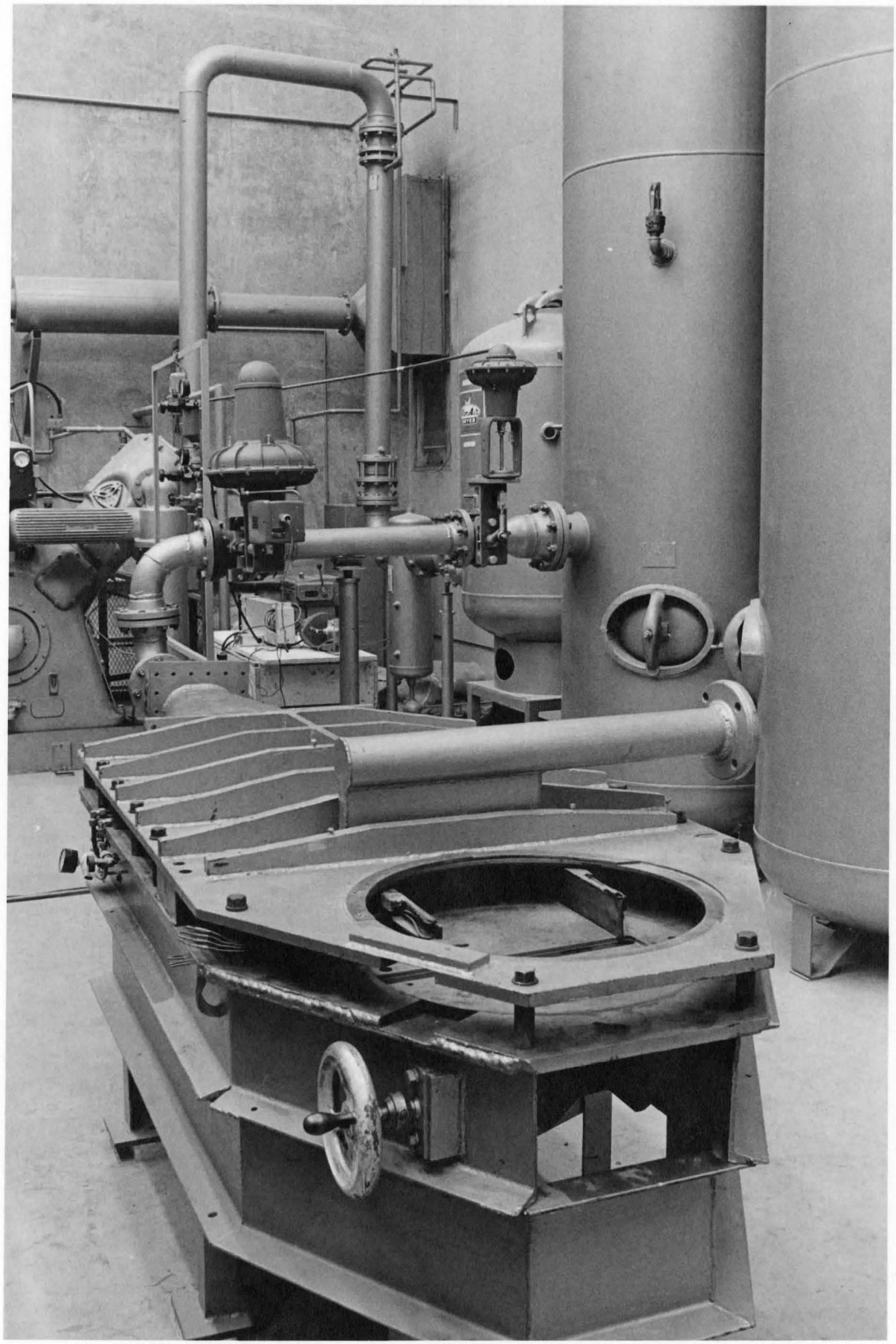

Figure 31 Overall View of the Test Rig

valves manufactured by Foxboro Ltd. are mounted in the positions shown in Figure 30. The first valve is an air actuated butterfly valve which is used in the on-off mode. It is arranged in a fail-safe manner so that a return spring closes the valve on the failure of the valve air-supply. The second valve is of the ball type and thus effectively offers a double throttling orifice. The angular position of the ball is controlled by a diaphragm air-actuator.

The component model numbers and a cost break-down is shown in Table 4.

4.1.2 The Cascade Wind-Tunnel

The main body of the tunnel was acquired from the National Research Council, Division of Mechanical Engineering, where it had been stored since the termination of the A.V. Roe "Arrow" project. This cascade tunnel was originally installed and used by Orenda Engines Ltd. to test compressor blade cascades. Consequently many of the component parts had to be reworked to higher tolerances and reinforced to withstand the greater operating loads when used at pressure ratios suitable for turbine blade testing with exhaust to atmosphere. A sketch of the tunnel including relevant dimensions is included (Fig.32). The working section is rectangular in shape with a maximum height of 2.40". The width is continuously variable from a maximum of 12.0" to a minimum of approximately 3.0". The angle of attack of the cascade can be varied by rotating the turntable on which the blade cascade is

TABLE 4

APPROXIMATE COST OF WIND TUNNEL (1970 PRICES)

Component	Model	Price
Air Compressor	Broom Wade VC500	15,000.00
Aftercooler	Armstrong ACF 660	1,000.00
Air Dryer	Van-Air D36	2,500.00
Installation of Above Items	----------	2,000.00
Air Receivers (4 of)	----------	4,400.00
Installation of Above	----------	1,000.00
Painting Interior of Above Receiver	----------	650.00
Butterfly Valve	Foxboro M3L	280.00
Control Valve	Foxboro V9000	1,081.00
Solenoid Valve	Numatics 2JLS AD3	87.00
Filter Regulator Set	B-110-AT (2 of)	78.00
Timer	Automatic Time Controls ATC 305D	80.00
Feedback Controller	Foxboro 62H	762.00
Mount for Above	Foxboro EH1	80.00
Pressure Transmitter	Foxboro E11AH	762.00
Machining on Tunnel		2,000.00
	TOTAL	$31,760.00

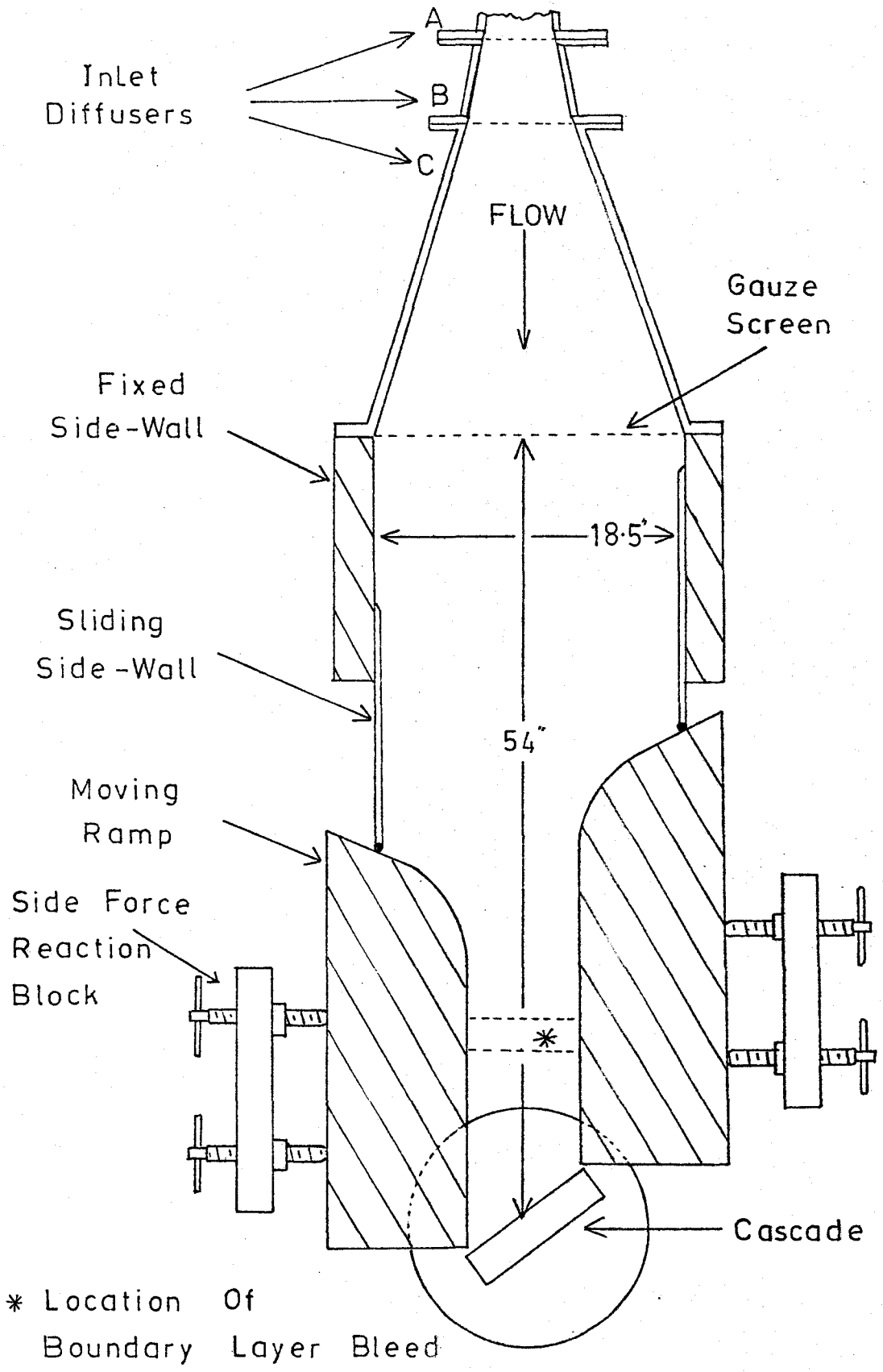

Figure 32 Plan View of the Wind Tunnel Working Section

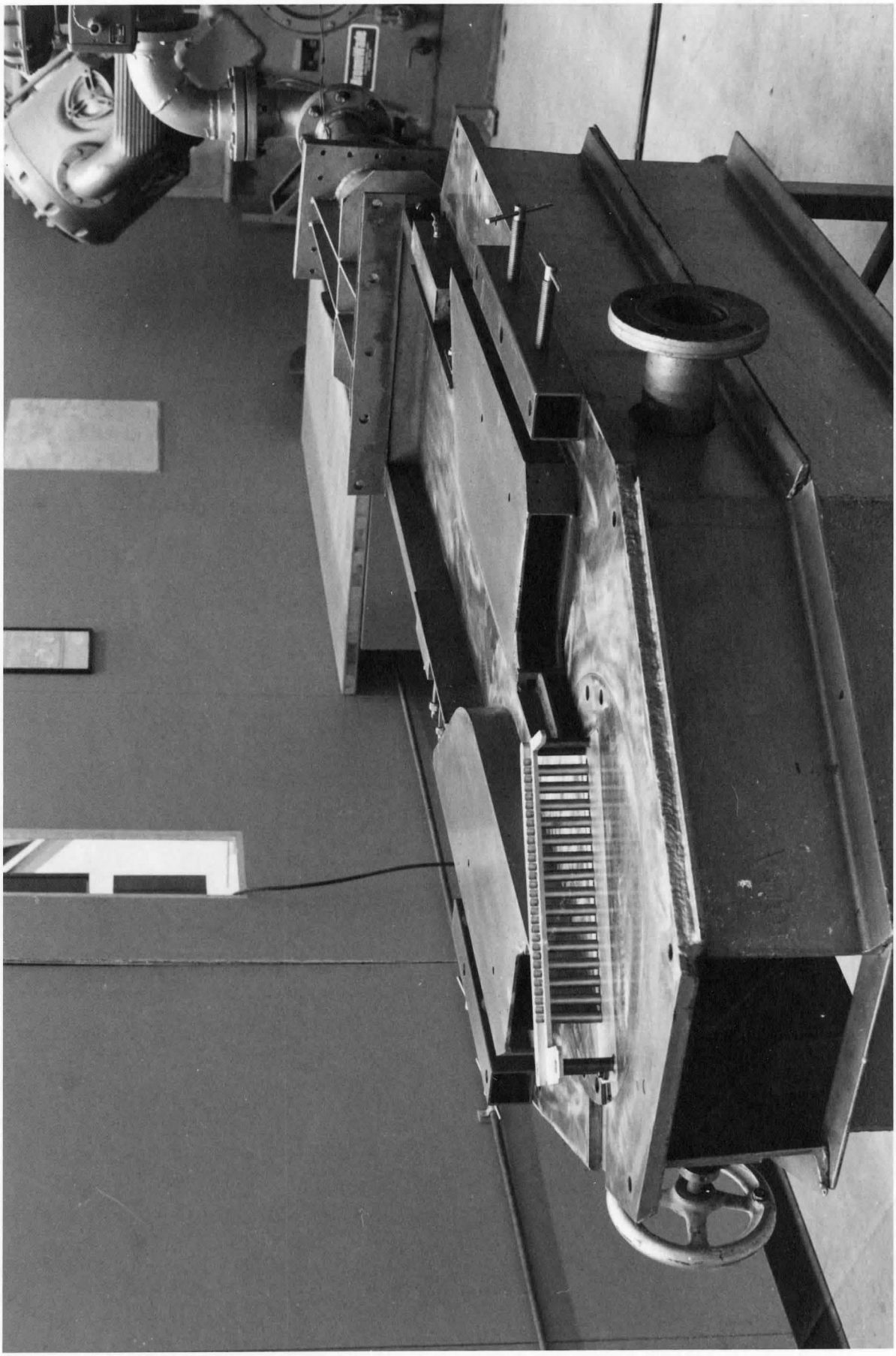

Figure 33 View of the Test Section with Upper Plate removed showing cylindrical Flow Obstructions

mounted (Fig. 33). The moving side-walls are operated by a parallelogram linkage so that they maintain their position with respect to the cascade at all angles of attack of the blades. As the side-walls change positions an air seal is maintained at their upstream faces by sliding seals. These are kept in contact with the ramps by separate air cylinders.

Provision is made just upstream of the working section for boundary layer bleed through slots or porous plates. The top and bottom plates of the rig are heavily reinforced by external ribs. The separation distance of the plates is maintained by a series of pillars and tie-bolts arranged around the periphery of the test-section. The plenum region immediately upstream of the working section is supplied with air from the 4" line through a series of diffusers. This plenum is approximately 18 ½"wide and the same height as the working section of the tunnel.

Flow control in the present diffuser installation (see Fig. 32) is achieved at the moment by using gauze screens designed to keep the diffusers running full. (Ref. 27, 28). The first diffuser (A) is conical in form with a change in diameter from 4" to 6". The cone is of 3^{o} half-angle. Diffuser (B) is a short section with very little area change. It changes the cross-section shape from a 6" diameter circle to a 5½" by 7" ellipse. The third diffuser (C) starts off with the above elliptical shape and diverges in one plane and converges in the other to mate with the 18½" by 2.4" shape of the plenum chamber. The diffusers are all of welded steel construction and (C) is reinforced by external ribs to prevent distortion of the side-walls under pressure.

The forces generated on the moving inlet ramps by internal air pressure are contained by reaction blocks mounted on either side of the test-section. These blocks have hand-screws which are arranged to bear on the ramps. These are tightened in position when the position of the ramps has been set. The ramp sliding seals run in slots milled in the top and bottom faces of the tunnel.

4.1.3. The Control System

The control system is shown schematically in Figure 3.4. The various units of the system are given identification numbers in the figure. To initiate flow in the wind tunnel, switch 1 is closed providing current to solenoid valve 2, and timer 3. The solenoid valve immediately admits air from the shop supply to the actuator of the main on-off valve 4. This valve is fully open in approximately ½ second. Before the run, main control valve 5 has been set to some opening on manual control, depending on the final test section pressure desired. Since both valves are open after this series of operations, pressure in the plenum section rises rapidly and is sensed by the pressure transducer 6 mounted on the plenum chamber top plate. At some pre-determined time after the start switch has been closed the timer cuts out coincident with the levelling off of pressure in the working section of the tunnel. This operation closes a pair of contacts which allow the automatic feedback controller 7 to go into operation. Its function is to compare the pressure measured in the plenum chamber with the required

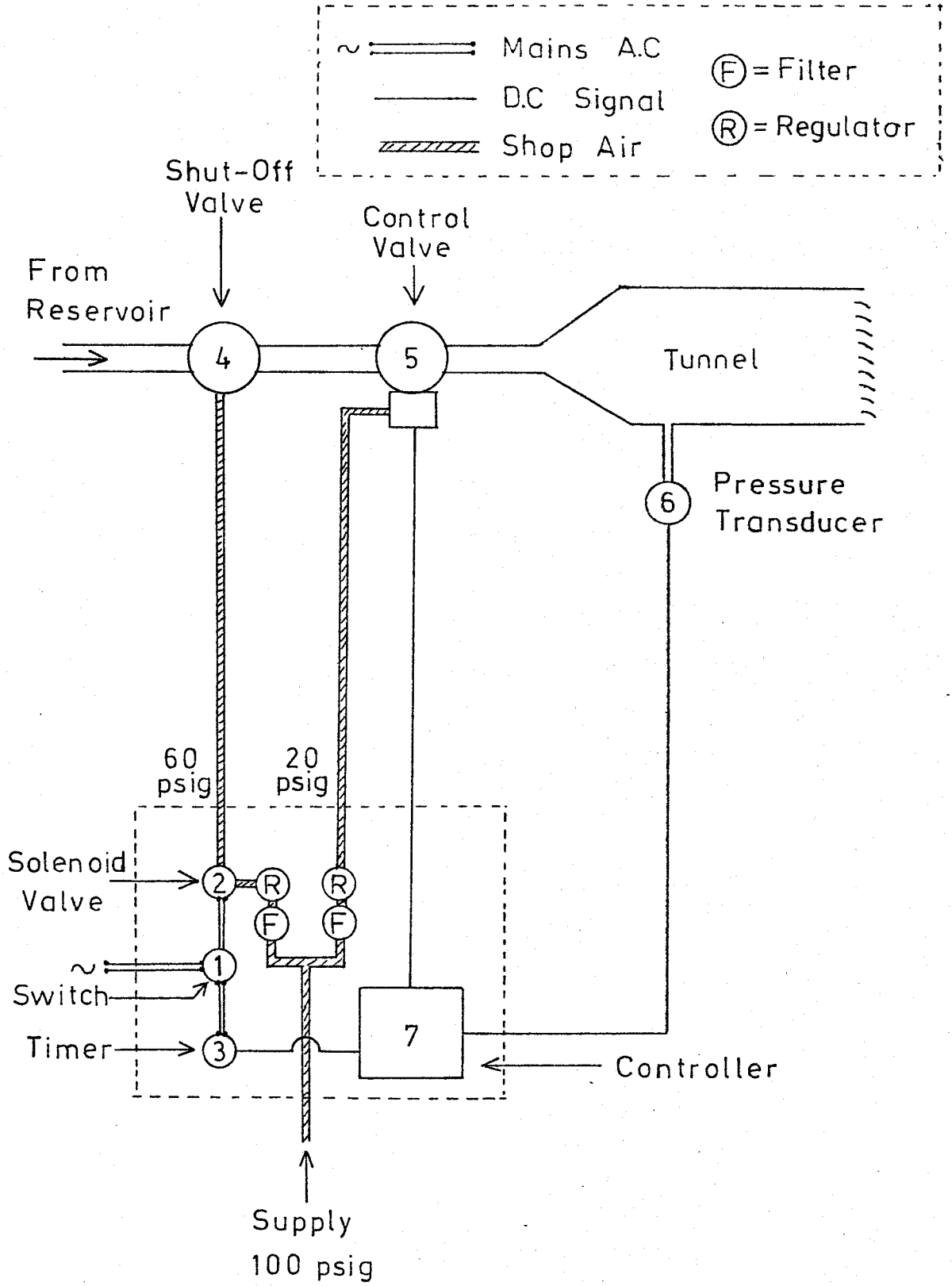

Figure 34 Schematic of the Pressure Control System

operating pressure and automatically adjust the angular position of the control valve. The controller is equipped with proportional, integrating and derivative loops, the actions of which are described in later sections of this thesis.

When the pressure in the reservoir has dropped so that the control valve is 100% open then further control is impossible and the start switch is opened manually. This returns the system to the pre-start condition and flow stops in the wind-tunnel. The air compressor cuts in automatically at a pressure set on its governor and pumps air into the reservoirs until the maximum allowable storage pressure is reached. The compressor then idles until the next cycle of operations.

If we assume that a pressure ratio of 2:1 is desired with a choked flow area of 10 sq.ins. then the present system will provide some 14 seconds of useable running time. This would necessitate 7 minutes of pumping time from the end of run condition(50 psig reservoir pressure) to the pre-start condition (100 psig reservoir pressure) (Fig. 35).

The original control system was designed by Dilworth, Secord, Meagher Associates on a minimum cost basis. The total cost based on 1970 prices was approximately $3,000.00. The individual units are operating at their design limits and it has required considerable patience and attention to detail to achieve the present operating standards.

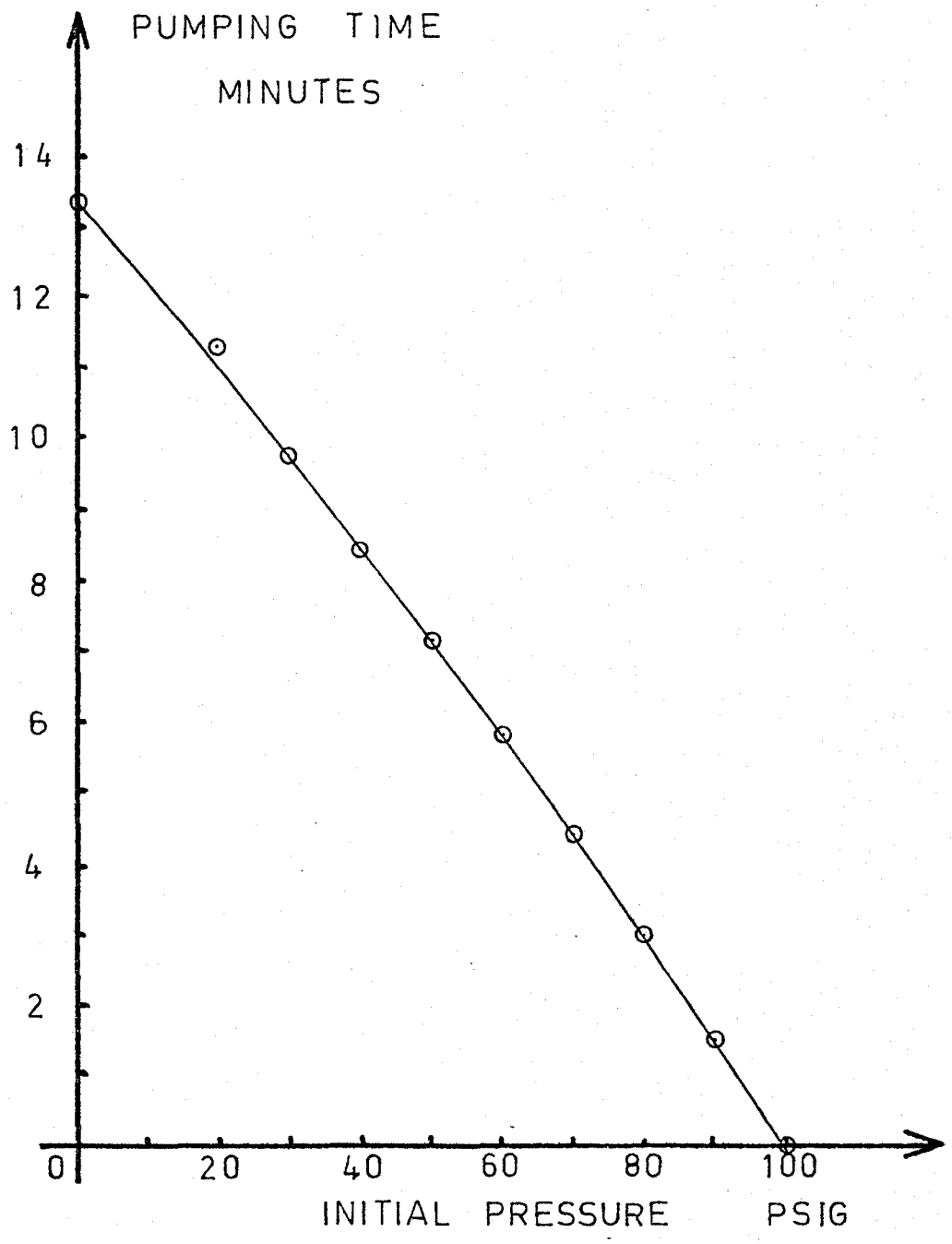

Figure 35 Time required for Pumping Air into Storage System

4.2.0 Development testing of the Cascade Wind Tunnel

The pressure and flow rate of the air at the working section depends on a number of variables. In the testing procedure and development of the wind tunnel the effects of these variables were first evaluated independently and then progressively in combinations until the goal of reliable operation with good pressure control and maximum running time was achieved. Pressure traces were obtained by tapping into the pressure transducer feedback circuit and recording on a chart recorder the varying voltage coming from the transducer. Similarly valve position was monitored by recording the voltage in the output control loop. However, in this instance it is more an indication of controller output than the angular position of the ball in the control valve housing. The pressure transducer was calibrated against a Wallace & Tiernan test gauge accurate to ±½%. This is considered sufficient accuracy for control transducer requirements (Fig. 36).

Each series of tests is described in separate sections below.

4.2.1. The Investigation of the effect of Reservoir Pressure

The first and perhaps most obvious parameter is the pressure available in the reservoir. A number of test runs were made with different initial control valve openings at three different reservoir pressures. The height of the initial pressure peak was noted in each

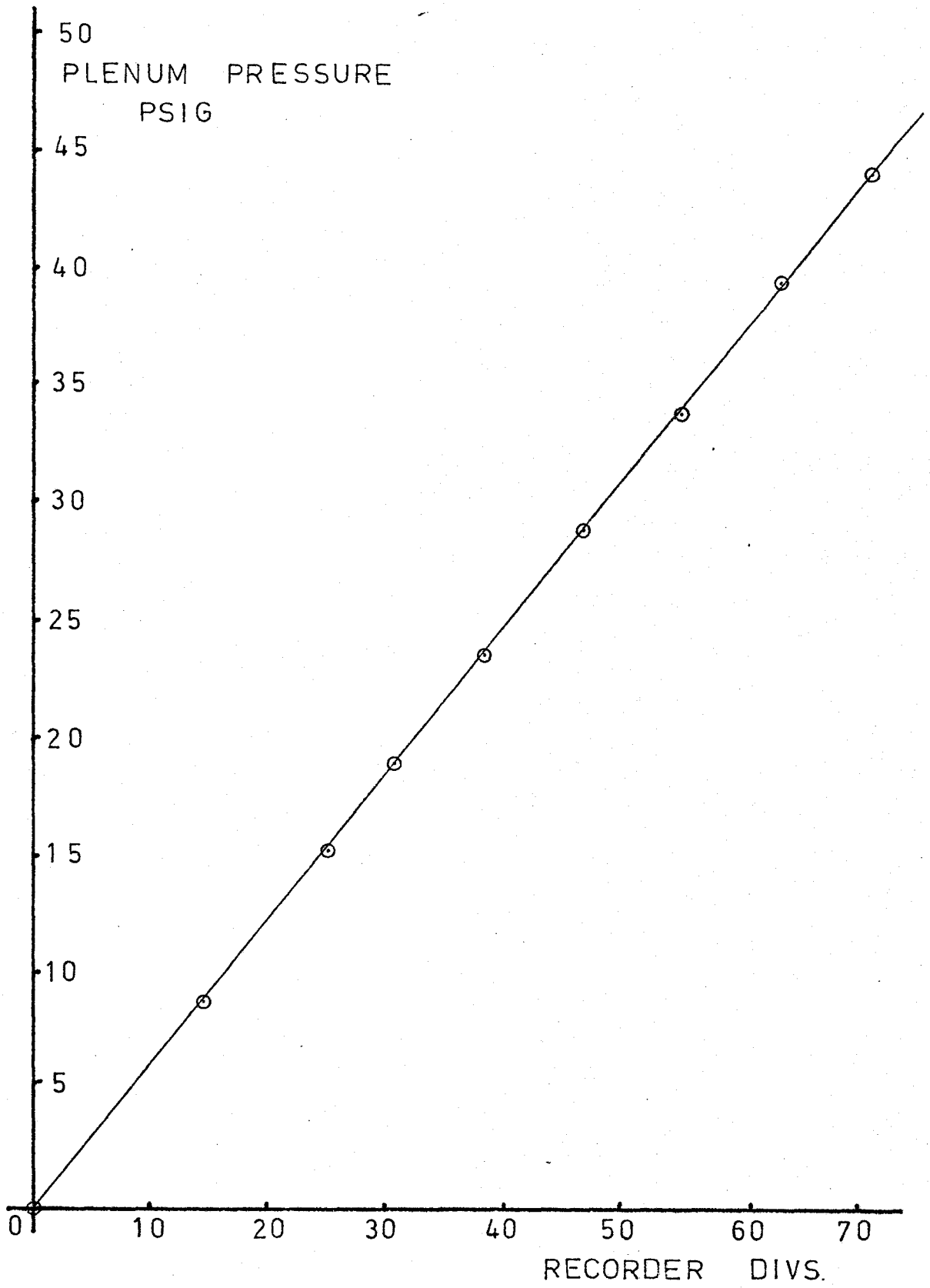

Figure 36 Calibration of the Control System Pressure Transducer

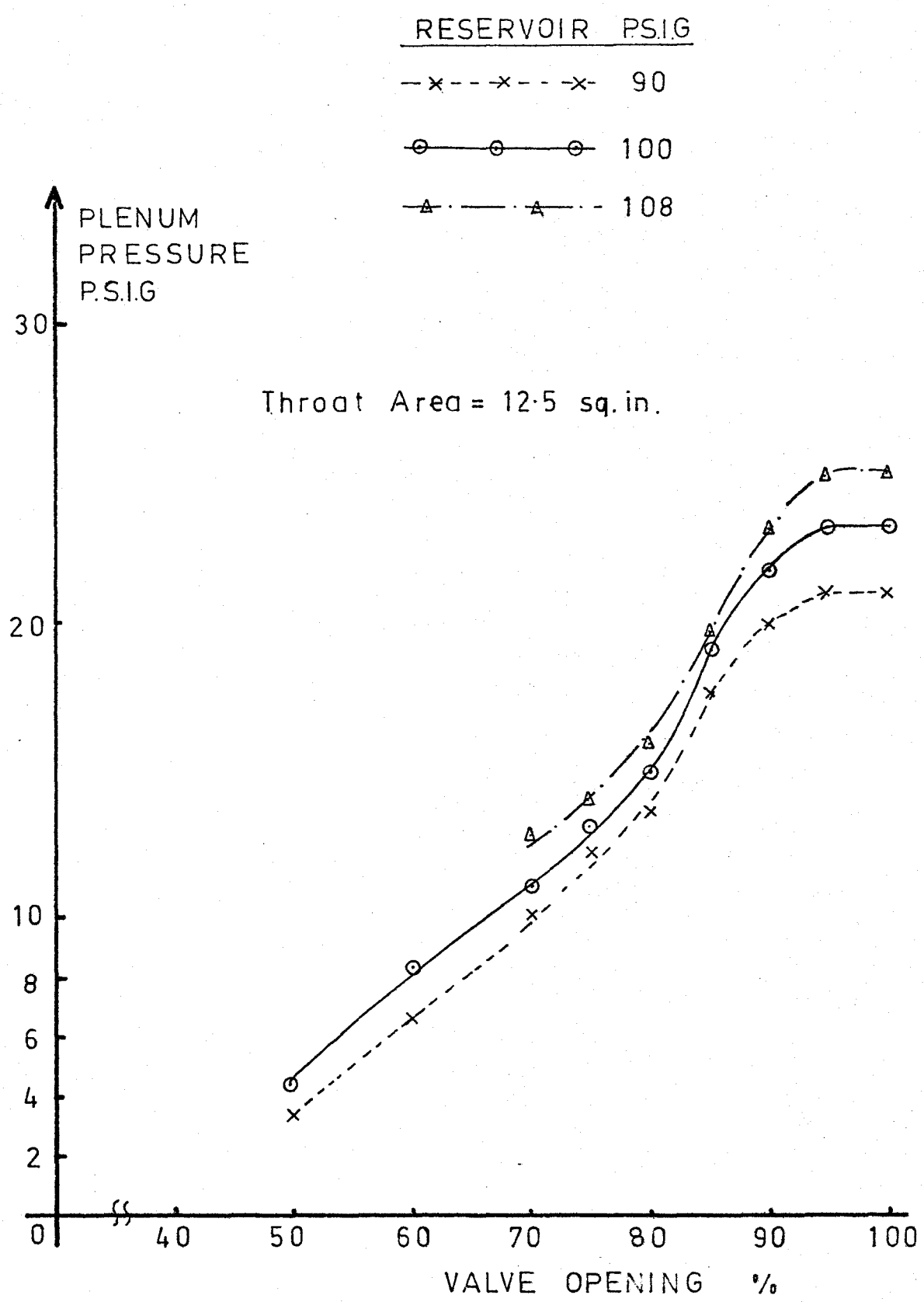

Figure 37 Investigation of the Effect of Reservoir Pressure on Plenum Pressure

case. The choked throat area was constant for all tests.

As expected (Fig. 37) it was found that downstream pressure available was increased at fixed valve opening by increasing the reservoir pressure. Also the downstream pressure increased with valve opening. It was also obvious however that the valve characteristic was highly non-linear, with an initial fairly gentle slope giving way to a rapidly rising pressure curve up to a plateau value for the last 5% of the travel.

On investigation of the valve mechanism it was found that the ball was being rotated past the fully open position so that the last 5% of actuator travel gave no throttling action. The stroke to input power ratio of the valve was adjusted until the valve was operating over its effective stroke rather than the maximum mechanical stroke built into the design. Early testing also revealed the important fact that although the air system was designed for maximum storage pressures of 125 psig, it was possible occasionally to thermally overload the present electrical supply to the drive motor. To enable continuous satisfactory operation the upper pressure limit in the storage system has been set to 100 psig.

4.2.2 The Investigation of the effect of Flow Area

The effect of flow area was investigated by varying the flow area of the cascade at constant initial reservoir pressure. The cascade consisted of a series of cylindrical flow obstructions giving the

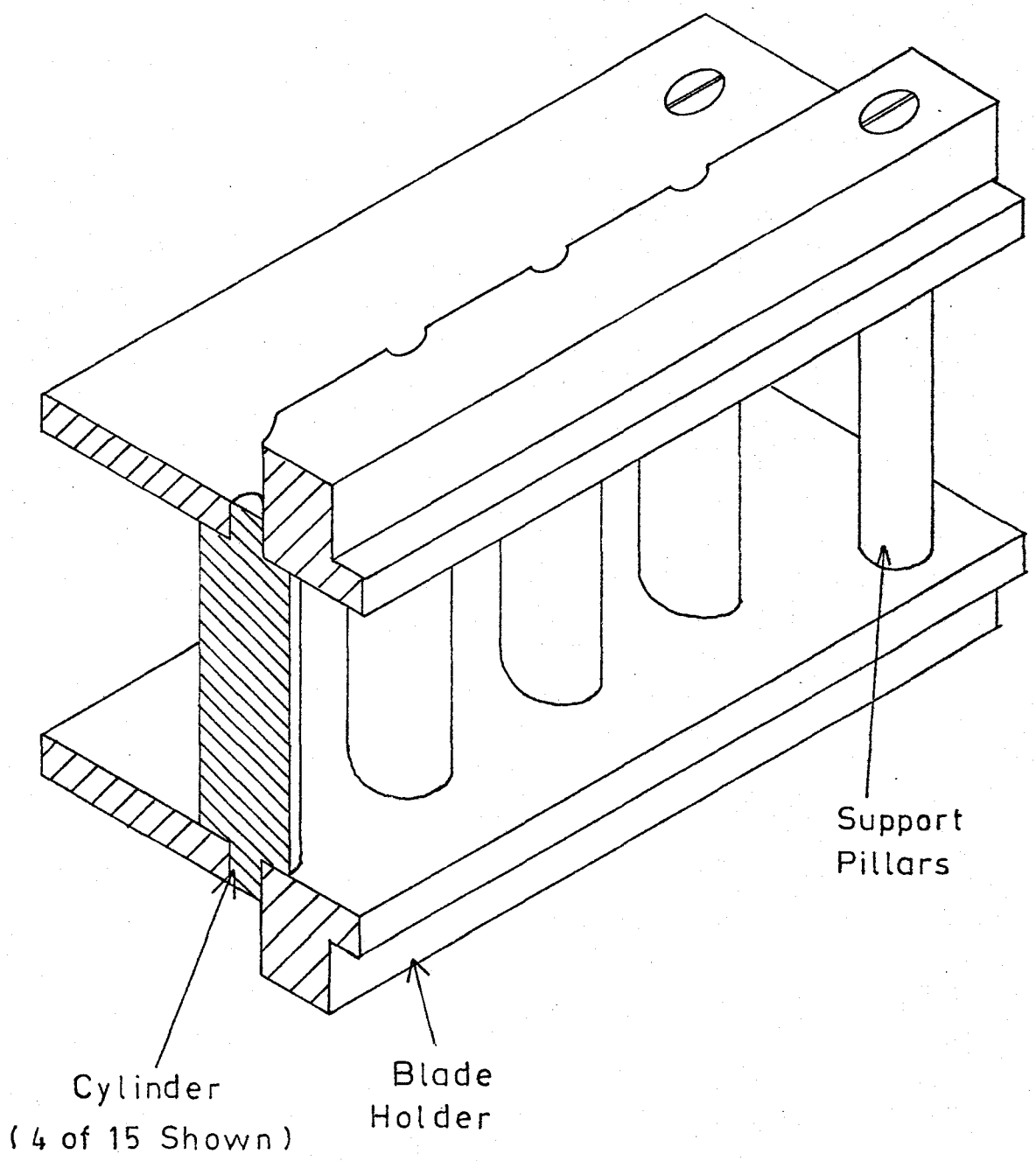

Figure 38 Crossection of Blade Holder showing Cylindrical Flow Obstructions

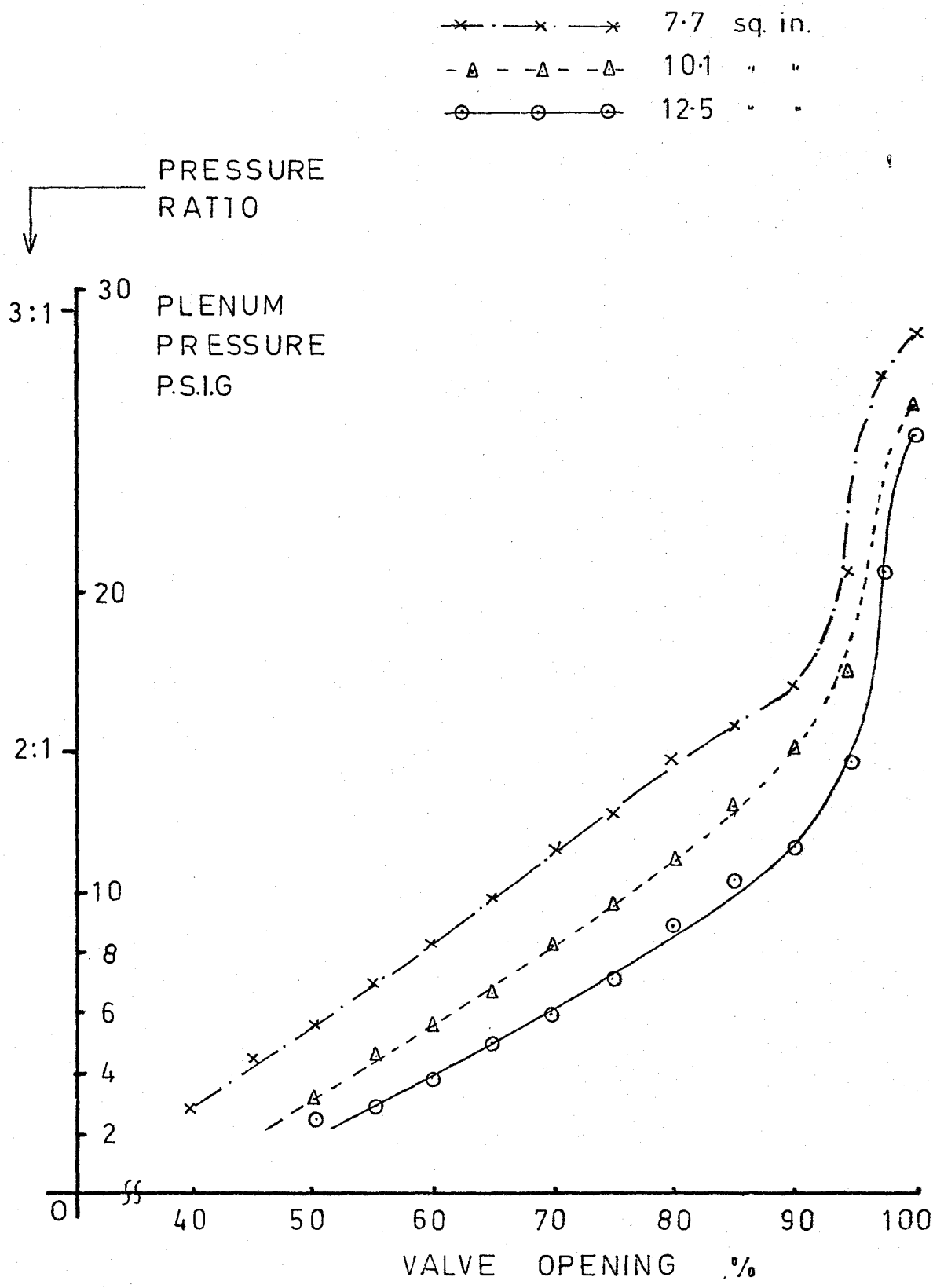

Figure 39 Investigation of the Effect of Throat Area on Plenum Pressure

required choked throat area (Fig. 38). This was done to avoid possible damage to the accurately machined cascade of turbine blades during development running in which unusual conditions might occur. Tests were carried out at three different flow areas and the peak initial pressure was recorded at different valve openings. It can be seen in Fig. 39 that the problem of over-stroking has been solved and the throttling action continues to 100% although the curves are still non-linear.

From Fig. 39 we can see the increased pressure ratios available at reduced flow areas. Also the valve opening characteristics which can be divided into two distinct regions centred about a value of 90% open.

4.2.3. The Investigation of the effect of Timer Setting

It is necessary from the point of view of air economy to allow pressure to rise very close to the set-point pressure value before allowing the automatic control to function. Otherwise, the system, even at its maximum response rate, would waste most of the reservoir air before achieving stable operation. Consequently, the setting of the timer is critical. The series of tests related above were also used to measure the length of time required to reach the initial peak from starting the system. At a fixed valve opening the pressure then slowly decays (see Fig. 40). This time to peak was then plotted as a function of valve opening and flow area. Although a great deal of

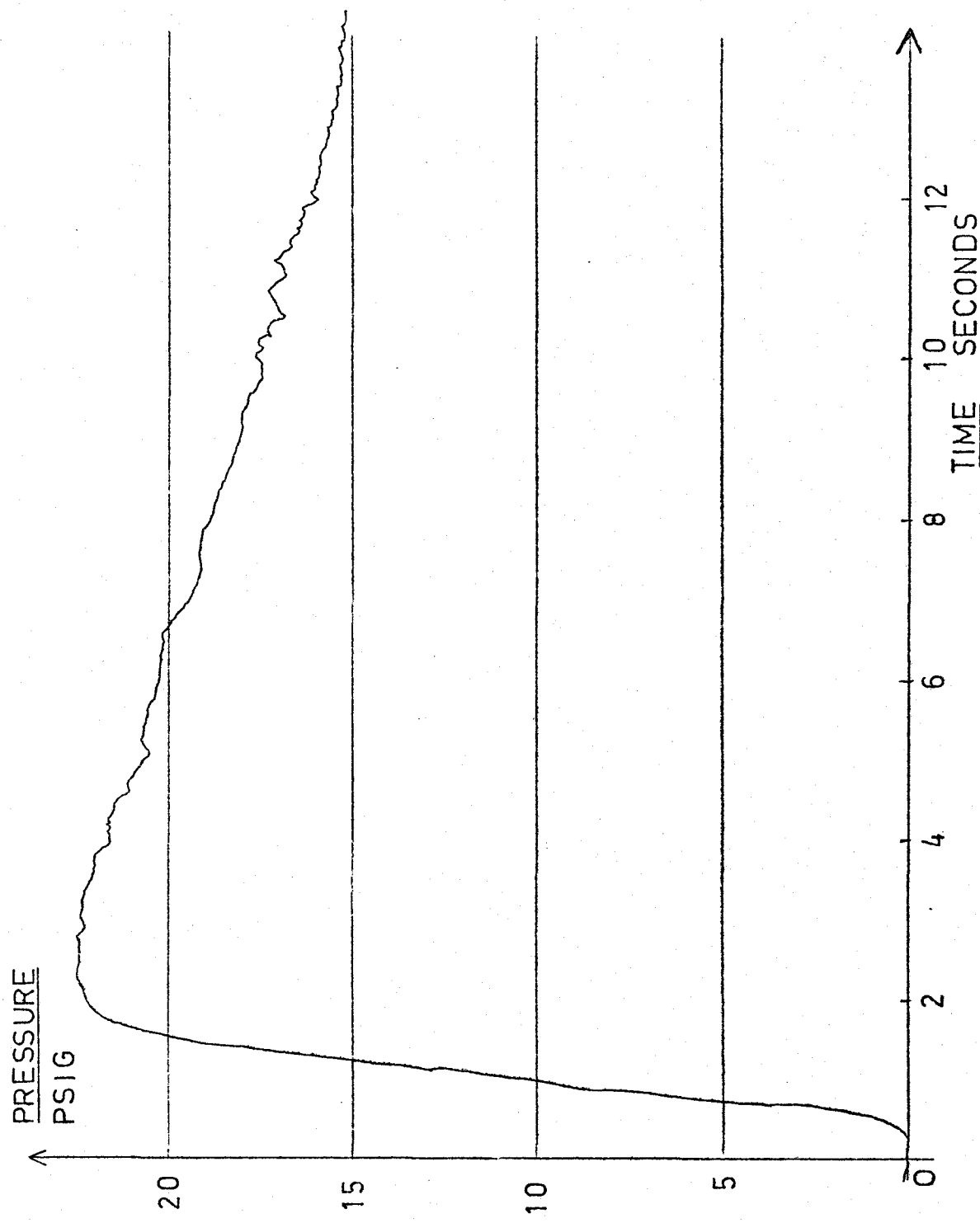

Figure 40 Typical Pressure Trace without Use of Automatic Control Systems

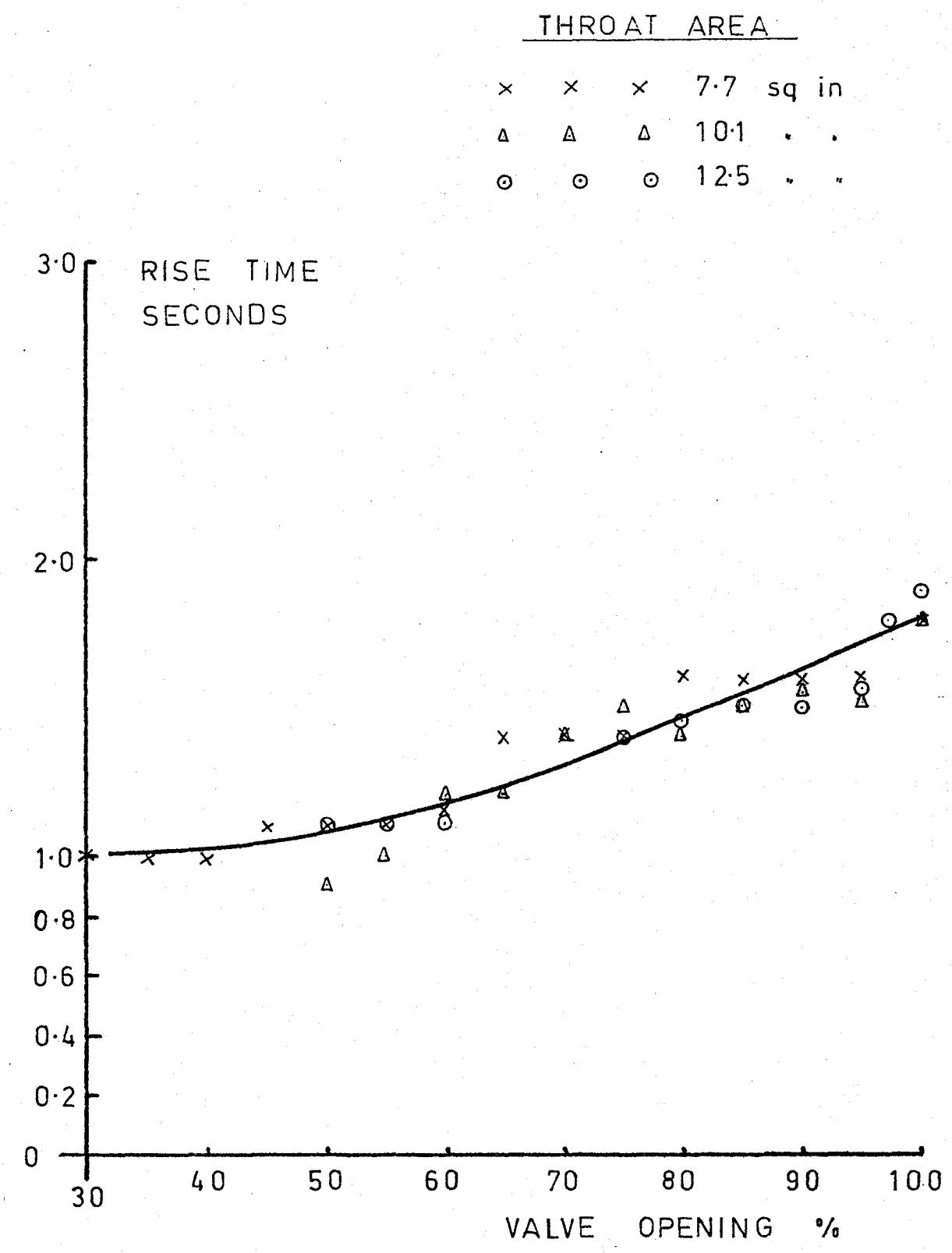

Figure 41 Time measured to the peak of the Pressure Curve of the type illustrated by Figure 40.

experimental scatter is obvious(Fig. 41)a trend is discernible. An allowance of one-half second added to the average time at a given valve opening will allow the pressure control system to take over smoothly at a given pressure very close to the set point pressure. With reference to both Fig. 40 and Fig. 41 it can be seen that this timing activates the automatic control system at a period of gentle pressure decay in the plenum chamber. Thus rates of change are low and air wastage is minimized.

A minimum time of one second was found to be necessary whatever the valve opening and this is attributed mostly to the time needed for the on-off valve to become fully open after starting the system. This time is independent of flow area or pressure required.

4.2.4 The Flow Control Pressure Transducer

The pressure range covered by the early tests was 0 - 50 psig as this was considered to be the whole range of interest. After some experience was gained the sensitivity was increased and the range reduced to 0 - 30 psig since this covered all the likely pressures that the rig was capable of. The siting of the transducer was found to be critical. The transducer is of a force balance design in which small movements of a bellows are resisted by an electro-magnetic force feed-back system. The output is very linear in the range 10 to 50 ma. at a line voltage of 83 volts D.C. The transducer can be sensitive to

vibration in certain planes, but these can be avoided in mounting. Also long pressure lines are undesirable since they can cause transducer "ringing" and generally poor response. In the best configuration tested the transducer was mounted directly above the center of the plenum with a short piece of connecting pipe (6" long, ¼" N.P.T.).

4.2.5 The Flow Controller Variables

The feedback controller is equipped with three control modes, namely proportional, integrating, and derivative loops. Each loop has a variable gain. The characteristics of the main control valve are slightly modified by the line pressure feeding the actuator and this subject is returned to later in the thesis. Initially the highest possible feed pressure was supplied with the intention of speeding valve response.

A process of elimination was possible with the three loop gains since it was found immediately that the use of derivative feedback at any loop gain caused violent cycling of the control valve and consequently downstream pressure. (Fig. 42). Investigation of this effect was carried out by simulation since the pressure changes could be destructive. The response of the controller to various input voltages and waveforms was investigated while monitoring output on an oscilloscope. It was found that the derivative loop was very sensitive to high frequencies; with the test rig set up as shown the pressure transducer signal contained some spurious signal from the turbulence and

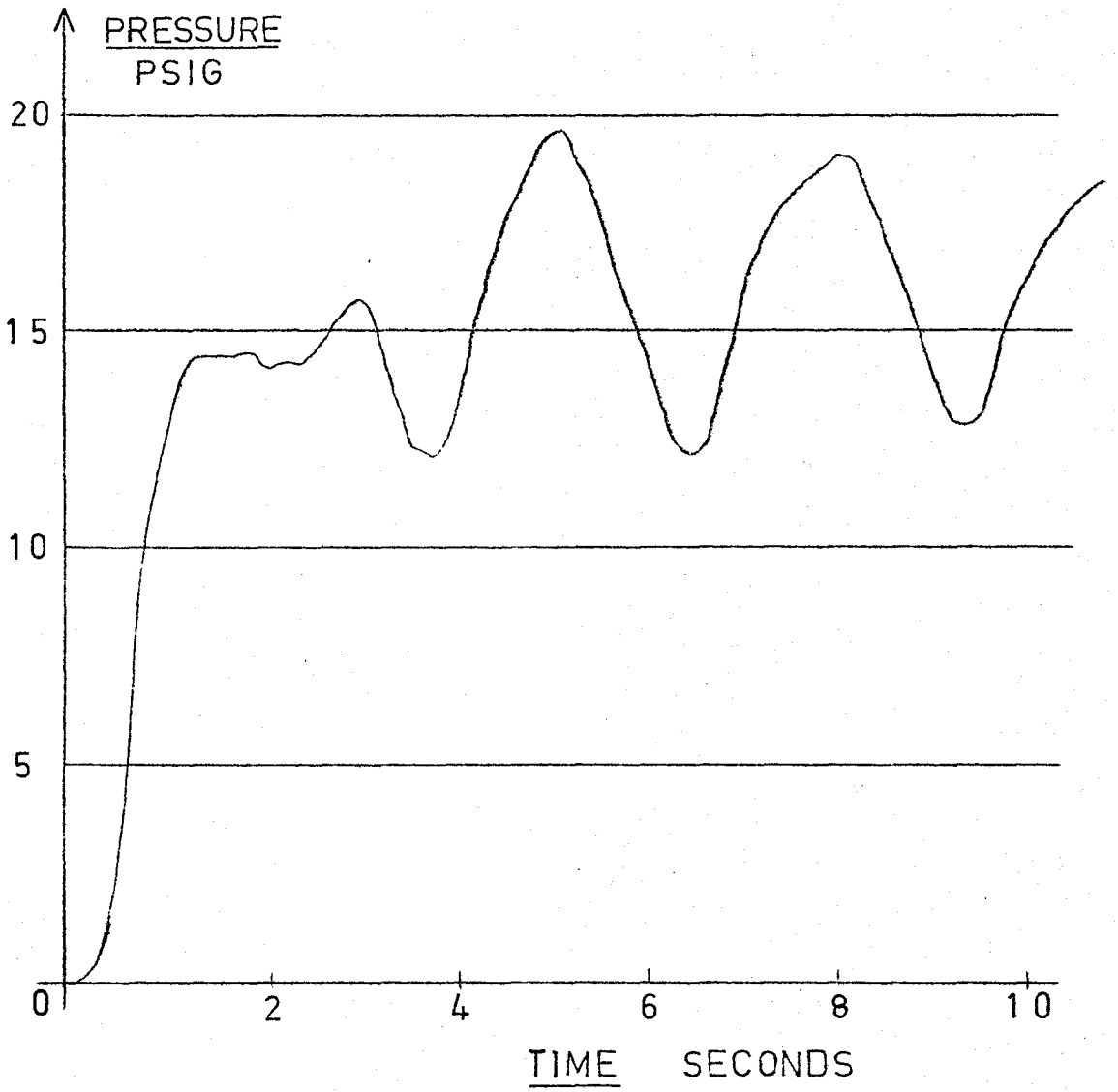

Figure 42 Violent Pressure Fluctuations Experiencedusing Derivative Feedback

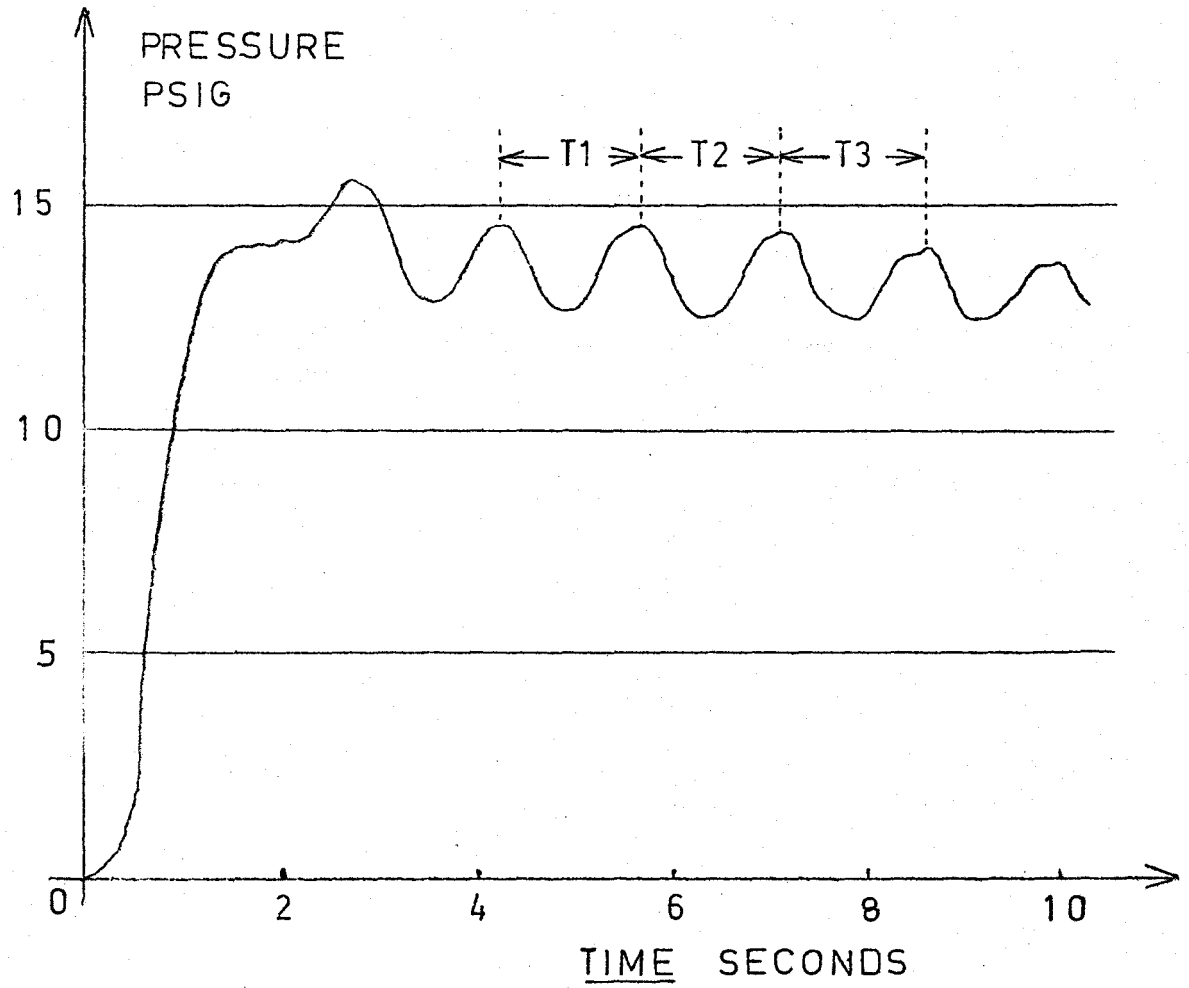

$T1 = 1{\cdot}41$ secs

$T2 = 1{\cdot}40$ "

$T3 = 1{\cdot}45$ "

$T_{av} = 1{\cdot}42$ secs

Figure 43 The Determination of Cycle Time with Proportional Feedback only.

noise generated by flow through the two valves and two right angle bends upstream. This was sufficient to cause large outputs from the derivative loop. Ideally one would filter out all frequencies above 2 or 3 Hz since it is in slower rates of charge that we are interested. However, a filter for this range would have to be digital in nature and quite expensive, and might also cause undesirable phase shift. It was found on further testing that adequate control was available using only the proportional and integrating loops.

Some theory was found of value in setting up the system. Values of various control parameters can be calculated using Pessen's formulae (29,30) using information gained from deliberately inducing cycling on proportional control and noting the system frequency and gain (Fig. 43). The calculated optimum parameters agreed well with those arrived at by trial and error. The calculated derivative gain is at the smallest setting available on our system, so little loss is felt by it's absence. (see Table 5).

After deriving optimum settings for the controls, a series of runs was carried out with different pressures and flow areas. Generally control was good after 2 to 3 seconds from the start of the run (see Figs. 44, 45, 46). If large flow rates at high pressure ratios were demanded then the system response was poor and the error from the set-point large. It was found that this occurred if initial valve opening required was greater than 90%. It was obvious that the change in valve characteristic at this opening was responsible. The deviation can be reduced by reducing the proportional gain to make up for the

increased sensitivity of the control valve setting.

It was also noted that the deviation of the trace was usually of constant amplitude whatever the absolute value of the set-point. This error of ± 1 psig was thus reduced by increasing transducer sensitivity as mentioned in Section 4.2.4 so that error signal was increased. This was at the expense of stability and the control at large valve openings was degraded. Analysis of the chart records showed that control response was 180^{o} out of phase with pressure records. This is a classical form of control instability and is not easily eliminated by a change of loop gains. The answer lies in the frequency versus phase angle characteristics of the components and system as a whole. In this sort of air control system it is usually the control valve which is the slowest element provided that the plenum volume is small (ref. 29). Thus it can be shown that changes to this part of the system will have the largest percentage effect on overall system response.

The system was changed by reducing considerably the feed pressure to the control valve so that its operation was slowed down. This greatly improved the stability at large openings without losing fine control at small openings.

Total running time available with a control accuracy of ± ½ psi is shown in Fig. 47 as a function of pressure ratio and flow area.

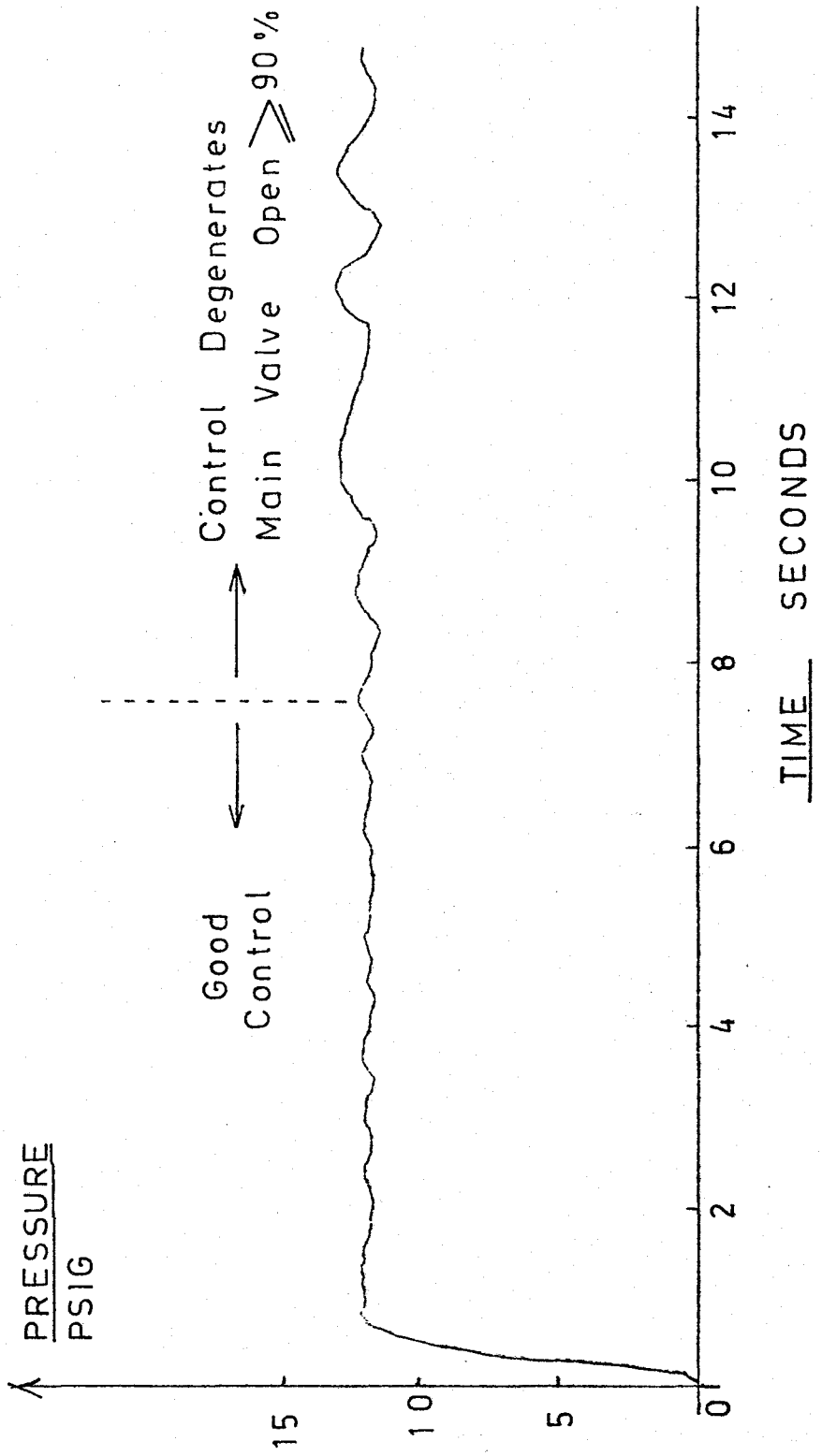

Figure 44 Typical Controlled Pressure Trace showing Deterioration at Large Control Valve Openings

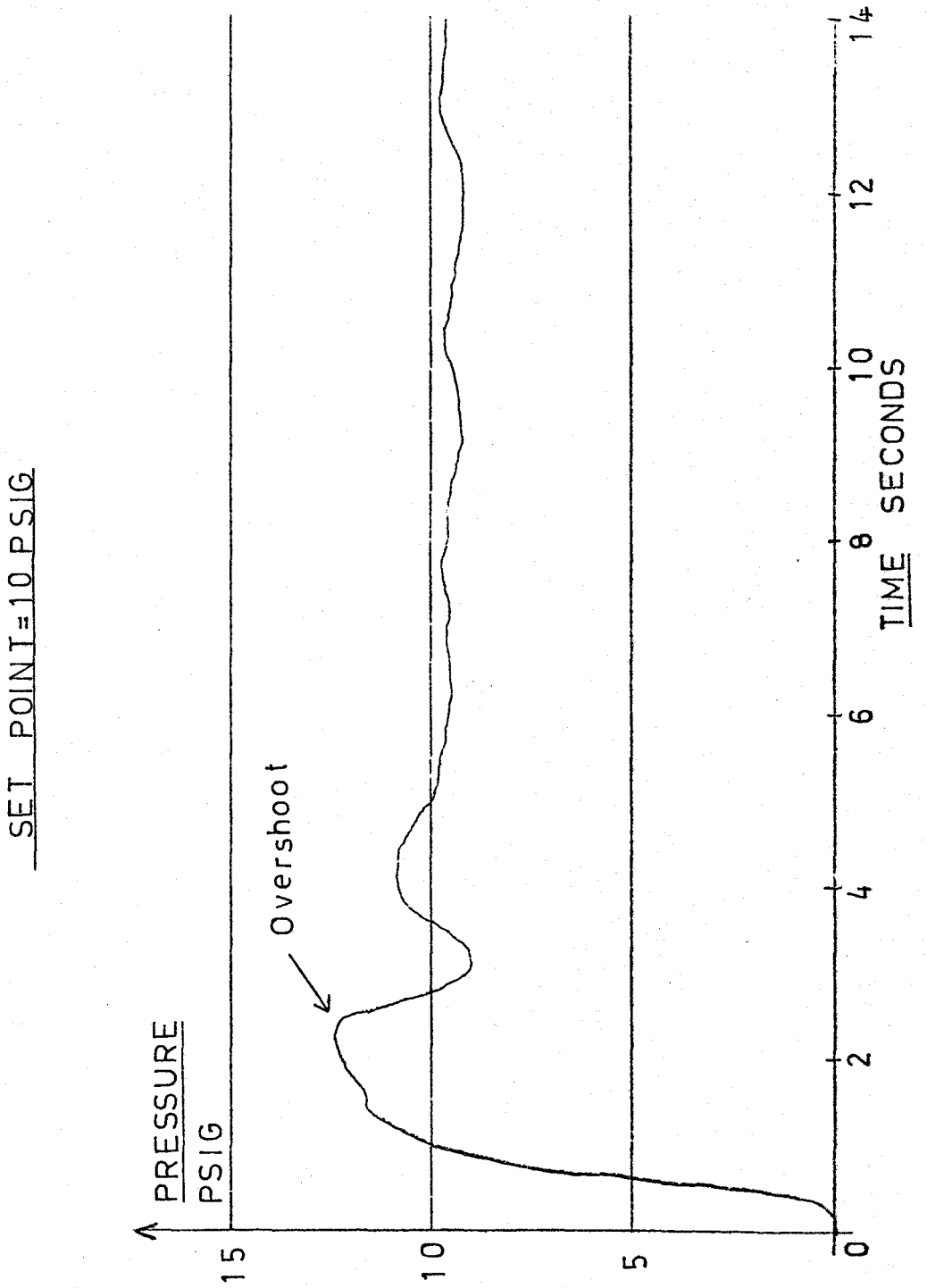

Figure 45 Illustration of Pressure Overshoot using Incorrect Initial Value Area.

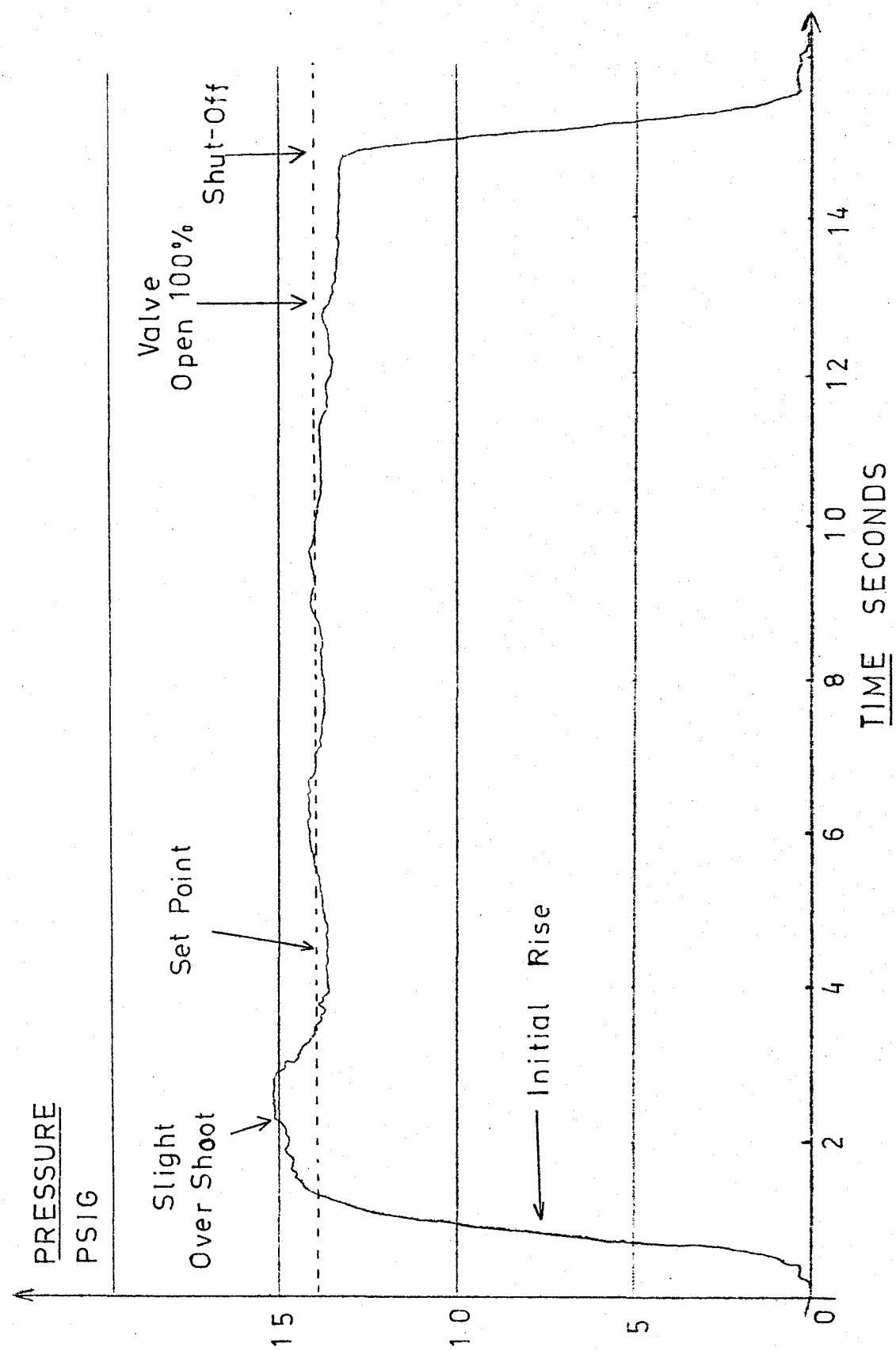

Figure 46 Illustration of Correctly Controlled Pressure

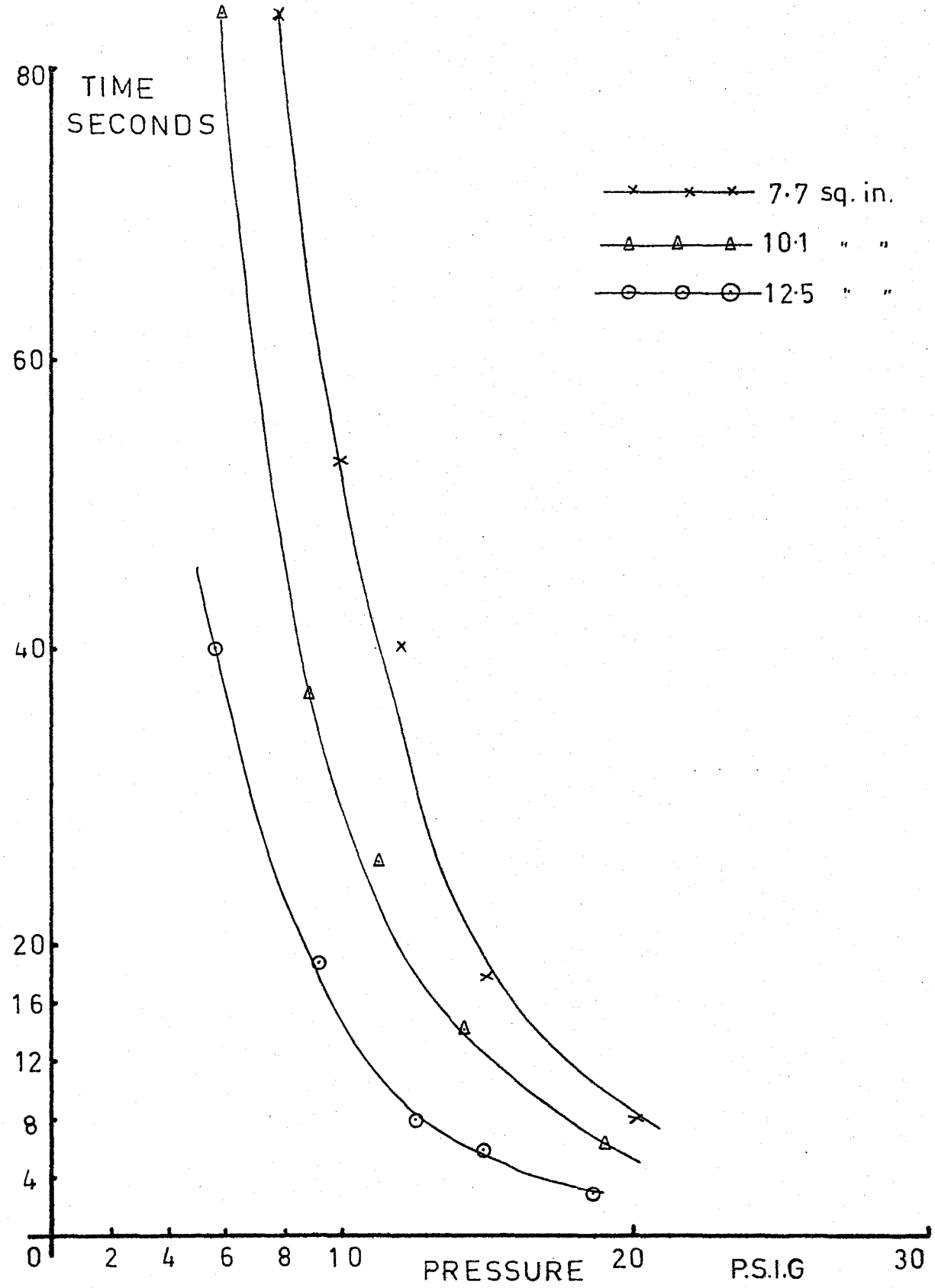

Figure 47 Total Running Time Available at Different Pressures and Throat Areas

4.2.6 Noise Levels during Wind Tunnel Operation

Any high speed aerodynamic system is accompanied by noise. This is especially true in this case since the cascade tunnel terminates in a series of choked turbine nozzles exhausting to atmosphere with consequent high shear rates and turbulence generation. The compressor is also noisy and noise levels are plotted for the compressor alone, and for the test rig during operation, at various points in the vicinity of the rig (see Fig. 48). Ear defenders were worn at all times. The Applied Dynamics Laboratory where the wind-tunnel is located is fortunately designed to contain high noise levels, the walls are designed to reduce noise by 60 dB and all exit planes are well sealed.

4.3.0 The Choice of Control Parameters

From the experience gained we can determine the following for a given desired pressure ratio at known flow area:-

(a) Initial control valve setting (Fig. 39)

(b) Timer setting (Fig. 41)

(c) Feedback loop settings (Table 5)

(d) Expected running time (Fig. 47)

The procedure is as follows:- The minimum flow area in the system (usually a choked throat) is found. From this value and the desired pressure ratio an initial valve opening is derived from Fig. 39. The set-point is set on the controller, and the valve set to the correct

TABLE 5

CONTROL SETTINGS

METHOD	PROPORTIONAL %	RESET MINUTES	RATE TIME MINUTES
Theory	140	0.0155 to 0.0067	0.0155 to 0.0067
Exptl. (Valve open <90%)	125	Minimum <0.015	----*
Exptl. (Valve open ≥90%)	150 to 200	0.015	----*

* see text

NOTE: RESET ≡ INTEGRATING LOOP

RATE ≡ DERIVATIVE LOOP

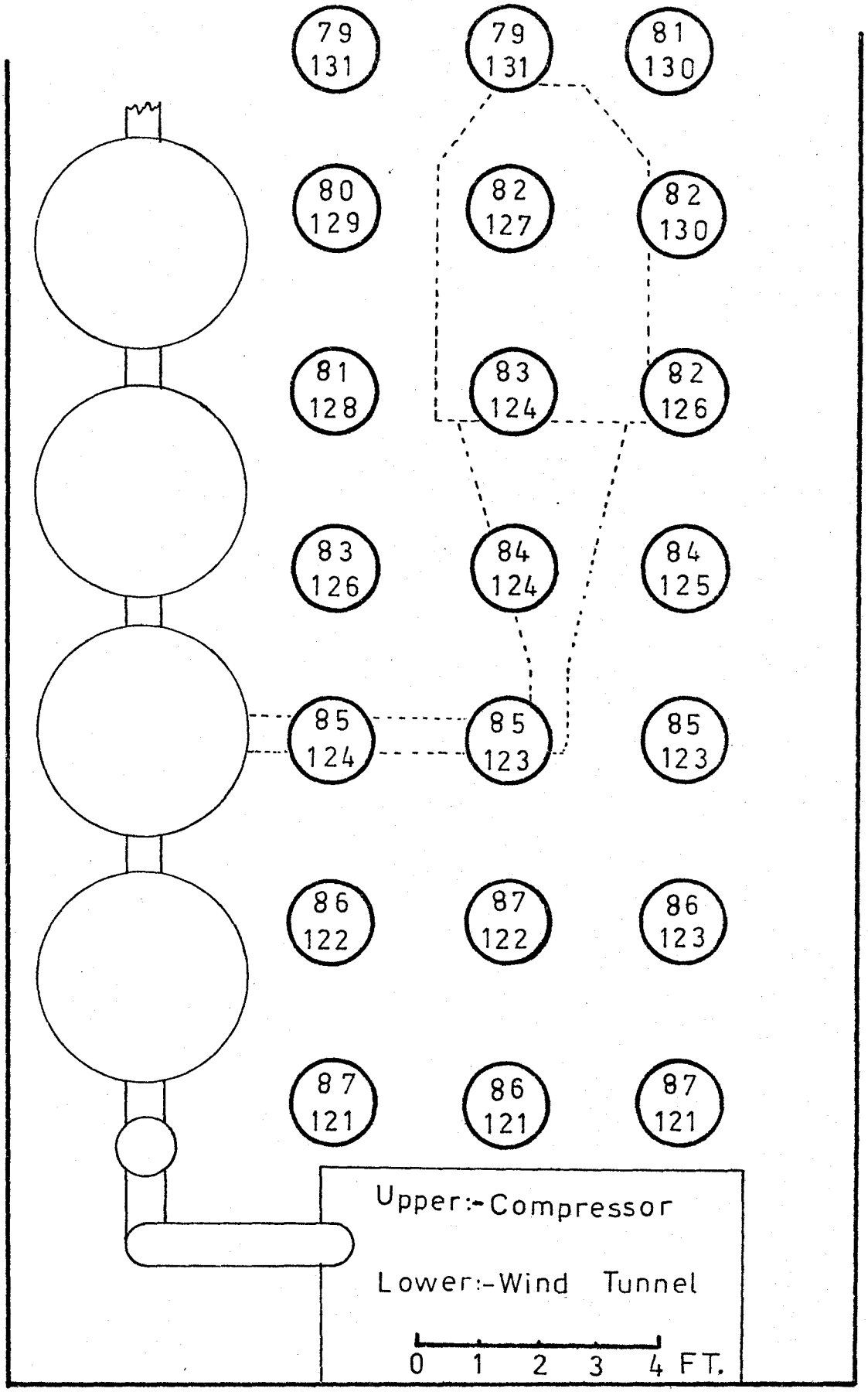

Figure 48 Noise Levels Measured in dBA in the Immediate Vicinity of the Test Rig for Operation of the Compressor alone and Wind Tunnel plus Compressor.

initial opening using the manual control. For any given valve opening the timer setting can be found by using Fig. 41 and adding 0.5 second to the value shown.

4.4.0 Discussion of the Wind Tunnel Performance

The wind tunnel has been developed to the point where it can confidently be used for pressure ratios up to 3:1. The running times obtained are sufficient when using data gathering equipment such as scani-valves. Alternatively pressure trapping systems might be employed. This subject is discussed further in chapter 5.0.

The most undesirable aspect of the system at present is the fact that both main valves are operating at their maximum flow limit for much of the time and excess pressure drops are unavoidable. Also pressure drops in the line and bends are appreciable since velocities up to M = 0.4 are possible in the straight portion of the pipe. An increase of valve and line size to 6" would put the control valve in its linear range and also reduce undesirable pressure drops.

The tunnel provides flows of the correct range of pressure ratios and velocities required for turbine blade testing. The total temperature varies slightly during a run. This variation is due to the polytropic expansion process in the reservoir system, and is common to all blow-down installations. In our case the variation is relatively small. For a typical test run at a pressure ratio of 2.0:1, the end of run total temperature has dropped to approximately $505^{o}R$ from an initial

value of $530^{o}R$. This will cause a small variation of Reynolds number, but for constant controlled pressure ratio, blade inlet Mach number is constant. Initial test section Reynolds number is 3×10^{5} based on a length of one inch. The calibration of the inlet flow for angular deviation and total pressure variation is discussed in Chapter 6.0.

CHAPTER 5.0 INSTRUMENTATION

The major problem associated with using blow-down wind tunnels is the fact that stabilised pressures and velocities are available for only a comparatively short period of time, of the order of ten or fifteen seconds. Most of the information that we require to define our flow, upstream of the blades, in the blade passage, and downstream of the blades is either primarily pressure information or velocities and flow directions deduced from pressure measurements. There are three basic methods of obtaining experimental information in such circumstances:

(a) Pressure trapping methods, such as guillotine manometers or solenoid controlled valves. (Fig. 49)

(b) Digital sampling and recording of pressures measured by individual transducers, or one transducer with a scanning valve connected to several input pressures. The scanning valve being driven by a stepper drive motor. (Fig.50)

(c) Use of a continuously motor driven scanning valve connected to a transducer with an electrical output, together with continuous analogue recording of the output signal Fig. 51.

We will examine each of these methods briefly. Method (a) has the major disadvantage that for the pressures envisaged for turbine blade testing (of the order of 30 psig) the manometers would have to be large, mercury filled and costly. Also the guillotine mechanism is

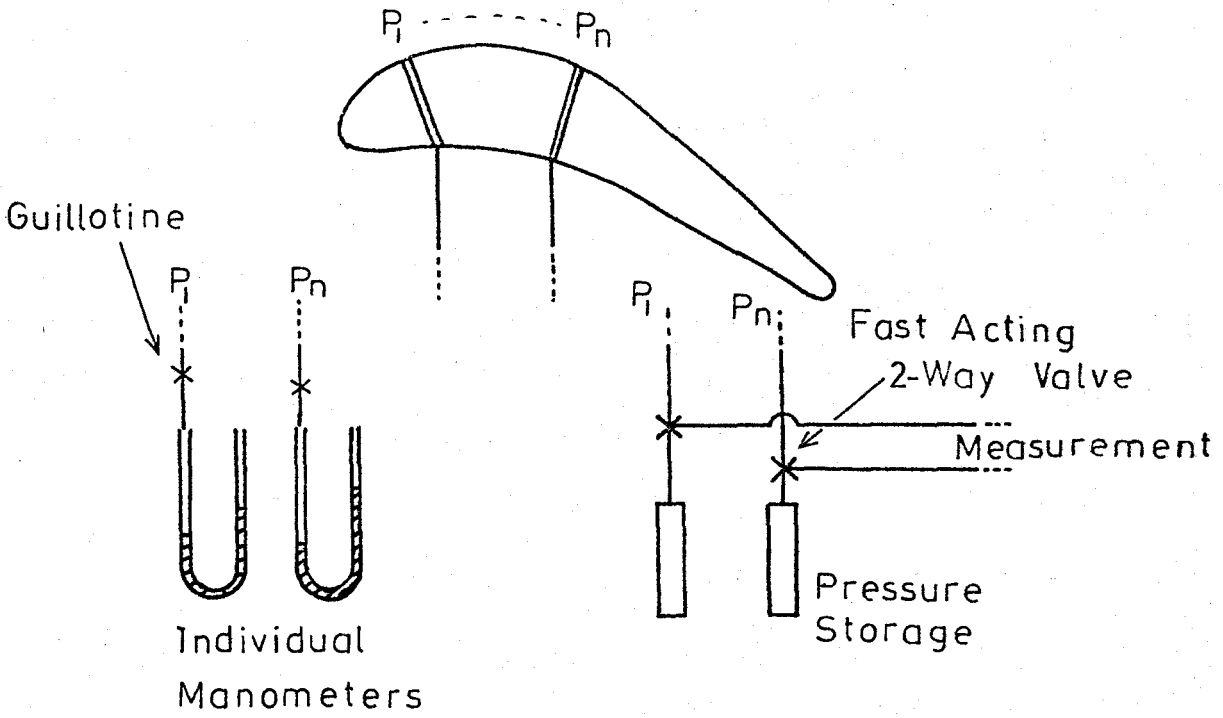

Figure 49 Schematic of Pressure Trapping Systems

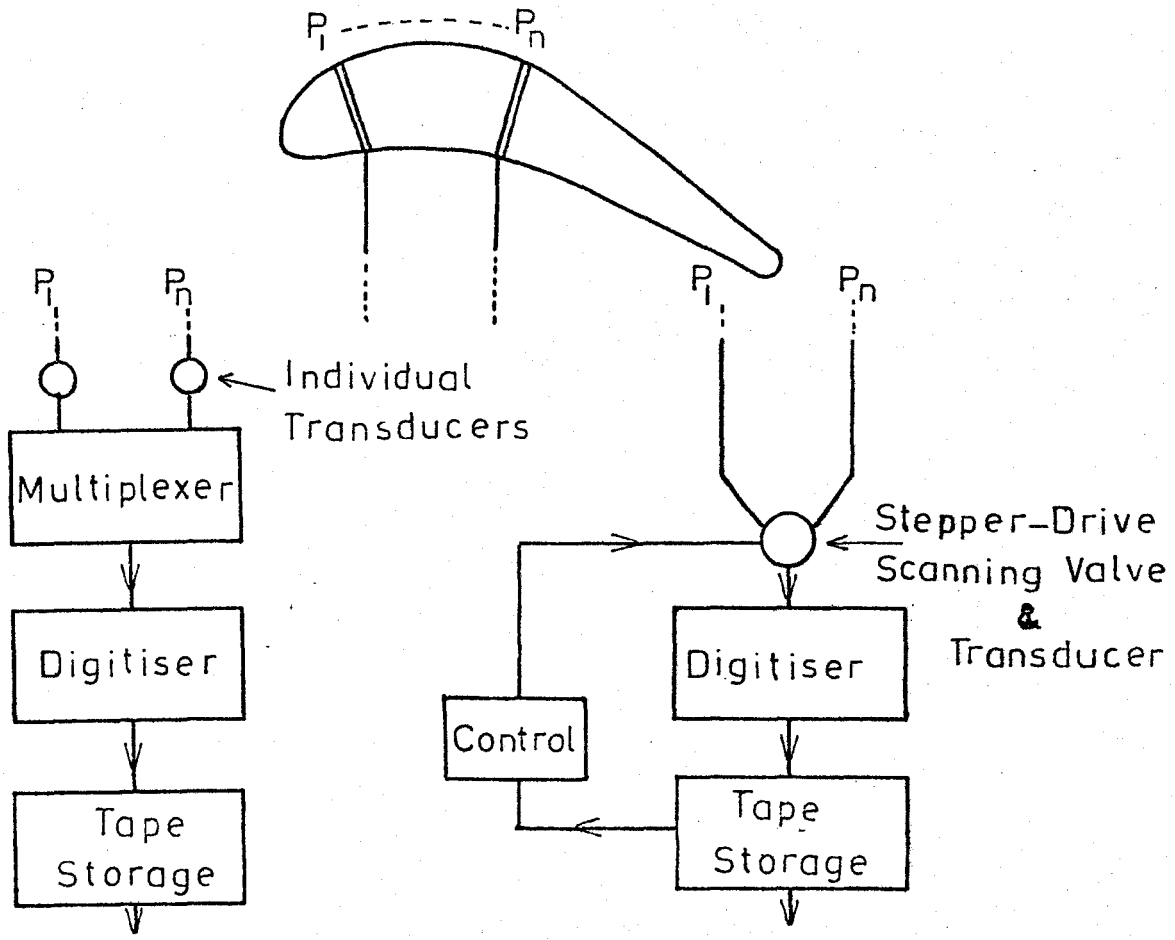

Figure 50 Schematic of Digital Data System

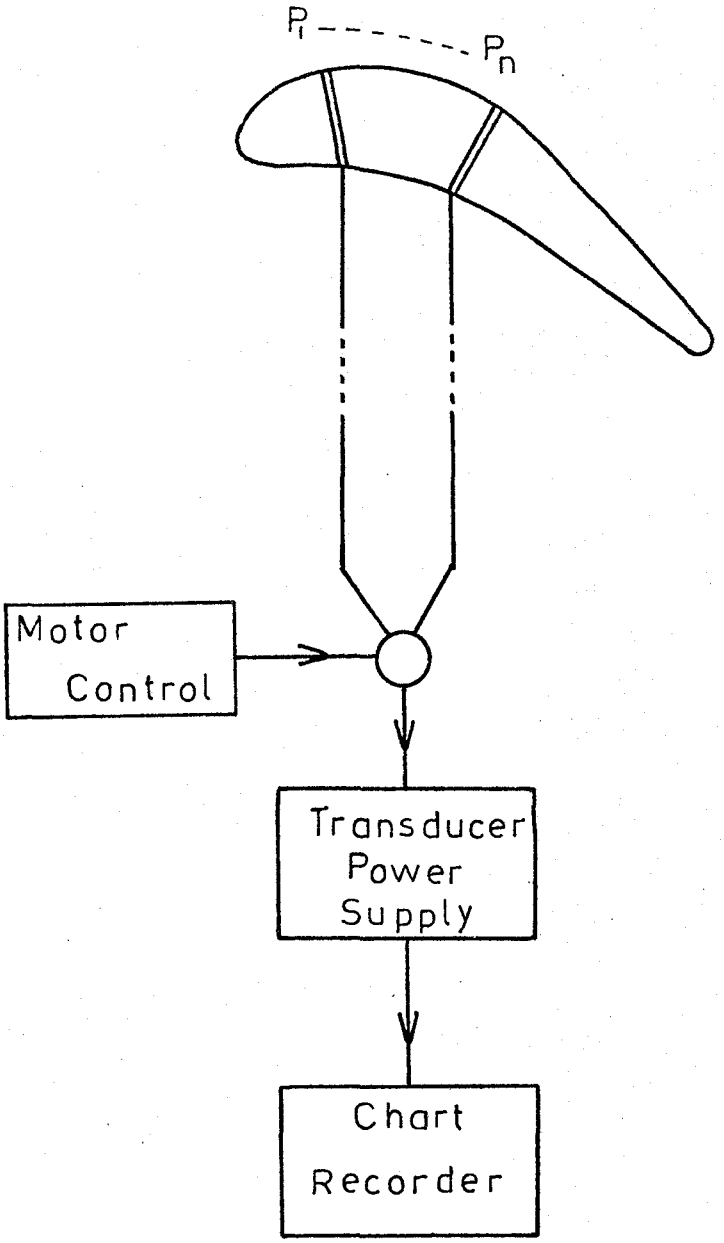

Figure 51 Schematic of Analogue Pressure Measuring System

a source of errors due to leakage. The very slow response and large internal volume require either many individual runs to reach equilibrium, or using a slave air system to "top" each tube up to near the expected final reading. Similar problems occur with bottle pressure trapping systems of the required quality, each individual bottle and its associated hardware costs approximated $500 commercially, thus for a minimum useful number of pressure taps of 10 say, large expenditures are necessary.

Method (b), the digital system, would be preferred given unlimited funds and time, if the same series of measurements were to be carried out on a series of similar blades. Experience with similar systems at the National Research Council and Orenda Engines Ltd (31, 32) suggested bare minimum costs of the order of $20,000 for a good system. Generally a great deal of "debugging" is necessary since it is very easy to record and process spurious signals with little chance of checking them until some time after each run.

Method (c) was chosen because the continuously driven scanning volume is relatively simple and reliable, and only one transducer is calibrated eliminating the problems of different zero drift and hysteresis experienced with multiple transducer systems. Another advantage is that the internal passages and volume of the transducer are all very small reducing the rise time in the system (see section 5.7). Ready availability was another factor in the choice. This system when used with a paper chart and pen type of recorder also offers the advantage that measured pressures can be visually checked during the run.

This enables great economy in total running time and cost since the test rig can be shut down immediately on achieving the desired results, thus reducing pumping time before the next run.

The chosen instrumentation, and ancillary equipment is described in the following sections of this chapter.

5.1 Instrumentation for the Upstream Flow

Knowledge of the flow in this region is vital, particularly with respect to the inlet boundary layers, since they can influence the flow over the blades to a great extent. Also the degree of free stream turbulence is important since it greatly effects the boundary layer growth on the blade surface.

To measure free-stream turbulence a simple miniature hot-wire probe manufactured by D.I.S.A. Ltd was used (Type 55A22). Outputs in the form of bridge D.C. voltage and bridge r.m.s. A.C. voltage allowed the measurement of turbulence without direct calibration using King's law (see section 6.1). The probe was however set up and the stability of the system checked at lower speeds (M≈0.1) using the calibration nozzle described in greater detail below (section 5.2).

Typically a cascade of blades is set up with sufficient number of blades (in our case 16) so that the central portion of the cascade (say the middle 5 blades) experiences a uniformity of both inlet and outlet flow angles and pressures (see Fig. 52). To verify this assumption the inlet flow immediately ahead of the blades was tested

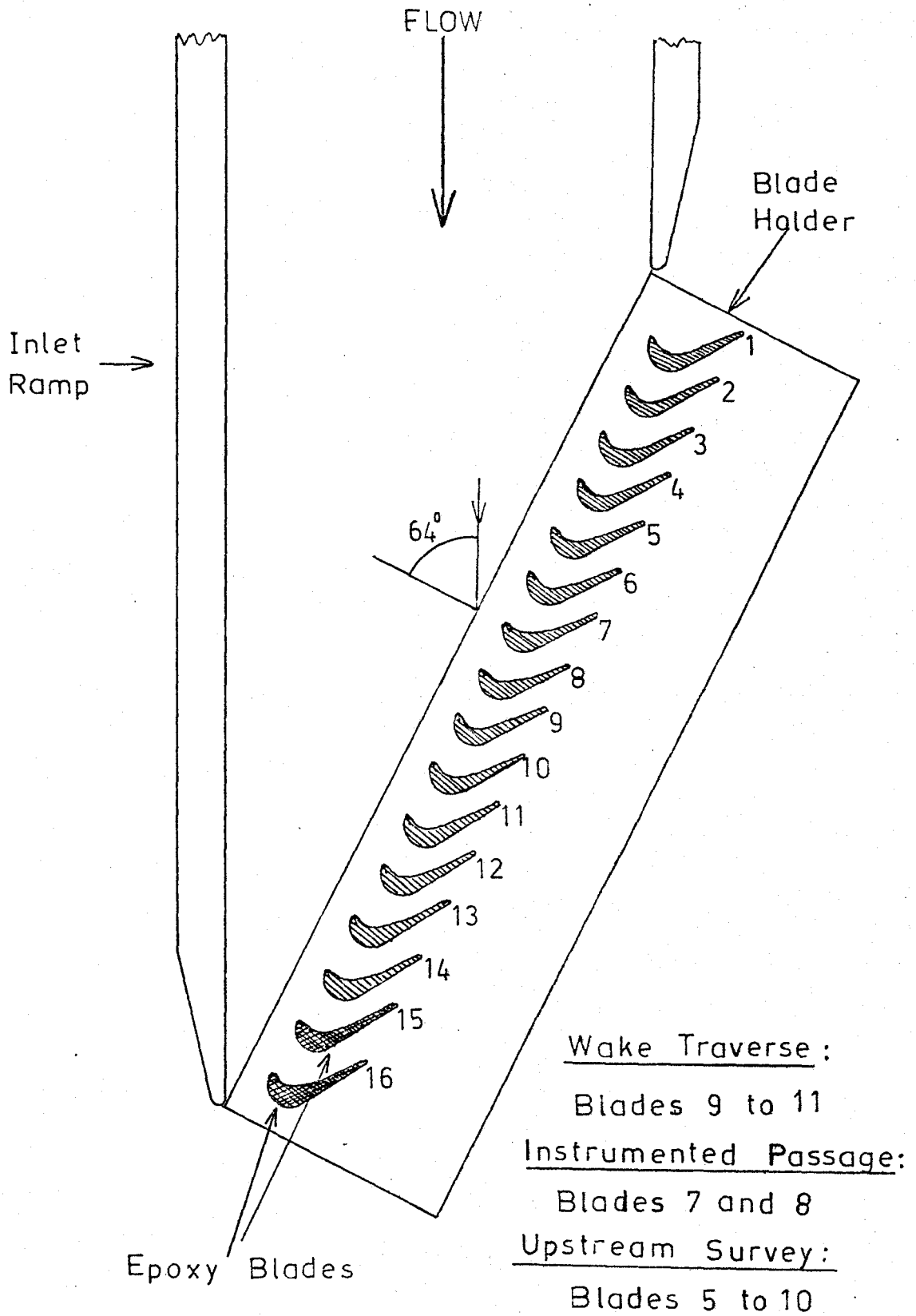

Figure 52 Arrangement of the Blade Cascade

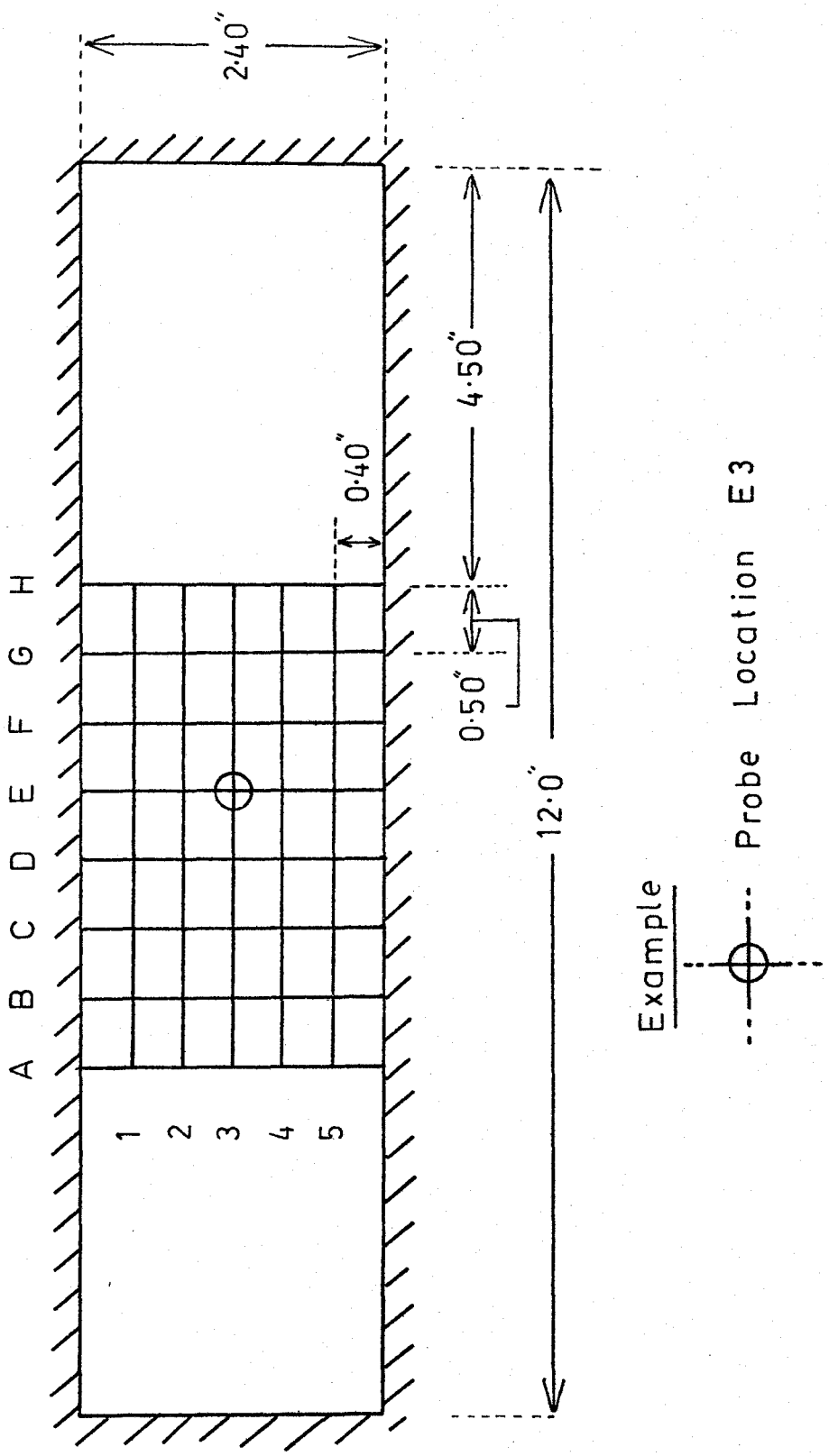

Figure 53 Position Grid used for Calibration of the Upstream Flow

at a number of points on a rectangular grid (Fig 53) in the manner suggested by Pope (33). A directionally sensitive probe of the "Cobra" type was used, the dimensions of which are shown in Fig. 54 . This probe has three pressure sensitive elements. The first is a forward facing tube which generally measures total pressure accurately to ± ½% over an angular range of ± 10^{o} (Refs 34, 35 36). The two other pressure taps on the probe are used to sense flow angular information. A yaw angle in the flow relative to the probe head will generate a measurable differential pressure. This type of probe can be used in one of two ways:

(a) As a null-seeking probe in which the probe is rotated until it faces dir ectly into the wind, the angle being read off a scale fixed relative to the tunnel axis.

(b) As a calibrated probe which is set up in one position relative to the tunnel axis, angular information being derived by comparing the differential pressure generated between the side parts to a calibration chart.

In our case it was chosen to use system (b) because once calibration of the probe is performed the tunnel running time is greatly reduced, since it is not necessary to keep resetting the probe seeking the null position. The null method is however more accurate, especially where large deviation angles (say 5^{o} and greater) are expected. (34, 35, 36). Use of the cobra probe also facilitates measuring tunnel total pressures as well as flow direction simultaneously. Our probe, as manufactured by United Sensors Corp. Ltd was of

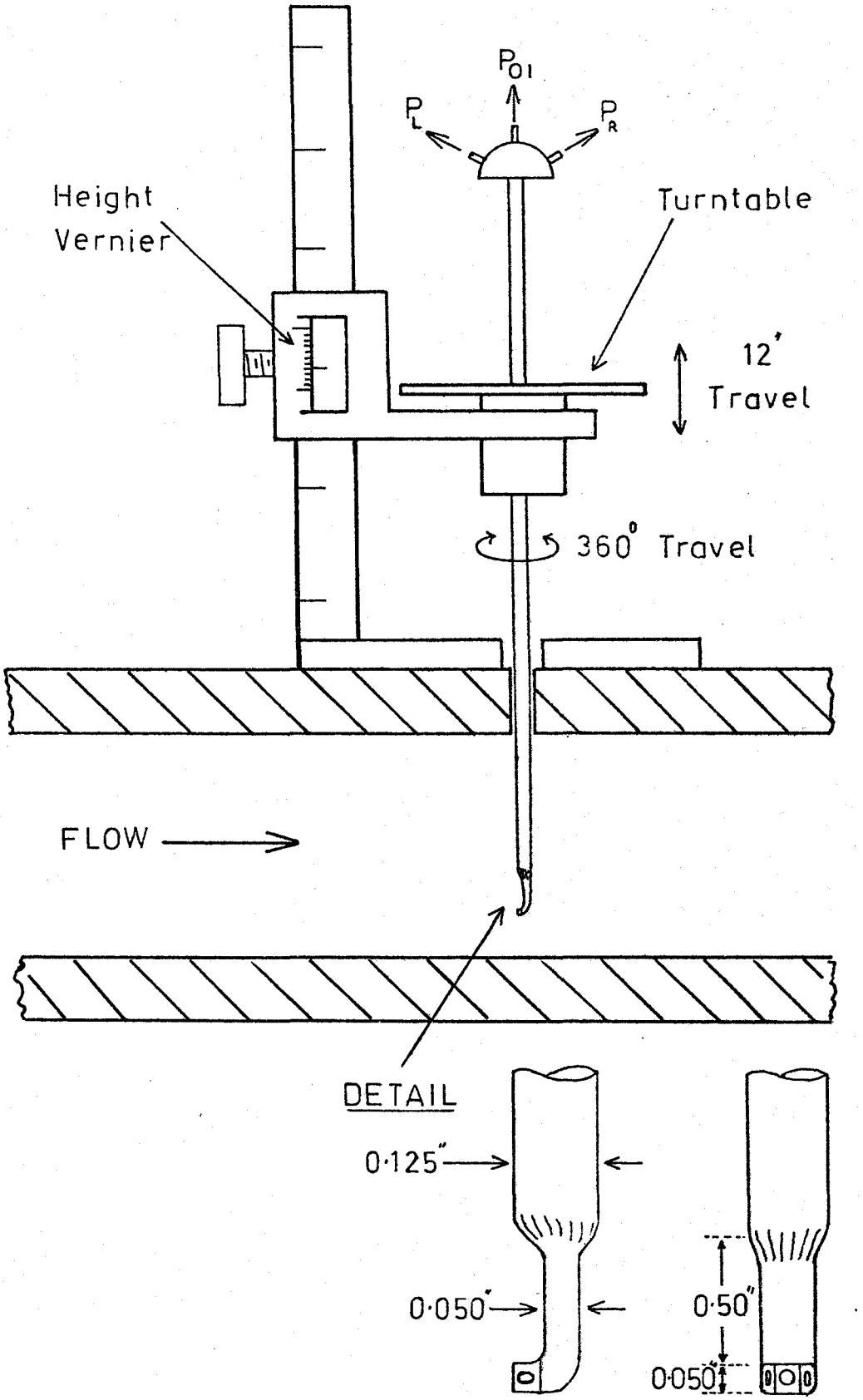

Figure 54 The Cobra Probe Traversing Gear and detail of Probe Head

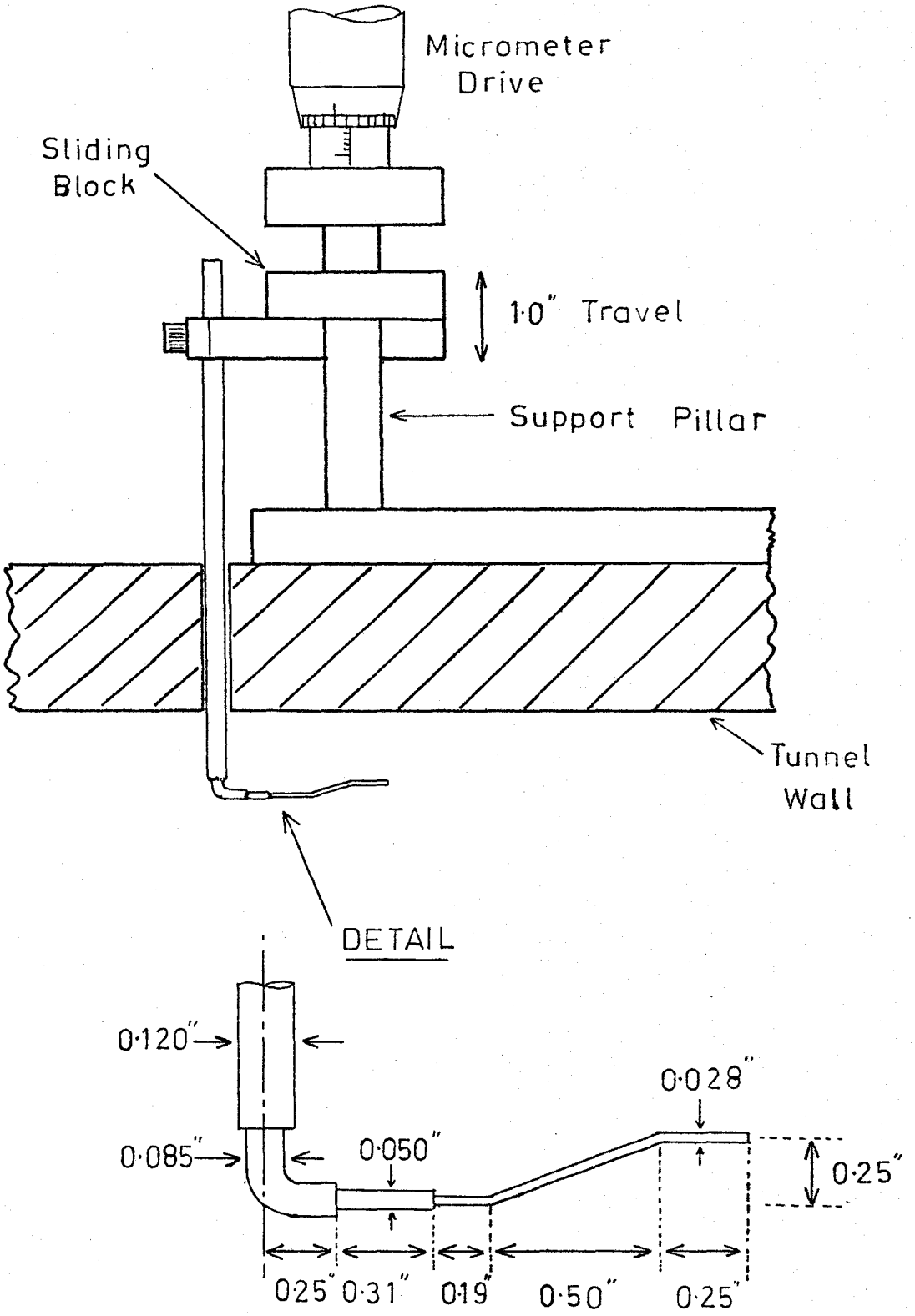

Figure 55 The Boundary Layer Probe Traversing Mechanism and detail of the probe head

sufficiently small dimensions to be regarded as a point relative to test section size (5.5" x 2.4").

To measure the boundary layer thickness on the top and bottom surfaces of the tunnels, the total head was recorded at a few points using the cobra probe. In this case however the probe is now too large relative to the typical flow dimension, (boundary layer height < 0.4"). A special boundary layer probe was thus constructed of the form shown in Fig. 55 . The tip of the probe was some 0.028" in diameter. The tip was not flattened in our case as it was felt that this was small enough for a valid check of boundary layer thickness. The "cranked" design of the probe head is used to reduce stem and support effects on the measurements, boundary layers are far more sensitive in this regard than free stream flows. The cobra probe was supported on the simple linear traversing gear shown in Fig. 54 The boundary layer probe used a more sophisticated design with a micrometer drive allowing more accurate positioning (Fig. 55).

5.2 The Calibration Nozzle

The sensitivity of cobra probes is a function of Mach number and less important than the Reynolds number. Also with most probes, unless one uses exceedingly high construction standards, the system will not be perfectly symmetrical. For this reason it was necessary to calibrate the probe in a known flow field of good accuracy. A carefully constructed calibration nozzle giving a low turbulence potential core

some 0.8" in diameter was available in the department. This nozzle has been very carefully checked for flow uniformity and turbulence level. (Ref 37). The nozzle uses a contour, one of several, suitable for wind tunnel contraction design, the curvature being arranged to give a flat velocity profile at the exit (Ref 38).

To achieve the Mach numbers necessary (0.4 to 0.65) it was modified by using a high pressure (100 psig) air line as the supply source, using pressure reducing valves to give plenum pressures of up to 5 psig. The exit plane of the nozzle exhausted to atmosphere (see Fig. 56). The scanning valve, transducer and chart recorder were used to record differential pressures, thus reducing the number of separate calibrations needed. The system was then transferred complete to the cascade wind tunnel eliminating wherever possible errors due to using different equipment for calibration and cascade testing.

It was necessary to settle on an arbitrary zero point at which the two side ports measured very nearly the same pressure. Once the probe was fastened to the turntable which carried it, and was no longer disturbed with respect to this turntable, then a calibration curve of the shape shown in Figure 57 was derived. If P_R was the pressure sensed by the right hand tube and P_L was the pressure sensed by the left hand tube the results were non-dimensionalised by the dynamic head $\frac{1}{2}\zeta u^2$ in the form:

$$C_p\psi = \left|\frac{P_R - P_L}{\frac{1}{2}\zeta u^2}\right| \qquad (49)$$

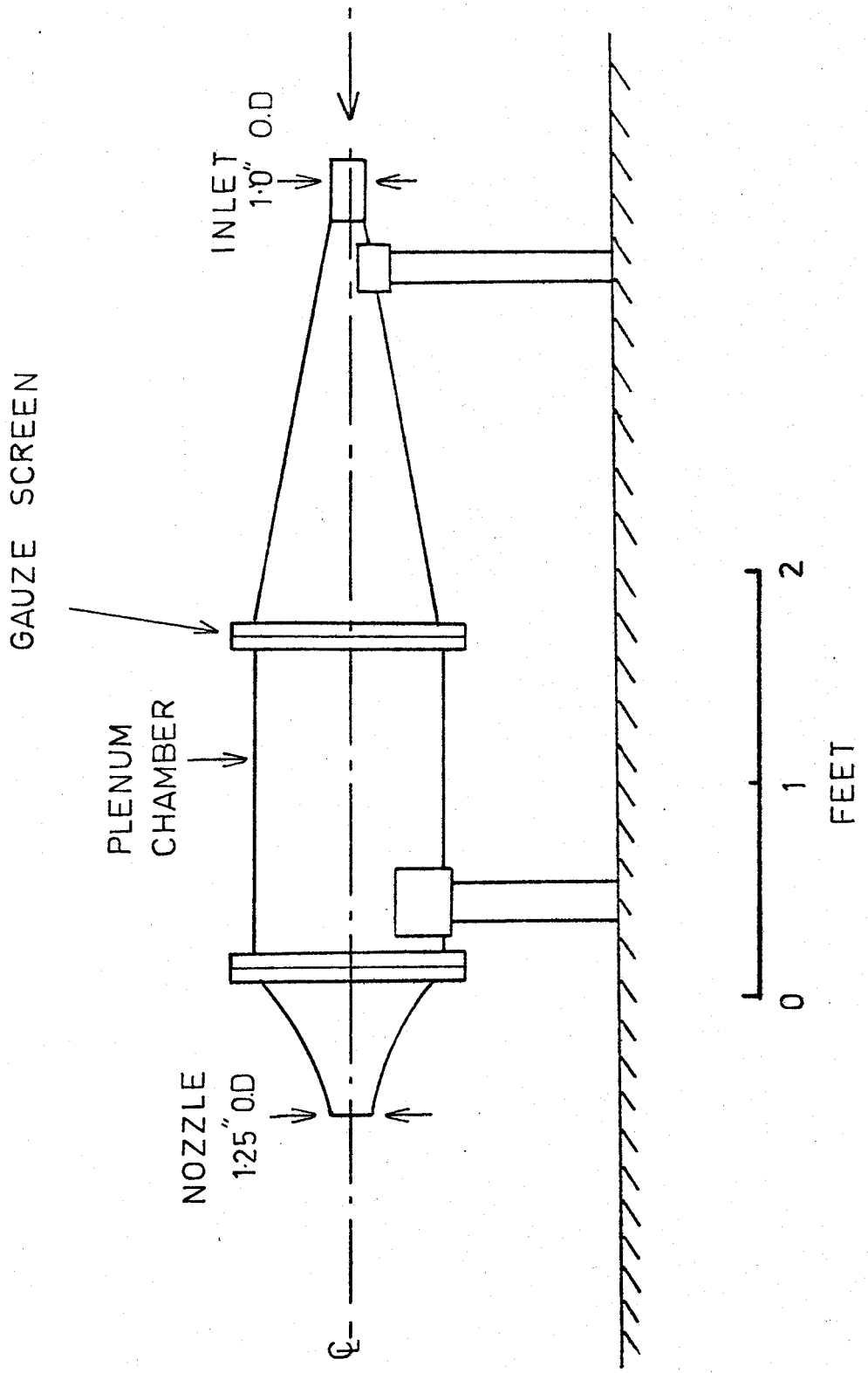

Figure 56 The Calibration Nozzle

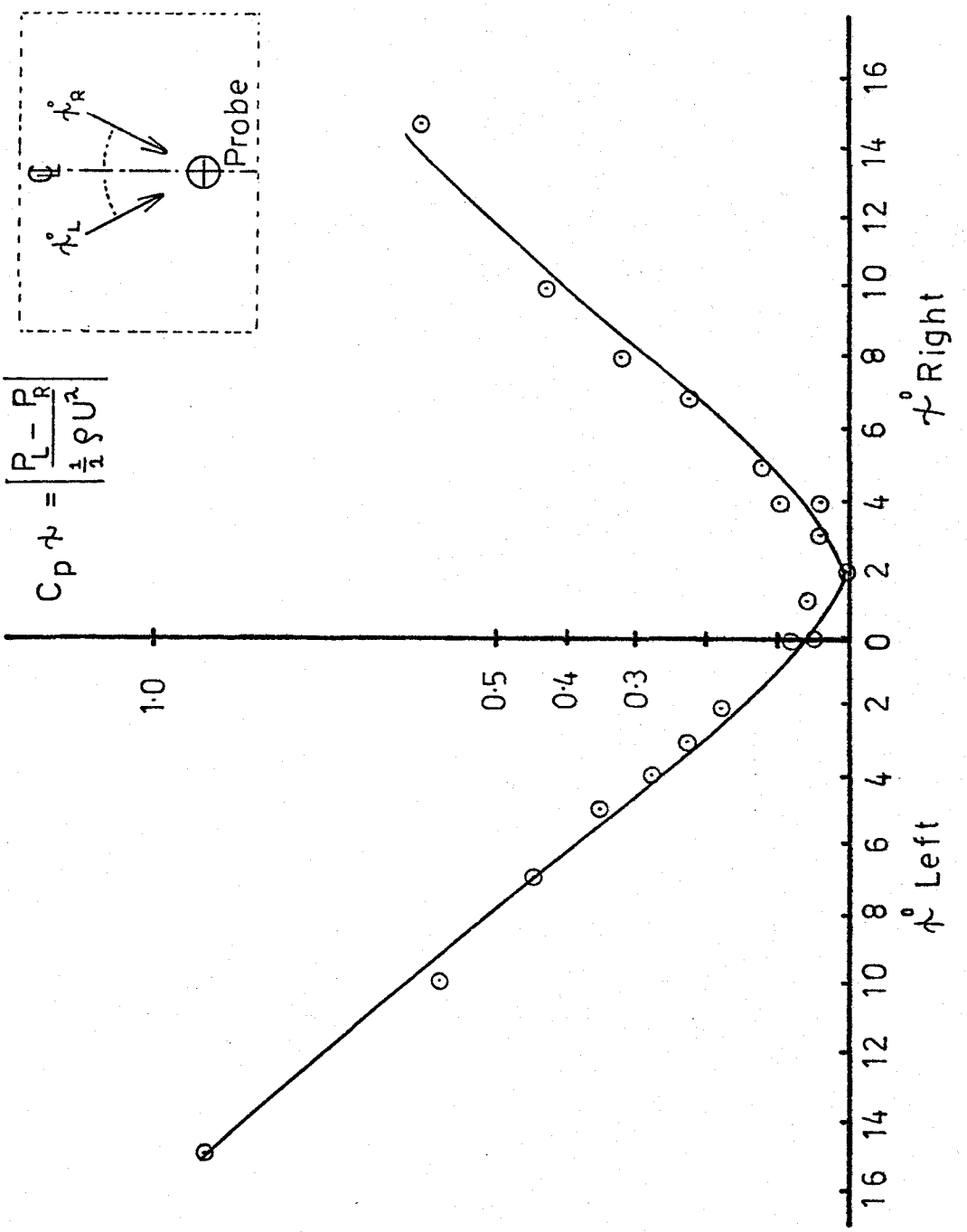

Figure 57 Calibration curve for the Cobra Probe used as a Yaw-meter

Note that the sign inside the modulus is preserved as ψ^{o} left and ψ^{o} right as can be seen by reference to Fig. 57. With further reference to this figure we can see that the whole curve is off-centre (our arbitrary zero) by some 2^{o} but this need not concern us unless the probe is disturbed relative to its holder. It was also found that within the experimental scatter plotted, there was little if any change of calibration with Mach number. This was to be expected since the range of interest was sufficiently small, (M = 0.4 to 0.65). This would not be true if the same probe was used in the incompressible regime (say M = 0.1) or at higher speeds when the blunt shape could cause local sonic conditions. This probe design is relatively immune to turbulence effects by virtue of the sharp corners which deliberately keep the flow over the side parts turbulent at all times.

5.3 Blade Surface Pressure Instrumentation

These measurements were made with the object of verifying the channel potential flow solutions. It was necessary to make these measurements without effecting the flow field. In order to study one particular channel the surface pressure taps were drilled through to the reverse side of the blades. There they communicated with grooves milled in the blade surface. The pressure taps themselves were 0.020" in diameter. The grooves were approximately square in cross section and 0.030" wide. Small diameter stainless steel hypodermic tubing with an I.D. of 0.015" and O.D. of 0.028" were cemented in the grooves using

epoxy resin (see Fig. 58 for details). These hypodermic tubes communicated the sensed pressure out of the top of the blade holder and to the scanning valve via plastic intermediate tubing.

The philosophy behind the particular static tap design shown was to replace unknown errors wherever possible by a known and smaller error. With the design shown the errors in sensing surface static pressure and of the order of ±½% (Ref 36). The tap located in the leading edge was used as a back-up system to measure inlet total pressure. This function was normally provided for by mounting the cobra probe just upstream and slightly off to one side of the blades.

In all a total of 20 pressure taps were used enabling a fairly precise definition of surface static pressure. These static pressure taps were staggered up and down 0.25" from the blade mid-height to reduce the effect of one tap on the next downstream tap (see Fig. 59).

5.4 Instrumentation for Downstream Wake Surveys

For the downstream flow we are concerned with Mach numbers usually in range 0.9 to 1.4. Thus the cobra probe can no longer be used to measure total pressure. Instead two probes with different sensing tips were constructed as shown in Figs. 60 (a,b). For our range of Mach numbers calibration is unnecessary and we can determine Mach number from the formula:-

$$\frac{P}{H'} = \left(\frac{2\gamma}{\gamma+1} M^2 - \frac{\gamma-1}{\gamma+1}\right)^{\frac{1}{\gamma-1}} \left(\frac{2}{(\gamma-1)M^2}\right)^{\frac{\gamma}{\gamma-1}} \qquad (50)$$

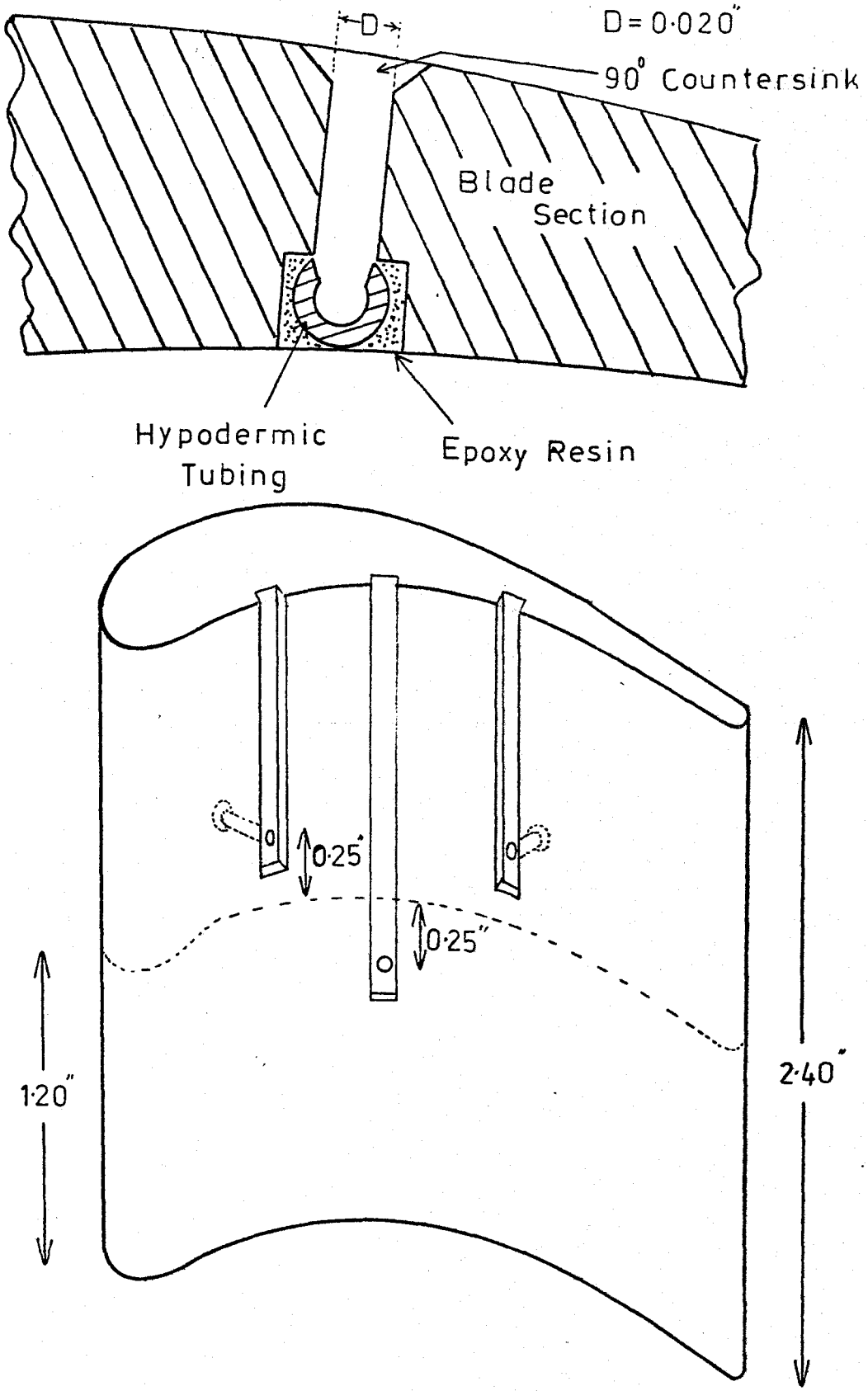

Figure 58 Illustration of the Blade Pressure Taps

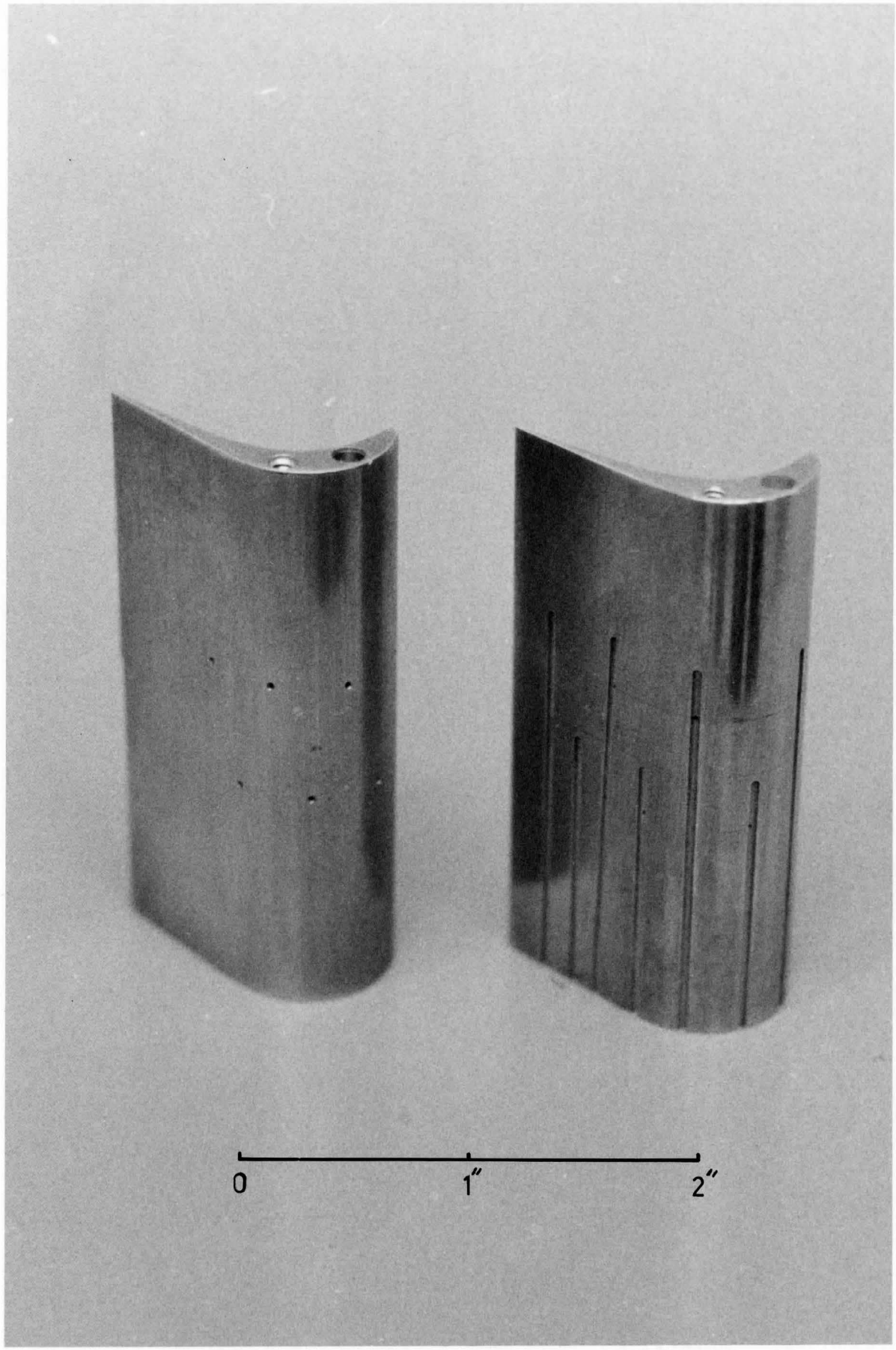

Figure 59 Photograph of Instrumented Blades showing Pressure Taps

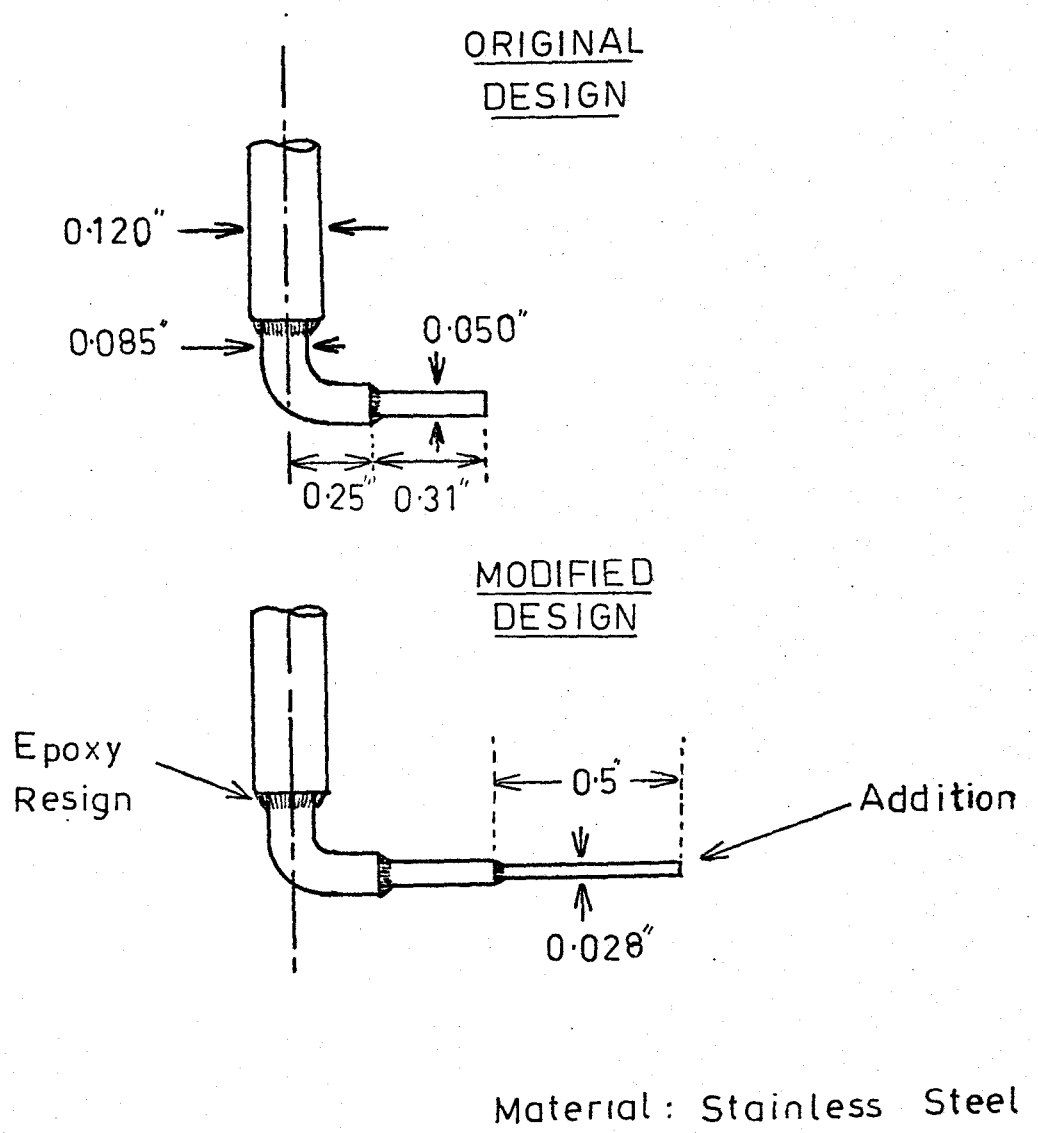

Figure 60 The Total Head Probe in its Original and Modified Form.

which for air with $\gamma = 1.4$ the equation reduces to:

$$\frac{P}{H'} = \left(\frac{7M^2 - 1}{6}\right)^{5/2} \left(\frac{5}{6M^2}\right)^{7/2} \qquad (51)$$

In this formula P is the undisturbed static pressure and H' is the total head measured by a pitot tube. In this situation the measured total head is less than the undisturbed total head due to pressure loss across the bow shock wave caused by the probe. (Ref. 34, 35) To obtain further information at different points within the downstream flow a traversing gear was built which was driven by a small synchronous electric motor (Fig. 61). This was arranged to traverse one of the total head probes across the back of the blade cascade in the direction '$\underline{y}$' shown in Fig. 62. The probe could be set at different heights ('$\underline{z}$') and the whole traversing gear could be bodily moved to allow measurements at different points in direction '$\underline{x}$'.

In operation the electric motor was allowed to spin up to operating speed before drive through the gears was started. This was accomplished by the driving gear being mounted on a smooth 20^{o} taper on the motor shaft. To engage drive the knurled nut was prevented from rotating by the operator, which caused it to wind down its left-handed thread until it firmly clamped the driving gear onto its taper. The system was stopped merely by switching it off. The driving gear could usually be released by finger pressure and the probe carriage was returned to the pre-start position by manual rotation.

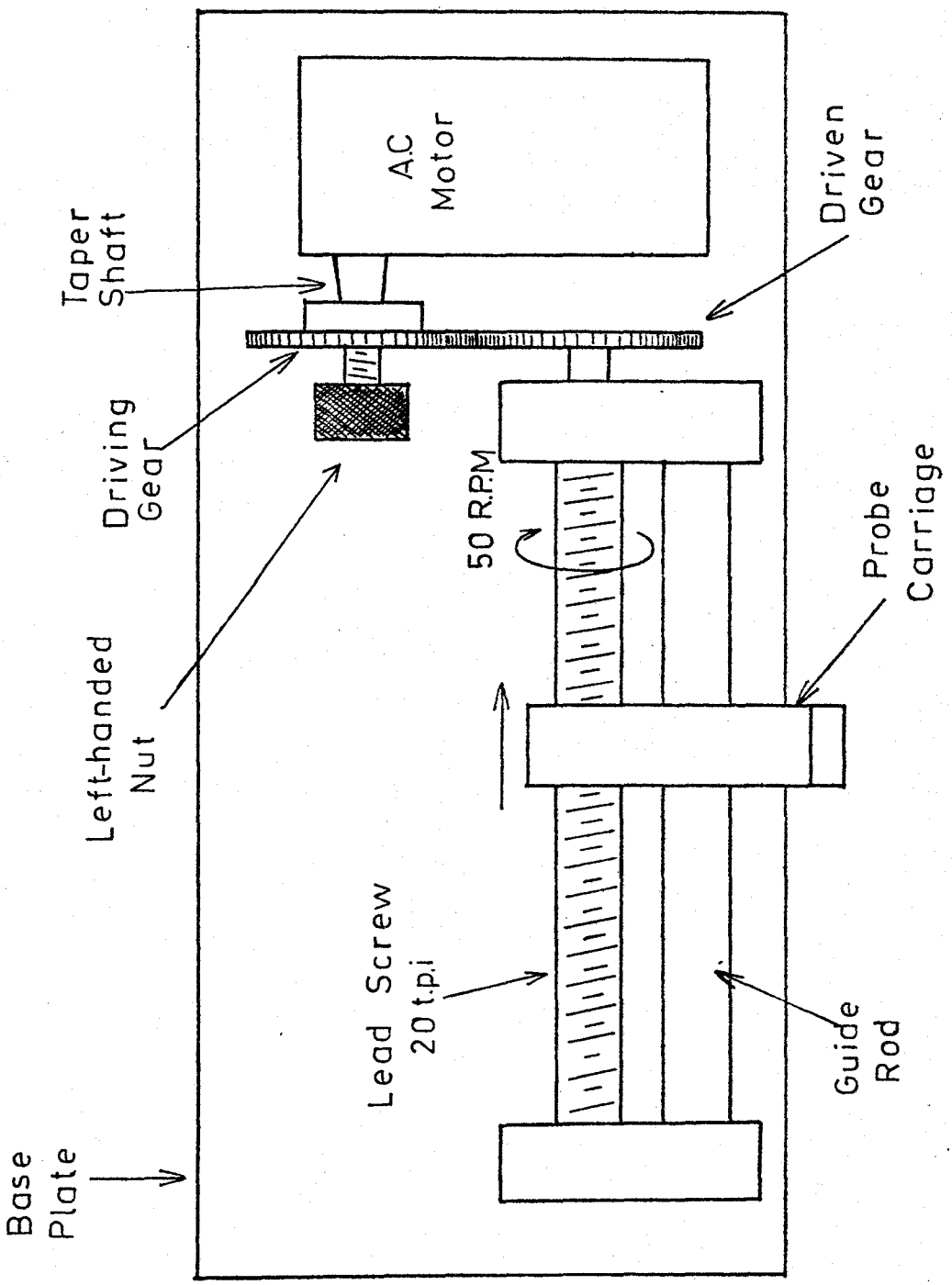

Figure 61 The Motorised Traversing Mechanism

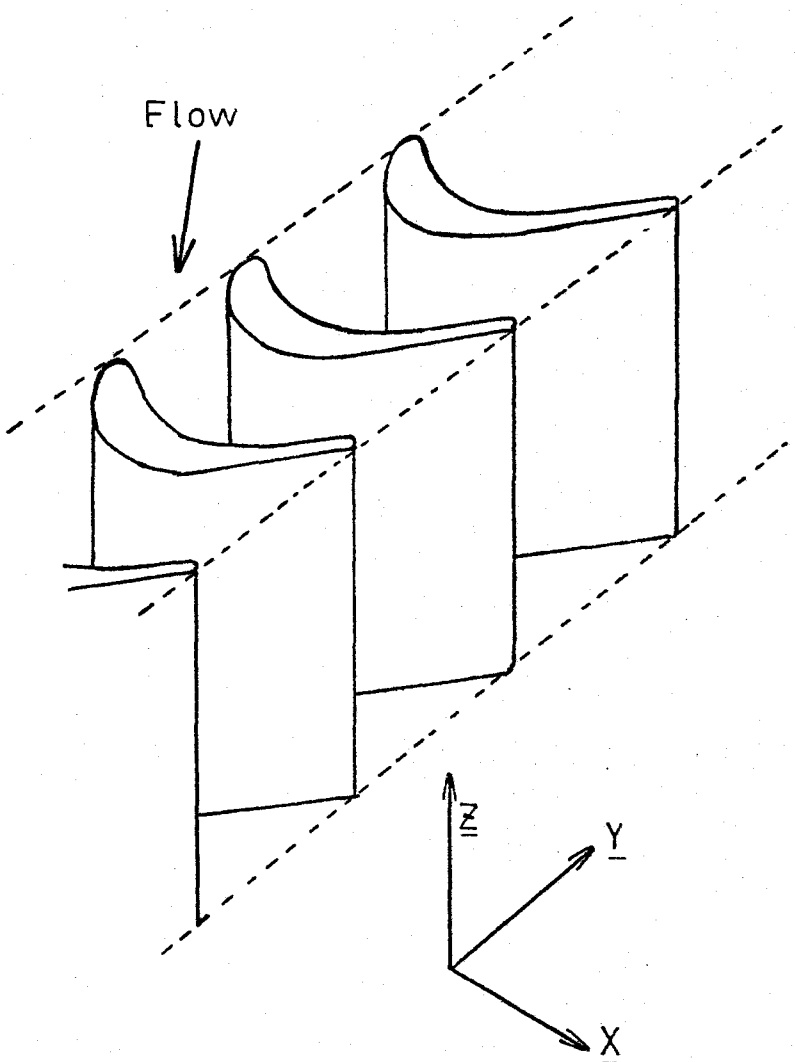

Figure 62 Coordinate Convention used for Measurements made Downstream of the Blade Cascade

5.5. Electrical Output Recording

Electrical outputs were recorded on a 2-pen chart recorder with a response time of 0.3 seconds for full scale. The twin pens allowed the continuous monitoring of upstream plenum pressure by one pen while the other pen recorded the variable of interest in the particular measurement, for example, scani-valve output. Monitoring up-stream pressure continuously also allowed one to choose the correct time to make measurements. The upstream total pressure was also used in the analysis of the data (see Chapter 6.0).

5.6. The Pressure Transducer

The pressure transducer (Druck PDCR-22) was of the diaphragm type using a semi-conductor element strain gauge bridge. The transducer and its supply were temperature compensated to prevent zero drift. This transducer was found to be exceedingly linear and stable, and zero drift was rarely noticeable and certainly not important when expressed as a percentage of full scale. (See calibration curve Figure 63). The transducer was designed for ± 50 psig and thus amply covered the intended range of operation without being used in a range of small pressures where hysteresis errors became important. Air pressures for calibration were supplied by the shop air system through a reducing valve. In the range of interest the Wallace & Tiernan gauge (Type FA 145) was found to be sufficiently accurate for calibration. It was however

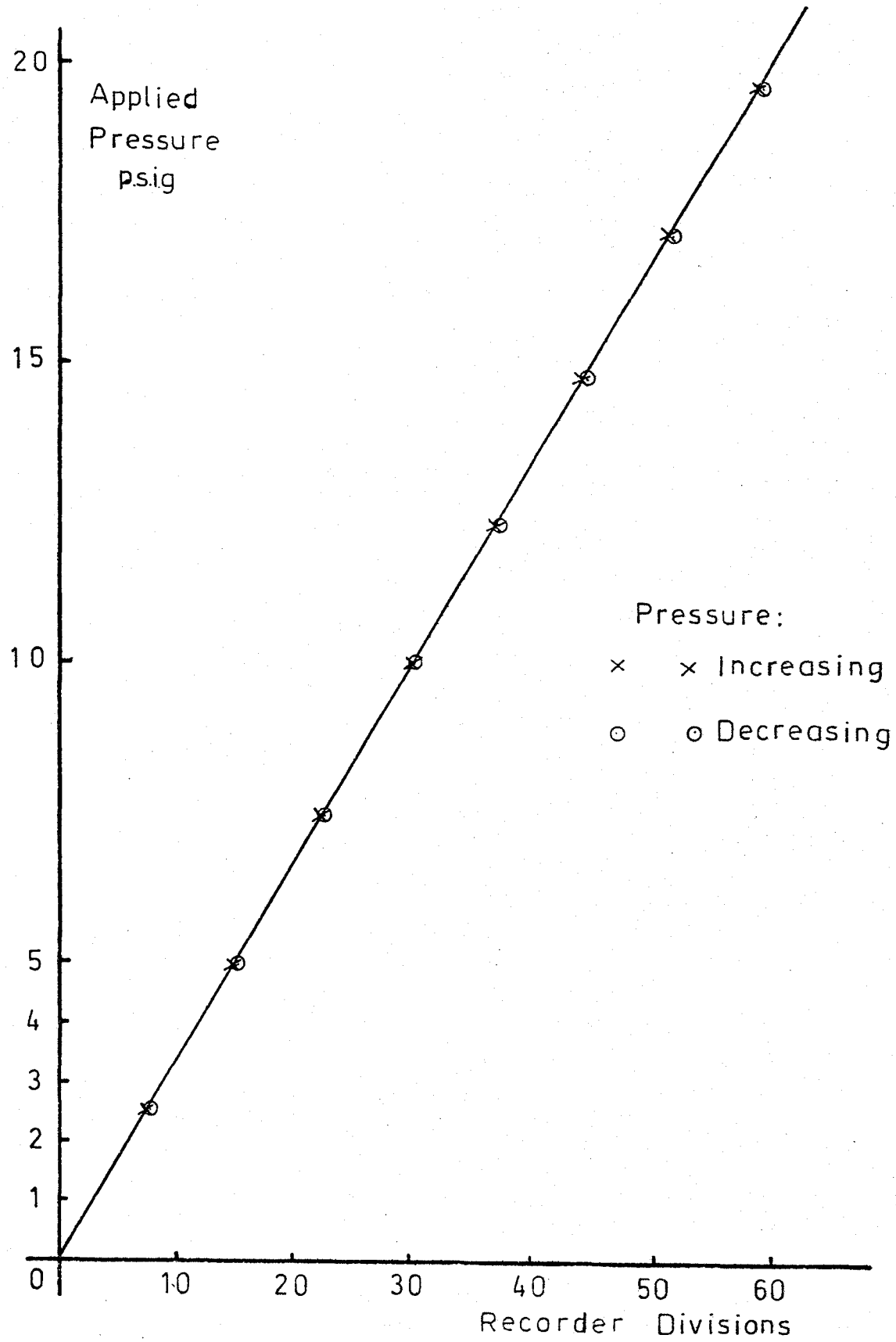

Figure 63 Calibration Curve for the Pressure Transducer installed in the Scanivalve

checked by a dead-weight system to support this conclusion.

5.7 The Scanivalve

A schematic of this system is shown in Fig. 51. These valves are widely used in the aerospace industry since they allow the rapid recording of many pressures using only one transducer. It consists essentially of a series of pressure ports connected sequentially by a rotating radial groove to a central pressure transducer. The pressure ports and central transducer port are located on a fixed highly polished disc. The radial groove is machined in the mating disc which is in running contact. To prevent the discs being separated by pressure forces, the system is balanced by a back pressure on the rotating disc supplied from a slave air supply. This pressure is chosen to be above the average pressure for all the ports, without exceeding the pressure which would cause the lubricating oil film to be squeezed from between the highly polished surfaces.

One problem that can arise with this sort of system is the rise time of the pressure at the transducer face. If it is too long then it would be impossible to measure an accurate final pressure before the scanning valve moved to the next port. This rise time is a strong function of internal diameter of the tubes to the pressure taps. The rise time to a pressure Pf from an initial pressure Pi, with final error e can be expressed by the formula (35):

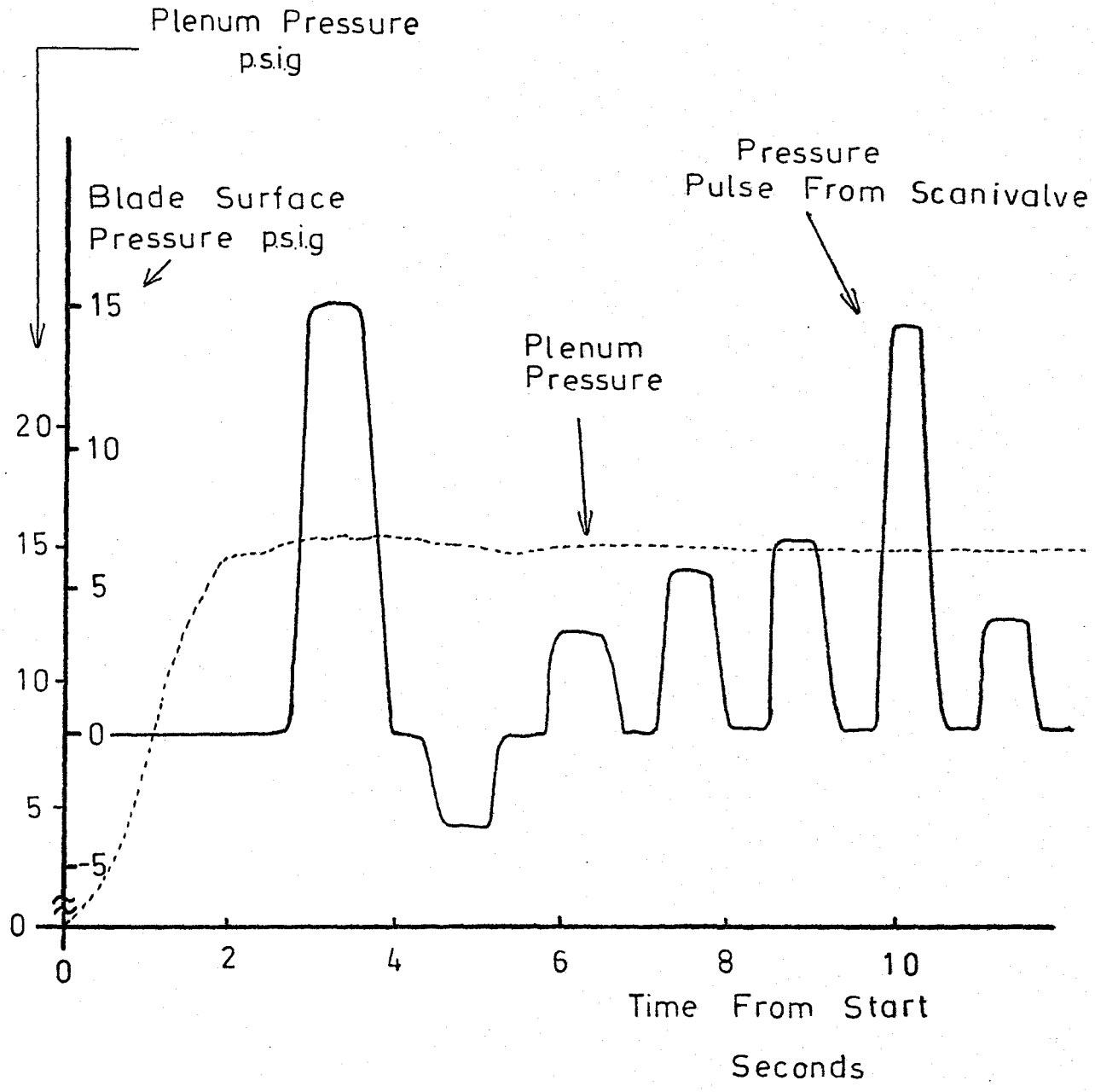

Figure 64 Typical Scanivalve Trace for Measurements made on Turbine Blade

$$t = \frac{l_1\,\alpha}{3P_f d_1(c+1)}\{V_1 + V_2(c^2+3c+3) + 3\,V_m(c+1)^2\} \qquad (52)$$

where $c = \frac{l_2}{l_1}\left\{\frac{d_1}{d_2}\right\}^4$ and $\alpha = 2.47\times10^{-7}\log\left\{\frac{\Delta P(2P_f + e)}{e(P_1 + P_f)}\right\}$

In this equation we have reduced our pressure communication system to two tubes, subscripts 1 and 2 where:-

l_1	=	length of first tube	inches
l_2	=	length of second tube	inches
d_1	=	diameter of first tube	inches
d_2	=	diameter of second tube	inches
e	=	error	p.s.i.
P_f	=	final pressure	p.s.i.
P_I	=	initial pressure	p.s.i.
ΔP	=	difference between initial and final pressures	p.s.i.
V_1	=	volume of first tube	in^3
V_2	=	volume of second tube	in^3
V_m	=	transducer volume	in^3

If we substitute in eqn. (52) for typical values for our system we have rise times to 99.5% of final pressure in a time of 0.050 seconds. This is sufficiently fast that the slowest part of our pressure recording system is in fact the chart recorder.

The system gives traces of the form shown in Fig. 64. It should be noted that only every other pressure port is connected to a pressure

sensing tap. The intervening pressure ports are open to atmosphere. This system allows the transducer to be more discriminating about the values of two pressures with similar absolute magnitudes as it helps eliminate hysteresis effects. It also aids in deciding the correct location of the parts of the trace to be measured.

5.8 Blade Temperature Measurement

It was necessary, for purposes of the boundary layer calculation, to know the blade surface temperature. To this end, a series of 5 thermocouples were embedded flush with the surface of the blade in holes which had been originally pressure taps (fig. 65). These pressure taps were increased in size to .030" to accommodate the thermocouple beads, the lead out wires used the grooves already existing in the blades. The sensing beads were cemented into the surface using a plastic filter material loaded with aluminium particles. The aim was to improve thermal conduction and reduce measurement errors due to distorting the temperature field in the blade. These effects can be significant if the coefficient of thermal conductivity for the cement is widely different from that for the blade material and thermocouple bead. (Ref. 39)

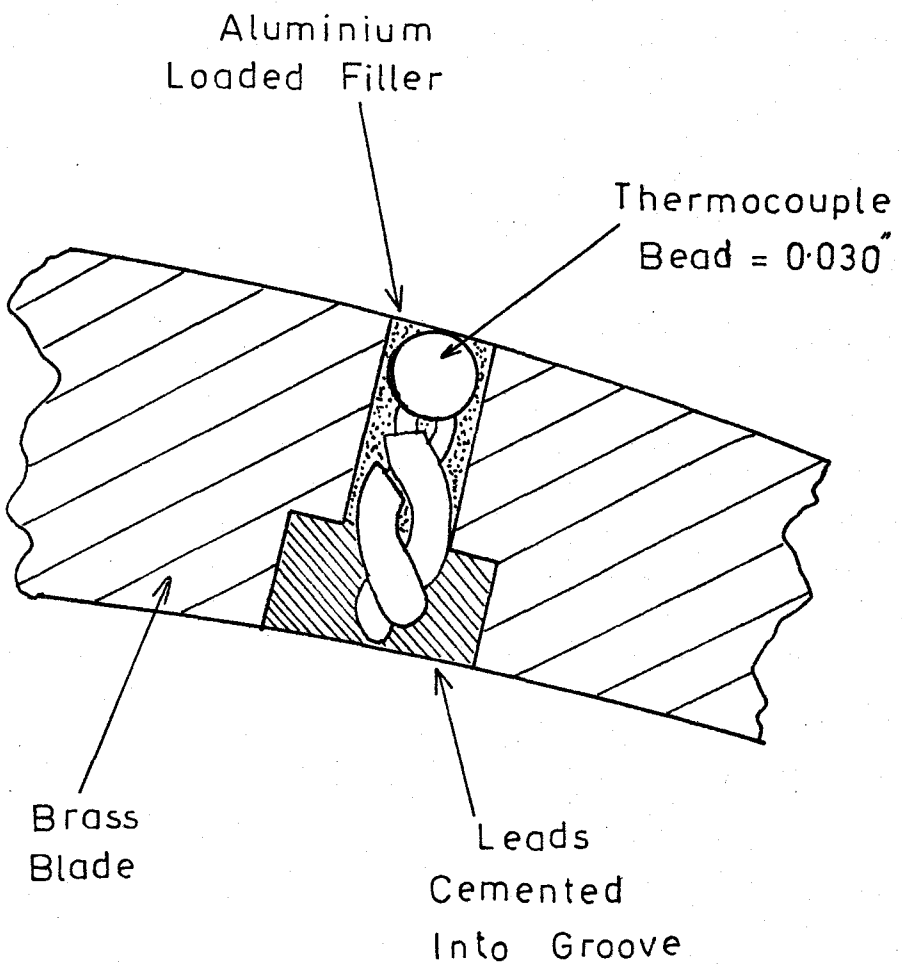

Table 65 Detail of the Thermocouple Installation

CHAPTER 6.0 DETERMINATION OF THE INLET FLOW TO THE BLADES

As in any wind tunnel, the quality of the flow in the working section determines the degree of confidence which can be placed on experimental measurements. This is particularly true in our case since it is known that highly curved turbine blades are very sensitive to input flow conditions. Another factor to be taken into account is that our flow has a time variation as well as spatial variation to be measured because our control system only gives us a quasi-static situation.

In chapter 4.0 we have already discussed the running time we can expect for a given flow area and pressure ratio. In light of the above remarks however it was still necessary to check at various points in the flow that the same good control exists. The rest of the chapter therefore is devoted to the calibration of the working section in the following areas of interest:

(a) Time dependency of the flow

(b) Total head distribution

(c) Flow direction

(d) Free stream turbulence levels

(e) Inlet boundary layers

(f) Wall Static pressure.

6.1 Time Dependency of the Working Section Flow

For this series of tests the total head measured by the cobra probe was recorded at different times during a test run as the plenum pressure was either controlled at a constant level allowed to decay in an uncontrolled manner. The probe sensing head was located at a number of the grid points shown in Fig. 53. At all times and pressure ratios it was found that the recorded total pressure at the grid points varied in a predictable smooth manner with upstream plenum pressure. This relationship was determined by the isentropic flow relations for flow along a streamline between plenum chamber and measurement point. In the boundary layer regions the flow would not necessarily be isentropic.

Having established therefore that upstream total pressure is directly related to plenum pressure at any time we can use this fact in the data reduction process for scanivalve pressure traces. Details of this are shown in Chapter 7.0.

6.2 Spatial Variation

These results were recorded using the total head tube of the cobra probe. The results are plotted in suitable non-dimensional form in Fig. 66. The total head profile is remarkably flat and distortion free across most of the test section passage. This series of tests was carried out at two different pressure ratios. At the lower wind

speed (pressure ratio = 1.5) the profile was not as good at the stations nearest the walls.

6.3 Flow Direction

Again the cobra probe was used, but for this measurement the two side tubes were employed as a simple yaw meter. Some difficulty was experienced in pointing the probe correctly. No vernier drive or rotation mechanism was incorporated into the turntable of the probe, and also the entire mechanism had to be aligned with the tunnel axis at each measurement location along the measurement grid. These effects together reduce the accuracy with which we can point our probe to the order of ±½%. However in this range a good pressure difference was available from the two pressure taps. These were measured using the scanivalve and transducer several times in each run by running the scanivalve forwards and backwards past the ports labelled P_{LEFT}, total P, and P_{RIGHT}. The results were plotted in the form as shown in Fig. 67.

As can be seen the central portion of the flow for the whole region upstream of the centre of the blade cascade is relatively consistent in flow direction, but the readings near the top plate of the tunnel are equally consistent but of different sign. However the range of angles is distributed about an average value 2^{o} left of the tunnel axis. Virtually all the measurements made are within ± 1^{o} of this mean.

It was thought at first that this was due to incorrect alignment

For Location Of Measurements
See Figure. 53

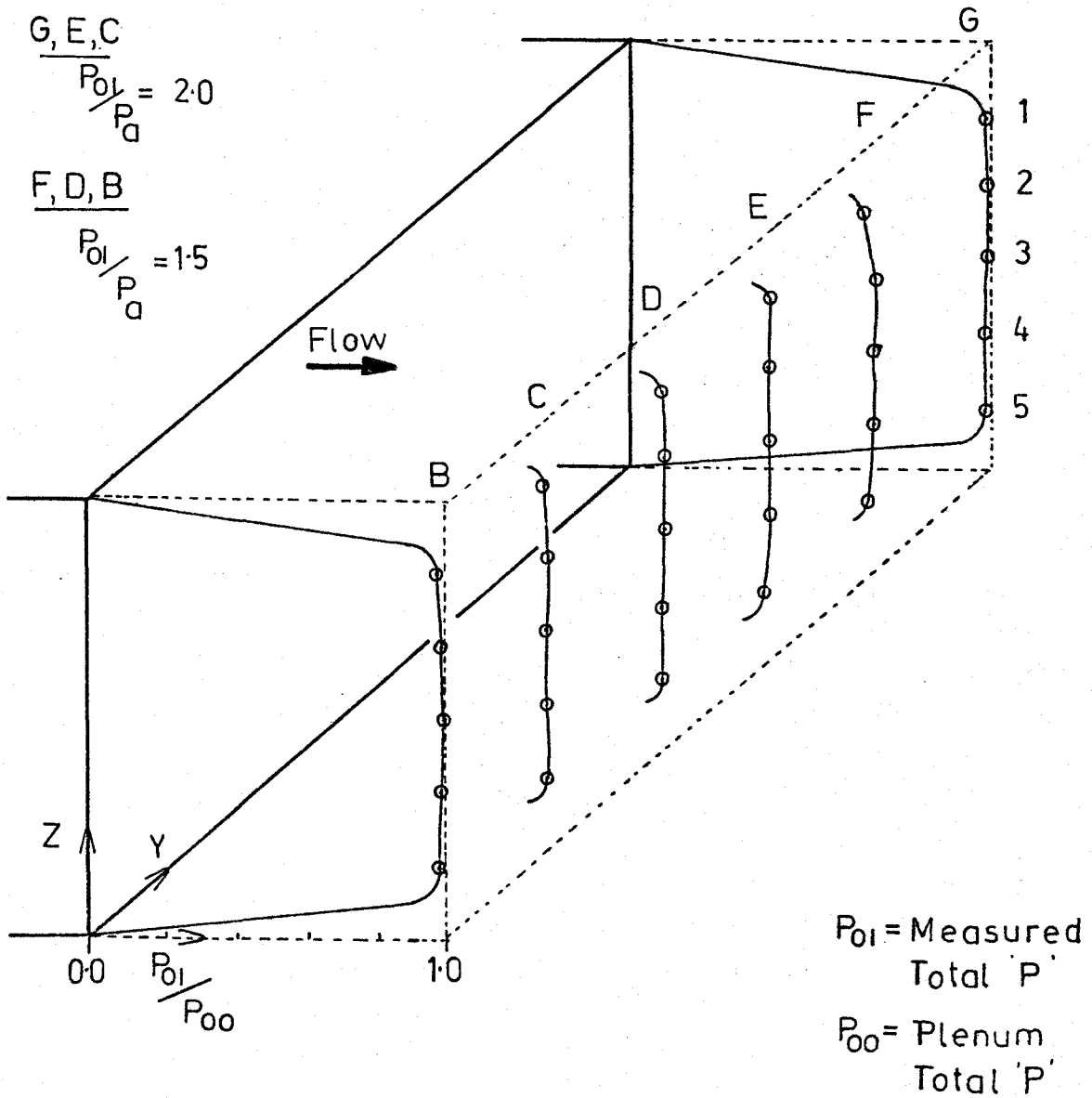

Figure 66 Variation of the Measured Total Head Across the Wind Tunnel Working Section

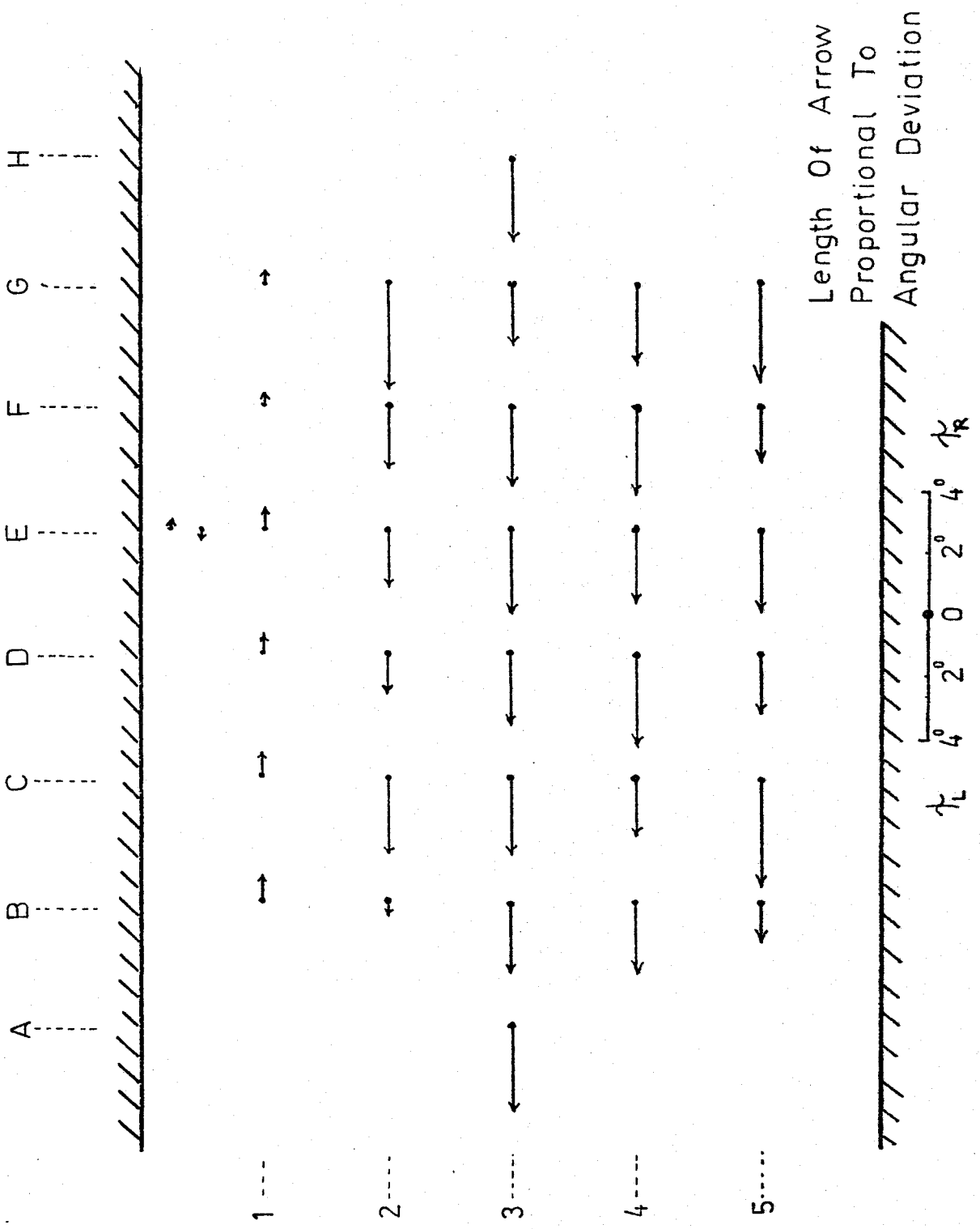

Figure 67 Variation of the Measured Flow Angle across the Wind Tunnel Working Section.

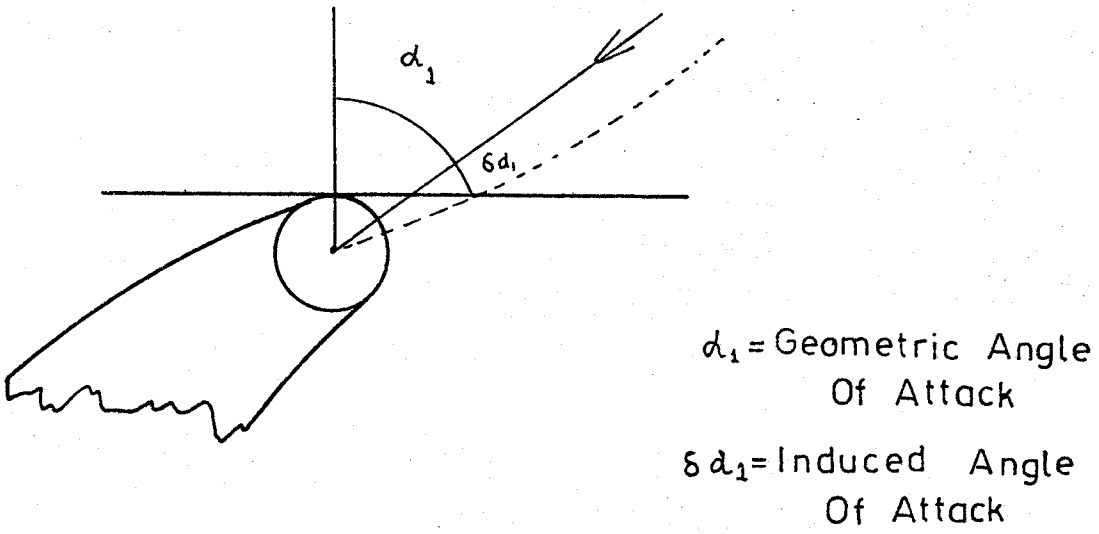

Figure 68 Illustration of the Induced Angle of Attack

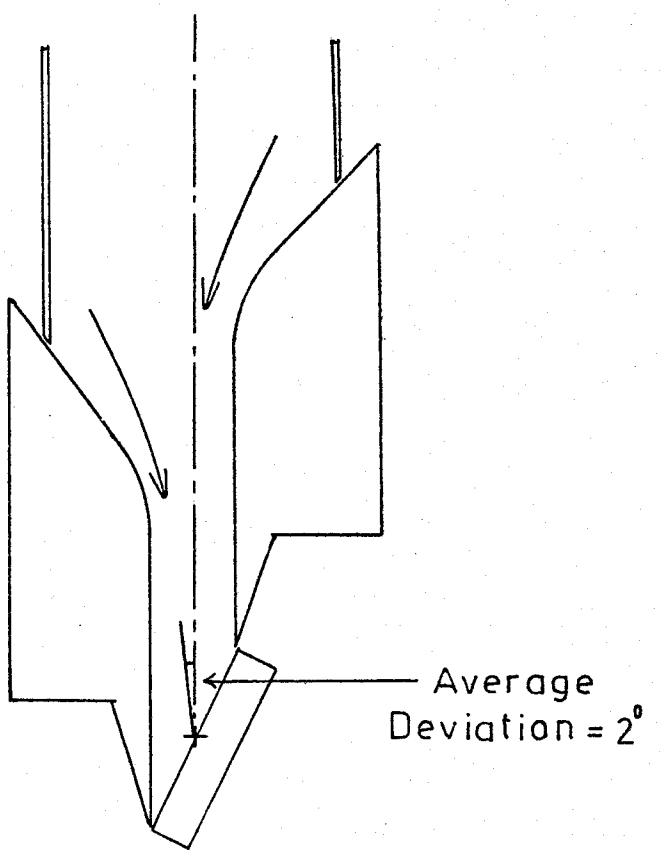

Figure 69 Illustration of the Offset Inlet Ramps

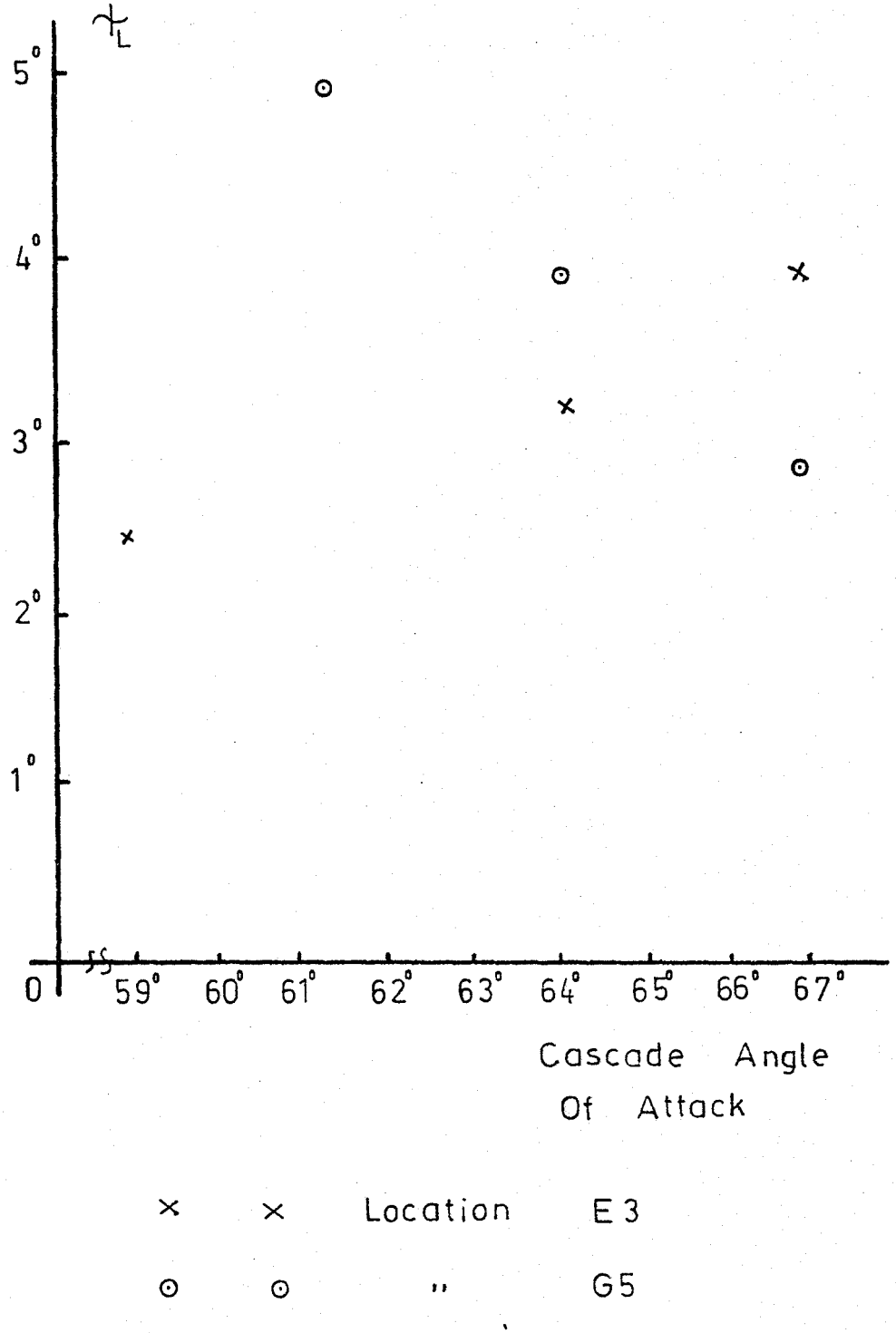

Figure 70 Variation of Flow Angle with Cascade Angle of Attack

of the test rig turntable or alignment of the probe holder. On further examination this did not seem capable of providing such large and consistent discrepancies. Another theory that was examined was the fact that the cobra probe was close to the leading edge of the blades. Thus in real flow, when the inlet streamlines are not exactly straight as assumed in Chapter 2.0, the induced angle of attack would have an influence upstream (see Fig. 68). Again on further examination this theory was not substantiated, the expected angular deviation being in the wrong direction.

It is probable that the real solution to this problem is the skewed nature of the inlet ramps to the test section, this is shown in Fig. 69 for the correct angle of attack of 64^{o}. To investigate this hypothesis the angle of attack was varied at constant pressure ratio. While the probe was mounted in a central location, free from boundary layer effects. As can be seen in Fig. 70 the deviation angle does change in some manner with ramp position but again not consistently. It might be possible for future experimentation to deliberately make assymmetric the gaps at the end of the cascade of blades, through which most of the side-wall boundary layer flows. In this way, with a sensitive probe placed at mid-channel, the flow angle at mid-stream might be "tuned" to the desired value.

6.4 Free Stream Turbulence Levels

These levels were measured with the hot-wire probe already

$$\% \text{ Turbulence} = \frac{U'_{rms}}{\bar{U}} \times 100$$

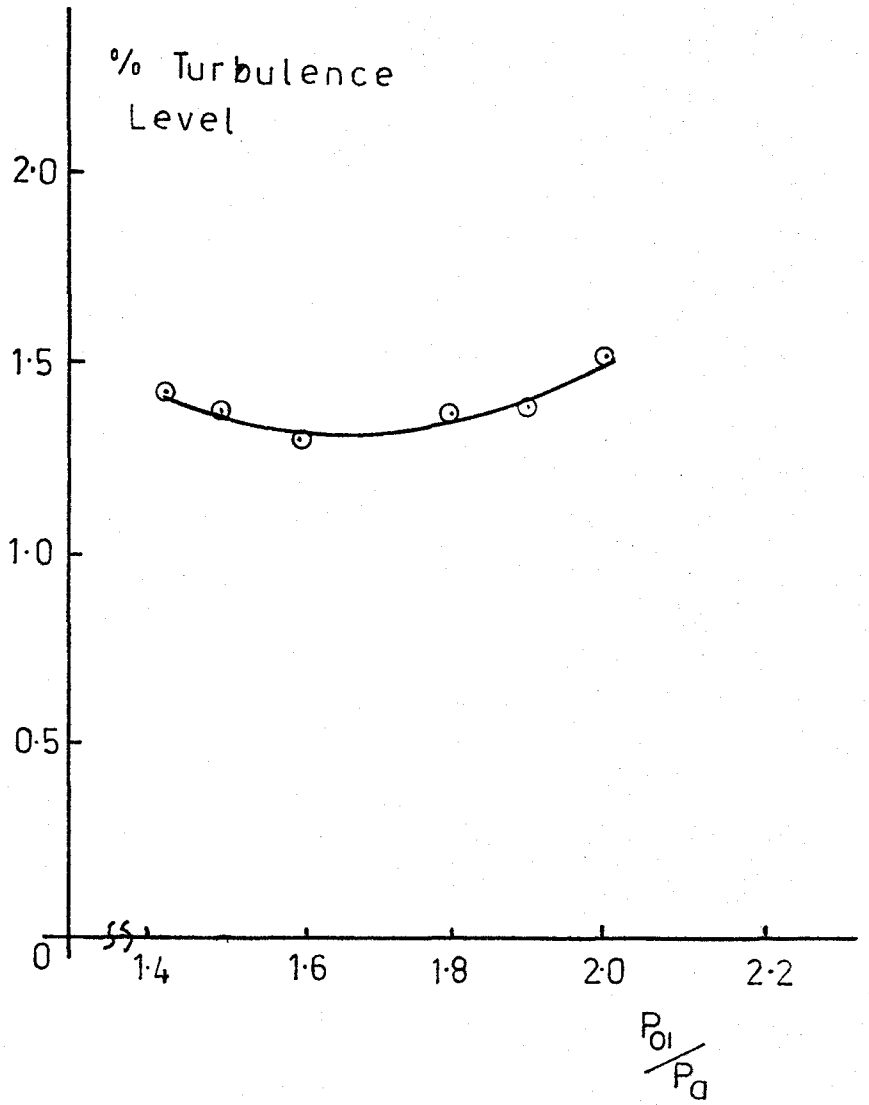

Figure 71 The Measured Turbulence Levels in the Working Section

described. This series of tests was performed at constant angle of attack with the tip of the probe some 2.5" upstream of the centre of the blade cascade. The pressure ratio was varied over the range between 1.4 to 2.3 and the turbulence level noted at various times during the run. The results were remarkably uniform (see Figure 71) at any pressure ratio. The variation during a run was so small that one average set of D.C. voltage and r.m.s. A.C. voltages were taken to represent the whole run.

In general the r.m.s. turbulence levels are remarkably low, of the order of 1.4% expressed as a percentage of mean flow velocity, if the past history of the flow is taken into account. Our aim was not to produce very low turbulence levels however since tests performed in this manner do not realistically represent turbomachine flows where turbulence levels of 2 - 5% are common. Turbulence levels as low as 0.25% have been used in cascade testing with the unfortunate result that performance was entirely unrealistic due to a different boundary layer growth in the turbine blade passage.

6.5 Tunnel Wall Static Pressure

The wall static pressure does to some extent govern the shape of the inlet boundary layers on the upper and lower surfaces of the test section. A series of static pressure ports located as shown were tested for uniformity of pressure (Fig. 72). Only four taps were available for the lower surface because of the difficulty of locating them near the turntable mechanism. Over the central region of the tunnel it was

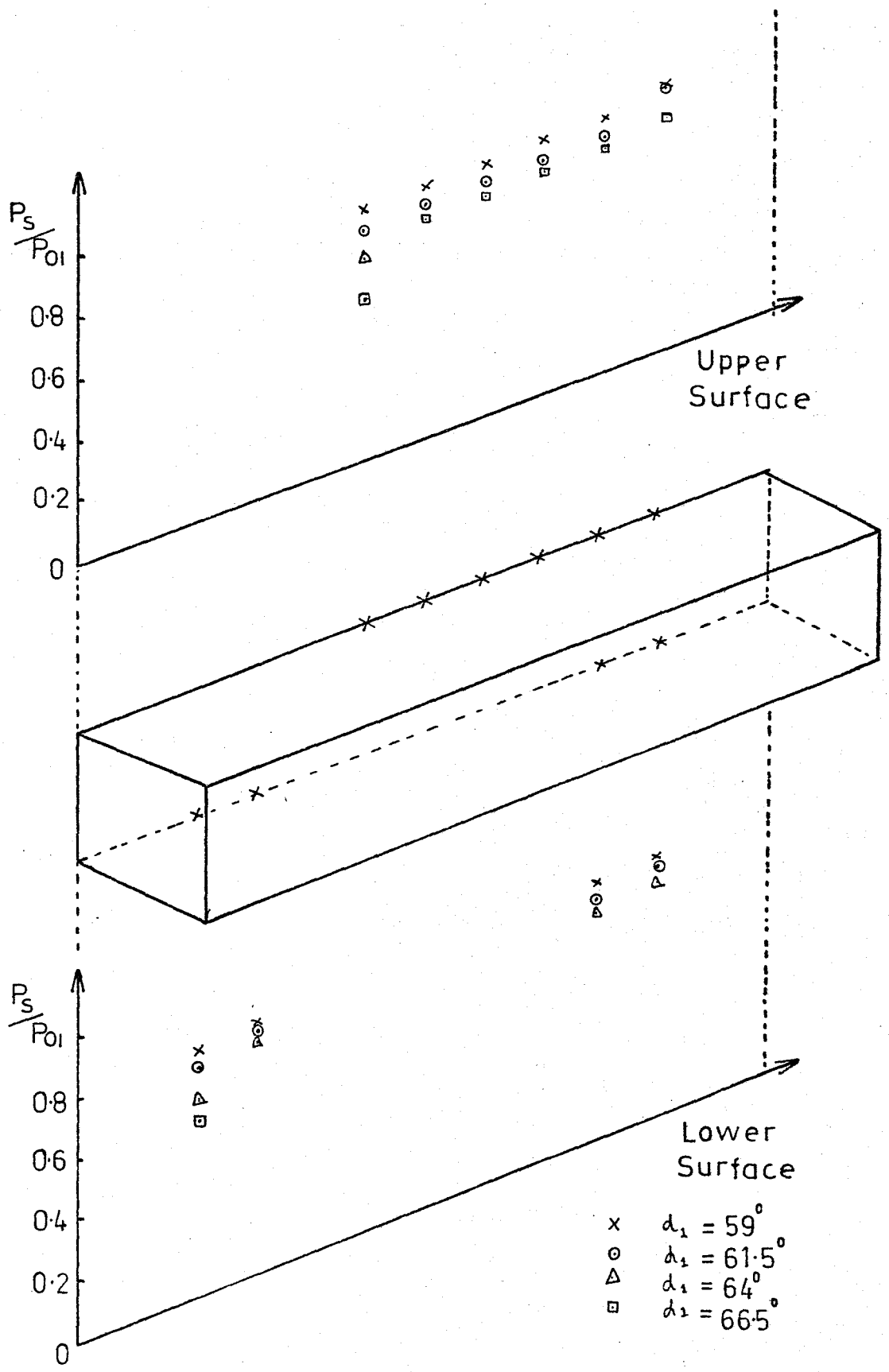

Figure 72 The Variation of the Static Pressure Measured on the Tunnel Wall

found that static pressure was constant but at the right-hand end (looking upstream) the pressures were above normal, and at the left hand end slightly below normal. These effects are almost certainly due to the variable blockage at the ends of the cascade. Over the critical central region upstream of the instrumented blades the results were quite acceptable.

6.6 Wall Inlet Boundary Layers

These were measured using the boundary layer probe drawn in Fig. 55. The results were obtained at two different pressure ratios and the difference in the profiles can be seen from Fig. 73. On this graph the points obtained with the cobra probe; which were few in number due to its size, are included for comparison. It should be noted that the results have been corrected in the case of the boundary layer probe, for displacement error in the form suggested by Young and Maas. (34)

$$\Delta z/D = 0.13 - 0.08\, d/D \qquad (53)$$

where Δz is the correction added to the measured height of a probe of tip O.D = D and tip I.D = d.

We must also correct for the fact that pitot probes do not correctly measure total pressure when within 2D of the wall and this is corrected using a non-dimensional graph supplied in Reference 34.

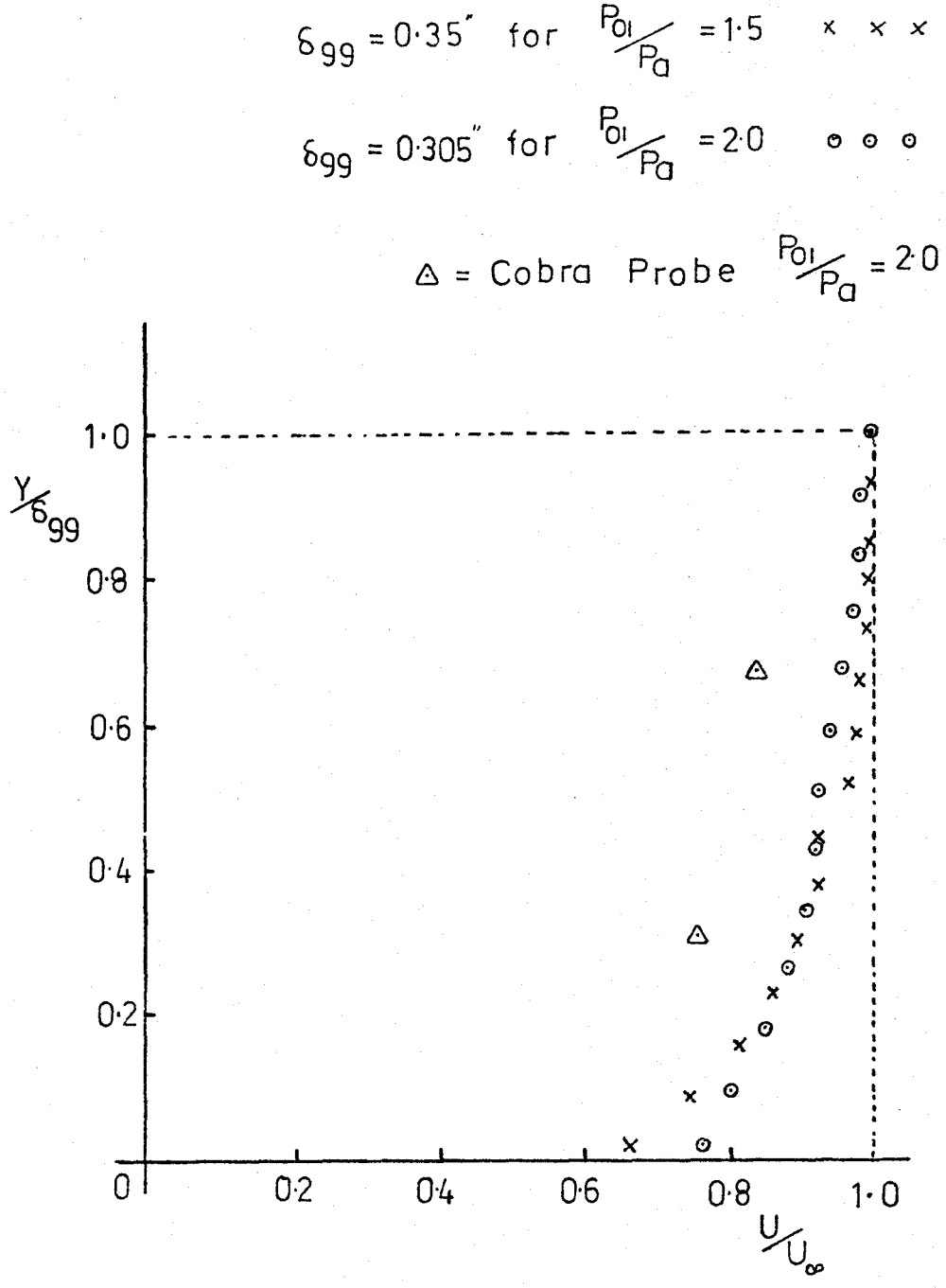

Figure 73 The Measured Inlet Boundary Layers on the top and bottom walls of the Wind Tunnel

6.7 Discussion of the Results

In general we can conclude that the wind tunnel provides us with a flow of the correct range of total head, inlet turbulence, and inlet flow angles with acceptably thin end-wall boundary layers. It should be borne in mind that in some cases the angle of attack measured from turntable position should be corrected for the consistent flow direction error noted in section 6.3.

CHAPTER 7.0 THE PRESSURE DISTRIBUTION STUDIES

As this work constituted the core of the experimental studies, the major proportion of the effort was aimed at determining experimental values for surface pressures. In order to reduce scatter in the experimental results the total head was monitored by a cobra probe situated near the blades. This was one of the inputs to the scanning valve system and thus total pressure was checked at intervals during the surface pressure measurements. The arrangement for the pressure ports is shown in Fig. 74.

Bearing in mind the dependence of pressure rise time on $(\frac{1}{d_1})^4$ it was felt that small errors in estimation the diameter of the pressure tubes could cause large increases in rise time. Thus all the pressure capillaries were reduced to the minimum possible length. (see Figs. 75 and 76).

The set of 16 turbine blades were held in a blade holder which was easily removable from the wind tunnel. The chief requirements for the design were that it held the blades in a rigid manner, at the correct spacing, while fitting into the machined grooves already existing in the wind tunnel turntable. Provision also was made so that the stagger angle λ^o could be varied.

The blade holder was made of aluminium, separated at each end by stainless steel pillars, the blades were pivoted at the ¼-chord point by silver-steel dowels which were an interference fit in the brass blade

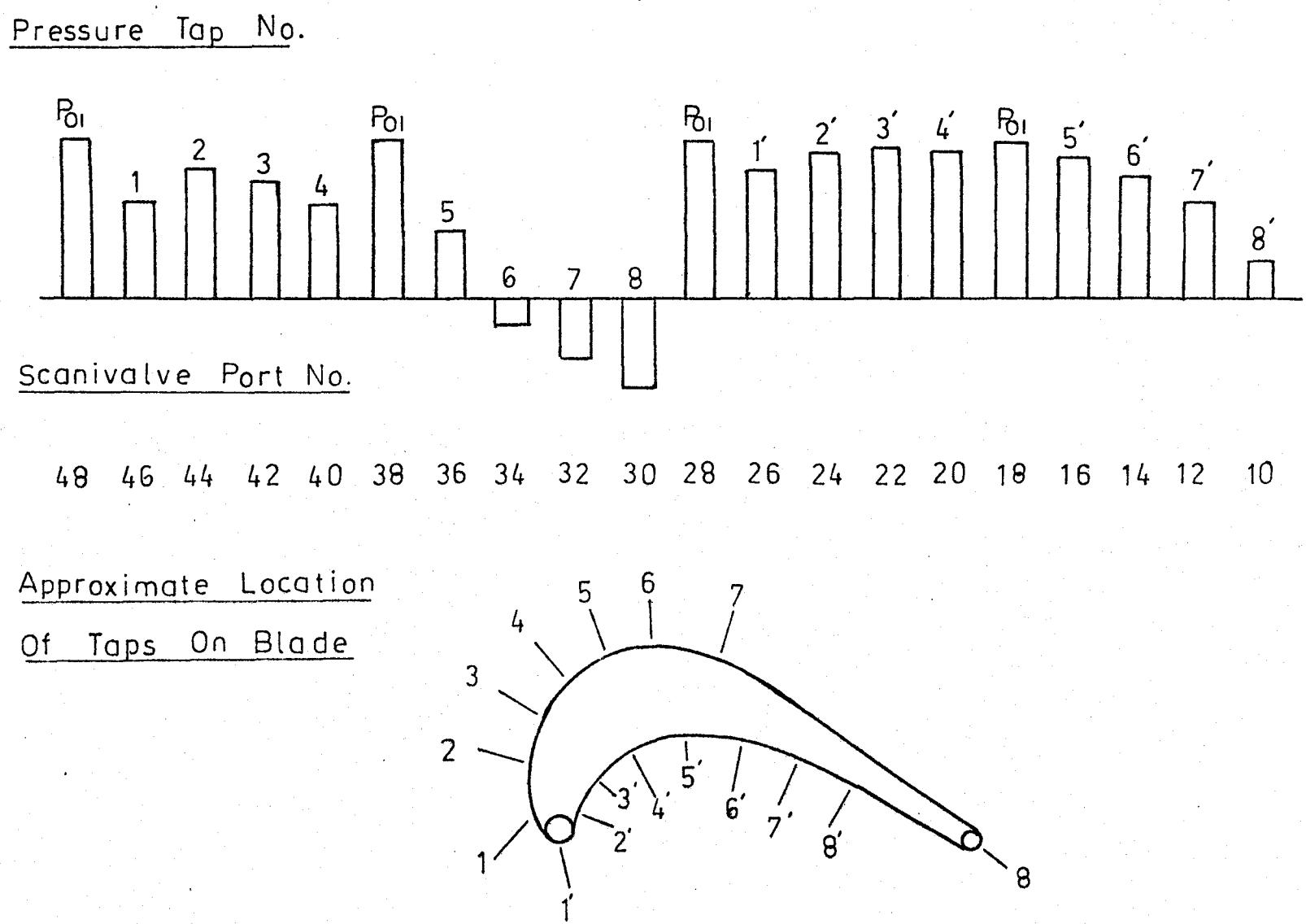

Figure 74 The Arrangement of Scanivalve Pressure Ports

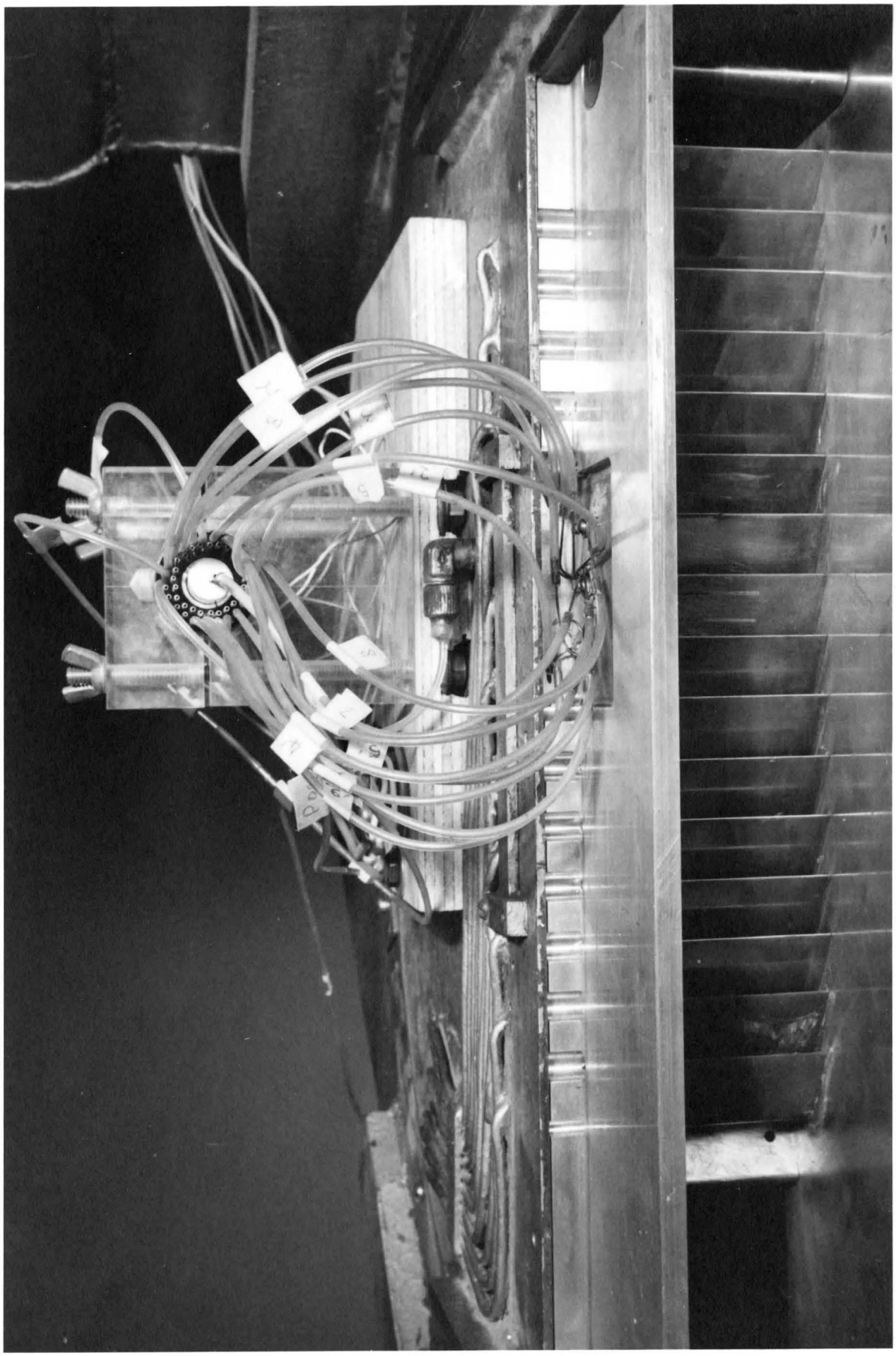

Figure 75 View of the Scanivalve Installation

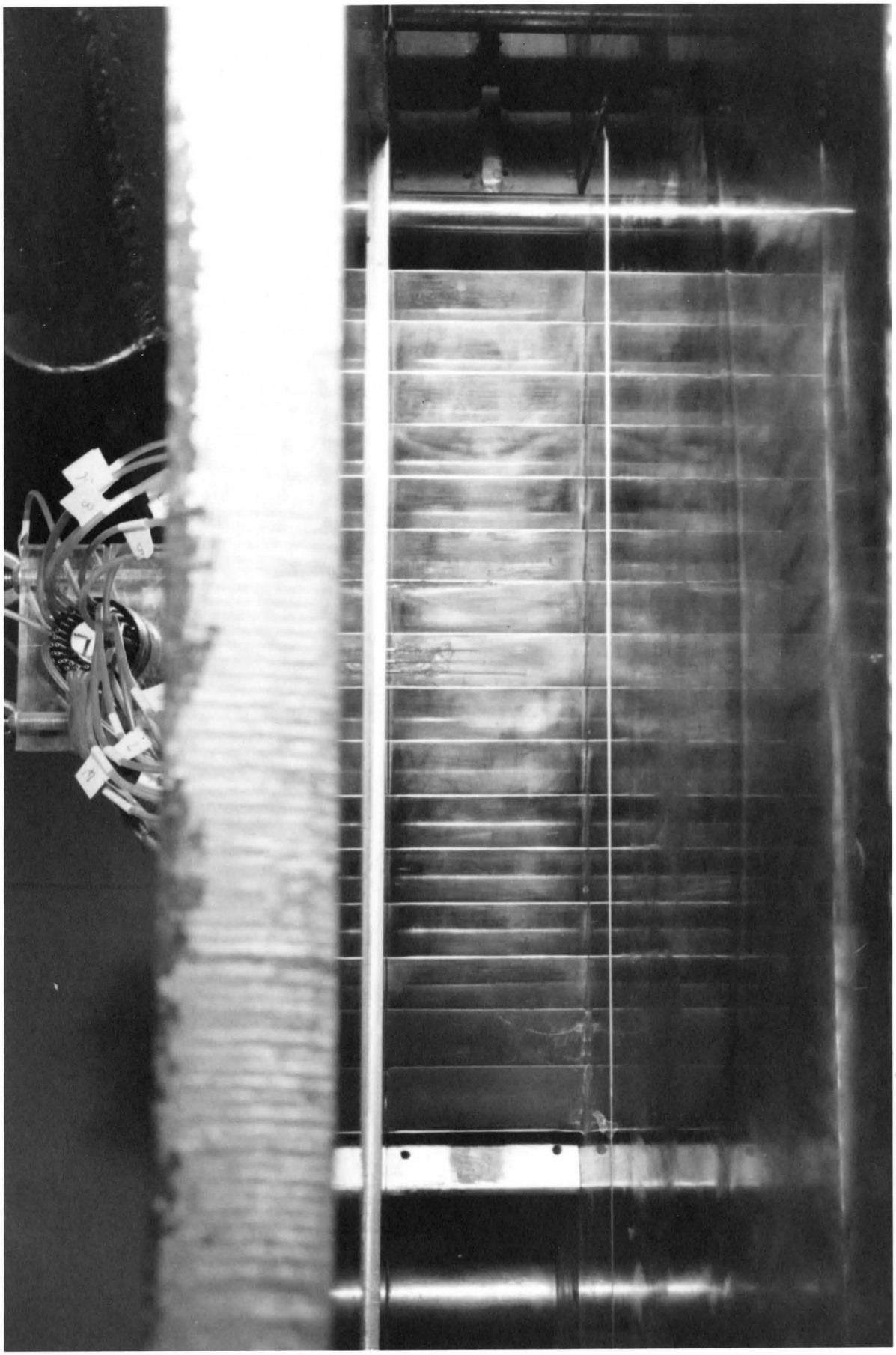

Figure 76 View of the Rear of the Installed Blade Cascade

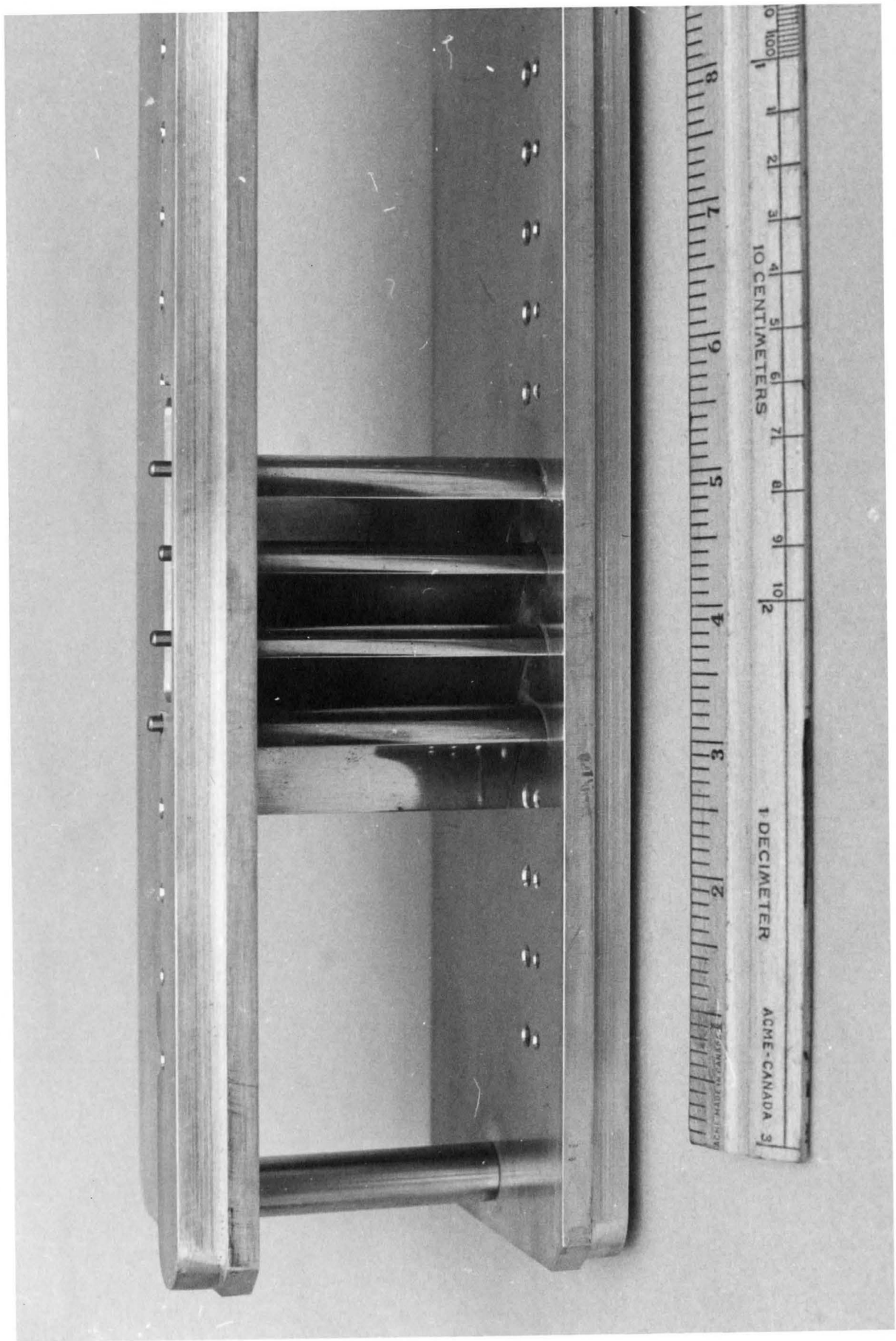

Figure 77 The Blade Holder

(Fig. 77). These projecting dowels were a tight movable fit in the blade holder. To resist aerodynamic loading moments about the dowel pin, the blades were locked in position relative to the holder by small screws, top and bottom, which fastened into tapped holes at the ½-chord point. These extended through oversize clearance holes in the top and bottom plates of the holder, allowing small angular changes to be made in stagger λ ($\pm 2^{o}$) after manufacture.

The blades were set in the correct relative position by a series of machined aluminium templates, which bore against the flat-back portion of the blades. The blades have a height of 2.400" and a design axial chord of 1.0". Due to a short-fall in the number of brass blades (kindly supplied by the Mechanical Engineering Division, National Research Council) a further two blades were cast in epoxy resin. One of the brass blades was used as a master and a mold made from silicone rubber. These blades proved very difficult to machine because the epoxy was silica loaded for strength. This resulted in the blades eventually being bonded in a fixed angular position to the holder bottom plate by epoxy resin. This allowed removal of the top plate for access to the other blades. They were placed at the extreme left hand end of the blade cascade thus minimizing the aerodynamic effect on the important central blades. The original brass blades were finished to a high polish and accurate to ± 0.001" on all dimensions.

7.1 Numerical processing of the Data

For each test it was found useful to use the value of P_{01} that

existed at the time of the pressure measurement in calculating the ratios P_s/P_{01} which were the derived end result. This was achieved by calculating from the continuously recorded plenum pressure, the value of P_{01} connected for supply fluctuations. This use of a "time local" P_{01} enabled a great reduction in the scatter of results. It was also found necessary to record atmospheric pressure at the time of the series of tests since both transducers, for plenum pressure and surface pressure, were zeroed relative to atmospheric pressure. For any particular angle, the test was repeated up to four times, to obtain a good average P_s/P_{01} at each pressure top location. For runs at pressure ratios of 1.5 to 1 it was possible to record all 20 pressures during each run with good accuracy. At higher pressure ratios the number of readings obtained was reduced, thus increasing the number of runs needed for a proper completion of the test.

7.2 First series of Tests at the Design Stagger Angle ($\lambda = 26^{\circ}$)

In this series of tests the pressure ratio was varied between 1.5 and 2.5 for the range of inlet angles between $66\frac{1}{2}^{\circ}$ and 59°. The type of blade we are testing would normally be installed in the first or second stage of a gas generator turbine and thus would see only small variation in angle of attack compared to saya power turbine blade.

In Figs. 78 and 79 the experimental results are compared to the theoretical results for a range of angles of attack each at a fixed pressure ratio. In Figs. 80 and 81 the variation with pressure ratio at

a fixed angle of attack is observed.

It has been found that the two series of graphs can be collapsed onto two curves, shown as Figs. 82 and 83 in which we have observed the following:

(a) That the effect of changing angle of attack is to increase or decrease pressures on the leading edge of the suction surface, the rest of the pressure distribution being virtually unchanged (Fig. 82).

(b) That the effect of changing pressure ratio is to increase or decrease the pressure ratio near the trailing edge, the rest of the pressure distribution being virtually unchanged (Fig. 83).

Conclusion (b) is qualified by saying that it is necessary for the pressure ratio to be at least enough for sonic conditions at the throat for this to be true.

We can further conclude that:

(c) For virtually all cases the pressure distribution is correctly predicted by our analytical method.

(d) That leading edge blockage, in the form of a sonic patch measured at inlet angles of 66½% severely limits the use of the blade since the design α_1 is 64°.

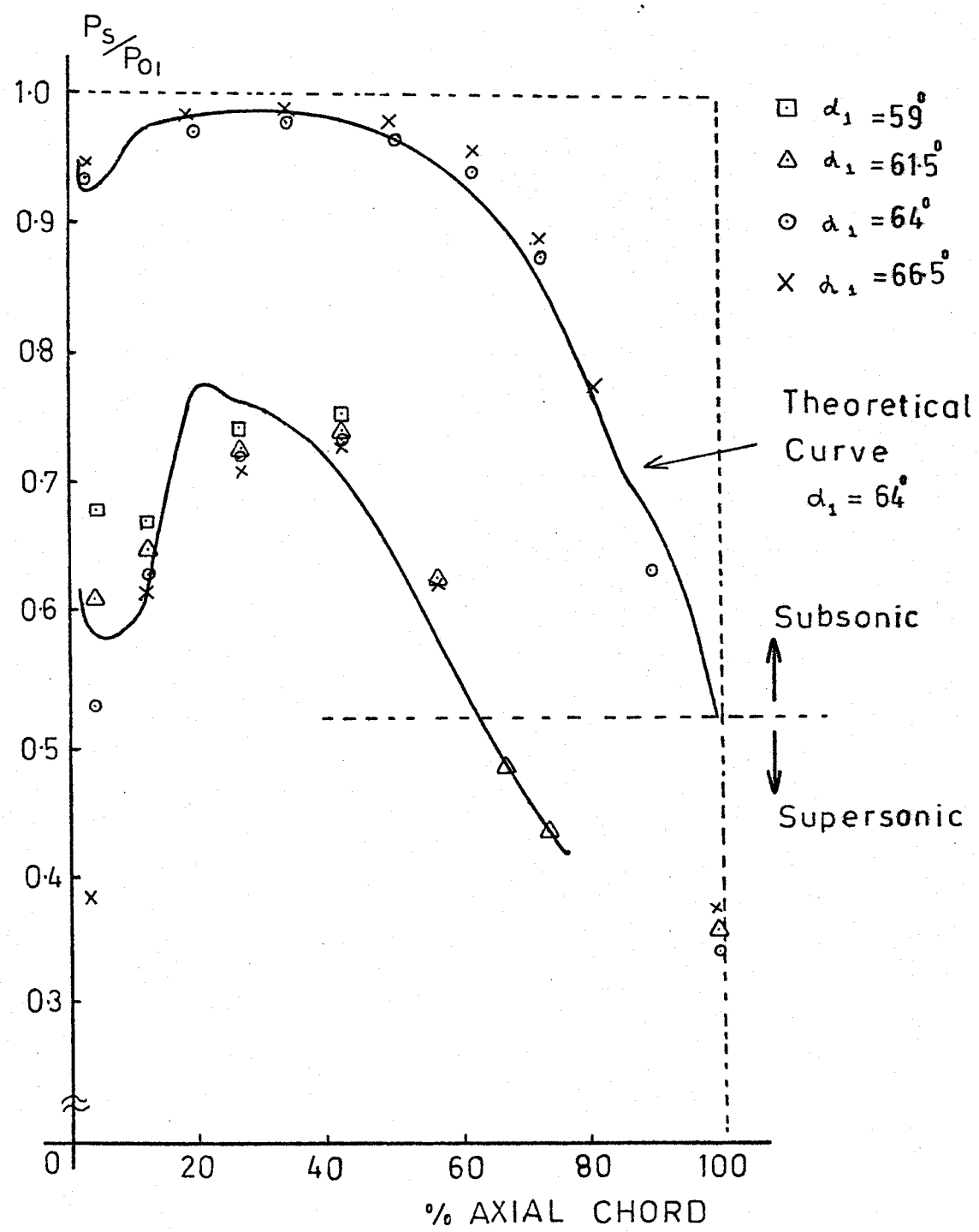

Figure 78 Comparison of Measured and Theoretical Non-Dimensional Surface Pressures (P_s/P_{01}) at a Pressure Ratio of 2.0:1 and varying angles of attack.

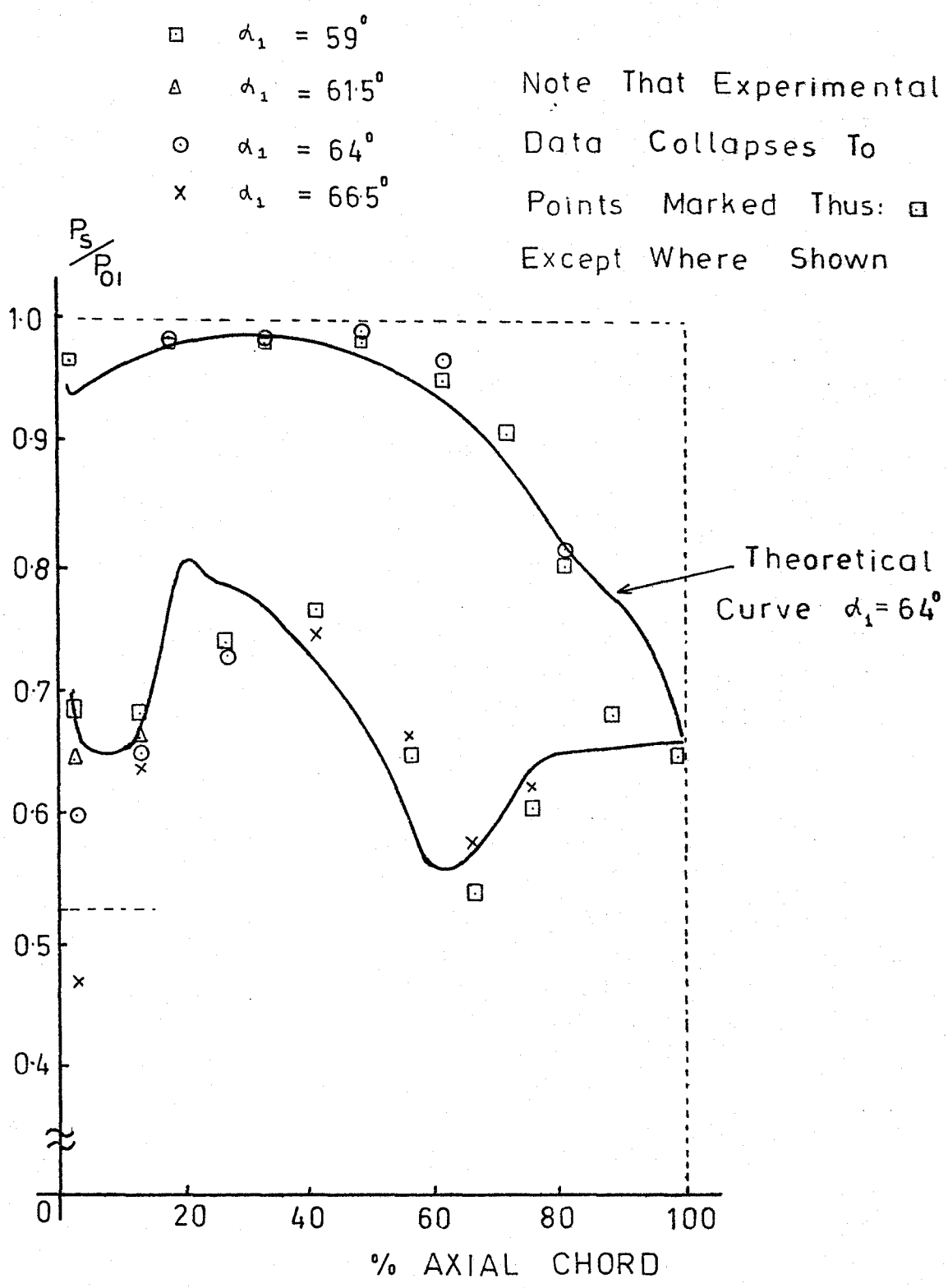

Figure 79 Comparison of Measured and Theoretical Non-Dimensional Surface Pressures at a Pressure Ratio of 1.5:1 and varying angles of attack.

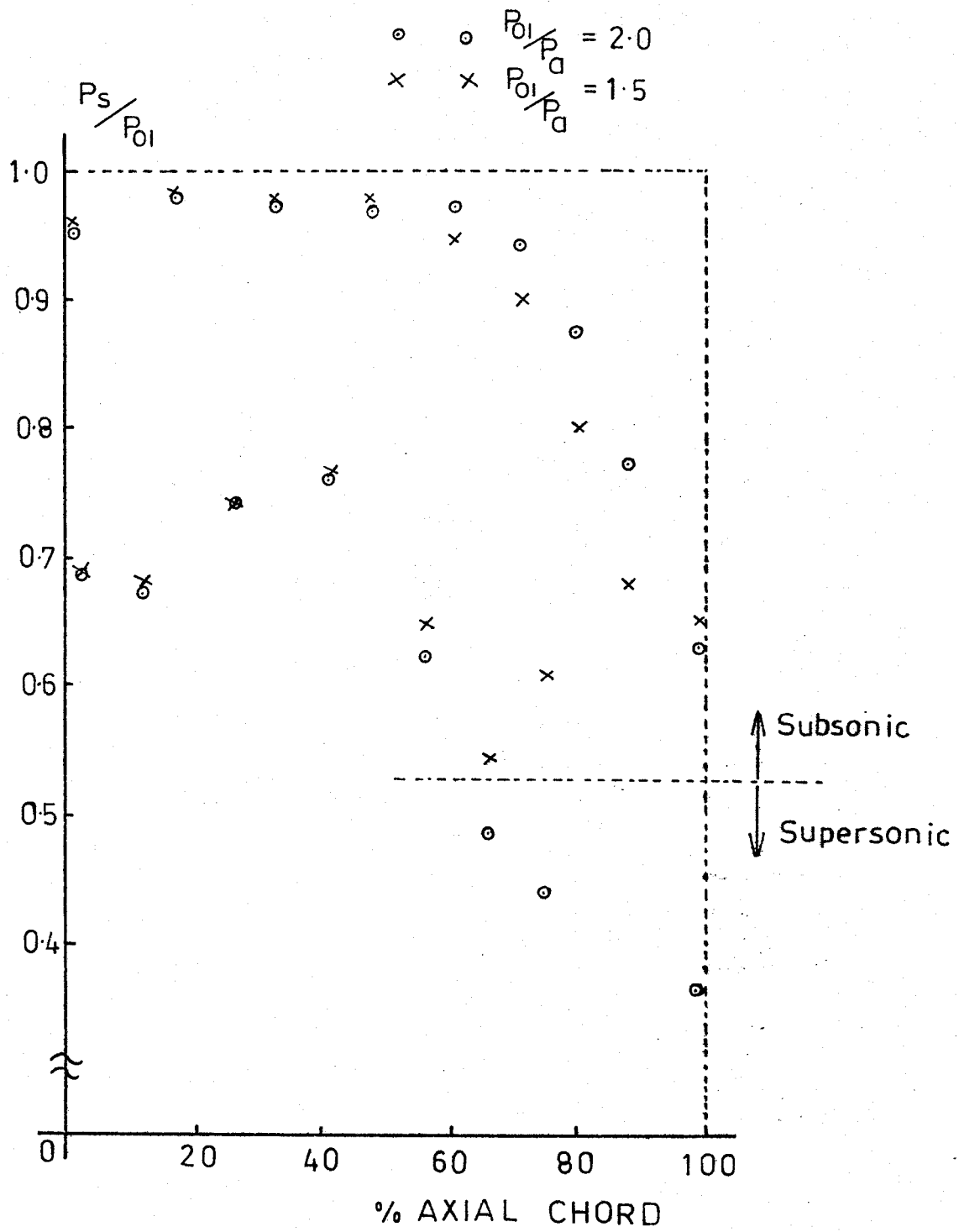

Figure 80 Measured Non-Dimensional Surface Pressures as a Function of Pressure Ratio at an Angle of Attack of 59°

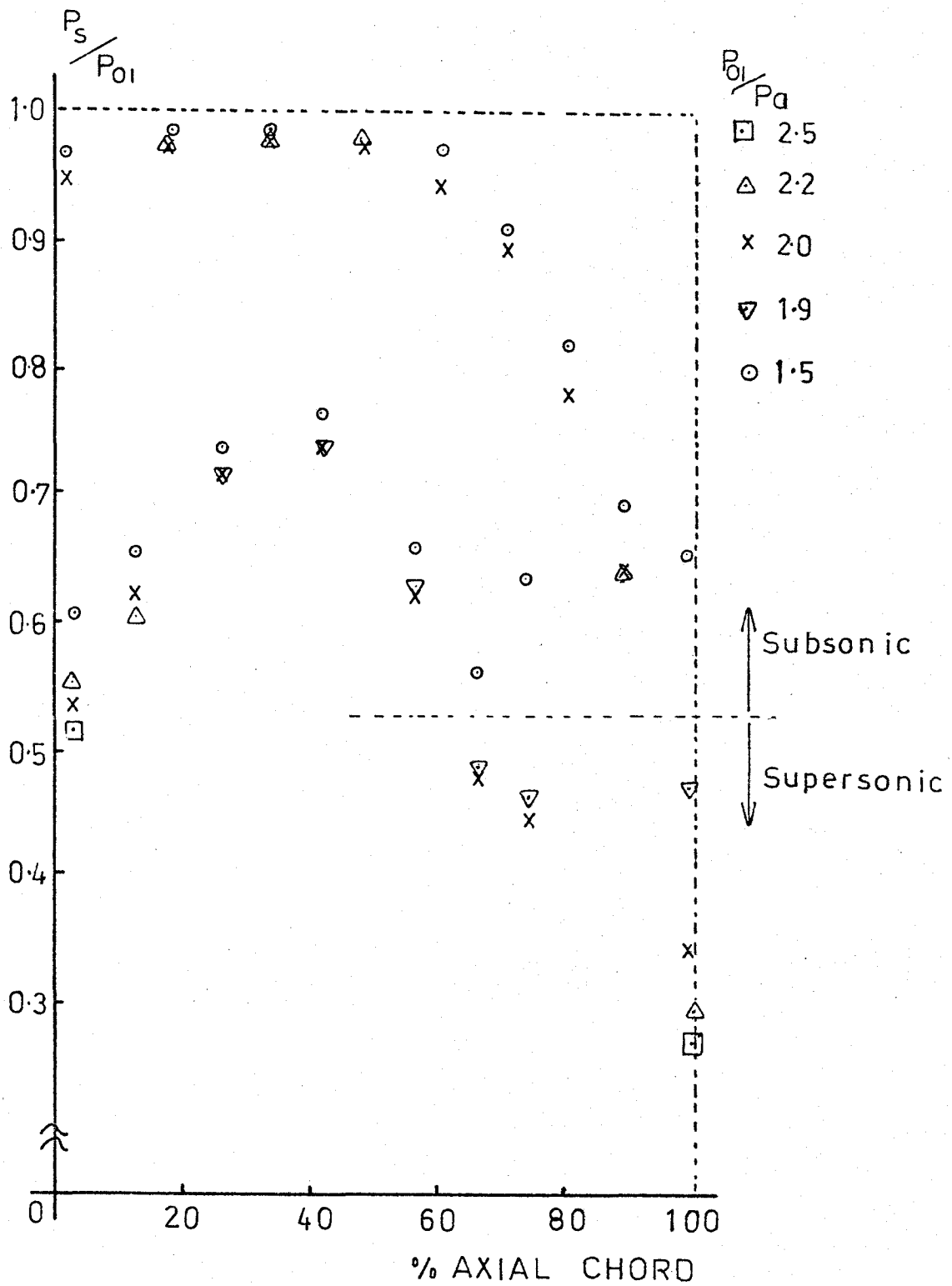

Figure 81 Measured Non-Dimensional Surface Pressures as a function of Pressure Ratio at an Angle of Attack of 64°.

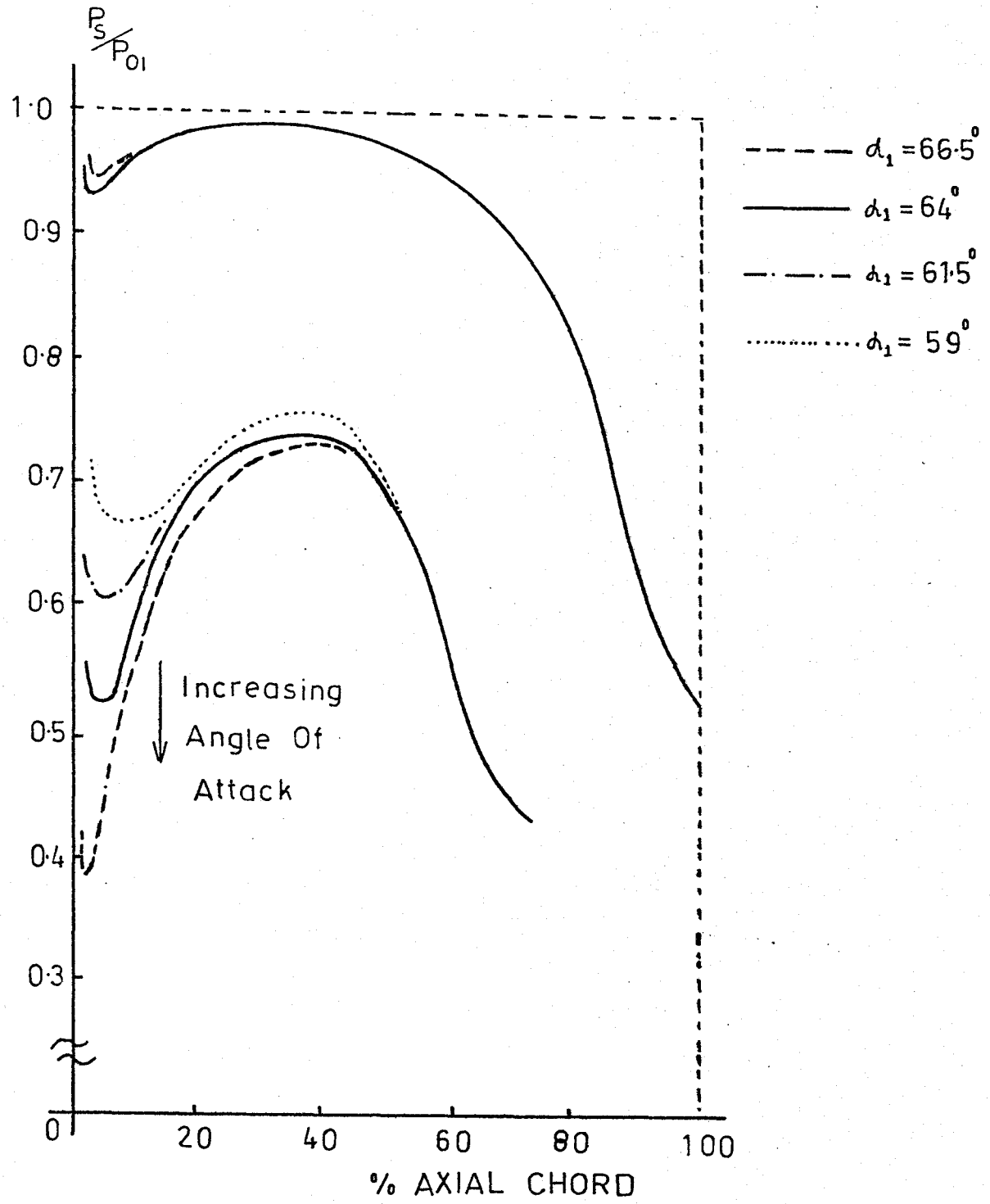

Figure 82 Summary of Results - Effect of Angle of Attack

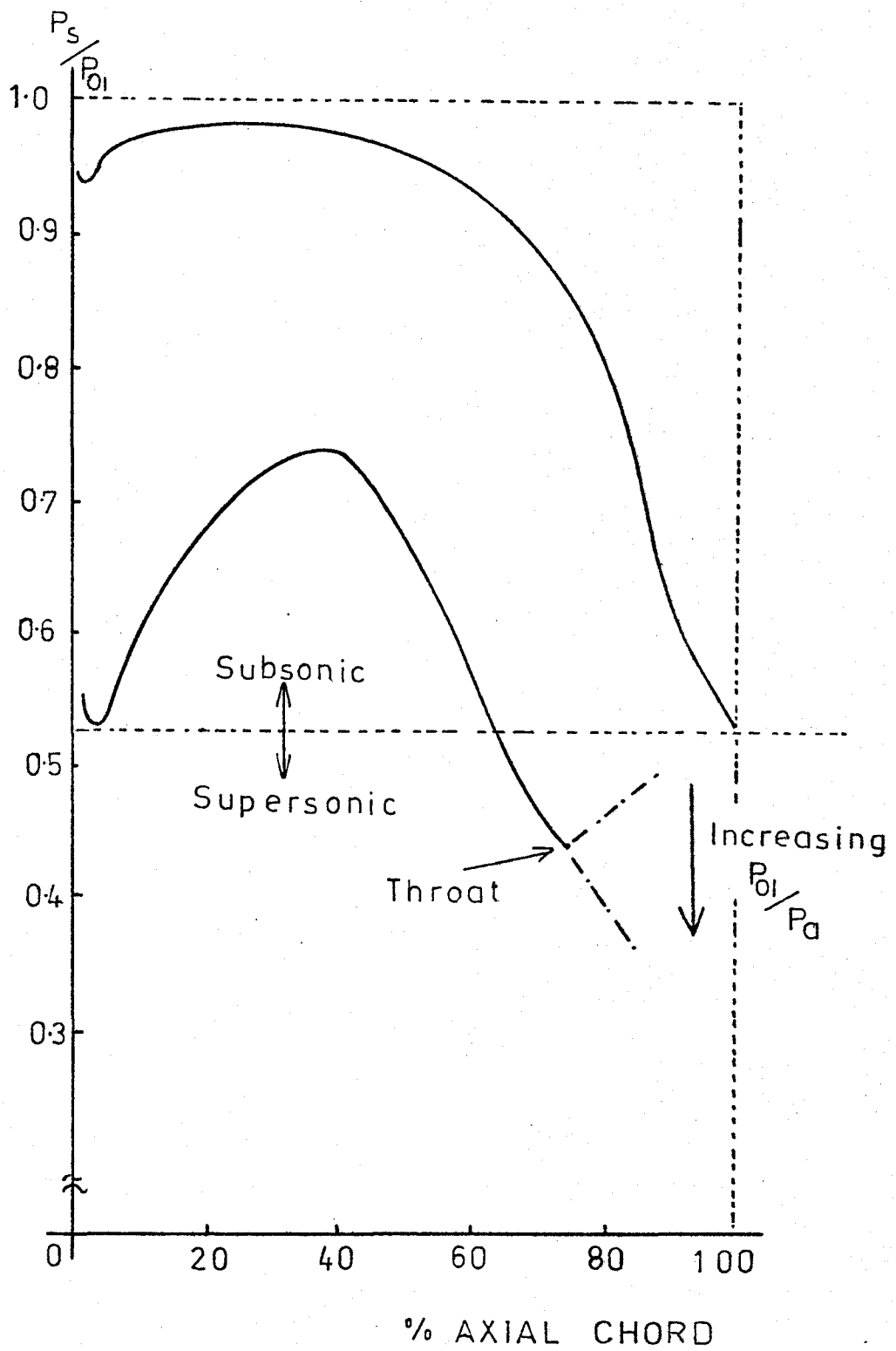

Figure 83 Summary of Results - Effect of Pressure Ratio

7.3 Second series of tests, with the Stagger Angle λ reduced to 24^{o}

Instant re-design of the blade passage was available by resetting the angle of the blades in the holder. Study of the blade shapes and curvature distributions showed that a reduction of leading edge suction was available with little change in total turning angle by reducing the angle of the flat-back to 24^{o}. The measured results for the new passage design are shown in summarised form in Fig. 84. The reduction achieved in leading edge suction has resulted however in a loss in total tangential force on the blade as computed from the area between the suction and pressure curves. An additional advantage given is the reduction in the severe adverse pressure gradient after the suction peak, thus reducing adverse effects on boundary layer growth.

7.4 Third series of tests, with the Stagger Angle λ increased to 28^{o}

This series was carried out to confirm our picture of the leading edge blockage. As can be seen from Fig. 84 the worsening of the situation was as expected.

7.5 The Effect of the Boundary Layer

As can be seen from Fig. 27 the prediction procedure is improved slightly when calculated boundary layer thickness is used to modify the potential flow calculation. These calculations were not carried out for

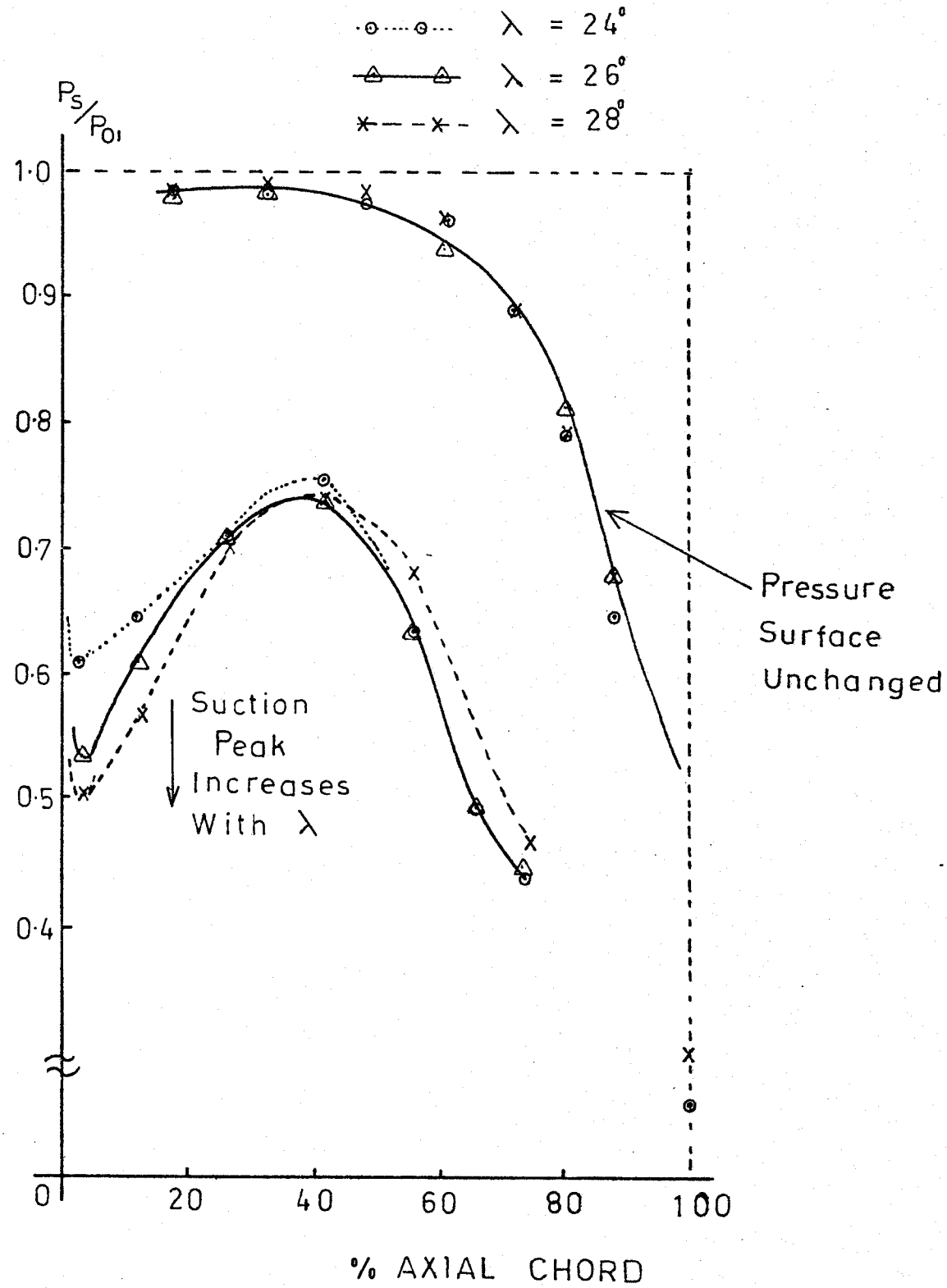

Figure 84 The Effect of Changing Stagger λ on Measured Non-Dimensional Surface Pressures

all tests , and the change is small enough not to be plotted. For the design stagger angle at an angle of attack of $66\frac{1}{2}^{o}$ the boundary program showed separation on the adverse pressure gradient zone after the leading edge suction peak. This point will be returned to in the wake survey tests reported in the next chapter.

7.6 Temperature Measurements

The thermocouples embedded in the blades were used to measure blade surface temperature. The measured values dropped during running to values between 492^{o} to 497^{o}R from a pre-run average reading of 528^{o}R. The good thermal conductivity of the brass blades is evident in that all 5 thermocouples read the same temperature to within $\pm \frac{1}{2}^{o}$R. This temperature corresponds to the recovery temperature for an adiabatic wall at the velocities that exist near the trailing edge of the blade. We can calculate this temperature from the relationship (Reference 40).

$$T_r = T_\infty (1 + P_r (\frac{\gamma-1}{2}) M_\infty^2) \qquad (54)$$

For example the last thermocouple was at a location of 74% axial chord. At a pressure ratio of 2.0 the Mach number in the free stream was 1.15 at this location. Substituting this Mach number into our equation and assuming $\gamma = 1.4$ and $P_r = 0.72$ for air:

$$T_r = 420\ (1 + 0.72\ (0.2)\ 1.15^2)$$

$$\underline{T_r = 499^{o}\text{R}}$$

It should be remembered at this point that because of the downward drift in total temperature noted earlier, our free stream static temperature is dropping during the test. Thus we have a difficult transient heat conduction problem, with the added complication of a varying boundary layer to take into account. The measured temperatures are in the correct range of values however since T_r at the end of a run has dropped to 478°R at the same location for which we have already quoted results.

CHAPTER 8.0 INVESTIGATION OF THE WAKE

The wake region of the blades is of interest because it enables the determination of some of the important parameters of a cascade of blades. From a traverse of the wakes it is possible to calculate the total head loss coefficient. Also the structure of the wakes is important because it will affect to some extent the performance of down-stream blade rows. In our investigation a total head probe driven by the mechanism shown in Fig. 61 was used. Since both the mechanism and the chart recorder were driven by constant speed A.C. motors, the chart-recorder trace gave us a record of P_{02} varying in the x-direction. We obtained a trace shown in idealised form in Fig. 85.

It is possible to show for a two-dimensional turbulent wake (Ref. 19) that the width 'b' of the wake is proportional to the downstream distance to the one half power:

i.e. $$b \propto l^2 \qquad (55)$$

and that the rate of decrease of the velocity difference between free stream and wake is given by the simple relationship:

$$u \propto (l^{-\frac{1}{2}}) \qquad (56)$$

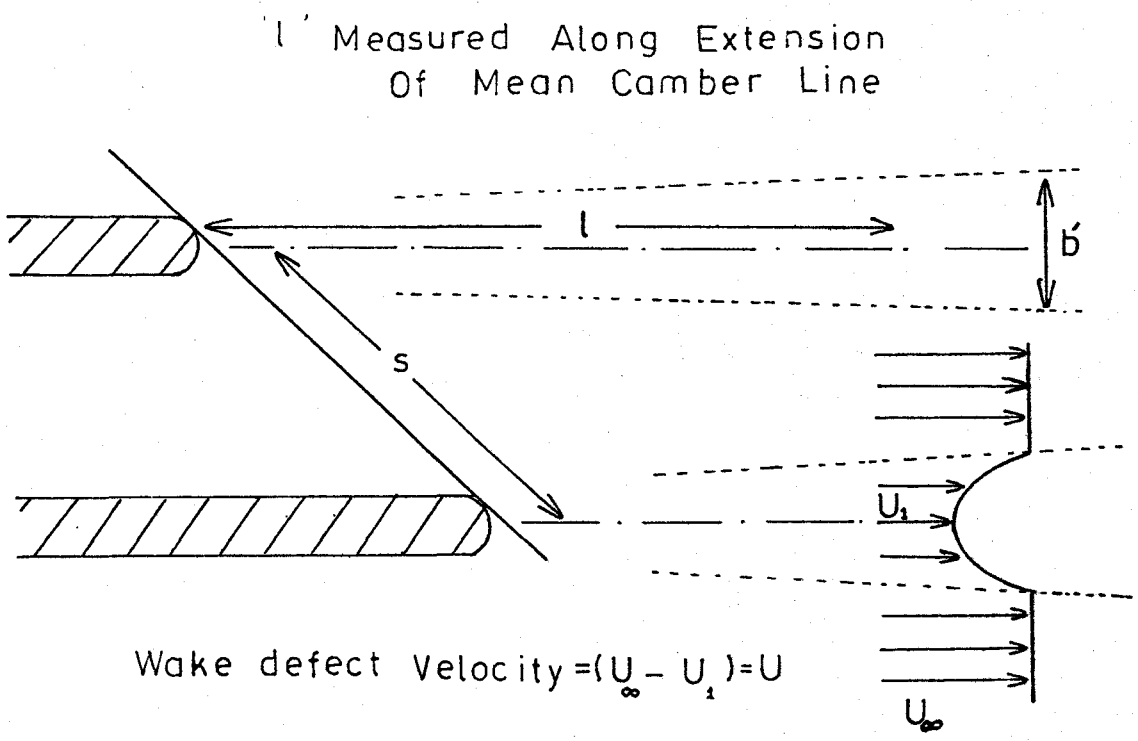

Figure 85 Nomenclature used for Wake Survey

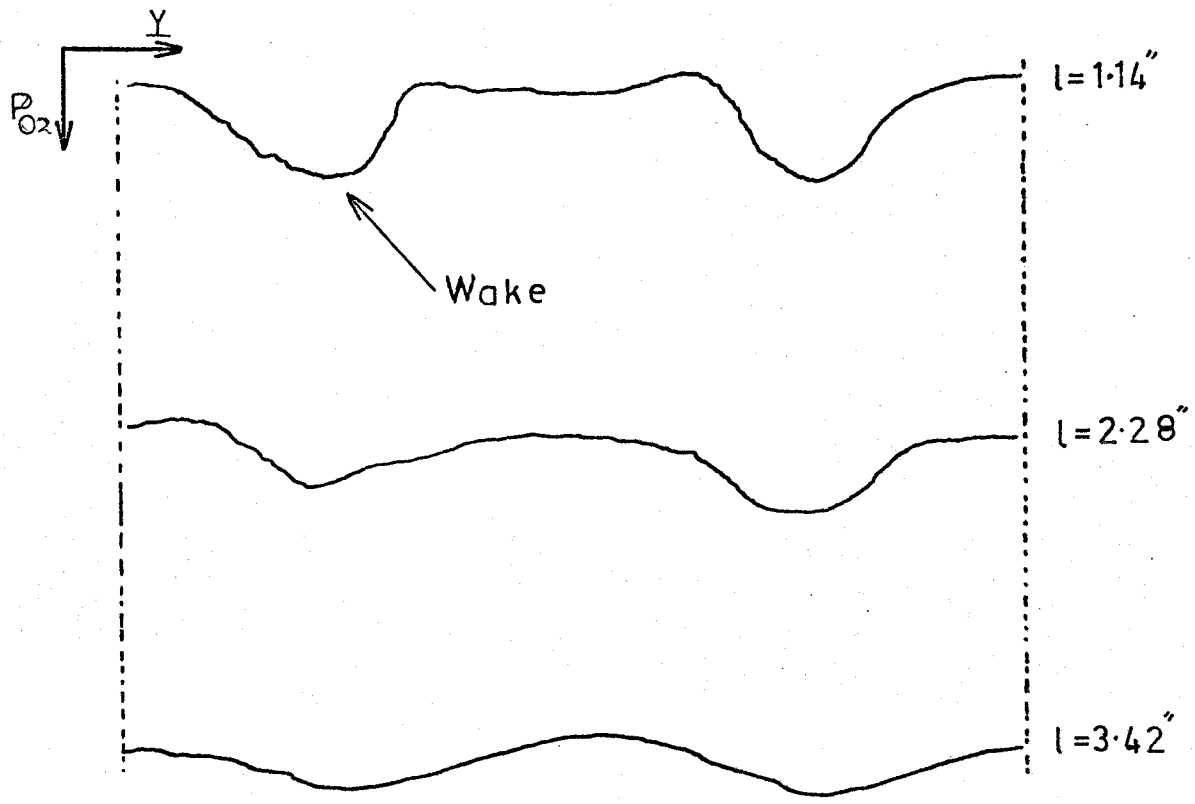

Figure 86 Variation in the Form of the Wake with distance from the Trailing Edge.

These relationships are however rather simple minded formulae and do not take into account such effects as the existence of shock waves or traverse velocity gradients. There is also the general limitation that these formulations can only be applied some four trailing edge thicknesses down-stream. This is only a small restriction when it is considered that this is only a total distance of 0.100", which is in fact 0.043" measured in the axial direction '$\underline{x}$'.

8.1 The Investigation of the Wake width as a function of distance from the Trailing Edge

Using the traversing gear mounted at different distances downstream, traces of the wake total pressure were recorded as shown in Fig. 86. The wake width can be found from the width at half-height using the well known relationship:

$$b'_{0.5} = 0.441\, b' \qquad (57)$$

The widths so obtained were devided by the pitch 's' and plotted against $(\frac{l}{s})^{\frac{1}{2}}$ in graph 87. The point plotted at $(\frac{l}{s})^{\frac{1}{2}} = 0$ is in fact obtained by adding the theoretical boundary layer thicknesses at the trailing edge to the trailing edge thickness. The simple theoretical relationship seems to be well justified in this instance because the experimental points lie about a straight line with little or no scatter.

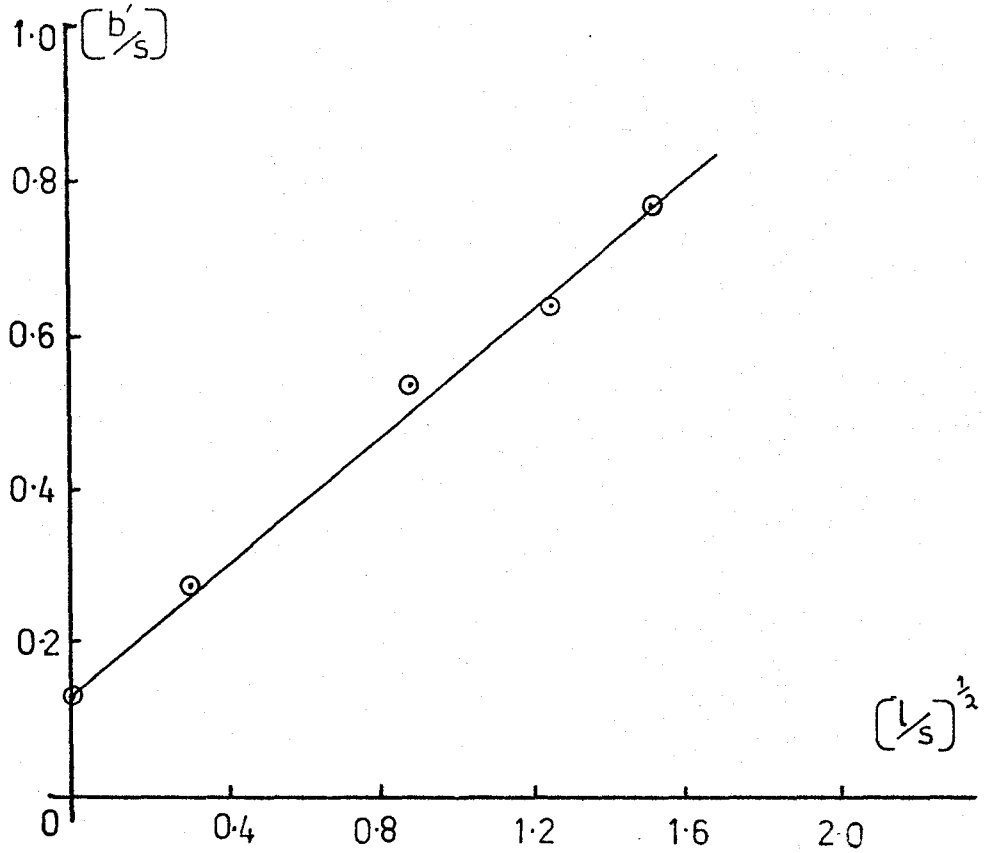

Figure 87 The Non-Dimensional Wake Width as a Function of Distance from the Trailing Edge.

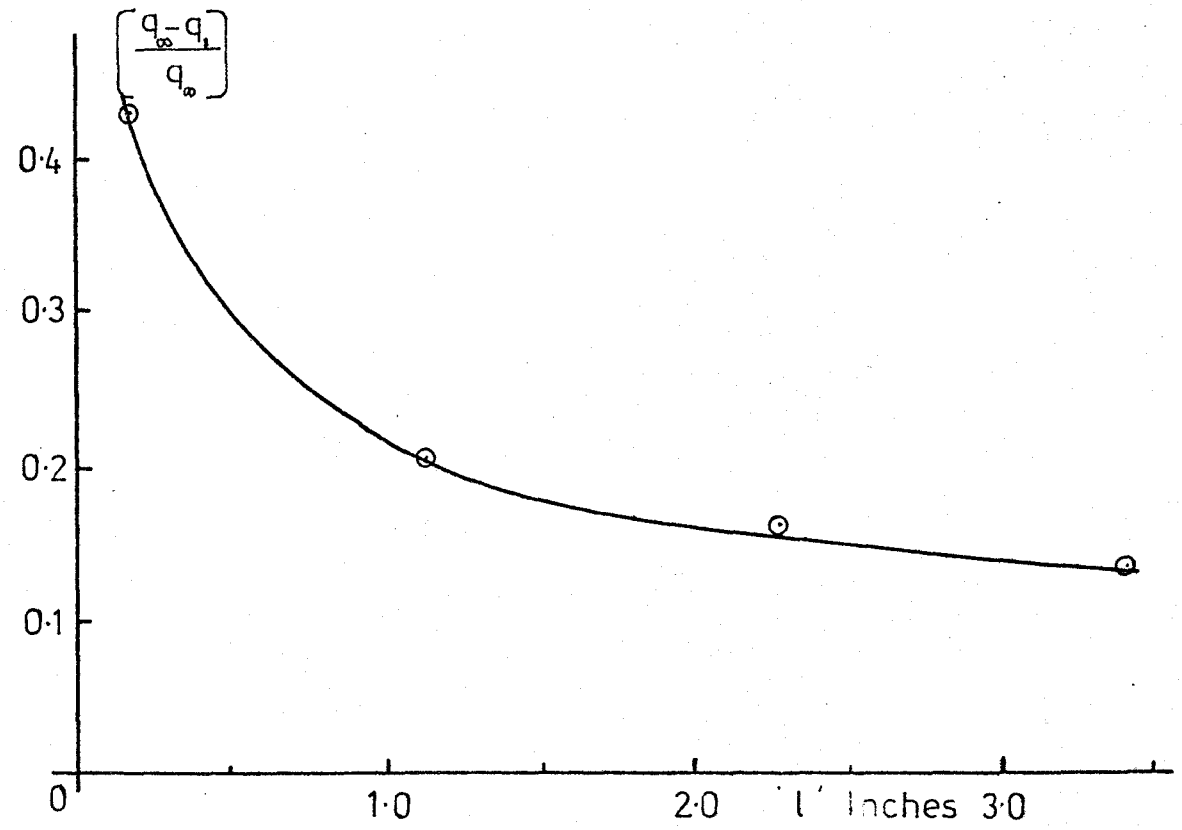

Figure 88 The Variation of the Defect in Total Head at the Wake Centre with Distance

Similar attempts made at plotting the velocity defect at the centre of the wake were less successful. The total head defect is plotted against distance(Fig. 88.) The reason for the lower degree of accuracy is probably due to the fact that we were attempting to make a point measurement while upstream conditions were varying slightly. Determination of wake width was not affected to such a great extent.

8.2 Investigation of changes in the Wake Width with Pressure Ratio

As can be seen from Fig. 89 the wake width decreases with pressure ratio. This is an analogous effect to the thinning of a boundary layer with increasing velocity. In the downstream region the velocity increases with pressure ratio. It would be expected that with the much higher velocity gradients and shear rates that exist at higher pressure ratios, that the mixing losses would increase, and that total head loss coefficients would increase. Also the friction losses on the blade surfaces would increase.

8.3 The Investigation of Blade Outlet Angle

It was hoped that it would be possible to determine the position of the wakes, and thus the overall outlet angle using the total head traversing method. Owing to the small size of the outlet passages (Throat = 0.257") it was found that insufficient precision was available,

especially when it was discovered that the probe itself was rather flexible. It is relatively easy to obtain a continuous traverse showing the variation of total head, but considerably more difficult to precisely pinpoint in space part of that traverse.

For the above reason the outlet angle was determined by a flow visualisation technique. A mixture of fine aluminium power in SAE 20 grade oil was made up and painted onto the lower surface of the blade holder downstream of the blades. A very short running time, of the order of two or three seconds, followed by a fast shut-off fixed the traces in the correct position. Too long a run dispersed the mixture downstream. The centre of the wake was determined visually and the angle measured with a protractor. Although the above method is not as accurate as results obtained with sophisticated traversing mechanism, it is very quick. This enables several runs to be made and an average angle calculated. The outlet angles so obtained certainly demonstrate the precision with which the blades direct the flow (see Table **6**). The simple theoretical results are those due to Taylors method which assumes isentropic flow between throat and downstream. This method is only applicable for small overpressures. For greater pressures the method of characteristics or system of waves described in Chapter 2.0 are more accurate.

TABLE 6

THE VARIATION OF OUTLET ANGLE WITH PRESSURE RATIO

Pressure Ratio	Measured Outlet Angle	Theoretical Outlet Angle
1.85	66°	---
2.52	64° 30'	63° 36'
2.62	64°	63° 6'
1.9	---	64° 30'

TABLE 7

THE VARIATION OF TOTAL HEAD LOSS COEFFICIENT $\frac{P_{01}-P_{02}}{P_{01}}$

Pressure Ratio	Angle of Attack	Total Head Loss Coefficient
1.89	66½°	0.059
1.9	66½°	0.067
1.9	64°	0.046
1.5	64°	0.021

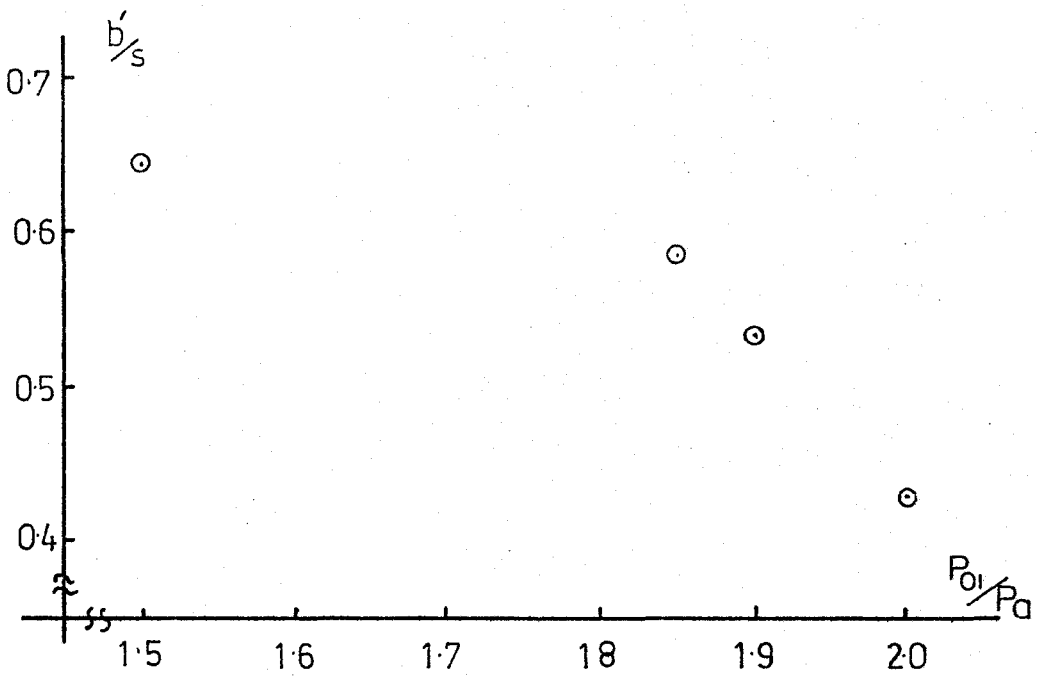

Figure 89 The Variation in Non-Dimensional Wake Width with Operating Pressure Ratio

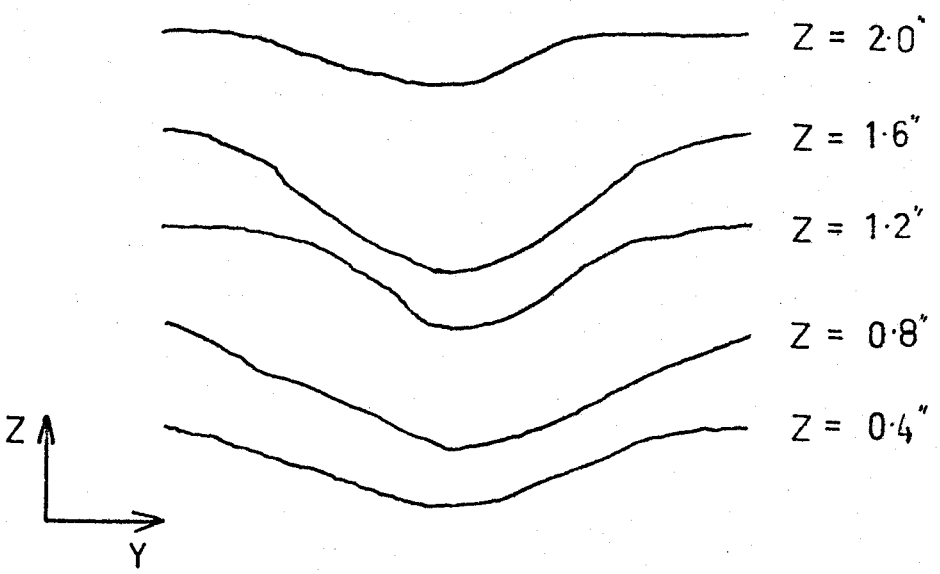

Figure 90 The Variation in the form of the Wake with Height.

8.4 The Investigation of the form of the Wake at Different Height and measurement of Total Head Loss Coefficients

As can be seen from the accompanying figure 90 the position of the wake changes at different measurement heights. These results were all taken at the same axial distance from the cascade, and at constant pressure ratio and angle of attack. A general "smearing" and increase in losses is observed nearer the end-walls. To reduce as much as possible errors due to the end wall boundary layers, total head loss coefficients were calculated from data taken at blade and height. At some locations it is possible to traverse the reduced total head at the core of the secondary flow vortices (see refs. 41, 42, 43) but this was not observed at any of our five measurement heights.

The measured total head loss coefficients are shown in Table 7 at two different angles of attack and two different pressure ratios. As noted in Chapter 3.0 the losses are much greater and the wake broader at the higher angle of attack (Fig. 91). At an angle of attack of 66½ degrees the theoretical results obtained with the computer program indicated separation immediately following the leading edge suction peak. As can be seen in Table 7 the loss coefficient is much more acceptable (0.045) at the design angle of attack and pressure ratio. This compares well with published data for similar designs although no comprehensive effort has been made to obtain diagrams for variation of loss coefficient as a function of Mach number and angle of attack.

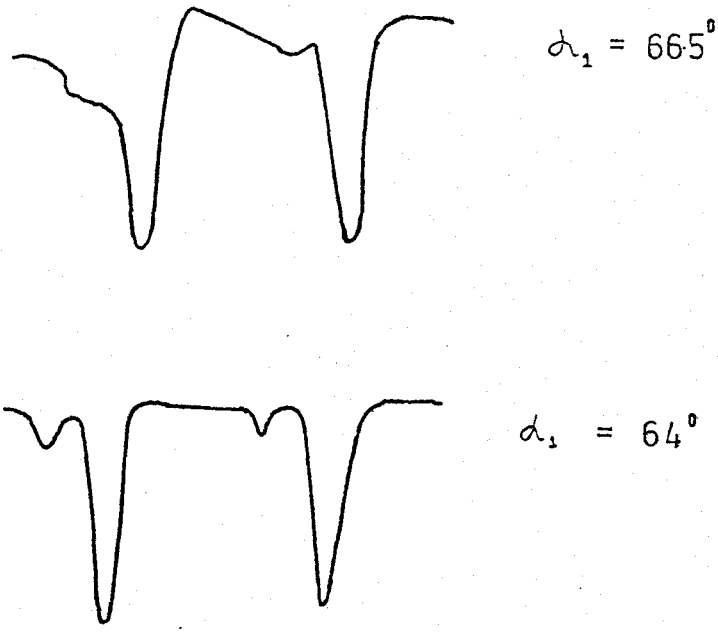

Figure 91 The Increase of Wake Width with Angle of Attack

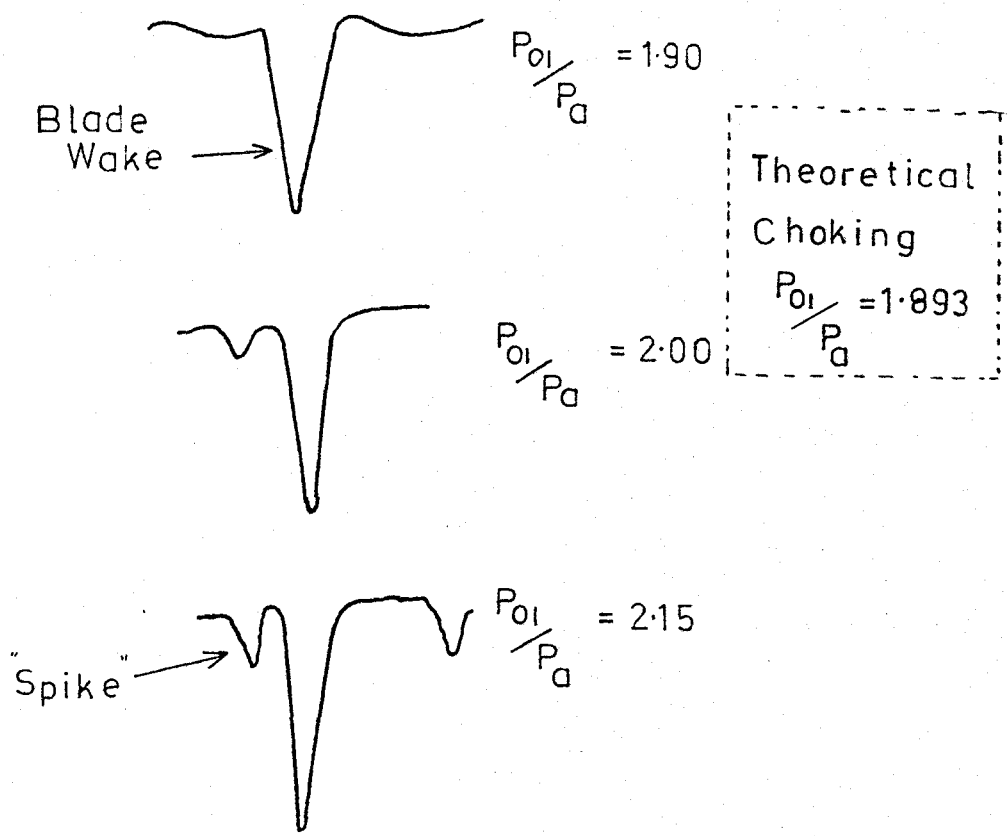

Figure 92 Wake Traces showing Shock Wave "spike"

8.5 Intersection of the Trailing Edge Shock

For some of the tests near the trailing edge the small diameter (0.028")probe was used. At pressure ratios greater than that required for choking sharp 'spikes" were seen on the pressure trace near the suction surface. (Fig. 92). These spikes were not observed at or below choking pressure ratio. The conclusion to be drawn is that this is the intersection of the probe with the trailing edge shock wave. In the series of three traces it is possible to see the spike height increase with pressure ratio.

8.6 Conclusions to be drawn from the Wake Survey

From the results obtained we can see that the blades as designed work quite well at the design angle of attack, but as predicted from our theoretical flow analyses, the flow losses increase greatly at increased positive angles of attack due to the adverse pressure gradients and leading edge blockage. With the blading used a height to axial chord ratio of 2.4:1 was sufficient to give us accurate two dimensional measurements.

CHAPTER 9.0 OVERALL CONCLUSIONS

From the experimental results and theoretical analysis reported in the present work the following general conclusions may be drawn:

(a) The cascade wind tunnel has been developed to the point where the correct range of pressure ratios, angles of attack and turbulence levels required for two-dimensional cascade testing are reliably produced.

(b) Correct predictions of the performance of the blade are made using the pressure distribution program. This is especially true with regard to the undesirable effects of leading edge blockage and over-expansion near the trailing edge.

(c) The boundary layer program effectively predicts the boundary layer parameters over the blade surface, enabling improvements of the blade shape to be made. Further development of the program is required however.

Supporting the above conclusion (a) the wind tunnel performance may be examined in more detail by reference to the Figures. The duration of steady operating conditions can be compared to the time required for accurate pressure measurements as shown in Figures 47 and 64. The average turbulence levels of 1.4% are sufficiently high to avoid problems with delayed transition of the boundary layer on the blade surfaces.

Excellent uniformity of total head is obtained in the critical central region of the test section (Fig. 66), where the flow direction is everywhere within ±1% of a mean value some 2^{o} from the tunnel axis (Fig. 67). Figure 72 indicates that, in this same region, the tunnel wall static pressure is of a uniform level. The end-wall boundary layers also are sufficiently thin to result in two-dimensional flow at the blade mid-height (Fig. 73).

The blade surface pressure measurements summarised in Figs. 82 and 83, are in good agreement with the theoretical analysis and the published results for this class of blades. With the results obtained to date we can apply our potential flow analysis to future turbine blade design.

The boundary layer calculation scheme works well for constant free stream pressure and mild pressure gradients. In common with most other methods the accuracy falls when strongly adverse or favourable pressure gradients are applied to the boundary layer edge. The predicted value for boundary layer thickness (Figs. 23 and 25) is substantiated to some extent by the wake measurements (Fig. 87). Additional operating experience is required before the program can be reliably applied to all classes of flows. It can however be used to calculate such integral parameters as displacement thickness to improve two-dimensional profile design.

In summary the overall conclusion can be made that the existing systems provide a simple and effective basis for the two-dimensional design of highly curved turbine blades.

REFERENCES

1. HORLOCK, J.H. "Axial Flow Turbines", Butterworth, 1966.

2. ZWEIFEL, O. "The Spacing of Turbomachinery Blading, especially with Large Angular Deflection". Brown Boveri Review, 1945.

3. LE FOLL, J. "A Theory of Representation of the Properties of Boundary Layers on a plane". Proc. of Seminar on Advanced Problems in Turbomachinery. V.K.I. 1965.

4. FOTTNER, L. "Analytical Approach for the Loss and Deflection Behaviour of Cascades in Transonic Flow Including Axial Mass Flow Variation". AGARD A6-164 1972. Conference Proceedings, "Boundary Layer Effects in Turbomachines" Surugue, J.Editor.

5. JOHNSEN I.A. & BULLOCK, R.O. (Editors) "Aerodynamic Design of Axial Flow Compressors" NASA SP-36, 1965.

6. MARTENSEN, G. "Calculation of Pressure Distribution over Profiles in Cascade in Two Dimensional Potential Flow by Means of a Fredholm Integral Equation" Archives of Rational Mechanical Analysis 3, 3, 1959.

7. STANITZ, J.O. "Design of Two-Dimensional Channels with Prescribed Velocity Distribution Along the Channel Walls".
   Part I "Relaxation Solution" NACA Tech. Note 2593, 1952.
   Part II "Solution by Green's Function" NACA Tech. Note 2595, 1952.

8. McDONALD, P.W. "The Computation of Transonic Flow through 2-D Gas Turbine Cascades". ASME, 71-GT-89. 1971.

9. DAVIS, W.R. & MILLAR, D.J. "A Matrix Method applied to the Analysis of the Flow past Turbomachine Blades". Carleton University, ME/A, 72-7.

10. KUMAR, V. "The Design of Three Related Gas Turbines for an Experimental Investigation of the Effect of Blade Loading on Performance". M.Eng., Thesis. Dept. of Mechanical Eng., Carleton University. 1968.

11. MALHOTRA, R.K. "The Two-Dimensional Development and Analysis of Blade Profiles having large Turning Angles". M.Eng Thesis. Dept. of Mechanical Eng., McMaster University, 1971.

12. COHEN, H., ROGERS, G.F.C., SARAVANAMUTTOO, H.I.H. "Gas Turbine Theory" 2nd Ed. J. Wiley & Sons, 1972.

13. OOSTHUIZEN, P.H. "A Simple Numerical Procedure for the Solution of Turbulent Boundary Layer Problems". Course Notes. Dept. of Mechanical Engineering. Queens University. 1970.

14. PLETCHER, R.H. "On a Finite Difference Solution for the Constant Property Turbulent Boundary Layer" A.I.A.A. Journal. Vol. 7. 1969.

15. McDONALD, H. & FISH, R.W. "Practical Calculations for Transitional Boundary Layers" AGARD. AG-164, 1972. Conference Proceedings. SURUGUE, J. Editor. "Boundary Layer Effects in Turbomachines"

16. WHITE, F.M. "Viscous Fluid Flow" McGraw-Hill, 1974.

17. BRADSHAW, P. "The Analogy between Streamline Curvature and buoyancy in turbulent Shear Flow". Journal of Fluid Mechanics, 1968. Vol 36.

18. THOMANN, H. "Effect of Streamwise Wall Curvature on Heat Transfer in a Turbulent Boundary Layer". Journal of Fluid Mechanics, Vol. 33. 1968.

19. SCHLICHTING, H. "Boundary Layer Theory". Trans by J. Kestin McGraw-Hill, 1968.

20. PAI, SHIH-I — "Viscous Flow Theory" Part II Turbulent Flow. Van Nostrand, 1957.

21. WADE, J.H.T., STANNARD, J.H. & GUPTA, S.K. — "A Finite Difference Calculation Method for the compressible Turbulent Boundary Layer over a curved surface". Dept. of Mechanical Engineering. McMaster University, ME/75/FM/TN/10

22. MAISE, G. & McDONALD, H. — "Mixing Length and Kinematic Eddy Viscosity in a Compressible Boundary Layer". AIAA, 5th Aerospace Meeting, 1967.

23. DUNHAM, J. — "Predictions of Boundary Layer Transition on Turbomachinery Blades". AGARD AG-164, 1972. SURUGUE, J. Editor.

24. DUNHAM, J. & EDWARDS. — "Heat Transfer Calculations for Turbine Blade Design". AGARD CP-73-71, 1970. Conference Proceedings "High Temperature Turbines".

25. DZUNG, L.S.(Editor) — "Flow Research on Blading". Brown Boveri Symposium Proceedings. 1969.

26. BETTNER, J.L. & BLESSING, J.U. — Design and Experimental results for a Turbine with Jet Flap Stator and Jet Flap rotor". NASA CR 2244, 1973

27. SCHUBAUER, G.B. & SPANGENBURG, W.G. — "Effects of Screens in Wide Angle Diffusers" NACA TN 1610

28. WADE, J.H.T. & FOWLER, H.S. — "An Introductory Note on Diffuser Design and Performance". Me-73-TF-1.

29. TUCKER, G.K. & WILLS, D.M. — "A Simplified Technique of Control System Engineering". Minneapolis-Honeywell Regulator Co. Ltd., 1958.

30. BREMER, J.W. — "Control Systems Analysis Design and Simulation". Prentice-Hall Inc. 1974

31. Private Communication - Orenda Engines Ltd.

32. Private Communication - Mechanical Engineering Division, National Research Council of Canada.

33. POPE, A. — "Aerodynamics of Supersonic Flight". Pitman, 1958.

34. BRYER, D.W. & PANKHURST, R.C. "Pressure Probe Methods for Determining Wind Speed and Flow Direction". HMSO 1971.

35. PARADIS, M.A. "Pressure and Velocity Measurements in Subsonic Flow". A Monogram. Department of Mechanical Engineering, Laval University.

36. DEAN, R.C. Ed. "Aerodynamic Measurements". Gas Turbine Laboratory, Massachusetts Institute of Technology, 5th edition, 1958.

37. SCHNEIDER, W. & WADE, J.H.T. "Investigation of Flow in the Mechanical Engineering Department Laboratory Air Jet". Mechanical Engineering Department, McMaster University, 1963.

38. WADE, J.H.T. AERONOTE 181. "A Review of the Literature on the Design of a Contraction Cone".

39. TURNER, A.B. "Heat Transfer Instrumentation" Conference Proceedings. "High Temperature Turbines". AGARD P-73-71.

40. LIEPMANN,H.W. & ROSHKO, A. "Elements of Gas Dynamics". J. Wiley & Sons, 1956.

41. DUNHAM, J. "A Review of Cascade Data on Secondary Losses in Turbines". Journal of Mechanical Engineering Science, Vol. 12, No. 1. 1970

42. KLEIN, A. "Investigation of the effect of the Entry Boundary Layer on the Secondary Flows in the blading of Axial Flow Turbines". British Hydromechanics Research Association, T1004, 1969.

43. PRUMPER, H. "Application of Boundary Layer Fences in Turbomachinery". Conference Proceedings "Boundary Layer Effects in Turbomachinery" SURUGUE J. Ed. AGARD AG-164, 1972.

44. PAPAILLOU, K.O. & SATTA, A. & NURZIA, F. "On the Two-dimensional Boundary Layers as they appear on Turbomachine Blades". Conference Proceedings. "Boundary Layer Effects in Turbomachinery". SURUGUE, J. Ed. AGARD AG-164 - 1972

45. BONHAM, D.J. "A System for the Synthesis of Machine Structures". Ph.D. Thesis. Department of Mechanical Engineering, McMaster University.

APPENDIX 1 FUTURE DIRECTIONS FOR RESEARCH

There are three major avenues for future research in this field.

(a) Three-Dimensional Effects

The major lack in the present work is the lack of detailed knowledge about secondary flows for this type of blade. The existing cascade wind tunnel can be used to study the effect of inlet boundary layers, and the larger three-dimensional test rig will provide more information to complete another "block" of our design diagram.

(b) The Boundary Layer Calculation

The existing program is clumsier and more expensive than it needs to be. The following improvements could be made:

(i) Entirely remove the non-dimensionalising system and process the "raw" equations. No loss of accuracy is expected because the accuracy of representation available with most computing machines greatly exceeds the accuracy of our equations.

(ii) It would be possible to implement a curvature correction scheme as a sub-routine in which shape factor was corrected between steps using suitable empirical data. (Ref. 44)

(iii) The effect of surface roughness could be taken into account by modifying the damping factor near the wall to allow for the effect of roughness on the viscous sublayer (15).

(c) Automation of the Design Procedure

With the existing computation blocks available it is now possible to exploit them more fully. The programs are simple and fast enough to use in a computer aided design scheme similar to that described by Bonham (45). The basic principle is to use a mini-computer such as the PDP8-L to organise the transferral of information from peripheral devices such as the digitiser to the large computer in a digestible form for processing. This processing could be the pressure distribution program for instance (see Fig. AI-1) or a three-dimensional blade stacking procedure.

In this way the designer selects the particular pre-programmed calculation to be performed and can design a blade extremely quickly. The tasks of drafting and information transferred are performed by the mini-computer, which has interface routines to convert information to a form suitable for each item of peripheral equipment. Thus the task of the designer, who is in command of the procedure, is reduced to that of DESIGN, since there are some aspects of experience and judgement that cannot be programmed.

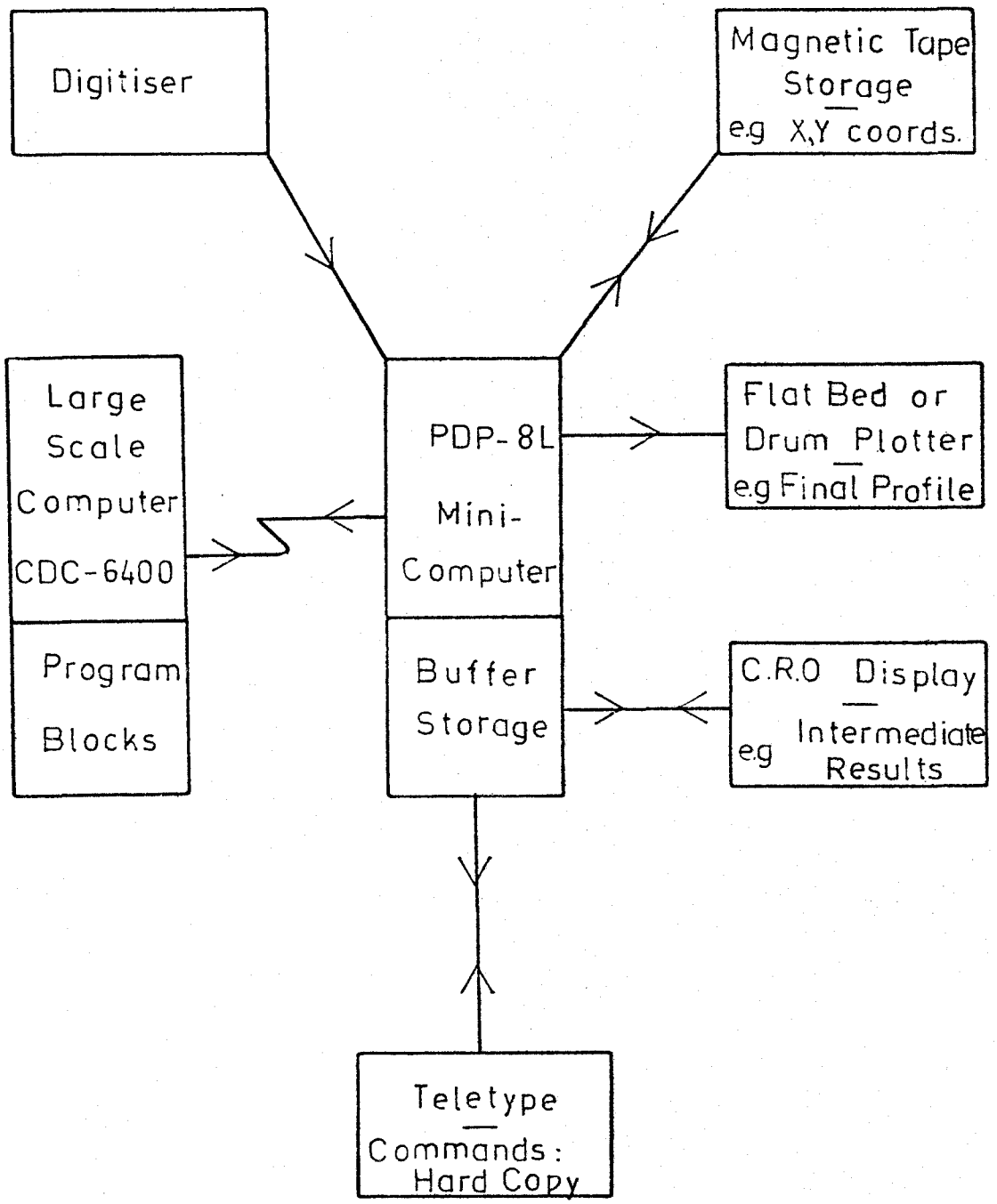

Figure A1-1 Schematic of Computer Aided Design Facility

APPENDIX 2

USERS MANUAL FOR THE PROGRAM

A flow chart and program listing are included in this appendix, together with a list of variables and sample output.

The program starts by reading in the inlet flow conditions and useful constants such as the specific heat ratio. It then proceeds to calculate a mass flow required to choke the blade or alternatively some design mass flow less than this if unchoked flow is required. Proceeding to the first quasi-orthogonal line it reads in values for suction and pressure surface curvatures, and also the length of the quasi-orthogonal. Using one of the expressions developed for velocity distribution a value for mass flow is calculated and compared to the design value. When convergence to a suitable accuracy is achieved the program prints out results for the flow variables at this station. It then moves on to the next quasi-orthogonal and repeats the process.

For choked flow at a throat the alternative calculation can be used.

At a typical orthogonal values for static pressure, Mach No., velocity, static pressure relative to inlet total pressure, static temperature and density are tabulated for the nine stream-tubes. The input variables to which numerical values have to be assigned are listed below.

VARIABLE	DESCRIPTION	UNITS OR VALUE
RETOPI	Relative Total Pressure at Inlet	psia
PEXIT	Static Pressure downstream of Cascade	psia
AMACHIN	Inlet Mach No.	----
RELTOT	Relative Total Temperature at Inlet	^{o}R
GASC	Specific Gas Content for Air	53.333ft-lb/lb_m ^{o}R
G	Acceleration due to Gravity	32.16 ft/sec^2
GAMMA	Ratio of Specific Heats	1.4
SPACE	Blade Pitch	Inches
JX	Control Card JX = 1 Curvature Variation is Linear JX = 2 Radius of Curvature Variation is Linear	
ACC	Required Accuracy for Iteration Loop	----
GAGE	Width of Flow passage defined by Inlet Streamlines. Normally Pitch x cosine of Inlet Air Angle	Inches
THROAT	Passage Width at Geometric Throat	Inches
RATIO	Iterating variable, given starting Value = 1	
AMCRIT	Critical Inlet Mach No. at which Geometric throat would choke.	
NDATA	Number of Quasi-orthogonals Used	
CP(k)	Curvature of Pressure Surface	Reciprocal "
CS(k)	Curvature of Suction Surface	Reciprocal "
GAUGE(k)	Quasi-Orthogonal Length	Inches

It is generally best to tabulate the data for Cp(k), CS(k) and GAUGE(k) when generated from the blade drawing along with the axial chord locations of each end of the quasi-orthogonal. Thus facilitating plotting of the pressure distribution as a function of axial chord. e.g

% AXIAL CHORD (SUCTION SURFACE)	% AXIAL CHORD (PRESSURE SURFACE)	CP(k) in^{-1}	CS(k) in^{-1}	GAUGE(k) in
25.0	5.0	1.28	2.72	0.455

The remaining variables in the program do not generally have to be assigned values.

VARIABLE	DESCRIPTION
A(I)	Speed of Sound
AMACH	Mach. No.
AMAS	Design channel mass flow
AP	Static Pressure
AR	Density
AT	Static Temperature
AV	Resultant Velocity
CMAS	Choking Mass Flow for Geometric Throat
D_1, D_2, D_3, D_4	Constants containing GAMMA
DELG	Distance between two adjacent streamlines
POW	Variable calculated within program used in velocity distribution expressions

RELTOP	Relative Total Pressure
RELTOT	Relative Total Temperature
RO(I)	Density
RPR(I)	Static Pressure
RPR(I)	Static Temperature
TMAS	Calculated mass flow in channel
W(I)	Velocity
Z(I)	Density x Velocity

FLOW CHART

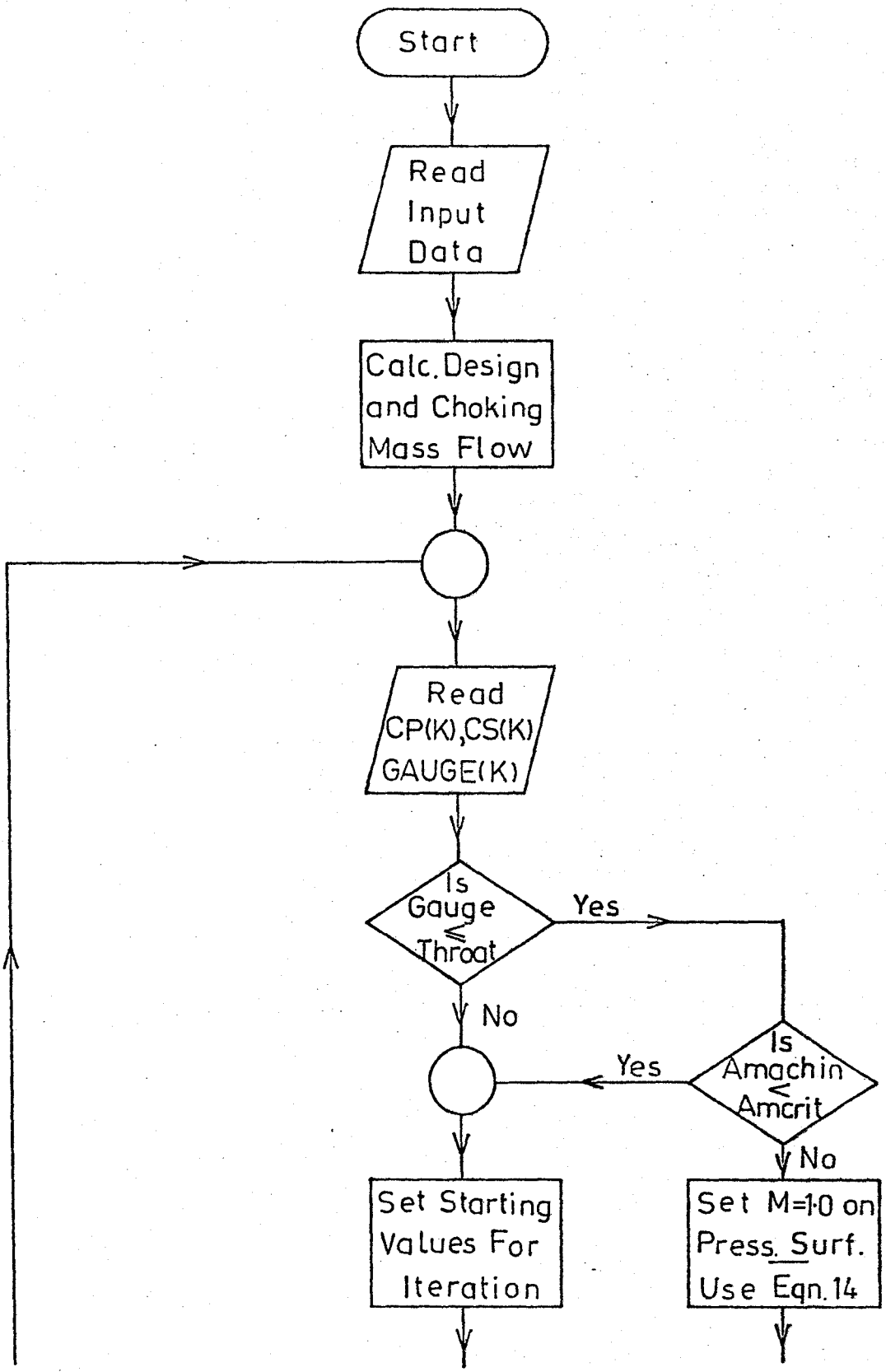
Start
Read Input Data
Calc. Design and Choking Mass Flow
Read CP(K), CS(K) GAUGE(K)
Is Gauge ≤ Throat
Yes
No
Is Amachin < Amcrit
Yes
No
Set Starting Values For Iteration
Set M=1.0 on Press. Surf. Use Eqn. 14

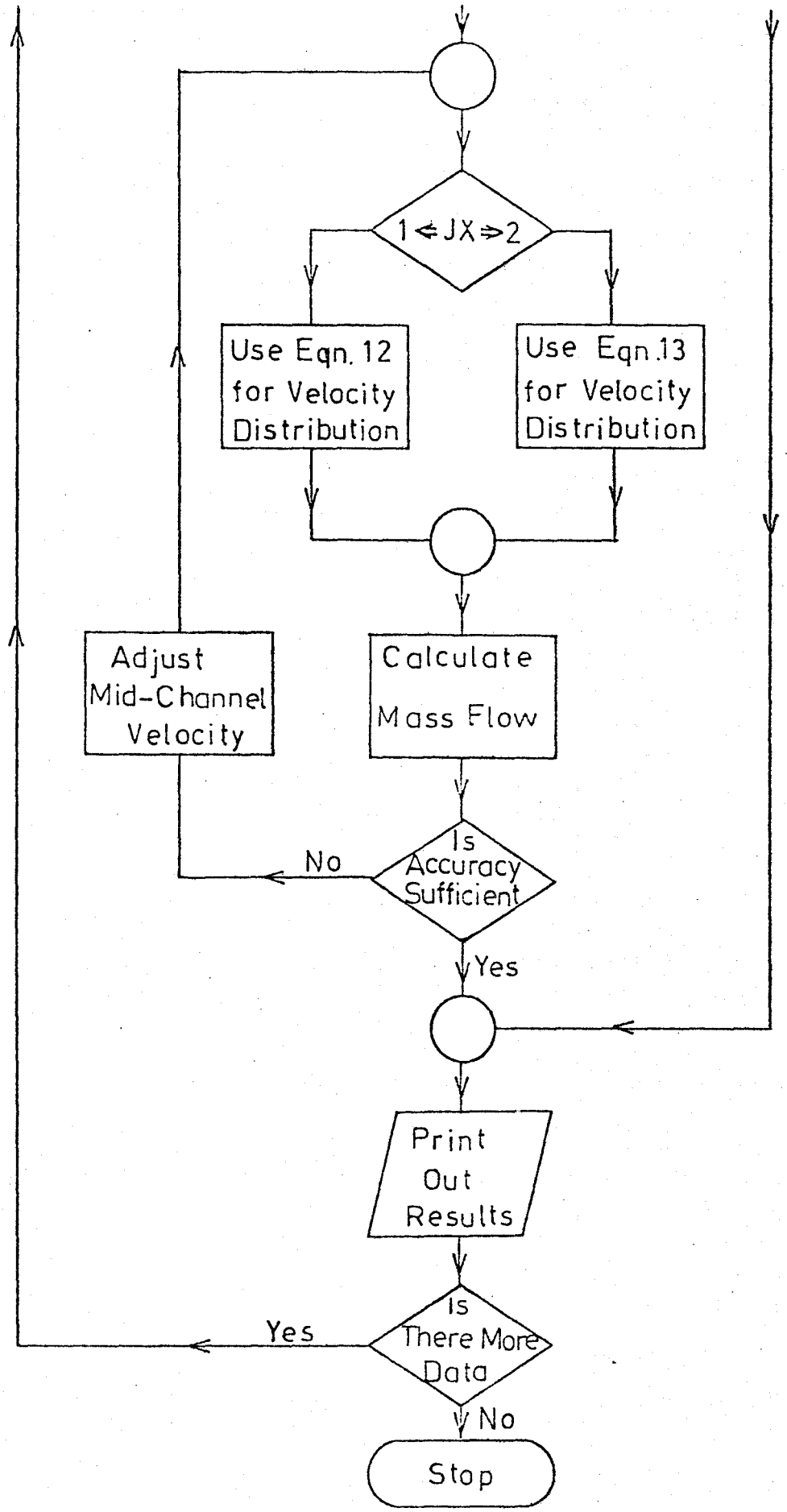
1⇐JX⇒2
Use Eqn. 12 for Velocity Distribution
Use Eqn.13 for Velocity Distribution
Adjust Mid-Channel Velocity
Calculate Mass Flow
No
Is Accuracy Sufficient
Yes
Print Out Results
Is There More Data
Yes
No
Stop

```
      PROGRAM TST (INPUT,OUTPUT,TAPE5=INPUT,TAPE6=OUTPUT)
      DIMENSION W(9),RPR(9),Z(9),AMACH(9),DRPR(9),
     1CP(12),CS(12),GAUGE(12),RT(9),A(9),RO(9)
      READ (5,15)RETOPI,PEXIT,AMACHIN,RELTOT
      READ (5,16) GASC,G,GAMMA,SPACE,JX
      READ(5,17)ACC,GAGE,THROAT,RATIO,AMCRIT,NDATA
15    FORMAT(4F8.3)
16    FORMAT(4F8.4,I2)
17    FORMAT(5F8.4,I8)
C
C
C     USEFUL CONSTANTS AND CHOKING MASS FLOW ARE CALCULATED
C
C
      D1=2.0*GAMMA*GASC*G
      D3=GAMMA-1.0
      D2=GAMMA/D3
      D4=GAMMA+1.0
      CMAS=(((G1MMA*G)/(GASC*RELTOT))**0.5)*THROAT*RETOPI*12.0/1.728
      WRITE(6,21)  CMAS
      WRITE(6,999)
      WRITE(6,999)
      WRITE(6,22)RETOPI,PEXIT,AMACHIN,RELTOT
      WRITE(6,999)
      WRITE(6,23) GASC,G,GAMMA,SPACE,JX
      WRITE(6,999)
      WRITE(6,25)ACC,GAGE,THROAT,RATIO,AMCRIT,NDATA
      WRITE(6,999)
C
C
C     THE DESIGN MASS FLOW IS CALCULATED AND THE SURFACE CURVATURES AND
C     QUASI-ORTHOGONAL LENGTH READ IN
C
C
      AT=RELTOT/(1+(D3*(AMACHIN**2.0))/2.0)
      AP=RETOPI*(AT/RELTOT)**D2
      AR=AP/GASC/AT*144
      AV=AMACHIN*((GAMMA*GASC*G*AT)**0.5)
      AMAS=AR*AV*GAGE/12.0
      WRITE(6,24)AMAS
      WRITE(6,999)
      DO 900 K=1,NDATA
      READ(5,24 )CP(K),CS(K),GAUGE(K)
      WRITE(6,999)
      WRITE(6,999)
      WRITE(6,999)
      WRITE(6,999)
      WRITE(6,28)
      WRITE(6,999)
      WRITE(6,241)CP(K),CS(K),GAUGE(K)
      WRITE(6,999)
      WRITE(6,999)
C
C
      IF(GAUGE(K)-THROAT) 63,63,62
```

```
63     IF(AMCRIT-AMACHIN) 64,64,62
C
C
62     W(5)=AV*GAGE/GAUGE(K)
51     IF(((W(5)**2)*D3/D1).LT.(RELTOT)) GOTO 52
       W(5)=W(5)/2.0
       GOTO 51
52     CONTINUE
66     W(5)=W(5)*RATIO
C
C
C
C
       DO 235 I=1,9
53     C=I
       DELG=(C-1.0)*GAUGE(K)/8.0
       IF(JX.EQ.2) GOTO 57
56     POW=GAUGE(K)*(CS(K)*(3.0/8.0-DELG/GAUGE(K))+.125*CP(K)-.5*
      $(CP(K)-CS(K))*(DELG/GAUGE(K))**2.0)
49     W(I)=W(5)*EXP(POW)
       GOTO 60
57     IF(CP(K)-CS(K))58,59,58
58     W(I)=W(5)*(2.0*(CP(K)+(CS(K)-CP(K))*DELG/GAUGE(K))/(CP(K)+
      $CS(K)))**UGAUGE(K)*CS(K)*CP(K)/(CP(K)-CS(K)))
       GOTO 60
59     POW=GAUGE(K)*(.5-DELG/GAUGE(K))*CS(K)
       GOTO 49
60     RELTOP=RETOPI
       RT(I)=RELTOT-(W(I)**2)*D3/D1
       A(I)=(GAMMA*GASC*G*RT(I))**0.5
       AMACH(I)=W(I)/A(I)
       RPR(I)=RELTOP/(RELTOT/RT(I))**D2
       DRPR(I)=RPR(I)/RELTOP
       RO(I)=144.0*RPR(I)/(GASC*RT(I))
235    Z(I)=RO(I)*W(I)
54     TMAS=(0.03489*(Z(1)+Z(9))+0.20769*(Z(2)+Z(8))-0.03273*(Z(3)+
      $Z(7))+.371023*(Z(4)+Z(6))-0.16014*Z(5))*GAUGE(K)/12.0
C
C
       RATIO=2.0-(TMAS/AMAS)
       IF(ABS(AMAS-TMAS).LE.ACC) GOTO 61
       GOTO 66
C
C
64     DO 245 I=1,9
       RT(9)=RELTOT*2.0/(GAMMA+1.0)
       W(9)=(GAMMA*GASC*G*RT(9))**0.5
       C=I
       DELG=(C-1.0)/8.0
       POW=GAUGEUK)*(CP(K)+CS(K)-2.0*CS(K)*DELG-(CP(K)-CS(K))*(DELG**2))
       W(I)=W(9)*EXP(POW)
       RELTOP=RETOPI
       RT(I)=RELTOT-(W(I)**2.0)*D3/D1
       A(I)=(GAMMA*GASC*G*RT(I))**0.5
       AMACH(I)=W(I)/A(I)
       RPR(I)=RELTOP/(RELTOT/RT(I))**D2
       DRPR(I)=RPR(I)/RELTOP
```

```
      RO(I)=144.0*RPR(I)/(GASC*RT(I))
245   Z(I)=RO(I)*W(I)
      TMAS=(.03489*(Z(1)+Z(9))+.20769*(Z(2)+Z(8))-.03273*(Z(3)+Z(7))
     $+.37023*(Z(4)+Z(6))-.16014*(Z(5)))*GAUGE(K)/12.0
      GOTO 61
C
C
61    WRITE(6,27)TMAS
      WRITE(6,999)
      WRITE(6,999)
      WRITE(6,30)
      WRITE(6,999)
      DO 26 I=1,9
21    FORMAT(1H1,40X,10HINPUT DATA/40X,10H----- ----//*
     $CHOKING MASS FLOW RATE =*,F10.3)
22    FORMAT(4F8.3)
23    FORMAT(4F8.4,I2)
24    FORMAT(1H1,40X,11HOUTPUT DATA/40X,11H------ ----//*
     $DESIGN MASS FLOW RATE =*,F10.3)
25    FORMAT(5F8.4,I8)
26    WRITE(6,29)RPR(I),AMACH(I),W(I),DRPR(I),RT(I),RO(I)
27    FORMAT(1HO,20X,*CALCULATED MASS FLOW RATE =*,F10.3)
28    FORMAT(1HO,20X,*CP(K)      CS(K)      GAUGE(K)*)
29    FORMAT(1HO,12X,F10.3,1X,F10.3,3X,F10.3,1X,F6.3,3X,F10.3,3X,
     1F6.3)
30    FORMAT(1HO,*                    RPR(I)      AMACH(I)      W(I)      DRPR(
     $I)      RT(I)      RO(I)*)
240   FORMAT(3F10.4)
241   FORMAT(16X,3F10.4)
999   FORMAT(10X,*    *)
900   CONTINUE
      STOP
      END
'         END OF RECORD
27.80617 14.69   0.61     530.0
53.353   32.16    1.4      0.685    1
0.0005   0.393    0.335    1.0      0.60          12
0.002      2.20       0.350
0.002      2.47       0.362
0.002      2.615      0.383
0.002      2.63       0.421
1.28       2.72       0.455
1.440      2.72       0.48
2.19       2.72       0.495
2.115      2.72       0.48
1.507      2.63       0.421
0.605      1.97       0.365
0.25       1.111      0.344
0.002      0.475      0.335
'          END OF FILE
```

OUTPUT DATA McDonald Blade

DESIGN MASS FLOW PATE = 2.574

CP(K)	CS(K)	GAUGE(K)
.0020	2.2000	.3500

CALCULATED MASS FLOW RATE = 2.573

RPR(I)	AMACH(I)	W(I)	DRPR(I)	RT(I)	RO(I)
13.406	1.076	1094.422	.482	430.277	.084
15.289	.965	999.986	.550	446.744	.092
16.783	.881	924.749	.604	458.801	.099
17.940	.817	865.513	.645	467.630	.104
18.815	.768	819.868	.677	474.035	.107
19.452	.733	786.022	.700	478.560	.110
19.883	.709	762.686	.715	481.569	.111
20.133	.695	748.993	.724	483.293	.112
20.216	.691	744.439	.727	483.859	.113

CP(K)	CS(K)	GAUGE(K)
.0020	2.4700	.3620

CALCULATED MASS FLOW RATE = 2.573

RPR(I)	AMACH(I)	W(I)	DRPR(I)	RT(I)	RO(I)
14.221	1.028	1053.495	.511	437.596	.088
16.309	.907	948.689	.587	455.067	.097
17.925	.817	866.319	.645	467.514	.103
19.149	.750	802.221	.689	476.418	.108
20.055	.700	753.309	.721	482.753	.112
20.703	.663	717.323	.745	487.159	.115
21.136	.638	692.658	.760	490.055	.116
21.386	.624	678.244	.769	491.700	.117
21.468	.619	673.465	.772	492.238	.118

CP(K)	CS(K)	GAUGE(K)
.0020	2.6150	.3830

CALCULATED MASS FLOW RATE = 2.574

RPR(I)	AMACH(I)	W(I)	DRPR(I)	RT(I)	RO(I)
15.722	.941	978.265	.565	450.322	.094
17.855	.821	869.924	.642	466.993	.103
19.456	.733	785.773	.700	478.593	.110
20.638	.667	720.949	.742	486.725	.114
21.495	.618	671.897	.773	492.413	.118
22.097	.583	636.051	.795	496.317	.120
22.495	.559	611.607	.809	498.856	.122
22.722	.545	597.371	.817	500.289	.123
22.796	.540	592.662	.820	500.756	.123

CP(K)	CS(K)	GAUGE(K)
.0020	2.6300	.4210

CALCULATED MASS FLOW RATE = 2.574

RPR(I)	AMACH(I)	W(I)	DRPR(I)	RT(I)	RO(I)
17.871	.820	869.100	.643	467.112	.103
19.371	.710	763.336	.715	481.487	.111
21.319	.628	682.134	.767	491.259	.117
22.356	.567	620.199	.804	497.975	.121
23.091	.522	573.720	.830	502.595	.124
23.598	.490	539.979	.849	505.724	.126
23.929	.468	517.085	.861	507.739	.127
24.115	.456	503.796	.867	508.868	.128
24.176	.452	499.408	.869	509.235	.128

CP(K)	CS(K)	GAUGE(K)
1.2800	2.7200	.4550

CALCULATED MASS FLOW RATE = 2.574

RPR(I)	AMACH(I)	W(I)	DRPR(I)	RT(I)	RO(I)
17.339	.850	896.432	.624	463.094	.101
19.714	.719	771.889	.709	480.394	.111
21.502	.617	671.489	.773	492.459	.118
22.836	.538	590.159	.821	501.002	.123
23.830	.475	524.016	.857	507.138	.127
24.572	.424	470.075	.884	511.602	.130
25.129	.383	426.025	.904	514.889	.132
25.549	.350	390.076	.919	517.331	.133
25.866	.323	360.836	.930	519.160	.134

CP(K)	CS(K)	GAUGE(K)
1.4400	2.7200	.4800

CALCULATED MASS FLOW RATE = 2.574

RPR(I)	AMACH(I)	W(I)	DRPR(I)	RT(I)	RO(I)
17.937	.817	865.704	.645	467.603	.104
20.316	.685	738.886	.731	484.545	.113
22.086	.583	636.728	.794	496.245	.120
23.390	.503	553.988	.841	504.448	.125
24.351	.440	486.649	.876	510.282	.129
25.061	.388	431.619	.901	514.489	.131
25.589	.347	386.504	.920	517.562	.133
25.984	.313	349.444	.934	519.833	.135
26.281	.285	318.985	.945	521.528	.136

CP(K)	CS(K)	GAUGE(K)
2.1900	2.7200	.4950

CALCULATED MASS FLOW RATE = 2.574

RPR(I)	AMACH(I)	W(I)	DRPR(I)	RT(I)	RO(I)
17.361	.849	895.318	.624	463.261	.101
19.965	.705	758.186	.718	482.139	.112
21.954	.591	644.695	.790	495.395	.120
23.443	.500	550.444	.843	504.774	.125
24.548	.426	471.903	.883	511.459	.130
25.364	.365	406.230	.912	516.261	.133
25.966	.314	351.133	.934	519.735	.135
26.412	.272	304.755	.950	522.267	.136
26.743	.237	265.590	.962	524.127	.138

CP(K)	CS(K)	GAUGE(K)
2.1150	2.7200	.4800

CALCULATED MASS FLOW RATE = 2.574

RPR(I)	AMACH(I)	W(I)	DRPR(I)	RT(I)	RO(I)
17.024	.867	912.478	.612	460.678	.100
19.622	.724	776.839	.706	479.755	.110
21.623	.610	664.370	.778	493.251	.118

23.136	.519	570.768	.832	502.876	.124
24.270	.445	492.584	.873	509.798	.128
25.117	.384	427.042	.903	514.817	.132
25.748	.333	371.905	.926	518.484	.134
26.221	.291	325.360	.943	521.186	.136
26.576	.255	285.935	.956	523.193	.137

CP(K)	CS(K)	GAUGE(K)
1.5070	2.6300	.4210

CALCULATED MASS FLOW RATE = 2.574

RPR(I)	AMACH(I)	W(I)	DRPR(I)	RT(I)	RO(I)
15.820	.935	973.361	.569	451.118	.095
18.227	.801	850.688	.655	469.749	.105
20.133	.695	748.983	.724	483.294	.112
21.623	.610	664.335	.778	493.255	.118
22.781	.541	593.619	.819	500.661	.123
23.680	.485	534.364	.852	506.226	.126
24.379	.438	484.590	.877	510.449	.129
24.923	.399	442.711	.896	513.682	.131
25.350	.366	407.449	.912	516.178	.133

CP(K)	CS(K)	GAUGE(K)
.6050	1.9700	.3650

CALCULATED MASS FLOW RATE = 2.573

RPR(I)	AMACH(I)	W(I)	DRPR(I)	RT(I)	RO(I)
15.056	.979	1011.691	.541	444.784	.091
16.712	.885	928.332	.601	458.248	.098
18.076	.809	858.499	.650	468.637	.104
19.188	.748	800.124	.690	476.698	.109
20.087	.698	751.546	.722	482.974	.112
20.807	.657	711.434	.748	487.860	.115
21.378	.625	678.726	.769	491.646	.117
21.822	.599	652.582	.785	494.543	.119
22.158	.579	632.349	.797	496.708	.120

CP(K)	CS(K)	GAUGE(K)
.2500	1.1110	.3440

CALCULATED MASS FLOW RATE = 2.573

RPR(I)	AMACH(I)	W(I)	DRPR(I)	RT(I)	PO(I)
15.129	.975	1008.030	.544	445.399	.092
16.021	.924	963.232	.576	452.752	.096
16.784	.881	924.694	.604	458.809	.099
17.429	.845	891.816	.627	463.782	.101
17.968	.815	864.096	.646	467.834	.104
18.410	.791	841.122	.662	471.096	.105
18.764	.771	822.556	.675	473.668	.107
19.037	.756	808.132	.685	475.626	.108
19.234	.745	797.643	.692	477.028	.109

CP(K)	CS(K)	GAUGE(K)
.0020	.4750	.3350

CALCULATED MASS FLOW RATE = 2.564

RPR(I)	AMACH(I)	W(I)	DRPR(I)	RT(I)	PO(I)
11.168	1.220	1208.501	.402	408.404	.074
12.028	1.163	1164.248	.433	417.146	.078
12.757	1.117	1127.183	.459	424.217	.081
13.360	1.079	1096.715	.480	429.858	.084
13.845	1.050	1072.368	.498	434.255	.086
14.216	1.028	1053.766	.511	437.546	.088
14.478	1.012	1040.627	.521	439.839	.089
14.635	1.003	1032.754	.526	441.198	.090
14.689	1.000	1030.027	.528	441.667	.090

APPENDIX 3 THE FORTRAN IV PROGRAM

The program philosophy has already been described in SECTION 3.5. The program control and a flow chart are included below together with a brief note on each sub-routine.

Program Control

The first data card to be read in contains values of a number of program control flags, these are listed below.

NAME	VALUE	MEANING
FLAG 1	0.0	Mixing length calculated i.e. turbulent
	1.0	" " = 0.0 ∴ laminar
FLAG 2	1.0	Controls first printout of boundary layer
FLAG 3	Unused in present program	
FLAGIT	0.0	Iteration is available between successive M-lines
	1.0	No iteration performed
FLAGPY	Unused	
FLAGTP	0.0	Uses simple temperature calculation
	1.0	Uses thermal energy equation
DAMP	0.0 — 1.0	Used to vary convergence rate of iteration usually 0.7
CUTOFF	0.99	Value of velocity at which B.L. thickness is evaluated
ERROR	5%	Accuracy to which iteration converges
CF	0.0	Starting value of skin friction
ITMIN	2 — 5	Minimum number of iterations allowed if FLAGIT = 0.0
NXTURB	2 — 10	Varies rate at which flow becomes turbulent during transition

Subroutine Descriptions

1 GRID

One input card is required to read in the following quantities:

a) N: number of steps in Y direction (initial)

b) NLIMIT: number of steps in Y direction (maximum allowed)

c) X: Initial value of X inches

d) XX: Final value of X inches

e) DXO: Interval between successive X-stations. This value can be manipulated in the program.

f) DY: Parameter to define Y-grid spacing. With present definition of grid total height of grid is approximately 500 DY.

In addition this subroutine defines the Y-location of points on the grid. The distance between two successive points in the Y-direction increases with distance from the wall.

2 BC

The given free stream and wall conditions are read in

a) Free Stream:

1st card NXDATA, number of points at which data given

Subsequent cards

XINCH: X-station in inches

DPDX: Pressure gradient psi/in

TFAR: Temperature ^{o}R

UFAR: Velocity ft/sec

PFAR: Pressure psf.

b) Wall Conditions:

1st card NWALL, number of points at which data given

Subsequent cards

XWALL: X-station in inches

TWALL: Wall Temp, ^{o}R

3 FLUID

Data is read in in dimensional form for the viscosity, density, conductivity and specific heat of air at different temperatures.

1st Card NPROP: Number of temperature stations at which data tabulated

Subsequent cards

PTEMP: Temperature ^{o}R

PRO: Density lbm/cuft

DCP: Specific Heat Btu/lbm^{o}F

PVIS: Coefficient of viscosity Ft^2/sec

PCOND: Coefficient of thermal conductivity Btu/sec-ft-^{o}F

4 DIMNON

The reference velocity and temperature are given as input. From these values the reference density, viscosity, specific heat and conductivity are obtained by interpolation from the properties of fluid table. The other reference parameters such as the reference length are calculated enabling the free stream data, wall data and grid dimensions to be non-dimensionalized.

5 TEMP

For any given x-station the free stream and wall temperatures are calculated in their non-dimensional form by interpolation.

6 START 2

The boundary layer data for the first x-station is read in.

Using this data the boundary layer profile is calculated using the model described in the main body of the report. (Section 2.2) If there is insufficient data a shape factor can be assumed.

7 TPROP

For a given temperature, air properties are calculated using simple linear interpolation from the non-dimensionalized air properties data.

8 PDX1

For a given x-station the free stream pressure gradient is calculated from the input data given in tabular form.

9 PDX2

For a given x-station the free stream pressure gradient is calculated from the input free stream velocity data.

10 ZLMIX

The mixing length is calculated using the empirical equations given in the report. (Section 2.3)

11 EDDY

The non-dimensional eddy diffusivity is calculated from the previously evaluated mixing length.

12 COEFF

The coefficients of the set of algebraic equations (representing the momentum and energy equations) are evaluated from the known conditions on the M = 1 line and the conditions at the wall and free stream.

13 CALC

This subroutine solves the above set of equations by the Thomas algorithm method. Velocity and temperature at the M + 1 line are thus obtained.

14 VELV

This subroutine calculates the velocities V in the y-direction on the M + 1 line from the equation of motion and the known x-direction velocities.

15 PRNTBL

The boundary layer variables below are printed out at suitable intervals down the surface depending on the value of FLAG 2.

a) The number of the grid point from the wall

b) The distance from the wall, inches

c) The x-direction velocity U/U_1 where U_1 = local free stream velocity

d) The y-direction velocity V/U_1

e) The non-dimensional temperature

f) Temperature ^{o}R

For the last y-station the free stream conditions are printed out.

16 BLX

Using the computed boundary layer solution the boundary layer thickness (D), displacement thickness (DI), momentum thickness (TI) and shape factor are evaluated and printed out.

17 PGL

This subroutine is a general purpose subroutine for linear

interpolation. In the program it is called to calculate free stream variables, wall variables and air properties at different x-stations and temperatures.

FLOW CHART

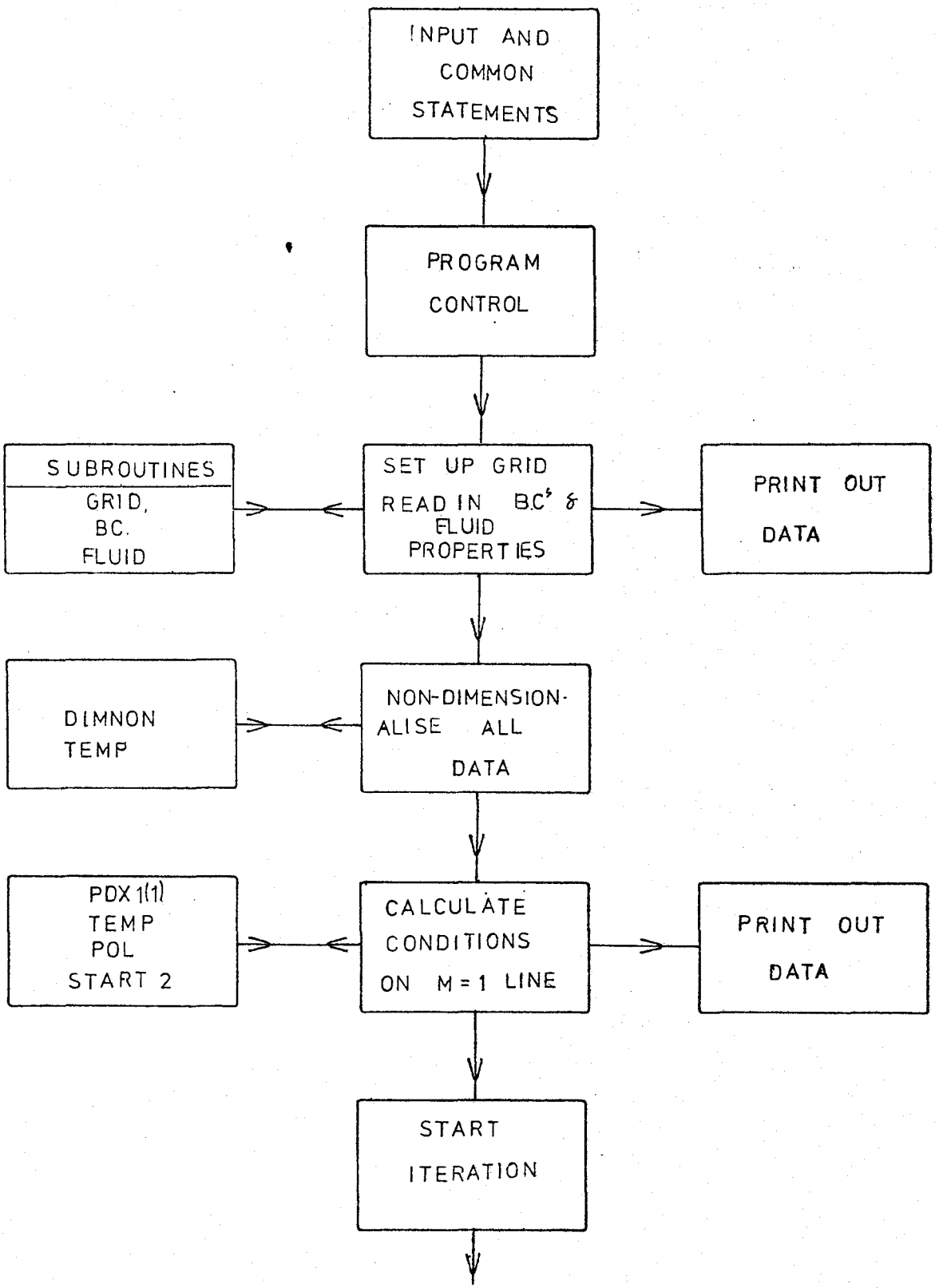
INPUT AND COMMON STATEMENTS
PROGRAM CONTROL
SUBROUTINES
GRID,
BC.
FLUID
SET UP GRID
READ IN B.C's & FLUID PROPERTIES
PRINT OUT DATA
DIMNON
TEMP
NON-DIMENSION-ALISE ALL DATA
PDX 1(1)
TEMP
POL
START 2
CALCULATE CONDITIONS ON M = 1 LINE
PRINT OUT DATA
START ITERATION

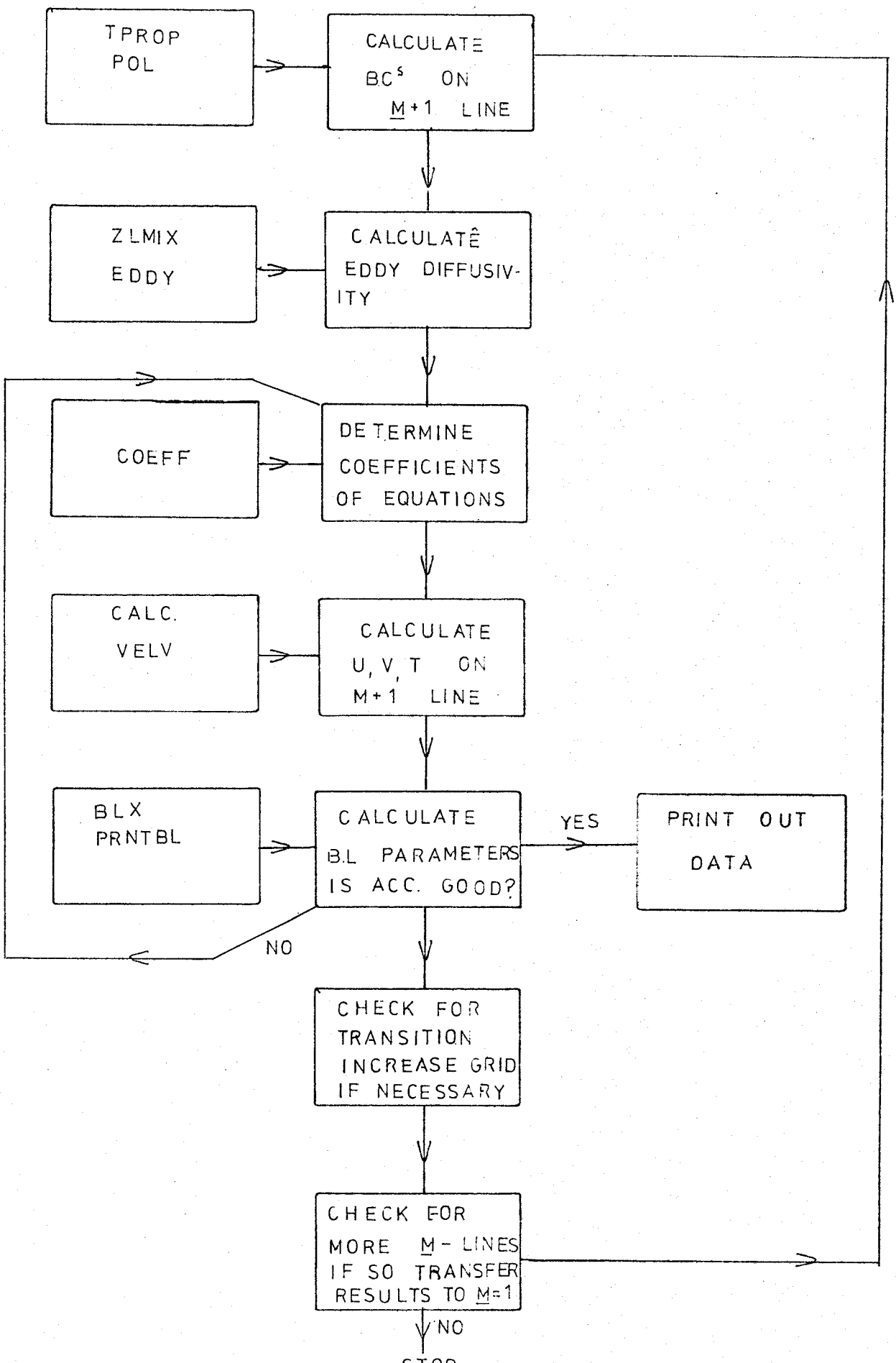
TPROP
POL
CALCULATE
BC^S ON
M+1 LINE
ZLMIX
EDDY
CALCULATE
EDDY DIFFUSIV-
ITY
COEFF
DETERMINE
COEFFICIENTS
OF EQUATIONS
CALC.
VELV
CALCULATE
U, V, T ON
M+1 LINE
BLX
PRNTBL
CALCULATE
B.L PARAMETERS
IS ACC. GOOD?
YES
PRINT OUT
DATA
NO
CHECK FOR
TRANSITION
INCREASE GRID
IF NECESSARY
CHECK FOR
MORE M- LINES
IF SO TRANSFER
RESULTS TO M=1
NO
STOP

BOUNDARY LAYER PROGRAM LISTING

```
      6400 END OF RECORD
      PROGRAM TST (INPUT,OUTPUT,TAPE5=INPUT,TAPE6=OUTPUT)
      COMMON/SKG1/U(2,100),V(2,100),T(2,100)
      COMMON/SKG2/AU(100),BU(100),CU(100),DU(100)
      COMMON/SKG3/AT(100),BT(100),CT(100),DT(100)
      COMMON/SKG4/UIT(100),VIT(100),TIT(100)
      COMMON/SKG5/RO(100),VIS(100),COND(100)
     1           ,PTEMP(50),PRO(50),PCP(50),PVIS(50),PCOND(50)
      COMMON/SKG6/XINCH(50),DPDX(50),TFAR(50),XWALL(50),TWALL(50)
     1,UFAR(50),PFAR(50)
      COMMON/SKG7/Y(100),E(100),HU(100),HT(100),ROM1(100),DPU(100)
     1           ,PY(100),ESX(100),EST(100),TL(100)
      COMMON/SKG8/DP1,DP2,X,XX,   DXO,DY,PR,PRT,CND,FACTOR
      COMMON/SKG9/N,NN,NXDATA,NWALL,NPROP,NLIMIT
      COMMON/SKG10/XR,RTH,D,DX,DI,TI,H
      COMMON/SKG11/UO,TO,TOO,ROO,CPO,VISO,CONDO,XLO,PRESSO
      COMMON/SKG12/ FLAG1,FLAG2,FLAG3,FLAGIT,FLAGPY,FLAGTP,DAMP
     1             ,CUTOFF,ERROR,CF,ITMIN,IPRINT
      COMMON/SKG13/U1,ICON
      COMMON/SKG14/TFSX,DTFSX
      COMMON/SKG15/TFX,TWX
C
C
C
C     PROGRAM CONTROL
READ(5,2)FLAG1,FLAG2,FLAG3,FLAGIT,FLAGPY,FLAGTP,DAMP,
     1CUTOFF,ERROR,CF,FACTOR,ITMIN,NXTURB
      TUBAR=1.5
      NXTURB=5
      ITMIN=2
      ERROR=5.0
      CUTOFF=0.99
      TRANS=1.0
      TRANS=0.0
      FLAGTP=0.0
      FLAGIT=1.0
      WRITE(6,2)FLAG1,FLAG2,FLAG3,FLAGIT,FLAGPY,FLAGTP,DAMP,
     1CUTOFF,ERROR,CF,FACTOR,ITMIN,NXTURB
C
C
      CALL GRID
C
C     READ FREE STREAM TEMP. AND PRESSURE GRADIENT ALONG X
C     IN DIMENSIONAL FORM
      CALL BC
C
C     PROPERTIES OF AIR AT VARIOUS TEMP.( DEG. F)
      CALL FLUID
C
C
C     REFERENCE QUANTITIES
      CALL DIMNON
C
C
C
C     BC,S AT M+1 LINE
```

```
      U(1,1)=0.0
      V(1,1)=0.0
      DP2=0.0
      RO(N)=1.0
      CALL PDX1(1)
      TFSX=1.0
      CALL TEMP(X,T(1,1),T(1,N))
C     FREE STREAM VELOCITY
      CALL POL(5,0,X,0.0,U(1,N))
      U(2,1)=0.0
      V(2,1)=0.0
C
C
C     INITIAL CONDITIONS ARE ASSUMED. IF NOT GIVEN
      CALL START2
C
C
      WRITE(6,66)
      WRITE(6,140)
      IF(FLAG1.EQ.0.0) WRITE(6,68)
      IF(FLAG1.NE.0.0) WRITE(6,67)
      WRITE(6,141)
      WRITE(6,64)
C
C
C     FLUID PROPERTIES ARE EVALUATED AT M=1 LINE
      CALL TPROP(T,1)
      CALL POL(6,0,X,0.0,PFARX)
      DO 3 J=1,N
 3    RO(J)=RO(J)*PFARX
C
C
C
C
C      ITERATION STARTS
      ICON=0
      IPRINT=0
      CF=1.0
100   CONTINUE
      DX=DXO
      XIN=X*XLO*12.0
      IF(XIN.GE.0.1)   DX=5.0*DXO
      X=X+DX
C     DETERMINE BOUNDARY CONDITIONS ON M+1 LINE
      V(2,1)=0.0
      U(2,1)=0.0
      CALL TEMP(X,T(2,1),T(2,N))
      CALL PDX1(2)
      CALL POL(5,0,X,0.0,U( ,N))
C
C
C
      DO 8 I=1,N
      TL(I)=0.0
 8    CONTINUE
      IF(FLAG1.EQ.0.0) CALL ZLMIX
      IF(ICON.EQ.NXTURB) FLAG1=0.0
      IF(ICON.EQ.NXTURB) WRITE(6,999)
```

```
      IF(ICON.EQ.NXTURB) WR+TE(6,68)
      IF(ICON.EQ.NXTURB) WR9TE(6,141)
C
      DO 82 J=1,N
      UIT(J)=U(1,J)
      VIT(J)=V(1,J)
      TIT(J)=T(1,J)
 82   CONTINUE
C
      CALL EDDY
      ITER=0
 80   CONTINUE
      ITER=ITER+1
C
C     CALCULATE THE COEFFIC9ENTS OF EQUATION 47A
      CALL COEF
C
C     SOLVE THE SIMULTANEOUS EQUATIONS 47A AND 47B
C     U AND T ON THE '(M+1) -INE
      CALL CALC(AU,BU,CU,DU,HU)
      IF(FLAGTP.EQ.0.0) GOTO 114
      CALL CALC(AT,BT,CT,DTYHT)
      GOTO 116
114   CONTINUE
      DO 115 J=1,N
      R=0.89
      TAW=TFX+R*((U(2,N)*U0**2)/(2.0*CPO)
      HT(J)=(TO-TWX-((TAW-TWX)*UIT(J)/U(2,N))+R*(UIT(J)*U0)**2
     1/(2.0*CPO))/(TO-TFX)
 115  CONTINUE
C
116   CONTINUE
      DO 16 J=2,NN
      U(2,J)=HU(J-1)
      T(2,J)=HT(J-1)
      IF(FLAGTP.EQ.0.0) T(2,J)=HT(J)
 16   CONTINUE
      IF(ITER.NE.1) GO TO 81
      DO 27 I=1,N
      ROM1(I)=RO(I)
 27   CONTINUE
 81   CONTINUE
      CALL TPROP(T,2)
      CALL POL(6,3,X,0.0,PF+PX)
      DO 4 J=1,N
 4    RO(J)=RO(J)*PFARX
C
C     CALCULATE VELOCITY V USING EQUATION OF CONTINUITY
      CALL VELV
C
      DO 83 J=1,N
      UIT(J)=UIT(J)+(U(2,J)-UIT(J))*DAMP
      VIT(J)=VIT(J)+(V(2,J)-VIT(J))*DAMP
      TIT(J)=TIT(J)+(T(2,J)-TIT(J))*DAMP
 83   CONTINUE
C     COEFFICIENT OF FRICTION
      CF1=CF
      U22=U(2,2)
```

```
      CF=(   U22/Y(2)-Y(2)*DP2/4.0)/U(2,N)**2
      CFERR=(ABS(CF-CF1)/CF1)*100.0
      IF((FLAGIT.EQ.0.0).AND.(ITER.LT.ITMIN)) GO TO 80
      IF((FLAGIT.EQ.0.0).AND.(CFERR.GT.ERROR)) GO TO 80
C
      IPRINT=IPRINT+1
      IF(IPRINT.GE.FLAG2) CALL PRNTBL
      XIN=X*XLO*12.0
      IF((XIN.EQ.22.0).OR.(XIN.EQ.47.0).OR.(XIN.EQ.65.0).
     1OR.(XIN.EQ.83.0)) CALL PRNTBL
C     TRANSFER THE RESULTS OF (M+1) LINE TO INITIAL LINE
      D-1=DP2
      DO 17 J=1,N
      V(1,J)=V(2,J)
      U(1,J)=U(2,J)
   17 T(1,J)=T(2,J)
C
C     B/L CHARACTERISTICS AO THE (M+1) LINE
      CALL BLX
C     HEAT TRANSFER COEFFICIENT
      HTNX=(T(2,1)-T(2,2))/Y(2)
      HTNX=HTNX*1.6/12.0/XLO
      ANX=0.0
      XIN=X*XLO*12.0
      DIN=D*XLO*12.0
      DIIN=DI*XLO*12.0
      TIIN=TI*XLO*12.0
      IF (TRANS.EQ.1.0) GO TO 7
      X1=X-DXO
      X2=X+DXO
      CALL POL (5,0,X1,0.0,U1)
      CALL POL (5,0,X2,0.0,U2)
      DUDX=(U2-U1)/(2.0*DXO)
      ALAMBDA=-(TI**2.0)*(RO(1)/VIS(1))*(DUDX)
      ACF=TIIN/12.0/XLO
      PART1=(0.27+0.73*EXP(-0.8*TUBAR))
      PART2=(550.0+680.0/(1.0+TUBAR-21.0*ALAMBDA)
      RCRIT=PART1+PART2
      IF(ACF.LT.RCRIT) GO TO 9
    7 ICON=ICON+1
      TRANS=1.0
    9 CONTINUE
      WRITE(6,65) XIN,DIN,DIIN,TIIN,H,CF,ACF,HTNX,ITER
C
C
C
C     INCREASE GRID SIZE IF NECESSARY
      IF(D.LT.Y(N-3))GO TO 800
      NMIN=N+1
      DY=Y(N)-Y(N-1)
      DY=1.5*DY
      DV=0
      NMAX=N+10
      IF(NMAX.GT.NLIMIT) GO TO 805
      DO 801 I=NMIN,NMAX
      Y(I)=Y(I-1)+DY
      U(1,I)=U(1,N)
      V(1,I)=V(1,I-1)+DV
```

```
      T(1,I)=T(1,N)
      RO(I)=RO(N)
      VIS(I)=VIS(N)
      COND(I)=COND(N)
  801 CONTINUE
      N=NMAX
      NN=N-1
      WRITE(6,999)
      WRITE(6,71) N
  800 CONTINUE
C
C
C
      IF (X .GT. XX) GO TO  8
      GO TO 100
  805 CONTINUE
      WRITE(6,806) NLIMIT
   18 CONTINUE
C
C
C
    1 FORMAT(1X,2I8,6F10.5)
    2 FORMAT(1X,11F6.2,2I6)
   52 FORMAT(3F10.2)
   64 FORMAT(7X,*X*,6X,*D(B/L THICK.)*,6X,*D'*,9X,*THETA*,8X,*H*,13X,
     1*CF/2*,6X,*          *=12X,*NX*,7X,*NO. OF ITER.*)
   65 FORMAT(3X,F8.4,3X,E10+3,3X,E 9.3,3X,E10.3,3X,F6.3,6X,E10.3,
     13X,E10.3,10X,F10.3,4X=I5)
   66 FORMAT(1H1,30X,*NUMERICAL SOLUTION OF BOUNDARY LAYER FLOW*//)
   67 FORMAT(5X,*NATURE OF BOUNDARY LAYER -LAMINAR*)
   68 FORMAT(5X,*NATURE OF BOUNDARY LAYER -TURBULENT*)
   71 FORMAT(10X,*NUMBER OF GRID POINTS*,5X,I3)
  132 FORMAT(10X,3F20.5)
  140 FORMAT(30X,*--------- ----------------------------------*///)
  141 FORMAT( 5X,*-----------------------------------------*//)
  806 FORMAT(///30X,*NUMBER OF GRID POINTS EXCFED*,5X,I5)
  998 FORMAT(1H1,*  *)
  999 FORMAT(10X,* *)
      STOP
      END
      SUBROUTINE GRID
      COMMON/SKG7/Y(100),E(100),HU(100),HT(100),ROM1(100),DPU(100)
     1           ,PY(100),FSX(100),FST(100),TL(100)
      COMMON/SKG8/DP1,DP2,X,XX,   DXO,DY,PR,PRT,CND,FACTOR
      COMMON/SKG9/N,NN,NXDATA,NWALL,NPROP,NLIMIT
      COMMON/SKG10/XR,RTH,D,DX,DI,TI,H
C
C
      READ(5,32) N,NLIMIT,X,XX,DXO,DY
      NN=N-1
      X=0.05
      XX=1.671
      DXO=0.001
      DXO=0.01
      DY=0.0001
      DX=DXO
      WRITE(6,33)
      WRITE(6,34)
```

```
      WRITE(6,35) X,XX,DXO,DY
C
C     THE Y-GRID
      WRITE(6,36)
      WRITE(6,37) N,NLIMIT
      Y(1)=0.0
      DO 41 J=2,5
 41   Y(J)=Y(J-1)+DY
      DO 42 J=6,10
 42   Y(J)=Y(J-1)+2.0*DY
      DO 43 J=11,15
 43   Y(J)=Y(J-1)+3.0*DY
      DO 44 J=16,30
      ZJ=J-12
 44   Y(J)=Y(J-1)+ZJ*DY
      DO 45 J=31,N
      ZJ=2*J-42
 45   Y(J)=Y(J-1)+ZJ*DY
      DO 50 J=1,N
 50   FSX(J)=Y(J)/DY
      WRITE(6,31)(FSX(J),J= ,N)
 31   FORMAT(10X,5F15.2)
      WRITE(6,998)
 32   FORMAT(1X,2I8,6F10.5)
 33   FORMAT(1H1,30X,*DEFINITION OF THE GRID*)
 34   FORMAT(///10X, *XO*,13X,*X-FINAL*,8X,*DXO*,12X,*DY*)
 35   FORMAT(//1X,4F15.5)
 36   FORMAT(///20X,*THE Y-+RID*//)
 37   FORMAT(/10X,*N*,2X,I5,10X,*N-MAX*,2X,I5//)
 998  FORMAT(1H1,*  *)
      RETURN
      END
      SUBROUTINE PDX1(N)
      COMMON/SKG5/RO(100)
      COMMON/SKG8/DP1,DP2,X,XX,DXO
      COMMON/SKG9/M
      COMMON/SKG11/UO,TO,T00,R00,CP0,VIS0,COND0,XL0,PRESS0
C
C
C     THIS ROUTINE CALCULATES PRESSURE GRADIENTS FROM GIVEN FREE
C                                        STREAM VELOCITY DISTRIBUTION
      X1=X-DXO
      X2=X+DXO
      CALL POL(5,0,X1,0.0,U1)
      CALL POL(5,0,X, 0.0,U4)
      CALL POL(5,0,X2,0.0,U2)
      UU=UU*RO(M)
      IF(N.EQ.1) DP1=-2.0*UU*(U2-U1)/(2.0*DXO)
      IF(N.EQ.2) DP2=-2.0*UU*(U2-U1)/(2.0*DXO)
      RETURN
      END
      SUBROUTINE TEMP (X,TW,TF)
      COMMON/SKG6/XINCH(50)TDPDX(50),TEAP(50),XWALL(50),TWALL(50)
      COMMON/SKG9/N,NN,NXDATA,NWALL,NPROP
      COMMON/SKG10/XR,RTH,D,DX
      COMMON/SKG11/UO,TO,T00,R00,CP0,VIS0,COND0,XL0,PRESS0
      COMMON/SKG14/TFSX,DTFSX
      COMMON/SKG15/TFX,TWX
```

```
C
      TF=1.0
      TFSX1=TFSX
      CALL POL(2,0,X,0.0,TFX)
      CALL POL(4,0,X,0.0,TWX)
      TW=(T0-TWX)/(T0-TFX)
      TFSX=TFX/T0
      DTFSX=(TFSX-TFSX1)/DX
      RETURN
      END
      SUBROUTINE BC
      COMMON/SKG6/XINCH(50)TDPDX(50),TFAR(50),XWALL(50),TWALL(50)
     1,UFAR(50),PFAR(50)
      COMMON/SKG9/N,NN,NXDATA,NWALL,NPROP
C
      WRITE(6,998)
      WRITE(6,149)
      WRITE(6,170)
      WRITE(6,999)
      WRITE(6,999)
      WRITE(6,145)
      READ(5,1) NXDATA
      DO 110 J=1,NXDATA
      READ(5,53) XINCH(J),DPDX(J),TFAR(J)
     1,UFAR(J),PFAR(J)
      PFAR(J)=PFAR(J)/2115.0
      DPDX(J)=DPDX(J)*10000.0
      WRITE(6,153) XINCH(J),DPDX(J),TFAR(J)
     1,UFAR(J),PFAR(J)
 110  CONTINUE
C     READ THE WALL TEMP.
      READ(5,1) NWALL
      WRITE(6,999)
      WRITE(6,999)
      WRITE(6,999)
      WRITE(6,152)
      WRITE(6,170)
      DO 109 J=1,NWALL
      READ(5,53) XWALL(J),TWALL(J),WALL
      WRITE(6,153) XWALL(J),TWALL(J)
 109  CONTINUE
 1    FORMAT(5X,I4)
 53   FORMAT(5F10.3)
 145  FORMAT(20X,*X,INCHES*,15X,*PRES,*,15X,*TEMP,R*,15X,*U,FT/SEC*///)
 149  FORMAT(25X,*GIVEN FREE STREAM CONDITIONS*)
 152  FORMAT(25X,*TEMP. B/C AT THE WALL*//,25X,*X,INCHES*,15X,*TEMP-R*)
 153  FORMAT(15X,F10.3,4(13X,E10.3))
 170  FORMAT(25X,*-------------------------*)
 998  FORMAT(1H1,* *)
 999  FORMAT(10X,* *)
      RETURN
      END
      SUBROUTINE FLUID
      COMMON/SKG5/RO(100),VIS(100),COND(100)
     1           ,RTEMP(50),RRO(50),RCP(50),RVIS(50),RCOND(50)
      COMMON/SKG9/N,NN,NXDATA,NWALL,NPROP
C
C
```

```
      WRITE(6,998)
      WRITE(6,148)
      WRITE(6,999)
      WRITE(6,999)
      WRITE(6,999)
      WRITE(6,171)
      WRITE(6,60)
      READ(5,1) NPROP
      DO 111 J=1,NPROP
      READ(5,54) PTEMP(J),PRO(J),PCP(J),PVIS(J),PCOND(J)
      PCP(J)=PCP(J)*25020.0
      PCOND(J)=PCOND(J)*25020.0
      PVIS(J)=PVIS(J)/(10.0**5)
      PCOND(J)=PCOND(J)/3600.0
      WRITE(6,131) PTEMP(J),PRO(J),PCP(J),PVIS(J),PCOND(J)
111   CONTINUE
1     FORMAT(5X,I4)
54    FORMAT(5F10.3)
60    FORMAT(10X,*  *)
131   FORMAT(10X,F6.1,5X,F6.3,3X,E10.3,3X,E10.3,5X,E10.3)
148   FORMAT(///30X,*PROPERTIES OF AIR*,/10X,*TEMP*,11X,*RO*, 9X,
     1*CP*, 8X,*VIS.* ,11X,*COND.*)
171   FORMAT(12X,*F*,8X,*LBM/CU FT*,3X,*BTU/LBM F*,2X,*SQ FT/SEC*,2X,
     1*BTU/SEC FT F*)
998   FORMAT(1H1,* *)
999   FORMAT(10X,* *)
      RETURN
      END
      SUBROUTINE DIMNON
      COMMON/SKG5/RO(100),VIS(100),COND(100)
     1           ,PTEMP(50),PRO(50),PCP(50),PVIS(50),PCOND(50)
      COMMON/SKG6/XINCH(50),DPDX(50),TFAR(50),XWALL(50),TWALL(50)
     1,UFAR(50)
      COMMON/SKG7/Y(100),E(100),HU(100),HT(100),ROM1(100),DPU(100)
     1           ,PY(100),FSX(100),FST(100),TL(100)
      COMMON/SKG8/DP1,DP2,X,XX,   DXO,DY,PR,PRT,CND,FACTOR
      COMMON/SKG9/N,NN,NXDATA,NWALL,NPROP
      COMMON/SKG11/UO,TO,TOO,ROO,CPO,VISO,CONDO,XLO,PRESSO
C
C
      TO=540.0
      UO=SQRT(2402.0*TO)
      POL1=TO
      CALL POL (0,1,0,POL1,POL2)
      ROO=POL2
      CALL POL (0,2,0,POL1,POL2)
      CPO=POL2
      CALL POL (0,3,0,POL1,POL2)
      VISO=POL2
      CALL POL (0,4,0,POL1,POL2)
      CONDO=POL2
      XLO=VISO/ROO/UO
      PRESSO=0.5*ROO*UO*UO
      CND=UO*UO/(CPO*TO)
      PR=CPO*VISO/CONDO
      PRT=0.9
      WRITE(6,999)
      WRITE(6,133) TO,UO,ROO,VISO,XLO,PRESSO,PR,PRT,CND
```

```
C       THE GIVEN DIMENSIONAL QUANTITIES ARE NONDIMENSIONALISED
        DO 113 I=1,NXDATA
        XINCH(I)=XINCH(I)/12.0/XL0
        DPDX(I)=DPDX(I)*XL0/PRESS0
        UFAR(I)=UFAR(I)/U0
  113   CONTINUE
        DO 118 I=1,NWALL
        XWALL(I)=XWALL(I)/12.0/XL0
  118   CONTINUE
        DO 112 I=1,NPROP
        PRO(I)=PRO(I)/RO0
        PVIS(I)=PVIS(I)/VIS0
        PCP(I)=PCP(I)/CP0
        PCOND(I)=PCOND(I)/COND0
  112   CONTINUE
        X=X/12.0/XL0
        XX=XX/12.0/XL0
        DX0=DX0/12.0/XL0
        DY=DY/12.0/XL0
        DO 110 J=1,N
        Y(J)=Y(J)/12.0/XL0
  110   CONTINUE
  133   FORMAT(///30X,*REFERENCE  QUANT.*,///10X,*WALL-TEMP*,5X,
       1E10.3,/10X,*VELOCITY*,9X,E10.3,/10X,*DENSITY*,9X,E10.3,/10X,
       2*VISCOSITY*,7X,E10.3,/10X,*LENGTH*,9X,E10.3,/10X,*PRESSURE*,8X,
       3E10.3,/10X,*PR. NO.*,9X,E10.3,/10X,*PR.NO-T*,6X,E10.3,/10X,*C*,
       414X,E10.3)
  999   FORMAT(10X,* *)
        RETURN
        END
        SUBROUTINE START2
        COMMON/SKG1/U(2,100),V(2,100),T(2,100)
        COMMON/SKG7/Y(100),F(100),HU(100),HT(100),ROM1(100),DPU(100)
       1           ,DY(100),FSX(100),FST(100),TL(100)
        COMMON/SKG8/DP1,DP2,X,XX,   DX0,DY,PR,PRT,CND,FACTOR
        COMMON/SKG9/N,NN,NXDATA,NWALL,NPROP
        COMMON/SKG10/XR,RTH,D,DX,DI,TI,H
        COMMON/SKG11/U0,T0,T00,R00,CP0,VIS0,COND0,XL0,PRESS0
C
C
C       GIVEN DATA
        DIIN=0.0
        TIIN=0.0
        H=1.0
        DI=DIIN/12.0/XL0
        TI=TIIN/12.0/XL0
        RTH=TI*U(1,N)
C       BL PROFILE POWER INDEX
        RBL=(H-1.0)/2.0
        IF(RBL.NE.0.0) D=(RBL+1.)*(2.0*RBL+1.0)*TI/RBL
        IF(RBL.EQ.0.0) D=0.0
        DIN=D*XL0*12.0
C
C
        V(1,N)=0.0
        DO 1 J=2,NN
        V(I,J)=0.0
        IF(Y(J).GT.D) GO TO 2
```

```
      U(1,J)=U(1,N)*(Y(J)/D)**RBL
      T(1,J)=T(1,1)+ (T(1,N)-T(1,1))*Y(J)/D
      GO TO 1
 2    CONTINUE
      T(1,J)=T(1,N)
      U(1,J)=U(1,N)
 1    CONTINUE
C
C
C     NEAR WALL
      IF(RBL.EQ.0.0) U12=U(1,N)
      IF(RBL.EQ.0.0) GO TO 5
      U12=(0.0288/(ALOG10(4.075*RTH))**2.0)*U(1,N)*U(1,N)*Y(2)
     1+0.25*Y(2)*Y(2)*DP1
 5    CONTINUE
C
      WRITE(6,30)
      WRITE(6,31)
      XIN=X*XL0*12.0
      WRITE(6,32) XIN,DIN,DIIN,TIIN,H,RBL,RTH
      WRITE(6,33)
      DO 11 J=1,5
      YIN=Y(J)*XL0*12.0
      U1J=U(1,J)/U(1,N)
      V1J=V(1,J)/U(1,N)
      WRITE(6,34) J,YIN,U1J, V1J,T(1,J)
 11   CONTINUE
      DO 12 J=6,N,5
      YIN=Y(J)*XL0*12.0
      U1J=U(1,J)/U(1,N)
      V1J=V(1,J)/U(1,N)
      WRITE(6,34) J,YIN,U1J, V1J,T(1,J)
 12   CONTINUE
      WRITE(6,35) U12
 30   FORMAT(1H1,30X,*CONDITIONS AT STARTING M-LINE*///)
 31   FORMAT(15X,*X*,14X,*D*,14X,*DD*,13X,*THETA*,10X,*H*,
     114X,*R*,14X,*RN-THETA*//)
 32   FORMAT(3X,7E15.4)
 33   FORMAT(///30X,*BL PROFILE*,//10X,*N*,20X,*Y*,14X,*U*,14X,*V*,14X,
     1*T*//)
 34   FORMAT(9X,I3,7X,4F15.4)
 35   FORMAT(///10X,*U12*,5X,F15.4)
      RETURN
      END
      SUBROUTINE ZLMIX
      COMMON/SKG1/U(2,100),V(2,100),T(2,100)
      COMMON/SKG5/RO(100),VIS(100),COND(100)
     1           ,PTEMP(50),PRO(50),PCP(50),PVIS(50),PCOND(50)
      COMMON/SKG7/Y(100),E(100),HU(100),HT(100),ROM1(100),DPU(100)
     1           ,PY(100),FSX(100),FST(100),TL(100)
      COMMON/SKG8/DP1,DP2,X,XX,   DXO,DY,PR,PRT,CND,FACTOR
      COMMON/SKG9/N,NN,NXDATA,NWALL,NPROP
      COMMON/SKG10/XR,RTH,DYDX,DI,TI,H
      COMMON/SKG13/U1,ICON
C
C
      FACTOR=2.0*FACTOR+0.1
      IF(FACTOR.GE.1.0) FACTOR=1.0
```

```
      DO 7 J=1,N
      DEL=D
      DEL=D*U(1,N)/VIS(J)/RO(J)
      YSC=SQRT(U(1,2)*VIS(J)/Y(2)-Y(2)*DP1/4.0)
      YD=Y(J)/DEL
      YS=Y(J)*YSC
      IF(YD.LT.0.1) TL(J)=0.41*(1.0-EXP(-YS/26.0))*YD
      IF(YD.GT.0.6) TL(J)=0.089
      IF((YD.GE.0.1).AND.(YD.LE.0.6)) TL(J)=0.41*(1.0-EXP(-YS/26.0))*YD
     1-1.54*(YD-0.1)**2+2.7*(YD-0.1)**3-1.08*(YD-0.1)**4
      TL(J)=TL(J)*DEL
 7    CONTINUE
      RETURN
      END
      SUBROUTINE EDDY
      COMMON/SKG4/UIT(100),VIT(100),TIT(100)
      COMMON/SKG7/Y(100),E(100),HU(100),HT(100),ROM1(100),DPU(100)
     1           ,PY(100),FSX(100),FST(100),TL(100)
      COMMON/SKG8/DP1,DP2,XTXX,   DXO,DY,PR,PRT,CND,FACTOR
      COMMON/SKG9/N,NN,NXDATA,NWALL,NPROP
C
C
      E(1)=0.0
      E(N)=0.0
      DO 10 J=2,NN
      K=J+1
      E(J)=TL(J)**2*ABS((UIT(K)-UIT(J-1))/(Y(J+1)-Y(J-1)))
 10   E(J)=E(J)*FACTOR
      RETURN
      END
      SUBROUTINE COEF
      COMMON/SKG1/U(2,100),V(2,100),T(2,100)
      COMMON/SKG2/AU(100),BU(100),CU(100),DU(100)
      COMMON/SKG3/AT(100),BT(100),CT(100),DT(100)
      COMMON/SKG4/UIT(100),VIT(100),TIT(100)
      COMMON/SKG5/RO(100),VIS(100),COND(100)
     1           ,PTEMP(50),PRO(50),PCP(50),PVIS(50),PCOND(50)
      COMMON/SKG7/Y(100),E(100),HU(100),HT(100),ROM1(100),DPU(100)
     1           ,PY(100),FSX(100),FST(100),TL(100)
      COMMON/SKG8/DP1,DP2,XYXX,   DXO,DY,PR,PRT,CND,FACTOR
      COMMON/SKG9/N,NN,NXDATA,NWALL,NPROP
      COMMON/SKG10/XR,RTH,D,DX,DI,TI,H
      COMMON/SKG11/UO,TO,TOO,ROO,CPO,VISO,CONDO,XLO,PRESSO
      COMMON/SKG12/ FLAG1,FLAG2,FLAG3,FLAGIT,FLAGPY,FLAGTP,DAMP
     1             ,CUTOFF,ERROR,CF,ITMIN
      COMMON/SKG14/TX,DTX
C
      LL=N-2
      DO 13 J=2,NN
      Y1=Y(J+1)-Y(J-1)
      Y2=Y(J+1)-Y(J)
      Y3=Y(J)-Y(J-1)
      E1=E(J+1)+E(J)
      E2=E(J)+E(J-1)
      VIS1=VIS(J+1)+VIS(J)
      VIS2=VIS(J-1)+VIS(J)
      RO1=RO(J+1)+RO(J)
      RO2=RO(J-1)+RO(J)
```

```
      COND1=COND(J+1)+COND(J)
      COND2=COND(J-1)+COND(J)
      PRT1=PRT+PRT
      K=J-1
      PRT2=PRT+PRT
      AL(K)=UIT(J)/DX+(VIS1/Y2+VIS2/Y3)/(RO(J)*Y1)+(RO1*E1/Y2+RO2*E2/Y3)
     1/(2.0*RO(J)*Y1)
      BU(K)=VIT(J)/Y1-VIS1/(RO(J)*Y1*Y2)-RO2*E1/(2.0*RO(J)*Y1*Y2)
      CU(K)=-VIT(J)/Y1-VIS2/(RO(J)*Y1*Y3)-RO2*E2/(2.0*RO(J)*Y1*Y3)
      DU(K)=UIT(J)*U(1,J)/DX-(DP1+DP2)/(4.0*RO(J))
      IF(FLAGTP.EQ.0.0) GO TO 116
      AT(K)=UIT(J)/DX+(COND1/Y2+COND2/Y3)/(RO(J)*PR*Y1)+(RO1*E1/
     1(Y2*PRT1)+RO2*E2/(Y3*PRT2))/(RO(J)*Y1)
      AT(K)=AT(K)+UIT(J)*(DTX+DTX)/(2.0*(TX-1.0))
      BT(K)=VIT(J)/Y1-COND1/(RO(J)*PR*Y1*Y2)-RO1*E1/(RO(J)*Y1*Y2*PRT1)
      CT(K)=-VIT(J)/Y1-COND2/(RO(J)*PR*Y1*Y3)-RO2*E2/(RO(J)*Y1*Y3*PRT2)
      DT(K)=UIT(J)*TIT(J)/DX+CND*UIT(J)*(DP1+DP2)/(4.*RO(J)*(TX-1.))
     1+CND*VIS(J)*((UIT(J+1)-UIT(J-1))/Y1)**2/(RO(J)*(TX-1.))
  116 CONTINUE
   13 CONTINUE
      DU(1)=DU(1)-CU(1)*U(2,1)
      DU(LL)=DU(LL)-U(2,N)*BU(LL)
      IF(FLAGTP.EQ.0.0) RETURN
      DT(1)=DT(1)-T(2,1)*CT(1)
      DT(LL)=DT(LL)-T(2,N)*BT(LL)
      RETURN
      END
      SUBROUTINE CALC (A,B,C,D,H)
C     *   *   *   THIS EVALUATES RESULTS USING THOMAS ALGORITHM   *   *
      DIMENSION A(100),B(100),C(100),D(100),H(100),W(100),Q(100),G(100)
      COMMON/SKG9/N
      N2=N-2
      N1=N-1
      W(1)=A(1)
      G(1)=D(1)/W(1)
      DO 1 K=2,N2
      K1=K-1
      Q(K1)=B(K1)/W(K1)
      W(K)=A(K)-C(K)*Q(K1)
    1  G(K)=(D(K)-C(K)*G(K1))/W(K)
      H(N2)=G(N2)
      N3=N-3
      DO 2 K=1,N3
      KK=N2-K
    2  H(KK)=G(KK)-Q(KK)*H(KK+1)
      RETURN
      END
      SUBROUTINE VELV
      COMMON/SKG1/U(2,100),V(2,100),T(2,100)
      COMMON/SKG5/RO(100),VIS(100),COND(100)
     1           ,PTEMP(50),PRO(50),PCP(50),PVIS(50),PCOND(50)
      COMMON/SKG7/Y(100),E(100),HU(100),HT(100),ROM1(100),DPU(100)
     1           ,PY(100),FSX(100),FST(100),TL(100)
      COMMON/SKG8/DP1,DP2,X,XX,   DXO,DY,PR,PRT,CND,FACTOR
      COMMON/SKG9/N,NN,NXDATA,NWALL,NPROP
      COMMON/SKG10/XR,RTH,D,DX,DI,TI,H
C
C
```

```
      V(2,1)=0.0
      DO 26 I=2,N
      Z=RO(I)*U(2,I)-ROM1(I)*U(1,I)+RO(I)*U(2,I-1)-ROM1(I-1)*U(1,I-1)
      ZY=Y(I)-Y(I-1)
      V(2,I)=RO(I-1)*V(2,I-1)-ZY*Z/(2.0*DX)
      V(2,I)=V(2,I)/RO(I)
   26 CONTINUE
      RETURN
      END
      SUBROUTINE PRNTBL
      COMMON/SKG1/U(2,100),V(2,100),T(2,100)
      COMMON/SKG5/RO(100),VIS(100),COND(100)
     1           ,PTEMP(50),PRO(50),PCP(50),PVIS(50),PCOND(50)
      COMMON/SKG7/Y(100),F(100),HU(100),HT(100),ROM1(100),DPU(100)
     1           ,PY(100),FSX(100),FST(100),TL(100)
      COMMON/SKG8/DP1,DP2,X,XX,   DXO,DY,PR,PRT,CND,FACTOR
      COMMON/SKG9/N,NN,NXDA A,NWALL,NPROP
      COMMON/SKG11/UO,TO,TOO,ROO,CPO,VISO,CONDO,XLO,PRESSO
      COMMON/SKG12/ FLAG1,FLAG2,FLAG3,FLAGIT,FLAGPY,FLAGTP,DAMP
     1             ,CUTOFF,ERROR,CF,ITMIN,IPRINT
      COMMON/SKG14/TFSX
C
C
      WRITE(6,999)
      WRITE(6,999)
      XIN=X*XLO*12.0
      WRITE(6,72) XIN
      WRITE(6,63)
      DO 84 J=1,5
      YIN=Y(J)*XLO*12.0
      U2J=U(2,J)/U(2,N)
      V2J=V(2,J)/U(2,N)
      T2J=TO*(1.0-T(2,J)*(1.0-TFSX))
      WRITE(6,61) J,YIN,U2J,V2J,T(2,J)
     1,T2J
   84 CONTINUE
      DO 85 J=6,N,3
      YIN=Y(J)*XLO*12.0
      U2J=U(2,J)/U(2,N)
      V2J=V(2,J)/U(2,N)
      T2J=TO*(1.0-T(2,J)*(1CO-TFSX))
      WRITE(6,61) J,YIN,U2J,V2J,T(2,J)
     1,T2J
   85 CONTINUE
      YIN=Y(N)*XLO*12.0
      T2N=TO*(1.0-T(2,N)*(1CO-TFSX))
      WRITE(6,61) N,YIN,U(2,N),V(2,N),T(2,N)
     1,T2N
      IPRINT=0
      WRITE(6,999)
      WRITE(6,999)
      WRITE(6,64)
      FLAG2=FLAG2+1.0
   61 FORMAT(25X,I3,4E20.5,5X,F10.2)
   63 FORMAT(/27X,*M*,13X,*Y(M)*,16X,*U(M)*,16X,*V(M)*,16X,*T(M)*,/)
   64 FORMAT(7X,*X*,6X,*D(B/L THICK.)*,6X,*D*,9X,*THETA*,8X,*H*,13X,
     1*CF/2*,6X,*          *,12X,*NX*,7X,*NO. OF ITER.*)
   72 FORMAT(///5X,*BOUNDARY LAYER AT X=*,E10.4)
```

```
 999  FORMAT(10X,*  *)
      RETURN
      END
      SUBROUTINE BLX
      COMMON/SKG1/U(2,100),V(2,100),T(2,100)
      COMMON/SKG5/RO(100)
      COMMON/SKG7/Y(100),E(100),HU(100),HT(100),ROM1(100),DPU(100)
     1           ,DY(100),ESX(100),EST(100),TL(100)
      COMMON/SKG8/DP1,DP2,X,XX,   DXO,DY,PR,PRT,CND,FACTOR
      COMMON/SKG9/N,NN,NXDATA,NWALL,NPROP
      COMMON/SKG10/XR,RTH,D,DX,DI,TI,H
      COMMON/SKG11/UO,TO,TOO,ROO,CPO,VISO,CONDO,XLO,PRESSO
      COMMON/SKG12/ FLAG1,FLAG2,FLAG3,FLAGIT,FLAGPY,FLAGTP,DAMP
     1             ,CUTOFF,ERROR,CF,ITMIN
C
C
C     B/L THICKNESS
      UU=CUTOFF*U(2,N)
      DO 14 J=1,NN
      JJ=J
      IF(U(2,J) .GE.UU)GO T- 15
   14 CONTINUE
      WRITE(6,150)
 15   CONTINUE
      D=Y(JJ)
C
      DY=Y(N)-Y(N-1)
      DV=V(2,N)-V(2,N-1)
      WRITE(6,999)
C     DISPLACEMENT AND MOMENTUM THICKNESS
      TI=0.0
      DI=0.0
      DX1=1.0
      TX1=0.0
      DO 930 J=2,JJ
      XX1=U(2,J)/U(2,N)
      XX2=(Y(J)-Y(J-1))/2.0
      DX2=1.0-XX1*RO(J)/RO(-)
      TX2=(1.0-XX1)*XX1*RO(1)/RO(N)
      DI=DI+(DX1+DX2)*XX2
      TI=TI+(TX1+TX2)*XX2
      DX1=DX2
      TX1=TX2
  930 CONTINUE
C
C     SHAPE FACTOR
      H=DI/TI
C
 150  FORMAT(///10X,*B/L THICKNESS GREATER THAN Y(N)*)
 999  FORMAT(10X,*  *)
      RETURN
      END
      SUBROUTINE TPROP(T,I)
      DIMENSION T(2,100)
      COMMON/SKG5/RO(100),VIS(100),COND(100)
     1           ,PTEMP(50),PRO(50),PCP(50),PVIS(50),PCOND(50)
      COMMON/SKG9/N,NN,NXDATA,NWALL,NPROP
      COMMON/SKG11/UO,TO
```

```
      COMMON/SKG14/TFSX
C
C
      DO 1 J=1,N
      TX=T0*(1.0-T(I,J)*(1.0-TFSX))
      CALL POL (0,1,0,TX,POL2)
      PO(J)=POL2
      CALL POL (0,2,0,TX,POL2)
      VIS(J)=POL2
      CALL POL (0,4,0,TX,PO-2)
      COND(J)=POL2
 1    CONTINUE
      RETURN
      END
      SUBROUTINE POL(NDP,NPR,XIN,TX1,ANS)
      DIMENSION X(50),Y(50)
      COMMON/SKG5/DUM1(300),X2(50),Y21(50),Y22(50),Y23(50),Y24(50)
      COMMON/SKG6/X1(50),Y11(50),Y12(50),X3(50),Y31(50)
     1,Y51(50),Y61(50)
      COMMON/SKG9/NX1,NX2,N1,N3,N2
      COMMON/SKG11/U0,XX2,DUM(5),XL0
C
      N=N2
      IF(NDP.NE.0) N=N1
      IF(NDP.EQ.4) N=N3
      DO 1 I=1,N
      IF(NDP.NE.0) GO TO 10
      X(I)=X2(I)
      IF(NPR.EQ.1) Y(I)=Y21(I)
      IF(NPR.EQ.2) Y(I)=Y22(I)
      IF(NPR.EQ.3) Y(I)=Y23(I)
      IF(NPR.EQ.4) Y(I)=Y24(I)
      GO TO 1
 10   CONTINUE
      X(I)=X1(I)
      IF(NDP.EQ.4) X(I)=X3(I)
      IF(NDP.EQ.1) Y(I)=Y11(I)
      IF(NDP.EQ.2) Y(I)=Y12(I)
      IF(NDP.EQ.4) Y(I)=Y31(I)
      IF(NDP.EQ.5) Y(I)=Y51(I)
      IF(NDP.EQ.6) Y(I)=Y61(I)
 1    CONTINUE
C
C
      XX=TX1
      IF(NDP.NE.0) XX=XIN
C
C
      DO 2 I=2,N
      ZED=X(I)-XX
      IF(ZED.GE.0.0) GOTO 4
 2    CONTINUE
      WRITE(6,30) NDP,NPR,XIN,TX1
 30   FORMAT(10X,*INTERPOLATION NOT POSSIBLE*,10X,I2,I2,2X,E10.1,2X,
     1E10.1//)
4     CONTINUE
      IF(ZED.EQ.0.0) GOTO 5
      ANS=Y(I)-(Y(I)-Y(I-1))*(X(I)-XX)/(X(I)-X(I-1))
```

```
      GOTO 3
5     ANS=Y(I)
3     CONTINUE
      RETURN
      END
'       6400 END OF RECORD
 1.0   1.0    0.0    0.0    1.0    1.0    0.7    0.98   1.0    1.0    0.0        5
       40      110   0.01        1.65        0.001      0.00001     0.7        0.9
        8
0.10        0.0         442.5       1026.0      2120.0
0.27        0.0         464.0       894.0       2500.0
0.44        0.0         493.0       754.0       2880.0
0.57        0.0         486.0       724.0       2960.0
0.74        0.0         460.3       915.0       2440.0
0.91        0.0         428.0       1112.0      1880.0
1.05        0.0         419.0       1153.5      1760.0
1.64        0.0         428.0       1112.0      1014.0
        2
0.0         492.0
2.0         492.0
       26
400.0       0.1058      0.2391      1.0         0.0122
410.0       0.0972      0.2392      1.017       0.0124
420.0       0.0949      0.2393      1.034       0.0126
430.0       0.0927      0.2394      1.051       0.0128
440.0       0.0906      0.2395      1.067       0.0130
450.0       0.0886      0.2396      1.083       0.0132
460.0       0.0866      0.2397      1.110       0.0134
470.0       0.0848      0.2398      1.128       0.0136
480.0       0.0830      0.2399      1.146       0.0138
492.0       0.0810      0.2400      1.165       0.0140
500.0       0.0797      0.2400      1.183       0.0142
510.0       0.0781      0.2400      1.201       0.0144
520.0       0.0766      0.2400      1.219       0.0146
530.0       0.0752      0.2400      1.237       0.0148
540.0       0.0738      0.2400      1.255       0.0150
550.0       0.0725      0.2400      1.270       0.0152
560.0       0.0712      0.2400      1.285       0.0154
660.0       0.0604      0.241       1.430       0.0174
760.0       0.0524      0.243       1.610       0.0193
860.0       0.0463      0.245       1.750       0.0212
960.0       0.0415      0.247       1.890       0.0231
1060.0      0.0376      0.250       2.00        0.0250
1160.0      0.0344      0.253       2.14        0.0268
1260.0      0.0316      0.256       2.25        0.0286
1360.0      0.0293      0.259       2.36        0.0303
1460.0      0.0273      0.262       2.47        0.0319
'         END OF FILE

                                                CDTOT   0019
```

APPENDIX 4 THE THOMAS ALGORITHM

After taking finite difference approximations we have a set of linear algebraic equations for momentum and energy in the form:

$$a_1x_1 + b_1x_2 = d_1$$

$$a_2x_2 + b_2x_3 + c_2x_1 = d_2$$

$$a_3x_3 + b_3x_4 + c_2x_2 = d_2$$

$$a_rx_r + b_rx_{r-1} + c_rx_{r-1} = d_r \qquad \text{A4 -1}$$

$$a_{m-1}x_{m-1} + b_{m-1}x_m + c_{m-1}x_{m-2} = d_{m-1}$$

$$a_mx_m + c_mx_{m-1} = d_m$$

In this equation the x-values are unknown. We can now define x_1 in terms of x_2, x_2 in terms of x_3 and so on until we define x_m in terms of x_{m-1}. But the last equation already gives us x_m in terms of x_{m-1} so we can solve for x_m and work backwards through the equations until we have defined all the unknown x values.

This is done numerically by defining the following

$$w_1 = a_1$$

$$w_r = a_r - c_rq_{r-1} \qquad \text{where } r = 2, 3 \ldots m$$

$$q_{r-1} = \frac{b_{r-1}}{w_{r-1}} \qquad \text{A4 -2}$$

$$g_1 = \frac{d_1}{w_1}$$

$$g_r = \frac{d_r - c_r g_{r-1}}{w_r} \qquad r = 2, 3 \ldots m$$

This set of equations further reduces to:

$$\left.\begin{aligned} x_m &= g_m \\ x_r &= g_r - q_r x_{r+1} \qquad r = m-1, m-2 \ldots 1 \end{aligned}\right\} \text{A4 -3}$$

Thus by substituting suitable values of 'r' in the equations (A4 -2) we can calculate w, q and g, then equation (A4 -3) can be solved for x starting with x_m. (For instance see Ref. 13)